

https://dspace.org/

Holistic approach to groundwater recharge assessment in the Upper Crocodile River Basin, Johannesburg, South Africa

Leketa, Khahliso Clifford

2019-07

https://hdl.handle.net/10539/29632

Leketa, Khahliso Clifford, Holistic approach to groundwater recharge assessment in the Upper Crocodile River Basin, Johannesburg, South Africa, University of the Witwatersrand, Johannesburg, <http://hdl.handle.net/10539/29632>

Downloaded from a DSpace repository. https://dspace.org/

Holistic approach to groundwater recharge assessment in the Upper Crocodile River Basin, Johannesburg, South Africa

By Khahliso Clifford Leketa

Student Number:

1436509

A thesis submitted to the Faculty of Science, University of the Witwatersrand, Johannesburg, in fulfilment of the requirements for the degree of Doctor of Philosophy.



WITS
UNIVERSITY

School of Geosciences

Supervisor: Professor Tamiru Abiye

July 2019

CANDIDATE'S DECLARATION

I declare that this thesis is my own, unaided work. It is being submitted for the Degree of Doctor of Philosophy at the University of the Witwatersrand, Johannesburg. It has not been submitted before for any degree or examination at any University.

……
(Signature of candidate)

July 2019

ABSTRACT

In the highly urbanised and water stressed Upper Crocodile River Basin (UCRB), Johannesburg, South Africa, which has wastewater induced surface water resources and a complex land use and geological setting, a holistic assessment of groundwater recharge was undertaken to understand the groundwater provenance and to address the prevailing water security issues. This work emanated from a project entitled, "Understanding Groundwater Recharge in the Limpopo River Basin (GRECHLIM)".

Samples from Johannesburg rainfall, surface water and groundwater were collected and analysed for $\delta^{18}O$, $\delta^{2}H$ and ^{3}H, while selected groundwater sources were additionally sampled and analysed for $\delta^{13}C$ and ^{14}C. Albert Farm spring was monitored monthly for stable isotopes and yield over a period of 14 months. The Thornthwaite Monthly Water Balance Model (TMWBM), Stream Segment Water Budget, Reservoir Water Budget, Baseflow Separation and Water Table Fluctuation methods were applied to assess groundwater recharge, while Precipitation Runoff Modelling System (PRMS) was applied to assess the impacts of changes in climate variables on the hydrology of the UCRB.

The temperature and amount effects were observed in rainfall and the Johannesburg Local Meteoric Water Line (JLMWL) was constructed as $\delta^2H = 6.7\delta^{18}O + 10‰$, while the temperature-$\delta^{18}O$ regression line was $\delta^{18}O = 0.552t - 14.1‰$. A high stable isotope variability was observed in the Johannesburg rainfall with the most depleted sample having $\delta^{2}H$ and $\delta^{18}O$ values of -131.6‰ and -17.82‰, respectively, and the most enriched rainfall having 51.4‰ and 7.03‰, respectively. A high variability was also observed in the monthly stable isotope samples of the Albert Farm spring with the signature ranging from -6.01‰ to -2.28‰ for $\delta^{18}O$ and from -21.6‰ to -10.48‰ for $\delta^{2}H$ with d-excess ranging from 3.23‰ to 18.7‰ for the review period. The majority of the groundwater samples across the UCRB plot close to the JLMWL and the most depleted samples were those from the dolomitic aquifer, while the most enriched were the boreholes positioned downstream of the Hartbeespoort Dam. The samples from the dolomite aquifer were enriched in stable carbon isotope ($\delta^{13}C$), while those from the granites, shales and quartzites were depleted, with intermediate values observed at the margins of granites and dolomites. The ^{14}C results indicated that groundwater in the UCRB has an MRT between 0 (present) and 3856 years, deducing high aquifer heterogeneity. The estimated daily air temperature at the time of recharge is similar to the current daily air temperature during rainfall, while the estimated annual air temperatures are lower than the present annual temperatures.

An average potential recharge estimate of 4.3% was obtained in the UCRB using the TMWBM with low amounts estimated in the warmer low elevation northern part of the UCRB and higher amount in the cooler elevated southern portion. This indicated the influence of temperature on recharge. The Stream Segment and Reservoir Water Budget methods indicated spatial and temporal net gain and net loss across the UCRB and the Reservoir Water Budget indicated that annually, the Hartbeespoort Dam experiences a net loss of 7% of its inflow, which is referred to as focused recharge amounting to 2 084 131 m^3. The focused recharge is deduced to occur through the Brits fault lines and the bedding planes in the Magaliesberg quartzite at the rate of 202 m/year deduced from tritium analysis. The application of the Baseflow Separation method in different quaternary catchments of the UCRB gave an area weighted average recharge estimate of 6.7% for the UCRB, while the Water Table

Fluctuation method gave an average recharge estimate of 11.4% in the dolomitic aquifers. The hydrograph and stable isotope analysis of the piezometers indicated the influence of interflow contribution, deducing that the baseflow estimate in the basement granites is inclusive of interflow.

It is concluded that change in seasons and moisture sources are the causes of the high variability in rainfall isotopes. The high temporal variability in stable isotopes and d-excess values from the same groundwater source further confirms that the UCRB receives rainfall from different moisture sources. This indicates that in regions that receive rainfall of different isotopic signature, the use of a single sample to characterise recharge may not be a good practice as this may erroneously yield biased interpretations. Effective recharge in the UCRB predominantly occurs through diffuse mechanisms, while focused recharge is mainly observed near the surface water bodies. The depleted nature (in $\delta^{18}O$ and $\delta^{2}H$) of groundwater samples in the dolomitic aquifers is deduced to be a result of altitude effect or possibilities of an exchange of oxygen between the dissolved CO_2 and groundwater. However, the possibilities of oxygen exchange have been recommended for further investigation. The stable carbon isotopes ($\delta^{13}C$) indicated closed system carbon evolution in the dolomitic aquifer and open system in the granites, shales and quartzites. From the signature of stable isotope of carbon, oxygen and hydrogen, it is further concluded that there is mixing of the two water types at the periphery of the dolomitic and granitic aquifers.

Combined interpretation of ^{14}C age and the estimated annual air temperatures indicates that recharge of older groundwater occurred at lower temperatures, while recharge of more recent groundwater occurred at warmer temperatures showing evidence of increase in annual air temperatures with time. The observed similarity between the calculated and the current daily temperatures on one side, and the observed variability between the calculated and current annual air temperatures on another side, could be related to the fact that regardless of the changes in global temperatures, the physical in-cloud condensation conditions, which dictate the isotopic signature in daily rainfall are not changing.

In general, the study indicates that the stable isotope effects in rainfall can successfully be used to assess the air temperature on the day of the rainfall that generated recharge and to determine the dependency of recharge amount on rainfall amount if the aquifer is recharged by rainfall without undergoing extreme evaporation prior to recharge.

The climate simulations indicate that as baseflow decreases due to changes in climate variables and wastewater increases due to growth in urbanisation, the amount of wastewater shall dominate baseflow in the UCRB leading to more polluted surface water. Therefore, better treatment and constraints on pollution are recommended for the future.

DEDICATION

I dedicate this effort to my late father Mr Rets'elisitsoe Garnet Leketa, my mother M'akhahliso Grace Leketa, my two sisters Bonang "Sis-bo" Leketa and M'aseabata "Sabby" Leketa. To my beautiful lovely wife Matumisang Phaello Brigitte Leketa, my son Tumisang Victor Leketa and my daughter Karabo Khauhelo Grace Leketa.

ACKNOWLEDGEMENTS

Sometimes we stand tall and firm looking as though we are invincible, while in fact it is only because of the strength of the great men and women on whose shoulders we have been standing.

By this, I would like to acknowledge the following persons and institutions for their contribution during the period of my study. Without their involvement, this study would not have been possible.

My supervisor Professor Tamiru Abiye who sourced the project fund and after seeing potential in me, he offered me a fully funded bursary giving me an opportunity to further my dream of pursuing a Doctor of Philosophy degree under his guidance. I would like to thank you Professor for the watchful supervision. It has been more than a thrill working with you. Like the clay when you take it in your hands when it almost has no shape or form, you took me under your supervision, and moulded me, imparted in me a passion for research, sculptured me to give me this shape that I am, which has now grown to become an asset in the field of water research. I thank you Prof! The best PhD supervisor I could have ever wished for.

The institutions that were financially responsible for my bursary: United States Agency for International Development (USAID) and the National Academies of Sciences, Engineering, and Medicine (NAS) through Partnership for Enhanced Engagement in Research (PEER) under cooperative agreement number AID-OAA-A-11-00012 Sub-Grant Number: 2000006304 and the Department of Science and Technology, South Africa (UID: 101594).

iThemba Labs, in particular, Mr Michael Butler for the analysis of radioactive isotopes. Department of Water and Sanitation (DWS), South African Weather Services (SAWS) and Council for Geoscience (CGS) for the provision of data.

I would like to pass my gratitude to the following students under the GRECHLIM project who have been very instrumental over my three year study period, particularly with field work assistance; Mr Khuliso Masindi (PhD Candidate), Ms. Silindile Zondi and Ms. Aqeelah Davis (MSc Hydrogeology 2016), Mr. Sipho Nyebelele, Ms. Thabisile Sibande, and Ms. Seeke Carol Mohuba (BSc Honours Geology 2017), Ms. Mashudu Mmbadi (MSc Hydrogeology 2017), Mr. Justin Press (MSc Hydrogeology 2018), Ms Ayanda Biyela (BSc Honours Geology 2018). I treasure those discussions we used to have, in particularly Khuliso Masindi, I enjoyed those geological excursions where we used to drive around and discuss the geology of the area.

Various professionals of the United States Geological Survey for a two weeks training they gave me in Denver Colorado, USA: Steve Robert Regan, Steve Markstrom and Lauren Hay for training on the Precipitation Runoff Modelling system; Dr Richard Healy for the training on estimating groundwater recharge; Don Rosenberry, Bridget Scanlon, Richard Webb, Kitty Walton-Day, David Parkhurst, Victor Heilweil for the various topics on groundwater assessment.

The whole of the School of Geosciences staff, particularly M'e Leenah Mtiyane and the Head of School Professor Roger Gibson for always processing my bursary payments with diligence.

I would like to thank my family and friends for all the support I received from them through this trying time. My lovely wife who has been motivating me from the onset and throughout this period of study; you were my support when my strength was challenged.

And in all these things, I saw the depth, the width and the breadth of the love of God, I learned that His grace is indeed amazing and that His promises are indeed yes and Amen!!!

PUBLICATIONS

Publication 1: Published in Groundwater for sustainable Development (Appendix C.1)

Leketa, K., Abiye T., Zondi, S., Butler M. 2019. Assessing groundwater recharge in crystalline and karstic aquifers of the Upper Crocodile River Basin, Johannesburg, South Africa Groundwater for Sustainable Development. 31-40. https://doi.org/10.1016/j.gsd.2018.08.002

Publication 2: Published in Journal of Environmental Earth Sciences (Appendix C.2)

Leketa, K., Abiye, T. & Butler, M. 2018. Characterisation of groundwater recharge conditions and flow mechanisms in bedrock aquifers of the Johannesburg area, South Africa. Environmental Earth Sciences, 77, 727. https://doi.org/10.1007/s12665-018-7911-7.

Publication 3: Published in Journal of Environmental Earth Sciences (Appendix C.3)

Leketa, K. & Abiye, T. 2019. Modelling the impacts of climatic variables on the hydrology of the Upper Crocodile River Basin, Johannesburg, South Africa. Environmental Earth Sciences, 78, 358. https://doi.org/10.1007/s12665-019-8353-6.

Publication 4: To be submitted to the Journal of Heliyon

Leketa, K. & Abiye, T. (Under preparation). Characterising stable isotopes in Johannesburg rainfall.

Publication 5: To be submitted to the Journal of Heliyon

Leketa, K. & Abiye, T. (Under preparation). Using the traces of stable isotope effects in rainfall to assess groundwater recharge conditions in Johannesburg, South Africa.

CONFERENCES/WORKSHOPS ATTENDED

Leketa, K. and Abiye, T. 2017. Characterising groundwater recharge in crystalline aquifer Johannesburg, South Africa. **Oral presentation at the 15th Biennial Groundwater Division Conference in Stellenbosch South Africa, 14th to 18th October 2017.**

Leketa, K., Abiye, T., and Butler, M. 2018. Using environmental isotopes to characterisation groundwater recharge conditions and flow mechanisms in the crystalline aquifers of the Johannesburg area, South Africa. **Oral presentation at the 2018 Geocongress, at the University of Johannesburg, South Africa 18th to 20th July 2018.**

Leketa, K., Abiye, T. 2017. Workshop on the Progress presentation on the Groundwater Recharge in the Upper Crocodile River Basin. **Oral presentation at the Consultative meeting for the project "Understanding Groundwater Recharge in The Limpopo River Basin" 9th to 20th October 2017**

Leketa, K., Abiye, T. 2018. Groundwater recharge assessment in the Upper Crocodile River Basin, **Oral presentation at Recharge training workshop at United States Geological Survey, Denver Colorado, USA 2nd to 13th April 2018.**

CONTENTS

CANDIDATE'S DECLARATION ii
ABSTRACT iii
ACKNOWLEDGEMENTS vi
PUBLICATIONS vii
CONFERENCES/WORKSHOPS ATTENDED viii
CONTENTS ix
LIST OF FIGURES xiii
LIST OF TABLES xvii
LIST OF SYMBOLS xviii
NOMENCLATURE xviii
1 INTRODUCTION 1
1.1 Background of the study 1
1.2 Research aims and specific objectives 3
1.3 Significance of the study and identification of potential beneficiaries to the research outcomes 3
2 DESCRIPTION OF STUDY AREA 4
2.1 Location of study area 4
2.2 Climatic setting 4
2.3 Land and water use 8
2.4 Geological Setting 10
2.4.1 The Basement Igneous Complex 12
2.4.2 The Witwatersrand Supergroup 12
2.4.3 The Ventersdorp Supergroup 13
2.4.4 The Transvaal Supergroup 14
2.4.5 The Bushveld Igneous Complex 16
2.4.6 The Sedimentary rocks of the Karoo Supergroup 17
2.5 Hydrogeological Setting 17
2.5.1 Intergranular aquifers 18
2.5.2 Fractured aquifers 18
2.5.3 Karstic aquifers 20
2.5.4 Intergranular and fractured aquifers 23
2.6 Hydrological Setting 23
2.7 Topographical Setting 24

3 A REVIEW OF LITERATURE ON GROUNDWATER RECHARGE PROCESSES 26
3.1 Groundwater recharge process and its interdependence with other processes in the Hydrological Cycle 26
3.2 Basic mechanisms of groundwater recharge 28
3.3 Groundwater recharge mechanism in fractured crystalline rock aquifers 29
3.4 Summary of previous investigations in the UCRB 31
3.5 Conceptualised recharge processes in the UCRB 33
4 THEORETICAL BACKGROUND ON THE RECHARGE ASSESSMENT METHODS 34
4.1 Introduction 34
4.2 Chemical and isotope tracer methods 34
4.2.1 Environmental isotopes 35
4.3 Classical water balance approaches 42
4.3.1 Thornthwaite Monthly Water Balance Model (TMWBM) 43
4.4 Physical methods of estimating groundwater recharge 45
4.4.1 Methods based on surface water data 45
4.4.2 Methods based on the saturated zone/groundwater data 47
4.5 Watershed modelling methods 50
4.5.1 Precipitation Runoff Modelling System 50
5 RESEARCH METHODOLOGY EMPLOYED 52
5.1 Desktop review and data collection 52
5.2 Aquifer characterisation 52
5.3 Assessment of baseflow versus interflow occurrence in the streams that are underlain by the basement granites 53
5.3.1 Assessment using borehole information and stream channel elevation 53
5.3.2 Assessment using piezometers in the stream that is underlain by the granites 54
5.4 Applications of chemical and isotope tracer methods 55
5.4.1 Sampling and field work procedure 55
5.4.2 Interpretation of environmental isotopes data 59
5.5 Applications of physical and water balance methods 60
5.5.1 Thorthwaite Monthly Water Balance Model 60
5.5.2 Baseflow Separation Method 61
5.5.3 Stream Segment Water Budget method 61
5.5.4 Reservoir Water Budget 63
5.5.5 Water Table Fluctuation method 63
5.5 Precipitation Runoff Modelling System 64

5.5.1 Construction of the model 64
5.5.2 Assessment of baseflow and groundwater recharge 67
5.5.3 Model sensitivity, calibration and validation 67
5.5.4 Simulation of climate-based scenarios 69
6 RESULTS AND DISCUSSIONS 70
6.1 Aquifer characterisation 70
6.1.1 Characterisation of aquifers in the basement granites 70
6.1.2 Characterisation of aquifers in the Transvaal Supergroup 72
6.1.3 Assessment of groundwater level response to rainfall through hydrograph analysis 73
6.2 Assessing the possibilities for baseflow and interflow occurrence in streams underlain by the basement granites 74
6.2.1 Assessing the elevations of stream channel and borehole log components 74
6.2.2 Assessment of interflow in the stream underlain by the Basement Complex 76
6.3 Application of chemical and isotope tracer methods 78
6.3.1 Stable isotope composition of Johannesburg rainfall 78
6.3.2 Characterising groundwater recharge mechanisms using stable and non-stable isotopes of the water molecule ($\delta^{2}H$, $\delta^{18}O$, ^{3}H). 82
6.3.3 Using the amount and temperature effects to assess the groundwater recharge conditions 89
6.3.4 Carbon isotopes to assess groundwater flow conditions and MRT 93
6.3.5 Hydrogeological characterisation of the dolomitic springs 97
6.4 Recharge assessment using classical and physical methods 101
6.4.1 Classical water balance methods 101
6.4.2 Baseflow Separation method 105
6.4.3 Stream Segment Water Balance method 106
6.4.4 Reservoir Water Budget method 109
6.4.5 Water table fluctuation method 110
6.5 Simulating the impacts of changes in climate variables on the stream flow using PRMS 112
6.5.1 Model calibration 112
6.5.2 Validation periods 113
6.5.3 Simulation of climate scenarios 115
6.6 Synthesis 119
6.6.1 Conceptual model of groundwater recharge and flow mechanisms in the UCRB 119
6.1.1 The sustainability of groundwater in the UCRB 119
7 CONCLUSION AND RECOMMENDATIONS 121
7.1 Conclusions 121

7.2 Main contributions of the study....123
7.3 Recommendations....124
REFERENCES....125
APPENDICES....134
A. Methodology on carbon14 sampling (Source is iThemba Labs, Johannesburg)....134
B. Borehole hydrographs....135
C. Publications....138
C.1. Publication 1-Journal of Groundwater for Sustainable Development....138
C.2. Publication 2-Journal of Environmental Earth Sciences....149
C.3. Publication 3-Journal of Environmental Earth Sciences....161

LIST OF FIGURES

Figure 2.1: Locality map of the UCRB and its location on South Africa map as insert. 4
Figure 2.2: Climate for the 20 year period (1996 to 2017) using data from four UCRB climate stations from South African Weather Services. 5
Figure 2.3: Locations of weather stations showing mean annual temperatures for the period 1997 to 2016 (A2E002 is for pan-evaporation). 6
Figure 2.4: Annual precipitation for the period between 1997 and 2016 from different weather stations. 7
Figure 2.5: Annual average temperature trends for the period between 1997 and 2016. 8
Figure 2.6: Annual pan-evaporation for the period between 1997 and 2016 for the station A2E002 (from an S-class pan). 8
Figure 2.7: Geological map of the UCRB shown relative to the quaternary catchments (Source of Geological data: Council for Geosciences, South Africa). 11
Figure 2.8: Locality map of the basement rocks (Source of Geological data: Council for Geosciences, South Africa). 12
Figure 2.9: Locality map of the Witwatersrand Supergroup (Source of Geological data: Council for Geosciences, South Africa). 13
Figure 2.10: Locality map of the Ventersdorp and Karoo Supergroup rocks (Source of Geological data: Council for Geosciences, South Africa). 14
Figure 2.11: Locality map of the Transvaal Supergroup rocks within the UCRB (Source of Geological data: Council for Geosciences, South Africa). 15
Figure 2.12: The north dipping bedding planes in the quartzites of the Magaliesberg Formation at the Hartbeespoort Dam wall. 16
Figure 2.13: Schematic representation of the Hartbeespoort Dam with its main fault lines showing the position of the graben. 16
Figure 2.14: Locality map of the Bushveld Complex rocks within the UCRB (Source of Geological data: Council for Geosciences, South Africa). 17
Figure 2.15: The vertical regional fractures that are typical in the quartzite of the Witwatersrand Supergroup on (a), (b) and (c), while (d) and (e) show the fractures that host the Albert Farm spring. 19
Figure 2.16: The outcrops of the basement rocks in the UCRB showing fractures (a) and the weathered part (b). 20
Figure 2.17: The Magaliesberg ridge, showing a conceptual model of the presumed recharge process from Hartbeespoort Dam through the bedding planes. 20
Figure 2.18: Discharge from Nouklip Spring in the dolomites (Courtesy of Prof. Tamiru Abiye)... 21
Figure 2.19: Geological map of the Malapa area showing the springs, the underlying lithology and the orientation of the faults (Courtesy of Prof. Tamiru Abiye) 22
Figure 2.20: Travertine that deposited downstream of Nouklip spring forming rapids (Courtesy of Prof. Tamiru Abiye). 23
Figure 2.21: Surface water bodies within the UCRB and gauging stations at the outlet of quaternary catchments on the main map and all UCRB gauging stations shown on insert map. 24
Figure 2.22: Topography and drainage of the UCRB. 25
Figure 3.1: Schematic representation of reduction of water through the recharge process. 26
Figure 3.2: Schematic of diffuse and focused recharge (Adapted from Healy (2010). 29
Figure 3.3: Conceptual representation of the unsaturated zone recharge and bypass flow through the weathered and fractured bedrock. 30

Figure 3.4: Schematic representation of saturation levels between fracture and matrix during both rising and falling water table. (Source: Healy (2010). 31
Figure 4.1: A schematic diagram of $\delta^{18}O$ versus $\delta^{2}H$ illustrating the global meteoric water line, the evaporation line (LEL), and the different d-excess values (adapted from Froehlich *et al.* (2002). ... 39
Figure 4.2: A schematic diagram showing a water balance of a water column (Adapted from Healy (2010)). 43
Figure 4.3: The Graphical User Interphase for TMWBM (Source: USGS). 44
Figure 4.4: An illustration of baseflow and interflow into the stream channel. 46
Figure 4.5: Hypothetical graph showing the magnitude of Δh measured from peak of the groundwater hydrograph to the point on the antecedent curve. 48
Figure 4.6: An illustration of a groundwater level fluctuation in a multi-layered geological setting. 49
Figure 4.7: Hydrologic processes simulated by Precipitation-Runoff Modelling System (adapted from Markstrom *et al.* (2008) and Markstrom *et al.* (2015)). 51
Figure 5.1: Locations of boreholes used for aquifer characterisation in the granites. 53
Figure 5.2: Locations of boreholes and adjacent river points. 54
Figure 5.3: Construction of the piezometers across Montgomery stream (NB: not drawn to scale). 55
Figure 5.4: Locations of sampling points for groundwater, surface water and rainfall. 56
Figure 5.5: The type of rainfall sampler used in this study. 56
Figure 5.6: Sampling procedure for ^{14}C and $\delta^{13}C$ using the drum method. 58
Figure 5.7: Location where the recharge methods were applied. 60
Figure 5.8: Location of gauging stations that were used in stream segment water-budget and a schematic of a water balance model. 62
Figure 5.9: Schematic of a reservoir water balance. 63
Figure 5.10: Examples of eliminated outlier points and boreholes with lack of response to rainfall. 64
Figure 5.11: Combo map of the model area and its location in RSA map as insert (Source of Geological data: Council for Geosciences, South Africa). 65
Figure 5.12: The constructed Hydrological Response Units (HRUs) in the UCRB with stream network, climate stations and a stream gauging station. 66
Figure 6.1: Lithology of the selected boreholes showing the positions of the water level, water strike and blow yield for each borehole (*mbgl is meters below ground level and masl is meters above sea level).* 71
Figure 6.2: Lithology of the selected boreholes in the karst aquifers of the Malmani Sub-group showing the positions of the water strike and water level fluctuation depth for each borehole. 73
Figure 6.3: Monthly groundwater levels versus rainfall. 74
Figure 6.4: Comparisons between groundwater level and the elevation of the nearby stream channel in meters above sea level. 76
Figure 6.5: Schematic of stream gain and stream loss at Montgomery Stream, which is underlain by the granites (NB: not drawn to scale). 77
Figure 6.6: Stable isotope plot of piezometers and stream water plotted against the Johannesburg Local Meteoric Water Line. 78
Figure 6.7: Time series of daily air temperature, amount of rainfall and stable isotopes in rainfall sampled at Montgomery Park rain sampling station during the period between November 2016 and November 2018. 80

Figure 6.8: $\delta^{18}O$ variation with daily air temperature (a) and average monthly air temperature (b) for two years. 81
Figure 6.9: Stable isotopes ($\delta^{18}O$, $\delta^{2}H$) plotted against precipitation to assess traces of amount effect in Johannesburg daily rainfall. The water types that show extreme deviation from linearity are encycled. 82
Figure 6.10: Stable isotopes of groundwater and surface water versus Johannesburg Local Meteoric Water Line (JLMWL), Pretoria Local Meteoric Water Line (PLMWL) and Global Meteoric Water Line (GMWL) (Craig, 1961). 84
Figure 6.11: Zoomed in view of the boreholes plotted against the JLMWL (solid line $\delta^{2}H=6.7\delta^{18}O+10‰$) with borehole evaporation line shown as a dotted line. 85
Figure 6.12: Plot of d-excess versus $\delta^{18}O$ for groundwater samples in the UCRB. 86
Figure 6.14: Schematic representation of Hartbeespoort Dam with the Brits fault lines (a) and north dipping quartzite bedding planes (b). 89
Figure 6.14: Plots of spring yield versus isotope signature at Albert Farm spring including the outlier points with (a) showing a correlation of 51% between yield and $\delta^{18}O$ and (b) showing no correlation between yield and $\delta^{2}H$. 90
Figure 6.15: Plots of spring yield versus stable isotopes excluding outlier points with (a) showing a correlation of 91% between yield and $\delta^{18}O$ and (b) showing 47% between yield and $\delta^{2}H$ 91
Figure 6.16: $\delta^{18}O$ versus ^{14}C (a) and calculated annual recharge temperatures (b) obtained from the Dansgaard (1964). 96
Figure 6.17: Stiff diagrams presenting the hydrochemistry of the dolomitic springs 99
Figure 6.18: EC, pH and ORP variation along the flow path. 99
Figure 6.19: ORP and pH variation along the flow path. 100
Figure 6.20: Temporal distribution of Si and pH in the Nouklip spring between 1980 and 2006 (Courtesy of Prof. Tamiru Abiye). 101
Figure 6.21: Mean monthly water balance components. 102
Figure 6.22: Time series of the annual components of the water balance. 103
Figure 6.23: Spatial distribution of mean annual values of PET, precipitation and the estimated potential recharge. 104
Figure 6.24: Components of a stream segment water budget underlain by the basement granites. 107
Figure 6.25: Components of Malmani dolomite stream segment water-budget. 107
Figure 6.26: Components of a stream segment water-budget model in the Pretoria Group. 108
Figure 6.27: Monthly net groundwater and surface water exchange ($Qseep$) for the 15-year review period. 109
Figure 6.28: Schematic of the reservoir water budget components for Hartbeespoort Dam. 110
Figure 6.29: Groundwater level fluctuations for the selected boreholes within the sub-catchment A21A, A21D and A21F indicating that there are different groundwater recharge mechanisms. 112
Figure 6.30: Correlation between simulated and measured annual flows for the station A2H012. 113
Figure 6.31: Daily measured and simulated time series discharge data of the A2H012 for model calibration period. 113
Figure 6.32: Correlation between simulated and measured daily stream discharge for the validation period 2007 to 2017. 114
Figure 6.33: Daily measured and simulated time series discharge data of the A2H012 for model validation. 114
Figure 6.34: Time series plot of baseflow simulated from a PRMS model and externally in a web-based tool called WHAT for the calibration period. 115

Figure 6.35: Scenario simulated for monthly average baseflow (a) and stream flow (b) with varying rainfall. 117
Figure 6.36: Scenario simulated for monthly average baseflow (a) and stream flow (b) with varying temperature..... 117
Figure 6.37: A Combined scenario simulated for monthly average baseflow (a) and stream flow (b) with increased temperature and reduced rainfall. 118
Figure 6.38: Graphical abstract for groundwater recharge in the UCRB. 119

LIST OF TABLES

Table 2.1: Wastewater discharge volumes in the UCRB (Department of Water Affairs and Forestry, 2008b). 9
Table 5.1: Stations used for reservoir water budget calculations. 63
Table 5.2: Input and output units in PRMS and the final unit conversions in this work. 67
Table 5.3: Names of modules used to build a PRMS model in this study. 67
Table 5.4: Scenarios used for PRMS simulations 69
Table 6.1: Locations of boreholes and elevation information. 70
Table 6.2: Locations of boreholes and elevation information. 72
Table 6.3: Location and elevation information for the stream channel points and boreholes water levels. 75
Table 6.4: Stable isotope and water level data for the piezometers and the stream. 77
Table 6.5: The environmental isotope results for the Albert Farm spring sampled monthly from June 2016 to June 2018 82
Table 6.6: Environmental isotope data for groundwater and surface water. 83
Table 6.7: Tritium in rainfall (*abstracted from Abiye *et al.* (2015)). 88
Table 6.8: Estimated groundwater flow period and flow velocity. 88
Table 6.9: The stable isotope and spring discharge data from the Albert Farm spring. 90
Table 6.10: The estimated mean annual and daily air temperatures at the time of recharge. 92
Table 6.11: Isotope data for selected groundwater samples with radiocarbon data. 94
Table 6.12: Hydrochemical data for the Malmani Dolomite springs. 98
Table 6.13: Mean monthly components of the water balance. 102
Table 6.14: The annual components of the water balance. 103
Table 6.15: Recharge estimations obtained through Baseflow Separation method. 105
Table 6.16: Components of the July stream segment water-budget obtained through Equation 11. 106
Table 6.17: Specific yield values used in this study and the relevant geological material. 110
Table 6.18: The recharge result for the water table fluctuation method. 111
Table 6.19: Annual baseflow and recharge for the period of study from PRMS and WHAT. 115
Table 6.20: Climate simulation results with impacts on baseflow and stream flow. 116
Table 6.21: Shows the number of days on which stream flow is less than $5m^3/s$ out of 7821 days of modelling period. 118
Table 6.22: Groundwater use as a percentage of recharge volume in the UCRB. 120

LIST OF SYMBOLS

‰	Permil
δ	Delta
$\delta^{18}O$	Oxygen-18 (‰)
$\delta^{2}H$	Deuterium (‰)
$\delta^{13}C$	Carbon-13 (‰)
^{14}C	Carbon 14 (pMC)
ENs	Nash-Sutcliffe model-efficiency coefficient
R^2	Coefficient of determination
$t_{1/2}$	Half life

NOMENCLATURE

AMD	Acid Mine Drainage
BFI	Baseflow Index
BFS	Baseflow Separation method
CMB	Chloride Mass Balance
DEM	Digital Elevation Model
DWS	Department of Water and Sanitation
GMWL	Global Meteoric Water Line
GNIP	Global Network of Isotopes in Precipitation
GRECHLIM	Understanding Groundwater Recharge in the Limpopo River Basin
GUI	Graphical User Interface
HRU	Hydrological Response Unit
IAEA	International Atomic Energy Agency
LMWL	Local Meteoric Water Line
LRB	Limpopo River Basin
MAE	Mean Annual Evapotranspiration
MAP	Mean Annual Precipitation
masl	Meters above sea level
mbgl	Meters below ground level
MRT	Mean Residence Time
NGA	National Groundwater Archive
PLMWL	Pretoria Local Meteoric Water Line
pMC	Percent modern carbon
PRMS	Precipitation Runoff Modelling System
SADC	Southern African Development Community
SAWS	South African Weather Services
TMWBM	Thornthwaite Water Balance Model
UCRB	Upper Crocodile River Basin
USGS	United States Geological Survey
VSMOW	Vienna Standard Mean Ocean Water
WHO	World Health Organization
WTF	Water Table Fluctuation
ZFP	Zero-flux plane

1 INTRODUCTION

1.1 Background of the study

Water has a significant contribution in the socio-economic development of any community. Moreover, in regions dominated by semi-arid/arid climate, groundwater in particular plays a central role because local surface water bodies in such climates are usually ephemeral (Scanlon *et al.*, 2006; Healy, 2010; Rivard *et al.*, 2014; Abiye, 2016). According to the World Health Organisation (WHO, 2017), in 2015, an estimated global population of 2.1 billion did not have access to clean drinking water at home, while a third of the Southern African Development Community (SADC) population lives in drought-prone areas (Braune and Xu, 2008).

South Africa in particular, partly situated in arid and semi-arid climate, relies extensively on groundwater resources particularly in rural communities (Department of Water Affairs, 2010). Wates *et al.* (2000) stated that groundwater constitutes 65% of water supply in rural communities of South Africa. This is because groundwater is usually suitable for decentralised water provision, making it ideal for dispersed agricultural activities and small-scale water supply compared to the localised surface water resources. Apart from the use of groundwater for human consumption and economic growth, its continual discharge through springs and river beds is able to contribute to stream flow and, despite the melting of snow in cold regions (e.g. snowmelt from the Lesotho Highlands in the Orange-Senqu River Basin, South Africa), groundwater discharge is often the main reason why perennial streams are able to sustain flows in dry seasons. Therefore, the assessment of groundwater recharge is of paramount importance, not only for management of water resources, but also for the support of downstream aquatic life and riparian vegetation.

South Africa is currently experiencing a water crisis as a result of climate change and over consumption of water, which led to a drought season where the most recent peak characterised by low rainfall and high temperatures was experienced between mid-2015 and early 2016 (ASSAf, 2017). The low rainfall and high temperatures give rise to increased evapotranspiration resulting in reduced terrestrial moisture (Engelbrecht *et al.*, 2015; ASSAf, 2017), which poses a threat to the sustainability of water resources for the current and future generations. The Intergovernmental Panel on Climate Change (IPCC) has predicted that with increasing carbon dioxide emissions into the atmosphere, by the year 2100, the global temperatures will rise to a range between 1.4 and 5.8°C (IPCC, 2001), while rainfall varies with ±20%. ASSAf (2017) provided the state of climate change in South Africa and predicted that South Africa will continue to warm at a rate higher than 0.15°C per decade.

The water crisis in South Africa is also exacerbated by ongoing pollution of available water resources, particularly in urban centres as a result of industrial activities besides agricultural and mining wastes. Predominant in Johannesburg is the acid mine drainage (AMD) problem from the abandoned West Rand mines and urban return flows from the wastewater treatment plants (Department of Water Affairs and Forestry, 2008b; Abiye *et al.*, 2015), which affect the quality of surface water and shallow groundwater (Abiye, 2011). Apart from the polluted groundwater resources, the total volume of available renewable groundwater in South Africa is 10 343 Mm^3/yr and 7 500 Mm^3/yr under drought conditions (Department of Water Affairs, 2010).

For groundwater to remain available as a source of water, there has to be a significant recharge, which exceeds or equals abstraction amount (Maliva and Missimer, 2012). Therefore, recharge must be quantified to attain sustainable groundwater management. The National Water Act (1998) of South

Africa also recognises the need to undertake continuous water resources assessment in order to establish an ecological reserve and ensure sustainable development for the benefit of future generations. It also advocates for an integrated management of both groundwater and surface water to provide for adequate protection of the water resource. Furthermore, the Act also recognises water as a fundamental resource in the alleviation of poverty through food production and advancement of economic growth.

Having highlighted the critical importance of groundwater resources in South Africa, groundwater recharge assessment is, without doubt, a fundamental need to attain sustainable groundwater development (de Vries and Simmers, 2002; Sun *et al.*, 2013). Recharge assessment is, however, complex in the semi-arid climate because of the complexity of how it occurs through the surface water bodies and preferentially through the fractured rocks (Scanlon *et al.*, 2006) and geological features such as lineaments and faults (Tessema *et al.*, 2012). Over and above these factors, recharge processes are also challenging because of high evapotranspiration that accounts for a big component of terrestrial moisture balance. Low rainfall that infiltrates the soil usually undergoes evapotranspiration back to the atmosphere even before reaching the water table (Allison and Hughes, 1983; de Vries *et al.*, 2000; Healy, 2010). However, in an assessment of rainfall intensity and recharge, Van Wyk (2010) indicated that significant recharge can still occur from high intensity rainfall in regions with high evapotranspiration through what is called episodic recharge. In addition to that, Abiye (2016) emphasised that effective recharge in South Africa usually occurs after extraordinarily high rainfall as observed by visible groundwater pulses following high rainfall.

Over and above the assessment of groundwater recharge, the controls and monitoring on groundwater exploitation form an integral part of sustainable groundwater management. In a fractured aquifer that is not readily recharged, long-term over-pumping can cause a permanent negative impact on the maximum yield of the borehole after termination of the pumping. Woodford and Chevallier (2002) stated that over-pumping of groundwater can greatly deform the fracture aperture size due to the weight of the overburden that is exerted in a dewatered fracture. As a result, the yield of such an aquifer shall decline. Overexploitation of groundwater also affects other hydrological processes within the water cycle, leading to the drying up of surface water bodies that rely on groundwater through springs, seepages and gaining streams, lakes and reservoirs.

Based on the complexity of the climate and hydrological setting, the diversity of recharge processes and management challenges associated with groundwater overexploitation, and above all, the economic significance of the Upper Crocodile River Basin (UCRB), the University of the Witwatersrand undertook a groundwater recharge assessment project in the UCRB. This is part of a project referred to as "Understanding Groundwater Recharge in the Limpopo River Basin (GRECHLIM)" funded by the United States Agency for International Development (USAID) and the National Academies of Sciences, Engineering, and Medicine (NAS) through Partnership for Enhanced Engagement in Research (PEER), under cooperative agreement number AID-OAA-A-11-00012 Sub-Grant Number: 2000006304 and the Department of Science and Technology, South Africa (UID: 101594).

It was from this project that a PhD research project entitled "*Holistic approach to groundwater recharge assessment in the Upper Crocodile River Basin, Johannesburg, South Africa*" was initiated. In the context of this PhD thesis, the definitions of terms apply as follows: "*holistic approach"* refers to an integrated methodology that engages various tools to give an assessment from different. perspectives "*Groundwater recharge"* as defined by Healy (2010) is the downward flow of water reaching the water table, adding to groundwater storage. "*Assessment"* refers to both qualitative and

quantitative determination. In simpler terms, therefore, the study is about application of an integrated methodology to qualitatively and quantitatively determine the component of water that flows into groundwater storage within the UCRB. The term "holistic" in this study also includes the assessment of different hydrological cycle components (rainfall, surface water, groundwater, interflow, baseflow etc.) that have significance to recharge within the UCRB.

1.2 Research aims and specific objectives

The aim of this study is to employ a holistic approach that integrates different techniques to assess groundwater recharge in the UCRB. The specific objectives of the study are:

- To characterise the stable isotope signature in local rainfall as a source of recharge by assessing the seasonality, predominant stable isotope effects, and determining the Local Meteoric Water Line in order to understand the isotopic input signal in terrestrial water bodies.
- To estimate groundwater recharge and determine the recharge mechanisms across the UCRB using environmental isotopes and physical recharge assessment methods.
- To assess the role of interflow using shallow piezometers in the alluvial channel aquifer underlain by massive basement granites.
- To assess groundwater fate and flow mechanisms using radioactive and stable isotopes.
- To test the applicability of using stable isotope effects in rainfall for characterising groundwater recharge conditions using spring data and for determining the influence of rainfall amount on recharge amount.
- To apply Precipitation Runoff Modelling System for the UCRB and assess the sensitivity of the streamflow components on changes in climate variables.

1.3 Significance of the study and identification of potential beneficiaries to the research outcomes

- The outcome of this study will form background and literature for further groundwater related research, which will benefit groundwater researchers and users such as the farmers who are the backbone of commercial food production in South Africa.
- The Johannesburg Local Meteoric Water Line shall be available for use by the water researchers interested in isotope hydrology.
- An approach that integrates recharge assessment tools will be better understood and, therefore, duplicated by groundwater researchers in other basins of similar complex nature.
- The water management authorities will benefit in that the findings will assist in giving guidance to setting the upper limits to groundwater abstraction.
- Recharge estimates and processes can also be used as input data for numerical models and for the estimation of sustainable groundwater yields.

2 DESCRIPTION OF STUDY AREA

2.1 Location of study area

The UCRB is located in South Africa, partly in Gauteng Province and partly in Northwest Province, as shown by the insert map on Figure 2.1. It occupies the geographical location at the range of 27.357° to 28.467° longitude and -25.27° to -26.199° latitude. The UCRB, with a surface area of 6336 km^2 (Department of Water Affairs and Forestry, 2008b) is situated north of the city of Johannesburg with its southern water divide within the compound of the University of the Witwatersrand. It extends to the north with the general slope to Hartbeespoort and Roodekopjes Dams, which are located north of Johannesburg. The UCRB is also referred to as "A21 Primary catchment" in the Water Management Area classification of the Department of Water and Sanitation. A21 and UCRB are, therefore, used interchangeably in this thesis.

Figure 2.1 shows the eleven (11) A21 sub-catchments, also referred to as "quaternary catchments"; A21A, A21B, A21C, A21D, A21E, A21F, A21G, A21H, A21J, A21K and A21L with locations of major dams and cities.

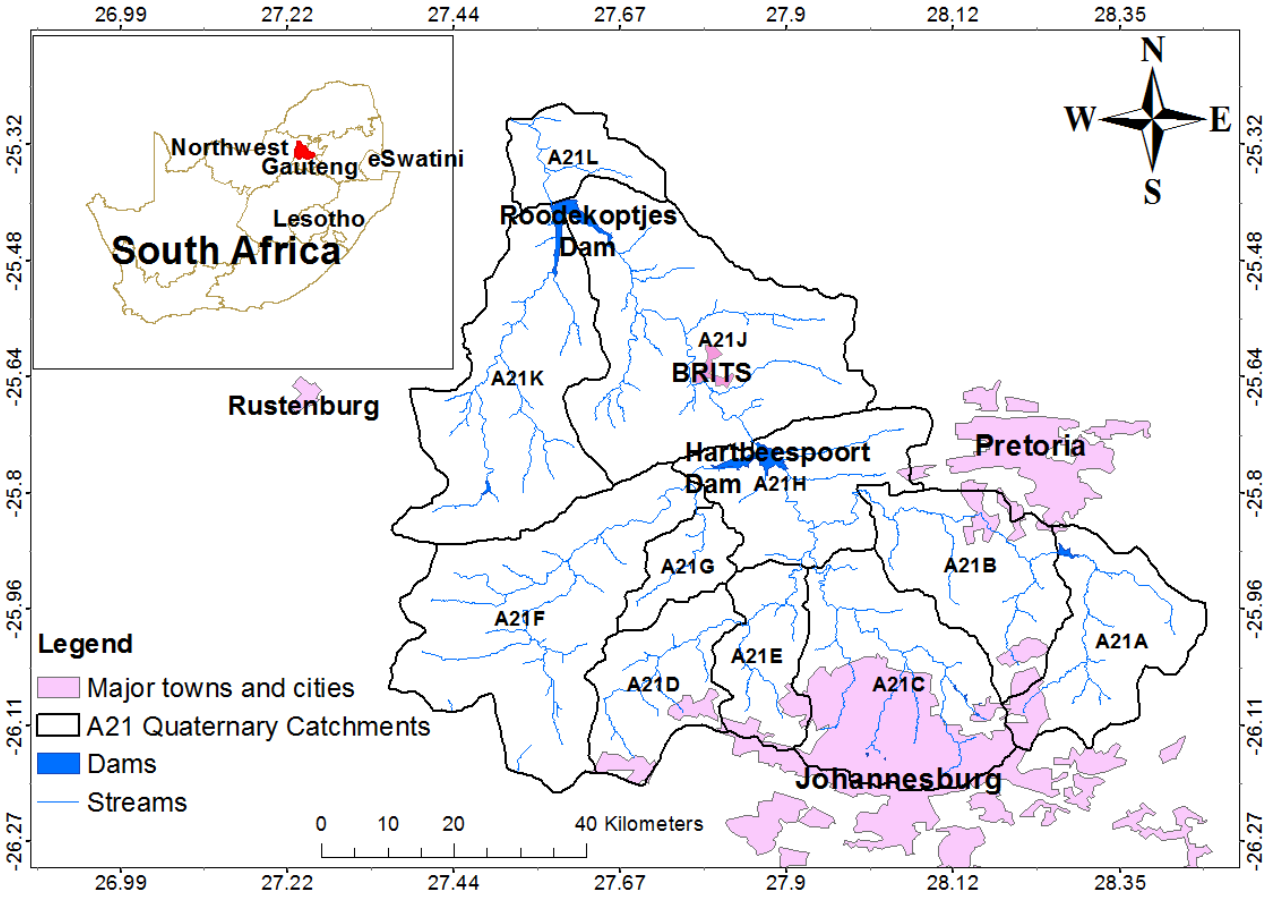

Figure 2.1: Locality map of the UCRB and its location on South Africa map as insert.

2.2 Climatic setting

The UCRB is classified as a subtropical highland climate (Cwb in the Köppen climate classification system), which predominantly receives summer precipitation in the form of rainfall with the Mean Annual Precipitation (MAP) of about 700 mm/year (Abiye, 2011), where the southern portion receives more precipitation than the northern portion. The UCRB predominantly receives convective rainfall with prevalence of cumulonimbus induced thundershowers, especially in the afternoons, and

occasional hail storms in summer (October to April) (Barnard, 2000; Department of Water Affairs and Forestry, 2004). It has a Mean Annual Evaporation (MAE) of 1700 mm/year (Barnard, 2000; Department of Water Affairs and Forestry, 2008b).

The UCRB experiences cold dry winters, which generally occur between May and July, while hot temperatures are experienced between October and March in summer. Daily temperature in winter usually ranges from a minimum of 1°C to a maximum of 20°C and ranges from 10°C to 30°C in the hot summers (Department of Water Affairs and Forestry, 2004). Figure 2.2 shows rainfall, maximum temperatures (T max), minimum temperatures (T min) and pan-evaporation for the climate stations that are based in the UCRB. Data was accrued from daily climate elements and averages were calculated for each month over the 20 year period from 1996 to 2017. The source of data is the South African Weather Services, South Africa.

The southern boundary of the catchment is elevated (see section 2.7) and generally has lower temperatures, which increase with decrease in elevation as shown on Figure 2.3 for the selected stations. When discussing the climate of the map-sheet 2526, which encompasses the UCRB, Barnard (2000) indicated that the MAE increases from approximately 1400 mm/yr in the southeast to about 2000 mm/year in the northwest. Evapotranspiration would, therefore, be expected to be higher in the northern part of the UCRB, thereby indicating possibilities of less recharge compared to the southern cooler areas.

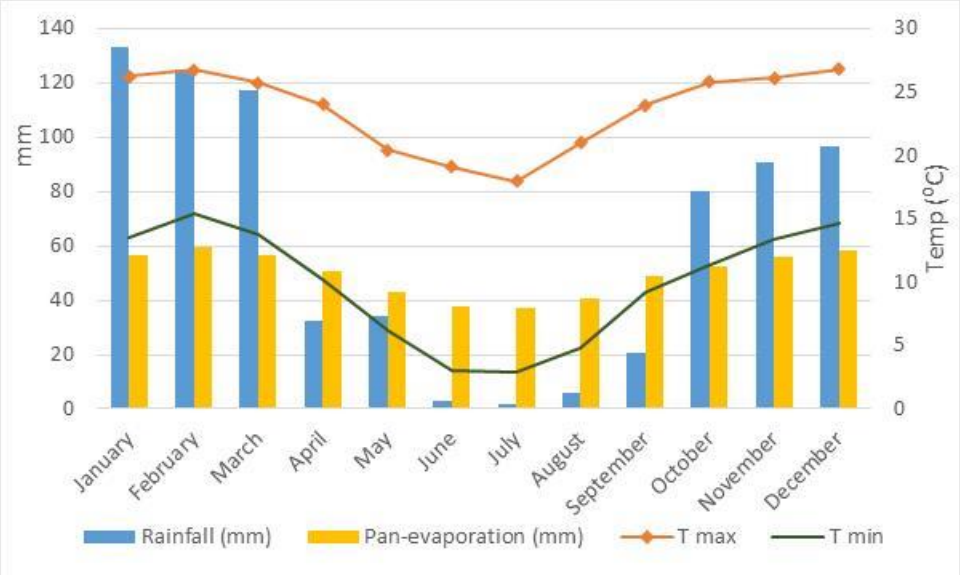

Figure 2.2: Climate for the 20 year period (1996 to 2017) using data from four UCRB climate stations from South African Weather Services.

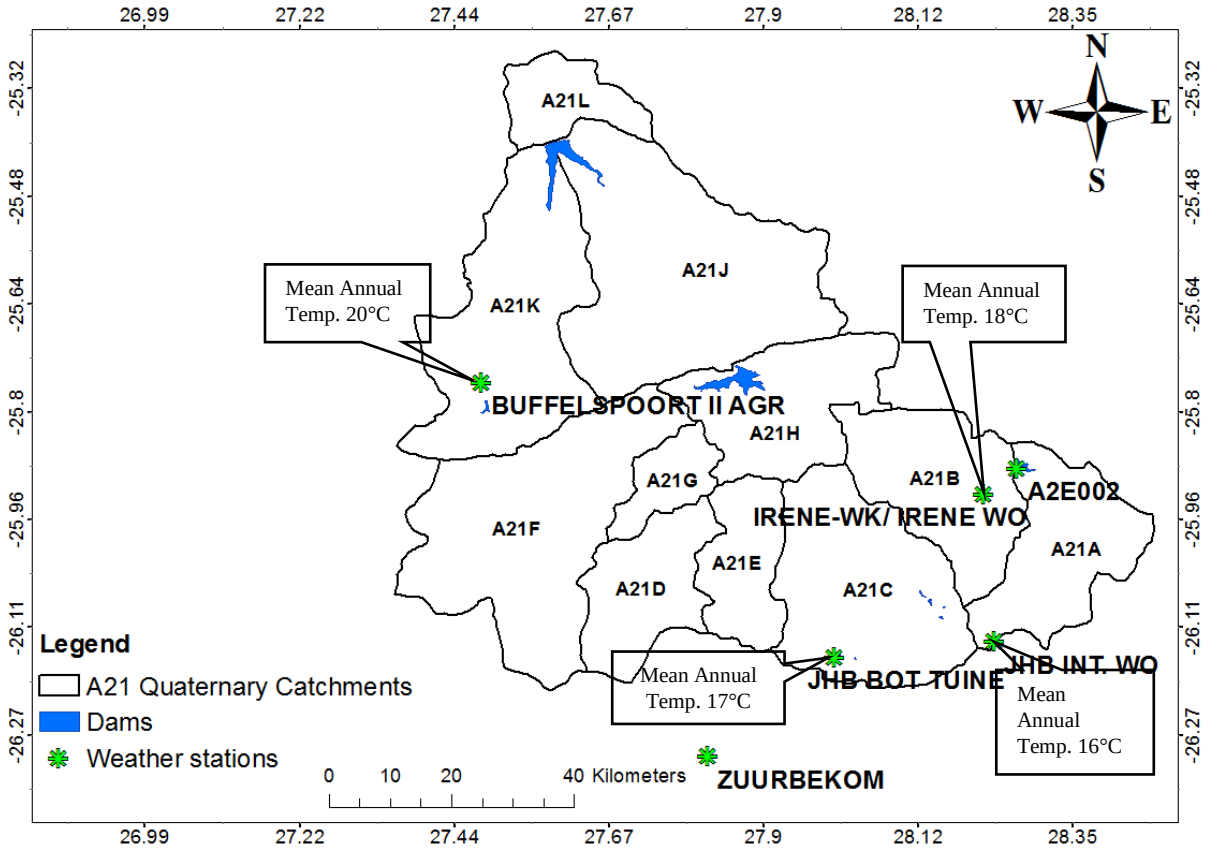

Figure 2.3: Locations of weather stations showing mean annual temperatures for the period 1997 to 2016 (A2E002 is for pan-evaporation).

Figure 2.4, Figure 2.5 and Figure 2.6 show the annual trends of precipitation, temperature and pan-evaporation, respectively, from 1997 to 2016 for the selected stations in the UCRB. Though these annual values have been fluctuating over the review period, the slopes of the trend lines indicate that precipitation has generally been decreasing in the range between 1.7 and 5 mm/yr, average temperatures have been increasing in the range between 0.069 and 0.115 °C/yr, while pan-evaporation has been increasing by 2.2 mm/yr. Collectively, these trends reveal that terrestrial moisture has been decreasing over the years. The locations of the stations are shown in Figure 2.3.

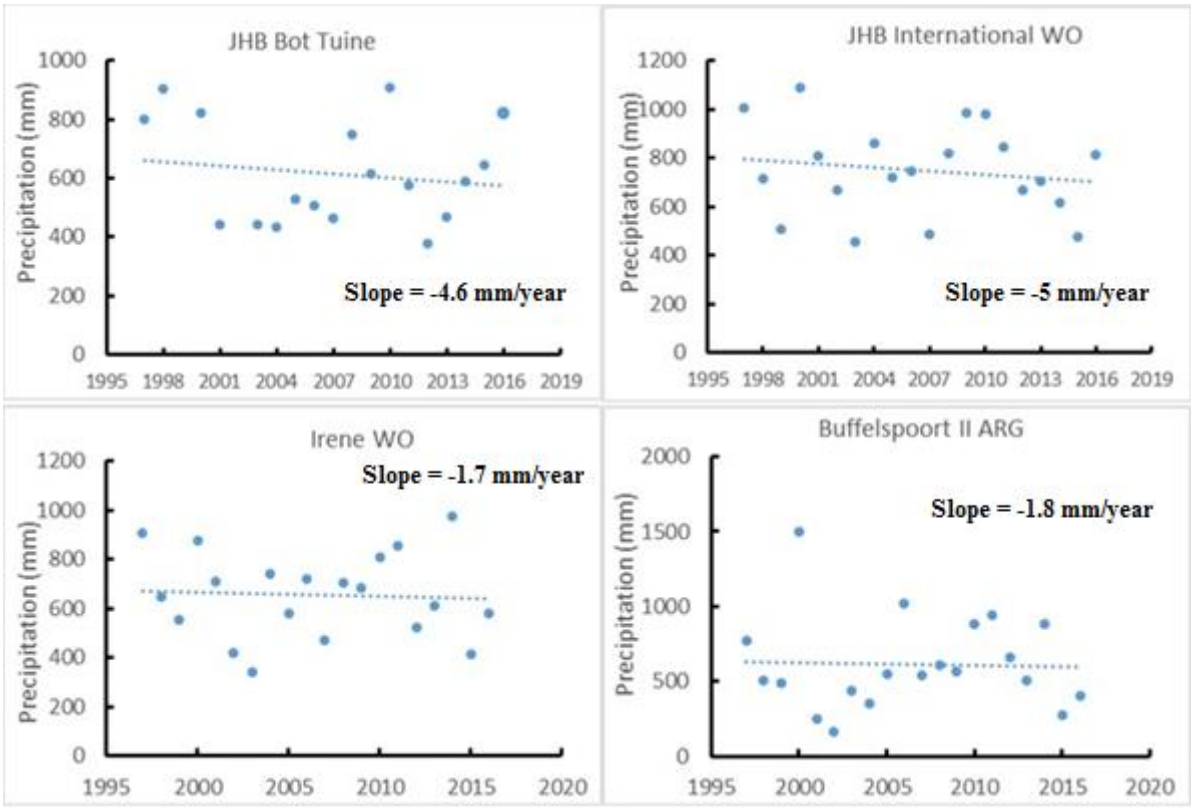

Figure 2.4: Annual precipitation for the period between 1997 and 2016 from different weather stations.

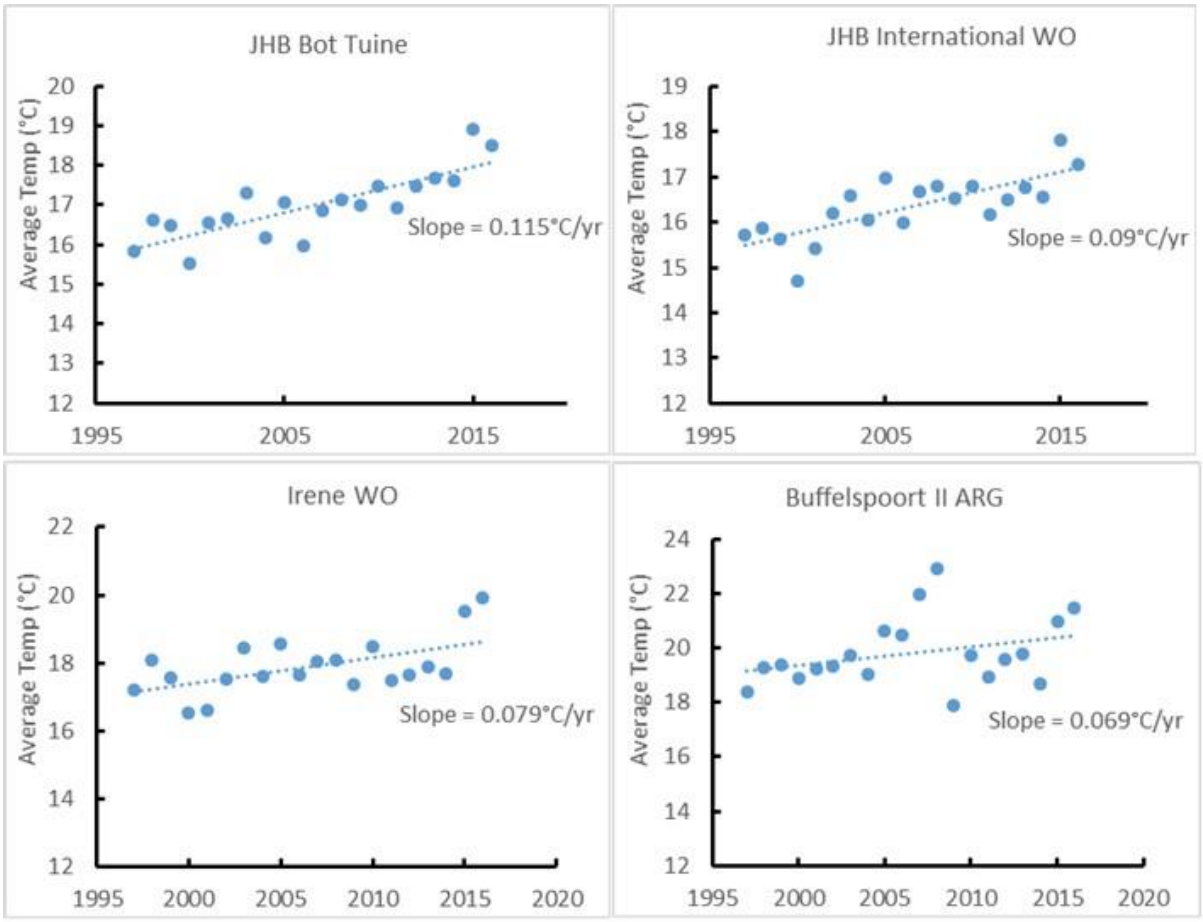

Figure 2.5: Annual average temperature trends for the period between 1997 and 2016.

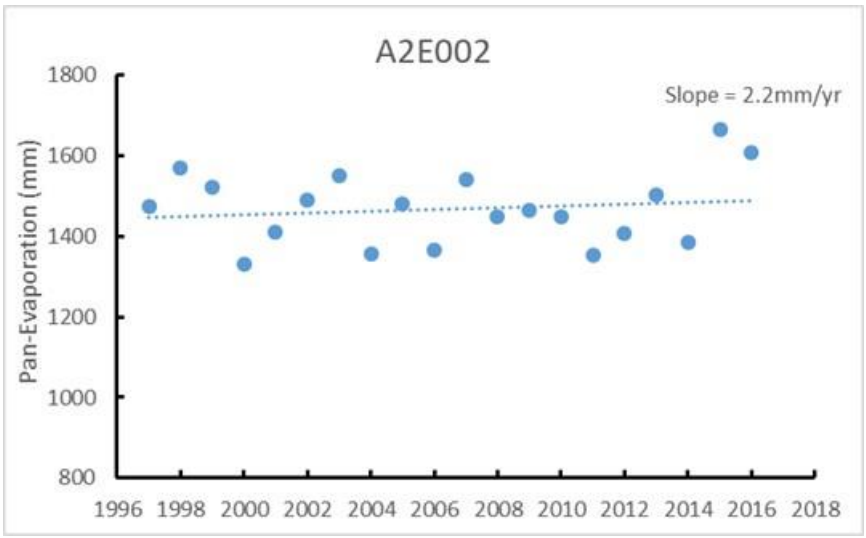

Figure 2.6: Annual pan-evaporation for the period between 1997 and 2016 for the station A2E002 (from an S-class pan).

2.3 Land and water use

Land and water use are very dynamic across the UCRB. The city of Johannesburg, situated in the southern and upstream part of the catchment is the industrial hub of South Africa, which due to its high water stress is augmented with more than 500 million m^3/yr, through a water transfer scheme from the Vaal Catchment (Department of Water Affairs and Forestry, 2008a). Surface water from the

Vaal Catchment is mostly used with minor groundwater abstractions in the southern end of the catchment where urban activities such as settlements and industries dominate. Groundwater on the other hand, is extensively utilised in the north and central parts for the catchment, while the use of surface water from the UCRB reservoirs is mostly centralised around the main reservoirs and along the valleys of the Crocodile River for agricultural activities. The annual water requirement in the UCRB is about 556 Mm^3 consisting of 292 Mm^3 in urban area, 208 Mm^3 for irrigation, 5 Mm^3 for rural areas, 38 Mm^3 for mining and 13 Mm^3 for power generation. It is projected that by the year 2025, the urban water requirement will have increased from 292 Mm^3 to 409 Mm^3 in the UCRB (Department of Water Affairs and Forestry, 2008b).

The water transfer from the Vaal Catchment has, however, increased the amount of wastewater that is disposed from the treatment works into the streams that drain Johannesburg and Pretoria (Dower, 2003; Department of Water Affairs and Forestry, 2008b). Poor surface water quality has, as a result, been a major concern for several decades, particularly in the Hartbeespoort Dam (Allanson and Gieskes, 1961; Zohary *et al.*, 1988), which is a receiver of wastewater from Johannesburg and Pretoria (Department of Water Affairs and Forestry, 2008a). Table 2.1 presents the water treatment works and their capacities, which sum up to approximately 400 000 m^3/day (5 m^3/s). The projected increase in urban water demand from 292 Mm^3 to 409 Mm^3 in the year 2025 shall lead to more wastewater disposal resulting in more polluted and unusable surface water in the UCRB.

Table 2.1: Wastewater discharge volumes in the UCRB (Department of Water Affairs and Forestry, 2008b).

Wastewater discharge station	**Wastewater volume (m^3/day)**
Hartbeesfontein	35000
Olifantsfontein	38000
Sunderland Ridge	35000
Esther Park	400
Johannesburg Northern works	220000
AECI	7000
Modderfontein	16000
Midrand South	5000
Percy Stewart	25000
Driefontein	15000

Agricultural activities are intense in the Crocodile River valley in A21J A21L and downstream of Hartbeespoort Dam. Some farms rely on surface water abstractions from the Crocodile River, Hartbeespoort Dam, and their distribution canals, while others depend entirely on groundwater abstractions. Generally, all A21 quaternary catchments have agricultural activities at various intensity levels. The majority of the land-cover in the UCRB is, however, uncultivated and consists of trees and highveld grasses and shrub vegetation. A21A, A21C, A21E and A21F have sparsely distributed agricultural activities, while A21G and A21K are mostly uncultivated grasslands. There is also animal husbandry in the UCRB for production of cow milk and meat, however, this type of agriculture is minimal in the catchment. Land use in A21K consists of mining of norite and the platinum-group metals (Cawthorn *et al.*, 2006), which utilise groundwater during processing and dewatering.

In the West Rand Gold Fields situated in A21D, there are abandoned gold mines where there is continual AMD into surface water. The West Rand is the major source of AMD into the UCRB, discharging between 24 and 29 Mm^3/yr, thereby deteriorating the quality of both surface water and shallow groundwater in the dolomitic aquifers (Abiye *et al.*, 2015). According to Abiye (2011), mine water has influenced the quality of shallow groundwater to about 1200 mg/L of iron and 5000 mg/L of sulphate. This adverse water quality has caused a broad spatial distribution of sulphate, which is a result of advection of mine water through the rock fractures (Abiye, 2014).

The southern tip of the catchment (A21A, A21B, A21C and A21E), which constitutes northern Johannesburg, Midrand, and southern Tshwane is in the highly developed area with industrial, urban and semi-urban sprawls (Department of Water Affairs and Forestry, 2008b). The study area also encompasses the Cradle of Human Kind World Heritage Site in the Malapa area where the high yielding dolomitic springs such as the Nash Farm and Nouklip springs are located. The region that covers the central part of the UCRB is dominated by grasslands, trees and shrub vegetation.

2.4 Geological Setting

The foundation of the geology of South Africa is represented by the Kaapvaal Craton, which is an ancient segment of the thick crystalline continental crust that formed in Southern Africa between 3.7 and 2.7 Ga (Robb and Meyer, 1995). The original Kaapvaal Craton has been shaped over time due to tectonic processes, which led to the present continental crust. Within the UCRB, the Kaapvaal Craton contains the basement Archaean granites upon which the sequence of sedimentary rocks were deposited (Armstrong *et al.*, 1991) and metamorphosed over time. The sedimentary cover has been stripped by the progressive upward movement of the basement Archaean granites through geological history (Anhaeusser, 1971).

The rocks of the UCRB are represented by the following Supergroups and Complexes overlying the basement in the following chronological order: the Witwatersrand Supergroup, the Ventersdorp Supergroup, the Transvaal Supergroup, the Bushveld Igneous Complex and the Karoo Supergroup, with a general younging direction towards the north relative to Johannesburg (Barnard, 2000; Johnson *et al.*, 2006).

In this study, no part of groundwater assessment was done within the Ventersdorp and Karoo Supergroups, and therefore, assessment of groundwater recharge in these lithologies is beyond the scope of this study. A brief description of the Ventersdorp and Karoo geology will be given but their aquifers will not be discussed.

Figure 2.7 shows a geological map of the UCRB relative to the quaternary catchments.

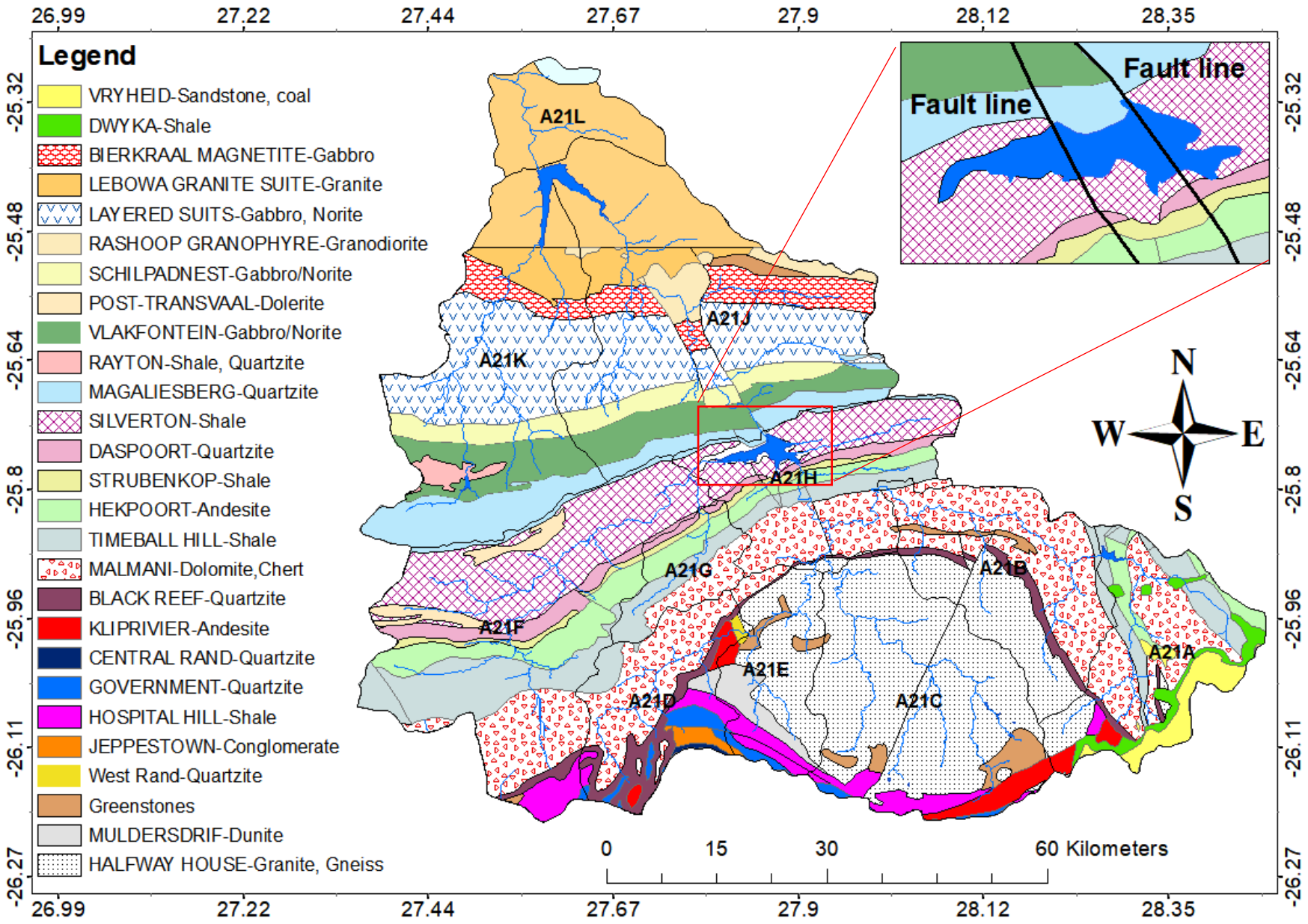

Figure 2.7: Geological map of the UCRB shown relative to the quaternary catchments (Source of Geological data: Council for Geosciences, South Africa).

2.4.1 The Basement Igneous Complex

The Basement Igneous Complex is the oldest rock exposure in the region with an approximate age of 3200 Ma, believed to have stabilised after the main period of plutonism that occurred 3.2-3.0 Ga ago (Anhaeusser, 1973). Its exposure in the central part of the Kaapvaal Craton (Brandl *et al.*, 2006) covers an approximate areal extent of 700 km^2 (Anhaeusser, 1971; Anhaeusser, 1992; Poujol and Anhaeusser, 2001). It is partially exposed in Johannesburg occupying the southern portion of the UCRB and in the Vredefort Dome (Armstrong *et al.*, 1991). It is represented predominantly by weathered and fractured Archaean granitic bodies of similar age that differ slightly in their composition (granitic, granodioritic, gneissose or migmatitic) (Barnard, 2000).

The Basement Igneous Complex outcrop in the UCRB is also referred to as Johannesburg Dome by Poujol and Anhaeusser (2001) due to its ovoid shape. Figure 2.8 shows a geological map of the basement rocks extracted from the geology of the UCRB.

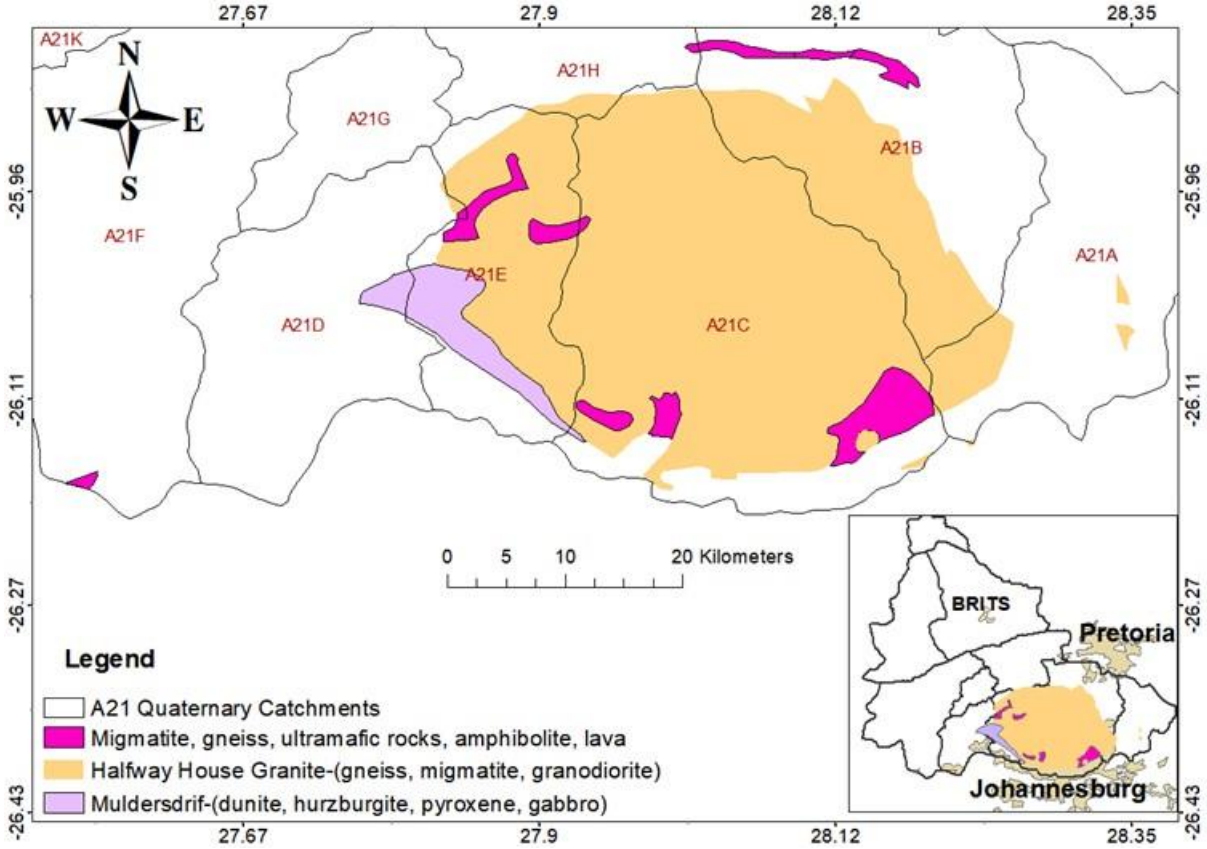

Figure 2.8: Locality map of the basement rocks (Source of Geological data: Council for Geosciences, South Africa).

2.4.2 The Witwatersrand Supergroup

The Witwatersrand Supergroup, which hosts the largest known gold deposit in the world (Armstrong *et al.*, 1991) unconformably overlies the basement rocks and forms a rimming structure predominantly exposed along the south to south western margins of the dome (Anhaeusser, 1971) as shown in Figure 2.7 and Figure 2.9. It was deposited over a period of 350 Ma (Armstrong *et al.*, 1991) (or 360 Ma by Robb and Meyer (1995)) through pulses of sedimentation that occurred in various periods resulting in stratigraphic divisions, which are West Rand Group (2970-2914 Ma) and the Central Rand Group (2894-2714 Ma) making up a total terrigenous thickness of approximately 7000 m (Robb and Meyer, 1995). The West Rand and the Central Rand Groups are sometimes referred to

as Witwatersrand sediments due to their rock content. In some parts, the Witwatersrand Supergroup overlies the basement granites while in some it overlies the Dominion Group, which is also referred to as the *volcano-sedimentary* by Robb and Meyer (1995) due to its lava and sediments content. However, within the UCRB, the Witwatersrand sediments directly overly the basement granites as illustrated by Barnard (2000).

The Witwatersrand Supergroup consists of a sequence of metamorphosed sedimentary rocks with alterations of shale, quartzites, grits and conglomerates (Pretorius, 1964) with siliceous ironstones, tillites and a band of intercalated lava found in the lower divisions of the Supergroup (Anhaeusser, 1971). Specifically, the stratigraphic divisions of the Witwatersrand Supergroup and their representative rocks are as thus: West Rand Group is represented by Orange Grove quartzites, reddish and ferruginous magnetic shales with a quartzite to shale ratio of 12:1; and Central Rand Group is represented by quartzites, shales and conglomerates with a quartzite to shale ratio of about 1 (Pretorius, 1976). Due to the historic upward movement of the Basement Igneous Complex, these rocks dip at varying angles and directions away from the Basement Igneous Complex (Anhaeusser, 1971). The dipping and fracturing in the quartzites is vividly observed in Johannesburg in the Northcliff Hills suburb.

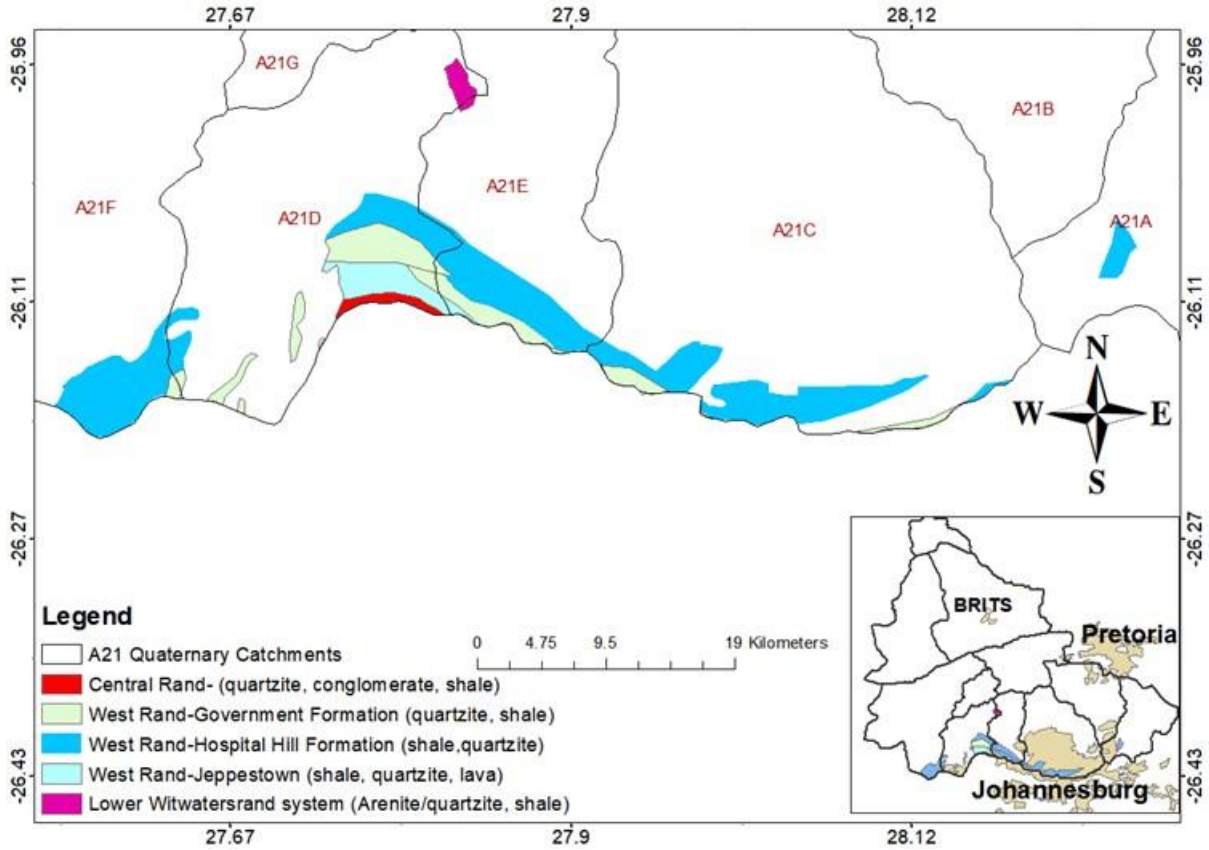

Figure 2.9: Locality map of the Witwatersrand Supergroup (Source of Geological data: Council for Geosciences, South Africa).

2.4.3 The Ventersdorp Supergroup

The Ventersdorp Supergroup, which was formed after 2714 Ma (Robb and Meyer, 1995) overlies the Witwatersrand Supergroup. Within the UCRB, rocks of the Ventersdorp Supergroup are exposed mainly on the south eastern part with patches also observed on the south-west of the Johannesburg

Dome as shown on Figure 2.7 and Figure 2.10. The rocks mainly consist of andesite and tuff from the Klipriviersburg Group (Barnard, 2000).

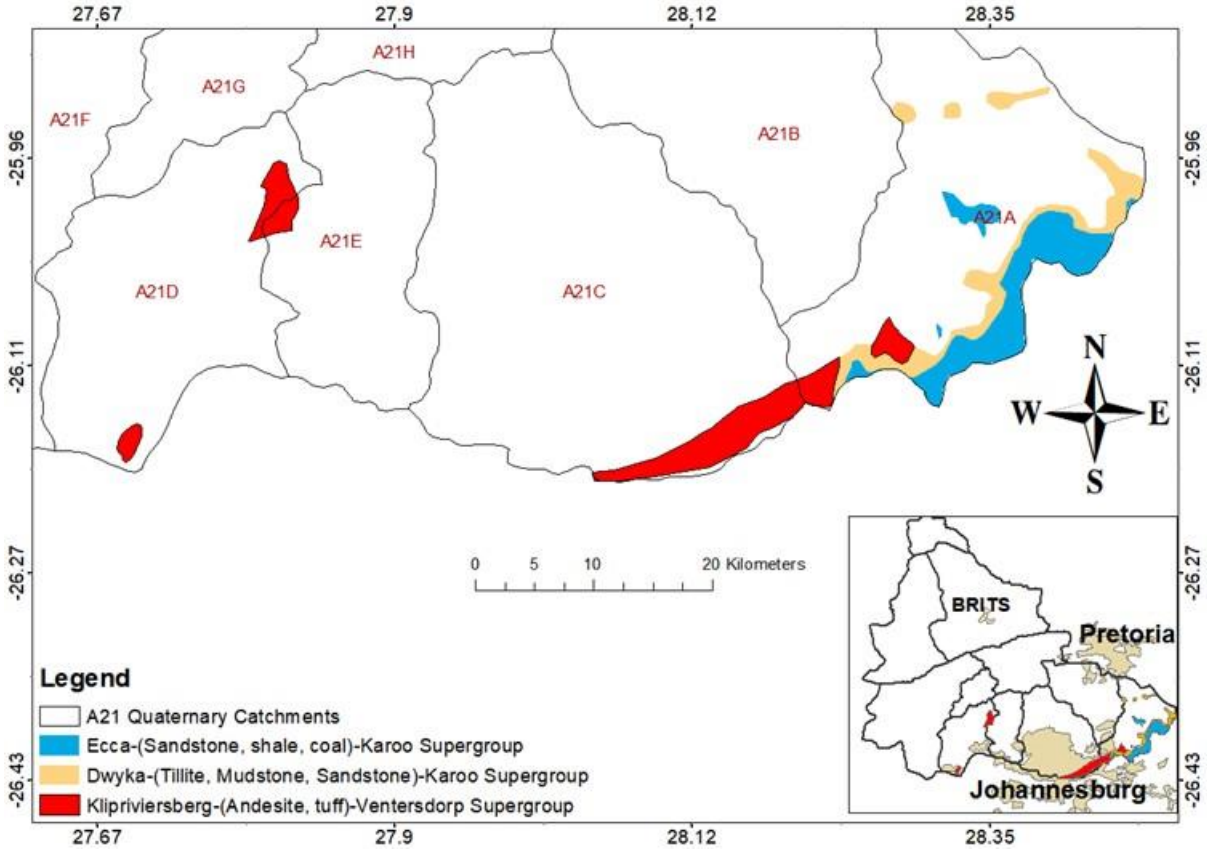

Figure 2.10: Locality map of the Ventersdorp and Karoo Supergroup rocks (Source of Geological data: Council for Geosciences, South Africa).

2.4.4 The Transvaal Supergroup

The rocks of the Transvaal Supergroup lie unconformably on the granites of the basement in the northern periphery, while in the east of the UCRB, they lie conformably on the Ventersdorp volcanic successions (Anhaeusser, 1971) as shown in Figure 2.7. The Transvaal Supergroup was formed between 2500 and 2100 Ma and has an approximate thickness of 15 000 m (Eriksson and Clendenin, 1990). It covers the middle portion of the UCRB and consists of the Chuniespoort Group and Pretoria Group. Within the UCRB, the Chuniespoort Group is represented by Black Reef Formation (quartzites) and Malmani Subgroup (dolomites). Its lowest formation, Black Reef forms a rimming structure along the northern periphery of the basement and consists of quartzites and conglomerates of significant lateral extent but that have a thickness of few meters (Eriksson *et al.*, 2006). The Malmani Subgroup is subdivided into five formations, which collectively make up a thickness of 2000 m and differ based on the chert content, stromatolite morphology, intercalated shales, and erosion surfaces (Eriksson *et al.*, 2006). The formations include, Oaktree Formation, Monte Cristo Formation, Lyttelton Formation, Eccles Formation and Frisco Formation (Eriksson *et al.*, 2006).

The Pretoria Group, which overlies the Chuniespoort Group, is represented by the following formations: Timeball Hill (shale, quartzite), Hekpoort (andesite), Strubenkop (shale), Daspoort (sandstone), Silverton (shale, lava), Magaliesberg (quartzite) and Rayton (sandstone, shale, volcanic rocks) (Barnard, 2000; Eriksson *et al.*, 2006). The shale of the Silverton Formation, being less resistant to erosion forms the valley floor that hosts the Hartbeespoort Dam, while the more resistant

quartzite of the Magaliesberg Formation forms the elongated ridge (Figure 2.11) from east to west constituting the Hartbeespoort Dam axis. Figure 2.11 shows the distribution of the Transvaal Supergroup rocks within the UCRB.

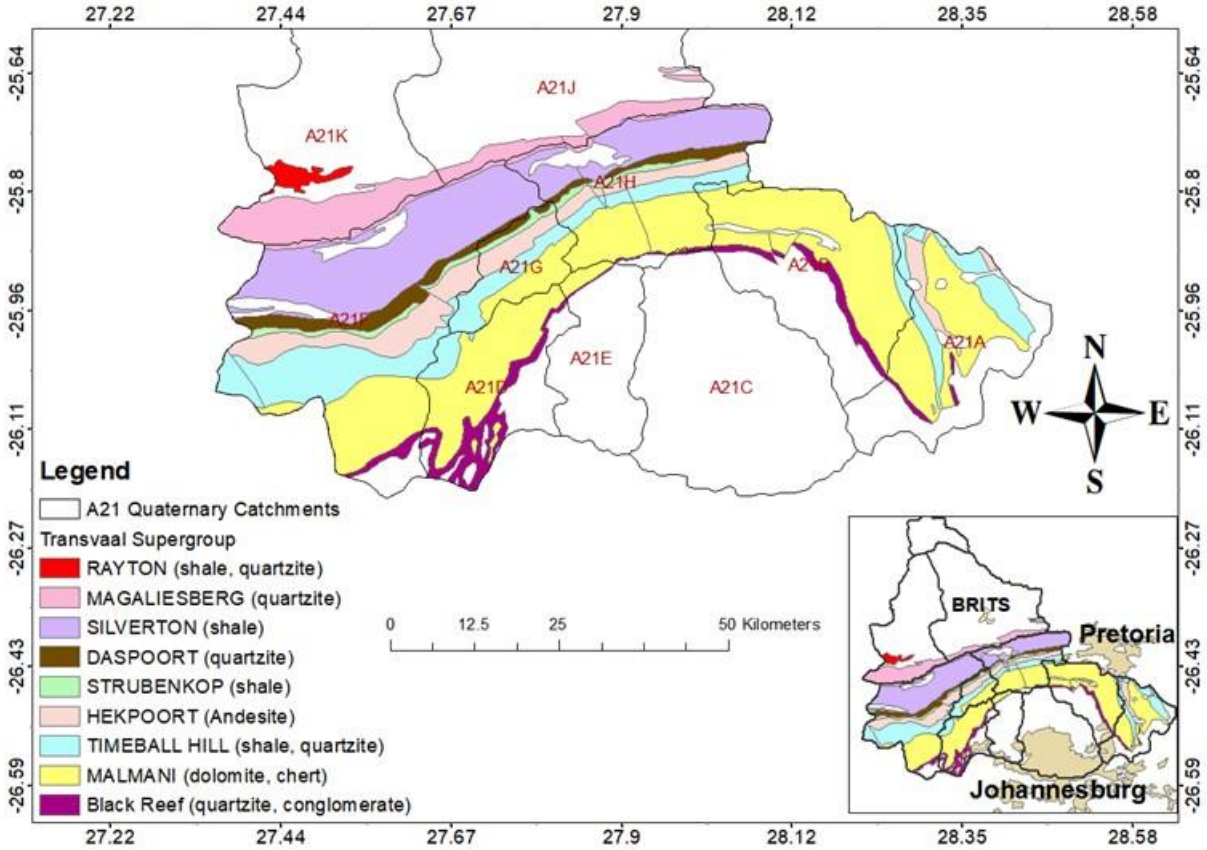

Figure 2.11: Locality map of the Transvaal Supergroup rocks within the UCRB (Source of Geological data: Council for Geosciences, South Africa).

The quartzite of the Magaliesberg ridge, has undergone structural deformation that tilted it to the north (Hall and du Toit, 1923). Figure 2.12 shows a cross section of the Magaliesberg ridge exposing the north dipping bedding planes in the quartzites with Hartbeespoort Dam reservoir to the south (which is the right side on the image). This area is also structurally modified by the two vertical semi-parallel northwest-southeast faults that cut across the Magaliesberg ridge and create a graben at the middle of the Hartbeespoort Dam. Figure 2.13 shows a bird's eye view schematic representation of the Hartbeespoort Dam with its two fault lines. This graben is characterised by a horizontal displacement of approximately 1280 m to the south, width of 5.6 km and a vertical displacement of 390 m (Hall and du Toit, 1923).



Figure 2.12: The north dipping bedding planes in the quartzites of the Magaliesberg Formation at the Hartbeespoort Dam wall.

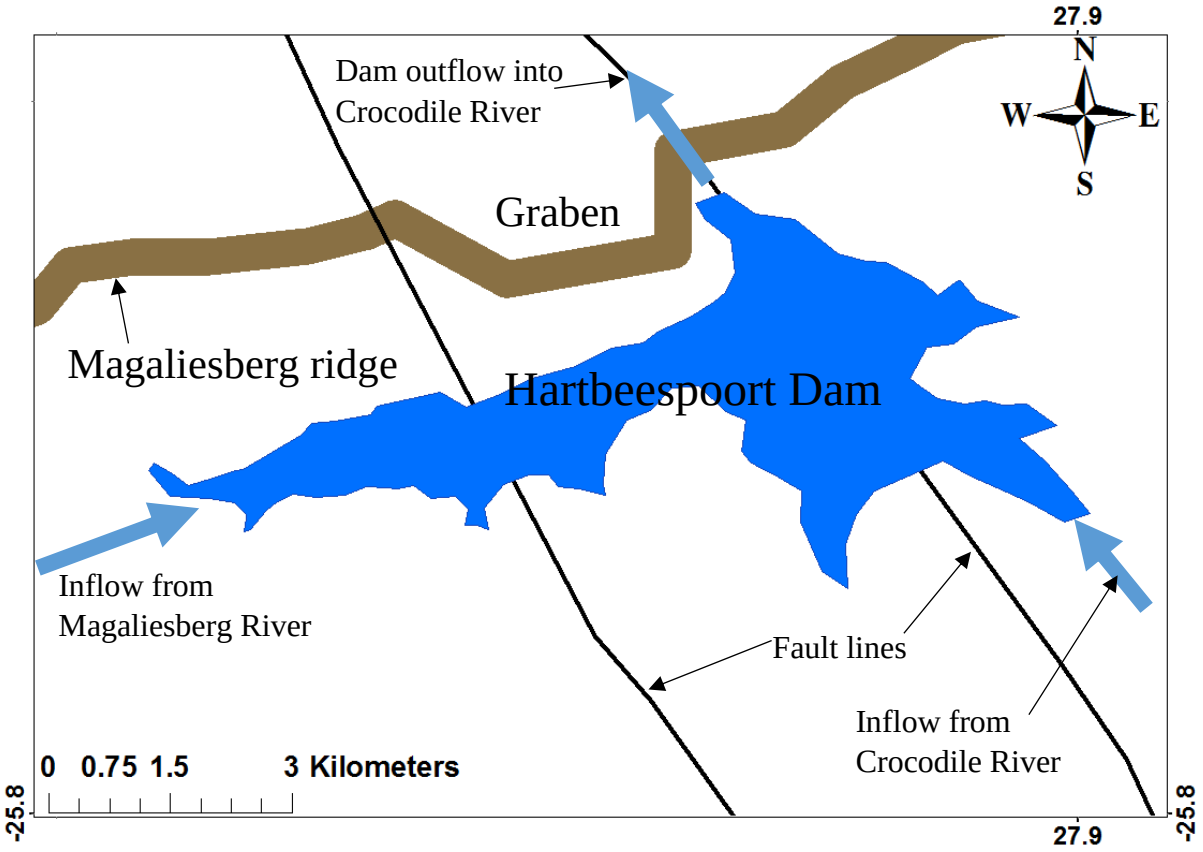

Figure 2.13: Schematic representation of the Hartbeespoort Dam with its main fault lines showing the position of the graben.

2.4.5 The Bushveld Igneous Complex

The Bushveld Igneous Complex was formed by a succession of magmatic intrusions. It consists of the Rustenburg Layered Suite, Rashoop Granophyre Suite and the Lebowa Granite Suite (Kent, 1980; Walraven *et al.*, 1990; Barnard, 2000; Vantongeren *et al.*, 2010). The Bushveld Igneous Complex is positioned on the northern part of the UCRB as shown on Figure 2.14. The Rustenburg Layered Suite consists of the mafic rocks (Walraven *et al.*, 1990), which are gabbro, norite and anorthosite (Cawthorn *et al.*, 2006). Within the UCRB, Rashoop Granophyre consists of granodiorite, while the Lebowa Granite Suite, which represents the last magmatic event of the Bushveld Igneous Complex consists of Nebo Granite (Cawthorn *et al.*, 2006).

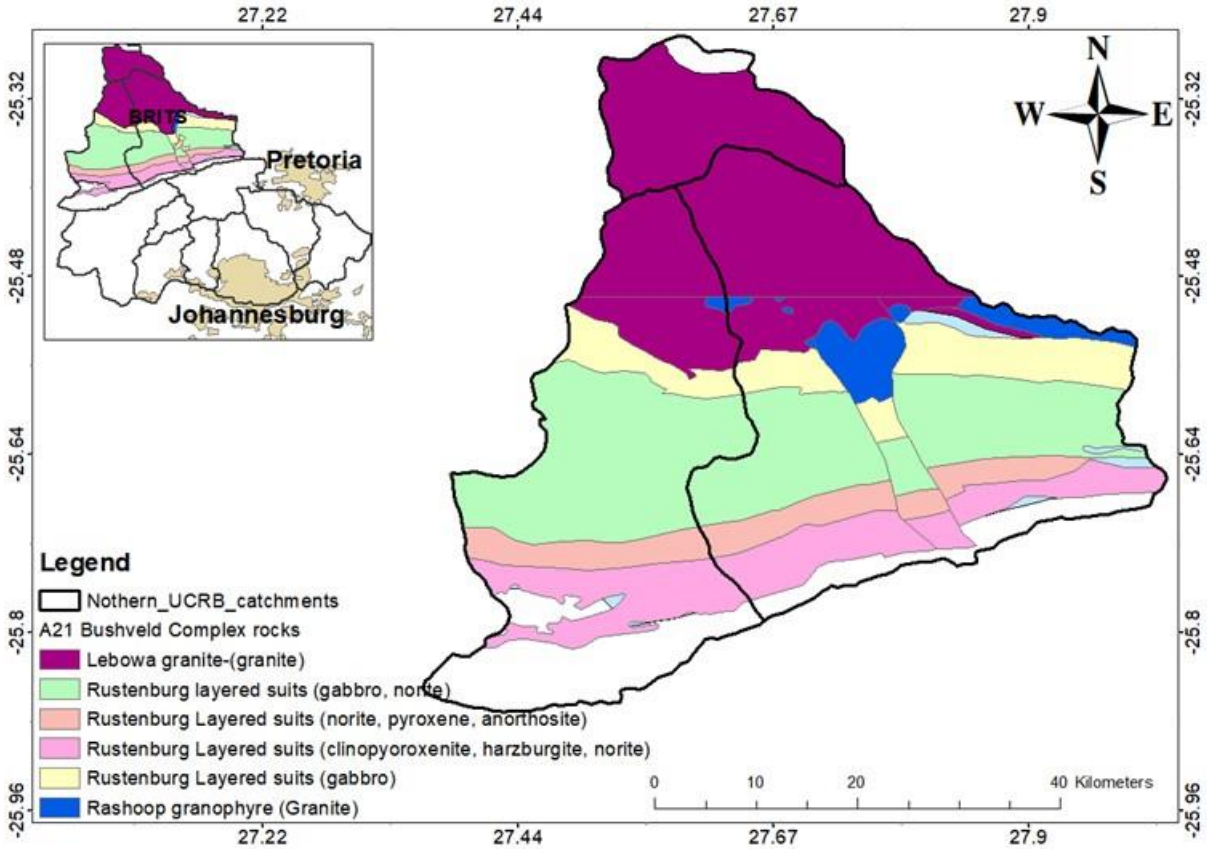

Figure 2.14: Locality map of the Bushveld Complex rocks within the UCRB (Source of Geological data: Council for Geosciences, South Africa).

2.4.6 The Sedimentary rocks of the Karoo Supergroup

The Karoo Supergroup is the youngest supergroup in the UCRB before the recent alluvial deposits. It is exposed as small patches on the eastern portion of the UCRB as shown in Figure 2.10. It is represented by the Dwyka Group (tillites, mudstone and sandstone) and Ecca Group (sandstone, shale and coal) within the UCRB.

2.5 Hydrogeological Setting

Groundwater recharge in a hard rock crystalline aquifer occurs via a combination of focused recharge from surface water channels and diffused recharge from rainfall through the soil matrix, and geological deformations such as lineaments, faults and fractured rocks (Scanlon *et al.*, 2006; Tessema *et al.*, 2012). Recharge amount, mode and groundwater flow mechanism are, therefore, dependant on the geological setting of an area.

The UCRB has a complex hydrogeological setting with aquifers of diverse hydraulic properties whose yields depend mainly on the secondary structures and weathering processes (Abiye *et al.*, 2015). This gives rise to highly site specific groundwater yields. Barnard (2000) observed that the dominant yield class among the boreholes that tap water from the basement granites is 2 L/s to 5 L/s constituting 35% of the sampled basement boreholes reaching a maximum yield of 36 L/s compared to the Malmani Subgroup dolomite, whose dominant yield class is more than 5 L/s constituting 50% of the sampled boreholes in the dolomites reaching a maximum yield of 126 L /s.

The hydrogeology of the UCRB is characterised by four types of aquifers, which are, *Intergranular aquifers*, *Fractured aquifers*, *Karstic aquifers* and *Intergranular and fractured aquifers* (Barnard, 2000; Abiye, 2011; Abiye *et al.*, 2011; Abiye *et al.*, 2015).

2.5.1 Intergranular aquifers

Intergranular aquifers consist of porous and unconsolidated material, composed of sand and gravel in the alluvial zones or ancient river deposition along river channels. It also represents geological material that has experienced extreme weathering to a porous state. This type of aquifer is found on the river banks and above the bedrock as weathered material mainly on the granites across the UCRB.

2.5.2 Fractured aquifers

Fractured aquifers consist of rocks that have fractures, fissures and joints capable of storing and transmitting large amounts of water. This type of aquifer is found in the granitic gneisses and quartzites. In this type of aquifer system, fractures are usually targeted for highly productive boreholes because the boreholes that are drilled in the core of the rock matrix usually yield small amounts of water.

The quartzite outcrops of the Witwatersrand Supergroup positioned on the southern boundary of the UCRB are intensively fractured (Figure 2.15). This fracturing is vividly observed in Johannesburg in the Northcliff suburb with a number of springs emerging at the base (e.g. Albert Farm spring) between the overlying quartzite and the underlying shale, acting as sources of small perennial streams in the catchment (Department of Water Affairs and Forestry, 2008a). Figure 2.15 shows the vertical fractures on the Witwatersrand quartzite, which are possibly responsible for the position of the Albert Farm spring. Figure 2.15 (a), (b) and (c) show fractures on the hill just above the spring, while (d) and (e) are at the spring itself. These fractures provide a suitable media for vertical recharge on the catchment boundary (Abiye *et al.*, 2011). Between June 2018 and June 2019, measurement of Albert Farm spring had an average discharge of 1.8 L/s.



Figure 2.15: The vertical regional fractures that are typical in the quartzite of the Witwatersrand Supergroup on (a), (b) and (c), while (d) and (e) show the fractures that host the Albert Farm spring.

The basement rocks give rise to a smooth topography represented by dome-like outcrops (Figure 2.16 (a)) that are weathered in some parts (Figure 2.16 (b)) and intersected by various fractures. This type of fractures could be responsible for infiltration from rainfall and from the stream channels.



Figure 2.16: The outcrops of the basement rocks in the UCRB showing fractures (a) and the weathered part (b).

The deformation of the Magaliesberg ridge and its northwards tilting nature as well as the fault lines and the graben have been discussed in section 2.4.4. Since Hartbeespoort Dam is constructed along the Magaliesberg ridge and intersected by the fault lines (Figure 2.13), it is deduced that the bedding planes and the fault lines may also be contributing to groundwater recharge from the dam. Figure 2.17 shows the north dipping bedding planes in the quartzite of the Magaliesberg ridge with the (b) part showing a conceptual model of the presumed recharge process from Hartbeespoort Dam.

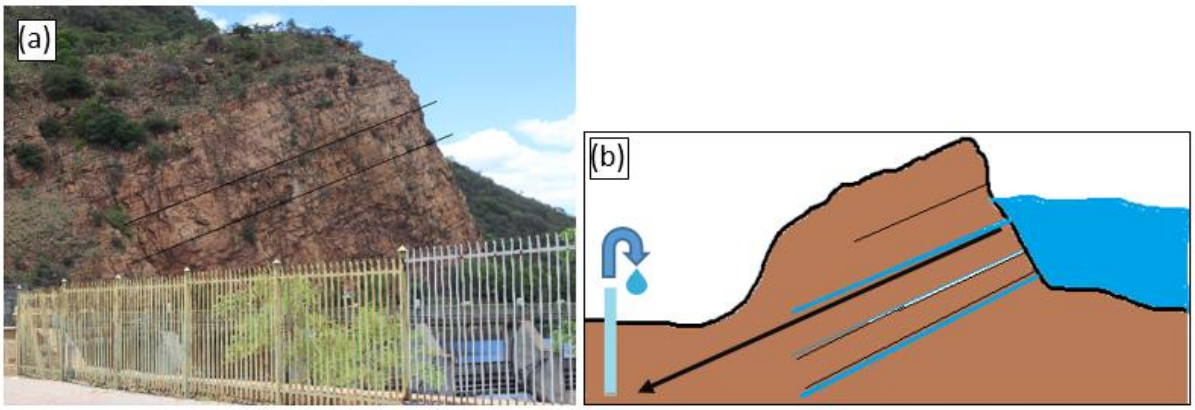

Figure 2.17: The Magaliesberg ridge, showing a conceptual model of the presumed recharge process from Hartbeespoort Dam through the bedding planes.

The frequency and aperture of the bedding plane fractures generally decreases with depth manly due to the lithostatic pressure (Daniel III, 1996). Therefore, recharge through the Magaliesberg bedding plane could only be impacting the shallow aquifer. There is intense irrigation on the northern side of Hartbeespoort Dam using the dam water. This intense irrigation also has a potential to aerially contribute to groundwater recharge.

2.5.3 Karstic aquifers

Karstic aquifers consist of carbonate rocks such as limestone and dolomite that have undergone dissolution (karstification), thereby creating cavities and sinkholes that aid in groundwater storage and movement giving rise to high yielding aquifers. Karstification is more prevalent within the chert-rich dolomite formations, which are the Monte Cristo and Eccles Formations (Kafri and Foster, 1989; Eriksson *et al.*, 1995). Since the chert layers are more resistant to erosion, they usually form the walls of the karsts within which the highly soluble dolomites have undergone dissolution. Because of their

high yields, the karst aquifers are considered as the most important aquifers in South Africa (Barnard, 2000; Holland and Witthüser, 2009).

The abundant cavities and fractures in the dolomites could also act as good recharge sites, which eventually generate high yielding aquifers through springs and tectonic depressions (Abiye *et al.*, 2015). Downstream of the Nash Farm spring in the Malapa dolomitic area (in A21G), the spring water totally infiltrates into the subsurface through the cavities. This is an indication of the potential impacts of dolomitic cavities on groundwater recharge from rainfall and stream channels. The tectonic lineaments and dissolution cavities also impact inter-basin groundwater flow in that, since the dolomites cut across the catchment in the east and west direction (Figure 2.11), groundwater can easily move across the water divides (Abiye *et al.*, 2011) leading to high yielding springs such as 130 L/s and 143 L/s at Nash Farm and Nouklip Springs (Figure 2.18), respectively (Hobbs, 2011).

Some studies have, however, reported that groundwater in the dolomites is compartmentalised by impervious and semi-pervious syenite and dolerite dykes that have intersected the dolomites, thereby retarding groundwater flow from one compartment to another (Holland and Witthüser, 2009; Abiye, 2011). According to Meyer (2014), these dykes are weathered close to the surface and, therefore, movement of water occurs at shallow depths, while at greater depths, the dykes are considered impermeable. However, it is also believed that due to tectonic processes at deeper levels, there could be trans-compartmental flow as a result of fracturing, indicating that dykes may not necessarily create no-flow boundaries (Meyer, 2014). The inter-basin flow could be the reason why Nash Farm and Nouklip springs have high yields in a small hydrological catchment as A21G.



Figure 2.18: Discharge from Nouklip Spring in the dolomites (Courtesy of Prof. Tamiru Abiye).

- *Hydrogeology of the Nash Farm and Nouklip dolomitic springs at the Malapa area*

These springs are located in the Malapa area within the Cradle of Human Kind World Heritage site, underlain by the Transvaal Supergroup rocks. As shown in Figure 2.19, in addition to the karst features, the area is also characterised by several west-north-west trending faults. These faults are steeply dipping with a shallow north-west plunging lineation accommodating the strike-slip faults, which have a total displacement of less than 2 meters. Together, the karst features and the faults are said to be oriented along the same strike and act as a prominent conduit for groundwater circulation.

The area has got small frequent springs that are identified by wet patches within the depressions and the big springs that are characterised by high yielding flows (Nash Farm and Nouklip springs). The

upslope spring is the Nash Farm spring (SP1), which yields about 130 L/s with a catchment area of about 11.6 km^2 (Hobbs, 2011). Water flows from Nash Farm spring for about 200 m in Grootvlei stream and finally forms a pool at SP2 and then flows for about 250 m after which it infiltrates through the sinkhole. After 2.2 km downstream, there appears Nouklip spring (SP3) at the contact between the Timeball Hill shale (Figure 2.19) where there are chert breccia layers. Nouklip spring is the highest yielding spring in the area with about 143 L/s (Hobbs, 2011). The downstream springs include SP4, which has a yield of 4.5 L/s and other smaller springs whose yields range from 0.05 L/s to 1 L/s, all discharging into the Grootvlei stream.

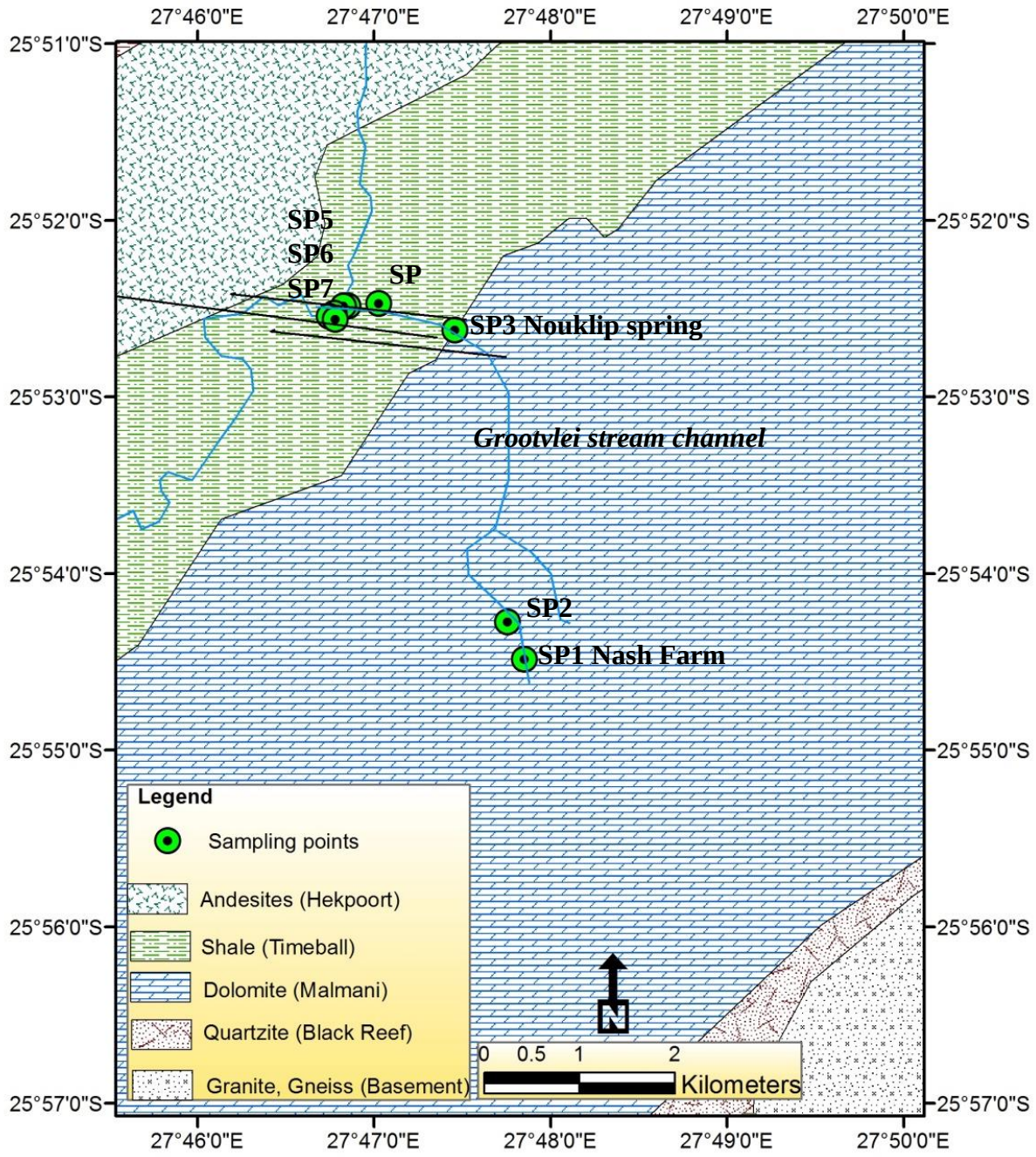

Figure 2.19: Geological map of the Malapa area showing the springs, the underlying lithology and the orientation of the faults (Courtesy of Prof. Tamiru Abiye)

As the Grootvlei stream flows, it intersects various lithologies including the dolomite and shale and, at about 100 m downstream of Nouklip spring, there are moulds of travertine (shown in Figure 2.20) The assessment of exploration pits indicate that the thickness of travertine goes up to a depth of 1.5 meters. Springs SP6 and SP7 are positioned downstream of the travertine moulds.



Figure 2.20: Travertine that deposited downstream of Nouklip spring forming rapids (Courtesy of Prof. Tamiru Abiye).

2.5.4 Intergranular and fractured aquifers

Intergranular and fractured aquifers in the crystalline rocks consist of aquifer material that is made of a combination of lose unconsolidated material and fractured aquifers (Barnard, 2000). The unconsolidated material is usually due to intense weathering that has given rise to the regolith of high permeability, which overlies the fractured hard rock aquifer, thereby, inferring a sort of two-layer system (Chilton and Foster, 1995; Barnard, 2000). Within the UCRB, this type of aquifer is mainly found in the basement granites, and the Bushveld Igneous Complex.

2.6 Hydrological Setting

The UCRB is drained by the Crocodile River, whose tributaries are the Jukskei River from Johannesburg in the south, the Hennops River from Pretoria in the southeast and the Magalies River from Magaliesberg in the west. Some of the tributaries are sustained by baseflow from stream seepage and spring flow in the dolomite, such as the Apies River from the Pretoria Fountains, the Rietvlei River from the Riet Dam springs, which all converge into the Crocodile River (Meyer, 2014). As shown on Figure 2.21, the Jukskei River from Johannesburg and Hennops River from Pretoria converge to form the Crocodile River before discharging into the Hartbeespoort Dam. The Crocodile and Magalies Rivers both discharge into the Hartbeespoort Dam. Crocodile River contributes 90% of Hartbeespoort Dam inflow (Tsoelopele-Environmental, 2006) after which it flows further northwards to discharge into Roodekopjes Dam, also called Rooikoppies Dam. In addition to the Crocodile River, the Roodekopjes Dam also receives inflow from the Gwatlhe Stream from the south west, which is on the northern side of the Magaliesberg ridge (Figure 2.21). Beyond the UCRB, the Crocodile River finally discharges into the Limpopo River.

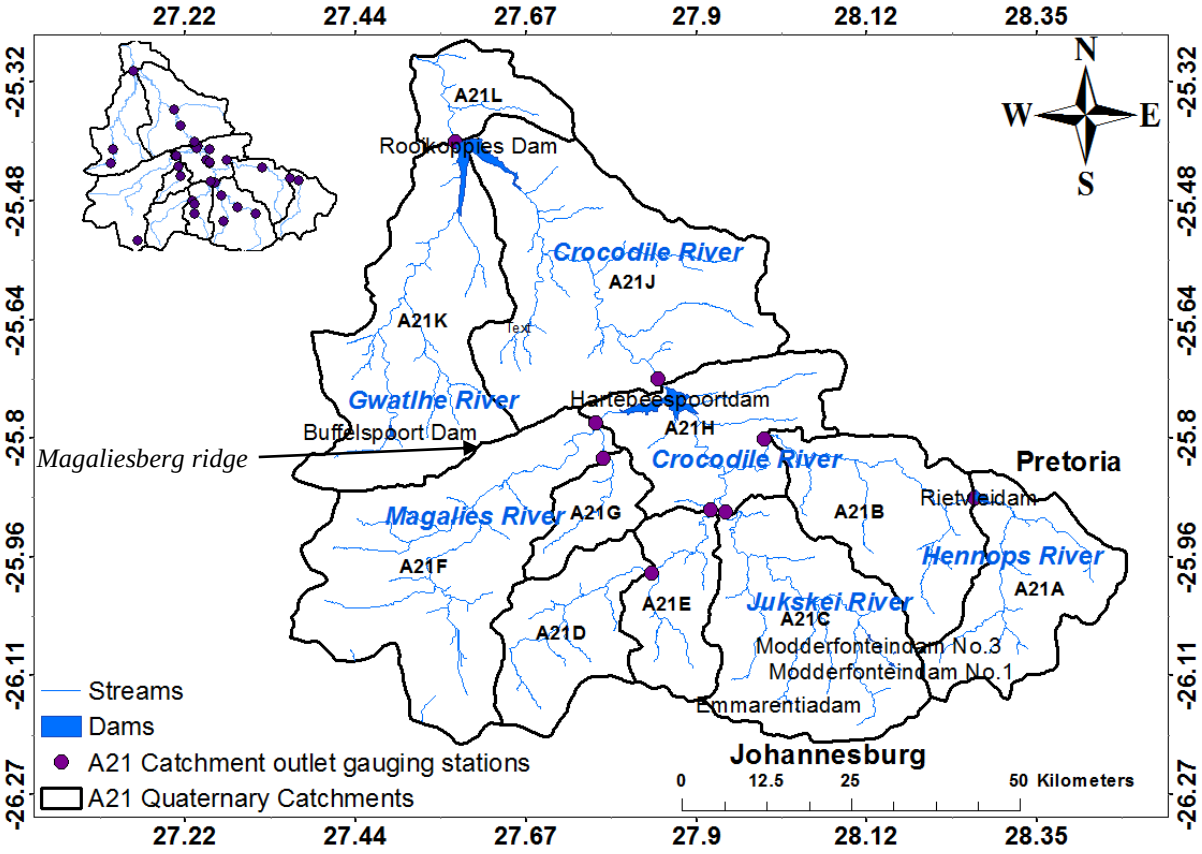

Figure 2.21: Surface water bodies within the UCRB and gauging stations at the outlet of quaternary catchments on the main map and all UCRB gauging stations shown on insert map.

Apart from Hartbeespoort and Roodekopjes Dams, there are other small surface water reservoirs (ponds and dams) within the UCRB. These are Rietvlei, Modderfontein and Emmarentia Dams, which eventually flow into Hartbeespoort Dam. Buffelspoort Dam, on the northern side of Magaliesberg ridge, discharges into Roodekopjes Dam as shown in Figure 2.21.

Due to the seasonality of rainfall in the UCRB, the streams are expected to be seasonal, however, partly as a result of continual disposal of urban wastewater from Johannesburg and Pretoria at an approximate rate of 400 000m^3/day (section 2.3), an artificial perennial state is observed in the UCRB. It has already been emphasised in section 2.3 that the wastewater discharge inflates stream discharge and renders surface water resources unsuitable for most uses, particularly the Hartbeespoort Dam, which is a depository of all return flows from Johannesburg (Dower, 2003; Department of Water Affairs and Forestry, 2008b).

2.7 Topographical Setting

Topography in the UCRB follows a general south east to north-west slope from the average elevation of 1873 to 963 masl (meters above sea level). Figure 2.22 shows the topography and drainage of the UCRB and its relation to surface water bodies.

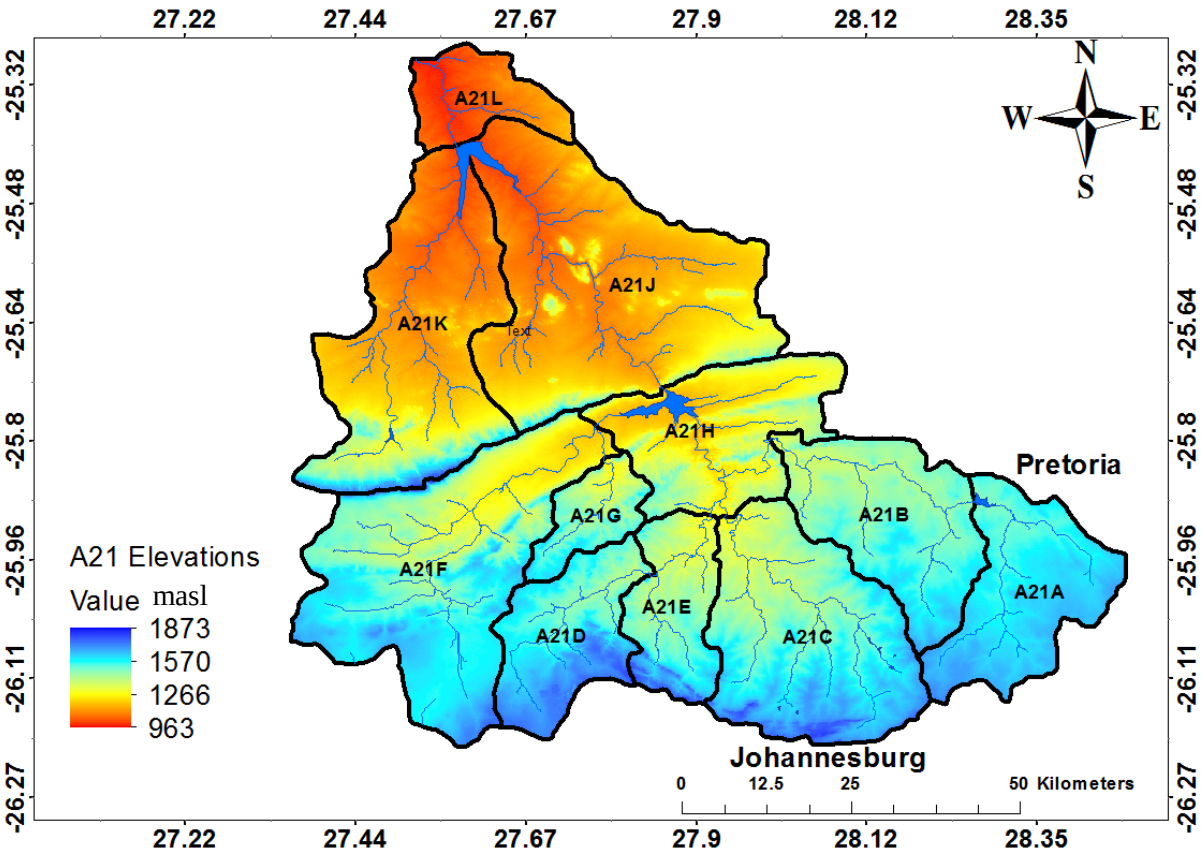

Figure 2.22: Topography and drainage of the UCRB.

The geological setting has contributed in shaping the topography of the UCRB. Through geologic history, the progressive upward movement of the basement granites stripped the sedimentary cover (Anhaeusser, 1971), thereby leading to the elevation of the older granites and the Witwatersrand Supergroup in the southern part of the catchment. This gave way for the younger Transvaal and Bushveld Igneous Complex to the low-lying areas of the basin. Erosion also contributed to the present day topography. The more resistant rocks are mostly protruding creating ridges and catchment boundaries, while the less resistant rocks form the valley floors. The structural deformation resulted in the dipping of rocks that could generate confined aquifers in the basin. This is observed in the Transvaal Supergroup among the alternating quartzite, shale and dolomites. Shale because of its less resistance to erosion has formed the valley floor where the Hartbeespoort Dam is based. The dolomite outcrop has a gentle undulating topography (Abiye, 2011; Meyer, 2014), while the quartzites of the Magaliesberg Formation, because of their resistant nature, form elongated ridges (average elevation 1400 masl) often marked by left lateral strike slip faults.

3 A REVIEW OF LITERATURE ON GROUNDWATER RECHARGE PROCESSES

3.1 Groundwater recharge process and its interdependence with other processes in the Hydrological Cycle

The hydrologic cycle is the endless circulation of water between the ocean (*surface water bodies)*, atmosphere, and land (Freeze and Cherry, 1979). In the hydrological cycle, precipitation is the main source of natural recharge and the major driving resource that provides for the hydrological cycle processes (Healy, 2010). Such processes include, but not limited to; interception, evaporation, run off, infiltration, evapotranspiration, percolation, actual recharge and groundwater discharge either naturally to stream channels or artificially by abstraction. In the context of this thesis, precipitation is assumed to be in the form of rainfall based upon the climate of the UCRB described in 2.2 (Climatic setting).

Figure 3.1 shows the processes that make up the hydrological cycle on a typical terrestrial watershed that has high evapotranspiration rates. It also shows quantitative reduction of water from precipitation down to available groundwater for consumption. It shows that only a small proportion of rainfall eventually becomes available for human consumption in a groundwater reservoir. This phenomenon emphasises the difficulty of recharge to occur in large quantities in a semi-arid climate and the difficulty of its assessment.

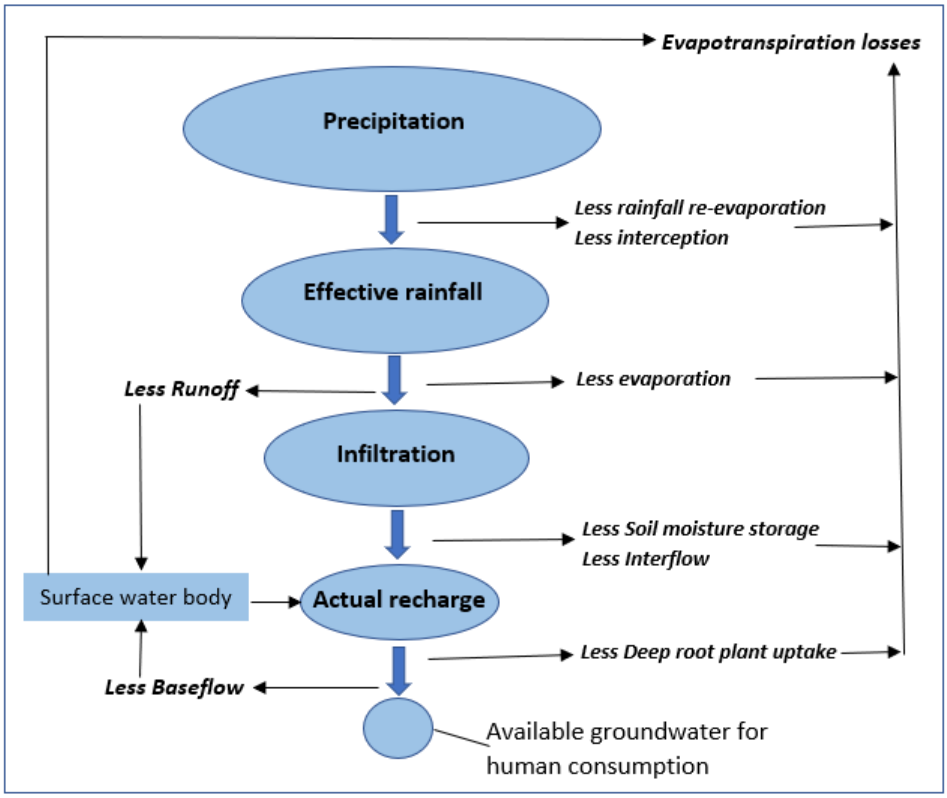

Figure 3.1: Schematic representation of reduction of water through the recharge process.

As *condensation* occurs in the atmosphere leading to rain droplets, the process of rainfall *re-evaporation* occurs as rain drops traverse through the atmosphere. Rainfall re-evaporation or *virga* is most prevalent in the arid and semi-arid environments due to high ambient temperatures and low humidity (Wang *et al.*, 2018). This leads to reduced rainfall that reaches the watershed. A portion of

rainfall is kept on plant leaves as *interception*, giving rise to *net rainfall* or *through fall* (Freeze and Cherry, 1979), which is the amount that reaches the land surface. Some of the intercepted rainfall is evaporated back into the atmosphere, while some is kept as *interception storage* and eventually falls onto the land surface. Unlike in humid areas, in arid and semi-arid areas, a big portion of *interception storage* is likely to evaporate rather than flow through to the land surface.

As net rainfall reaches the land surface, it is distributed into *infiltration*, *ponding* and *surface runoff*. The nature of the land cover and geo-pedological materials control the infiltration rates, which in turn influence the timing and spatial distribution of surface runoff (Freeze and Cherry, 1979). The impermeable concrete surfaces and semi permeable natural surface material such as fine-grained soils and massive rock outcrops will favour ponding and surface runoff, from which *evaporation* will occur. The more permeable surface material such as coarse-grained soils and fractured weathered rocks will experience more infiltration. The different mechanisms through which infiltration and subsequent recharge occur, are given in section 3.2.

The amount of water that infiltrates the land surface is further reduced in the unsaturated zone by soil moisture storage and *evapotranspiration*. Evapotranspiration is more severe in arid and semiarid climates to an extent that percolation into the saturated zone only occurs after extremely high rainfall (Van Wyk, 2010; Abiye, 2016). There is a *zero-flux plane* above the capillary zone (Figure 3.2), which marks the interface between water that moves upwards in response to capillary force, and downwards as a result of gravitational force in the form of *percolation*.

Percolation is the downward drainage of water below the root zone often equated to *groundwater recharge* (Scanlon *et al.*, 2002). It should not be confused with infiltration, because infiltration is the addition of water into the subsurface (Scanlon *et al.*, 2002; Healy, 2010). In order to make a distinction between groundwater recharge and infiltration, some references use *actual recharge* to refer to water that reaches the water table and *potential recharge* referring to water that enters the unsaturated zone from the soil surface (Scanlon *et al.*, 2002; Healy, 2010).

Essentially, as potential recharge flows downward, it might undergo evapotranspiration back to the atmosphere, or get stored in the unsaturated zone as pore water or get kept by a shallow impermeable layer forming a perched aquifer or reach groundwater storage, in which case it becomes actual recharge. Water that is kept by a shallow impermeable layer, often flows laterally and joins the stream network as *interflow*. Actual recharge, therefore, consists of an excess of pore water, which percolates further past the unsaturated zone into the *saturated zone*, joining the groundwater store.

The above discussion on actual and potential recharge processes applies in the case of diffuse mechanism through the unsaturated zone. However, recharge that occurs from a surface water reservoir when the water-table intersects the surface water channel is referred to as actual recharge, while potential recharge occurs if the stream is disconnected, such that an unsaturated zone exists between the channel and the water table (Lerner, 2003; Healy, 2010). The various interactions between groundwater and surface water are explained in section 3.2.

The quantitative illustration presented in Figure 3.1 is well defined by the low recharge estimates given by different authors for the semi-arid areas and areas with high evapotranspiration as compared to rainfall amount. Scanlon *et al.* (2006) presented a global synthesis of groundwater recharge in semi-arid areas, and observed that diffuse recharge over large areas (40-374 000km^2) ranges from 0.1

to 5% (0.2 to 35mm/year). On the other hand, focused recharge mechanism, which occurs beneath ephemeral streams and lakes, and preferential flow in fractured rocks results in variable recharge rates of up to 720 mm/year (Scanlon *et al.*, 2006).

Groundwater undergoes continual motion until it is discharged onto the land surface through deep rooted trees by evapotranspiration, abstraction boreholes, and through springs and stream beds, which constitute *baseflow* that sustains streams during dry periods (Kuniansky, 1989). Studies have shown that there is more baseflow in humid climates than there is in arid and semi-arid climates (Scanlon *et al.*, 2002; Lerner, 2003) as observed by perennial streams being more prone to humid areas, while ephemeral and intermittent streams are prone to arid and semiarid areas (Pitman and Vegter, 2003; Abiye, 2016).

The hydrological cycle is completed by a continual evaporation of water back to the atmosphere from surface water bodies, soil moisture and evapotranspiration of shallow groundwater through deep rooted plants.

3.2 Basic mechanisms of groundwater recharge

Groundwater recharge mechanisms can be classified as *diffuse* and *focused* based on the source of recharging water (Lloyd, 1986; Lerner *et al.*, 1990; de Vries and Simmers, 2002; Healy, 2010). Diffuse recharge occurs from precipitation or irrigation over a large area percolating through the unsaturated zone to the water table (Scanlon *et al.*, 2002; Healy, 2010). Diffuse recharge is also referred to as local recharge by Allison (1987) and direct recharge by Scanlon *et al.* (2002). Focused recharge is percolation of water from a surface water body such as a dam, lake or stream channel to an underlying aquifer, or through the joints and cracks (Lerner *et al.*, 1990; Xu and Beekman, 2003a; Healy, 2010). Lerner *et al.* (1990) proposed a further classification of focused recharge into *localised* recharge and *indirect* recharge. Localised recharge was defined as recharge from small depressions, joints or cracks and indirect recharge was defined as recharge from the map-able features such as rivers, canals and lakes (Xu and Beekman, 2003a; Scanlon *et al.*, 2006). However, for the purposes of this thesis, the author maintains the two definitions, diffuse and focused recharge.

Figure 3.2 depicts a schematic representation of diffuse and focused recharge through infiltration and percolation into the saturated zone. In the semi-arid climate, diffuse recharge is limited, while focused recharge is more predominant and tends to increase with aridity (Gee and Hillel, 1988; Lerner *et al.*, 1990; Scanlon *et al.*, 2006). This is because of high evapotranspiration on infiltrating water, which limits percolation, such that actual recharge is restricted to line and point sources such as streambeds and reservoir basins (Xu and Beekman, 2003a; Scanlon *et al.*, 2006).

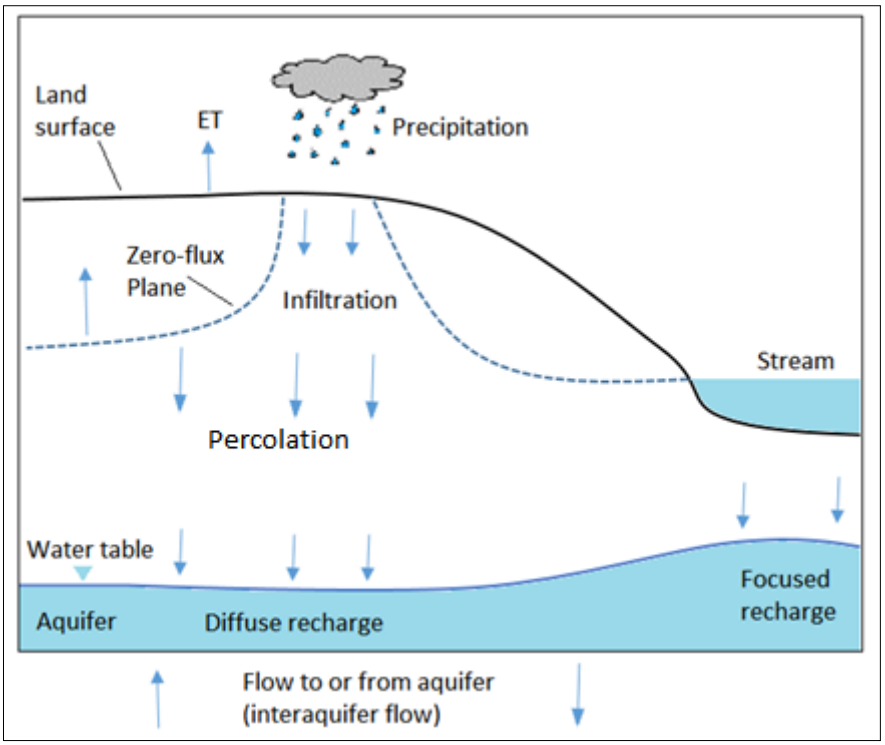

Figure 3.2: Schematic of diffuse and focused recharge (Adapted from Healy (2010).

As observed in Figure 3.2, focused recharge occurs as a loss of water from a stream channel into groundwater storage. However, in some cases, the opposite occurs whereby groundwater discharges into the stream channel. The direction of flow occurs in response to head difference between groundwater table and surface water (Brodie *et al.*, 2007; Healy, 2010). The interaction between groundwater and surface water may vary in space and time characterising streams as *gaining* and *losing* streams (Winter *et al.*, 1998; Sophocleous, 2002). In a gaining stream, groundwater is discharged into the stream channel as baseflow, while in a losing stream, water is lost from the stream channel into groundwater storage through the stream bed (Winter *et al.*, 1998; Scanlon *et al.*, 2002; Healy, 2010). In a particular space along the stream channel, a stream might be characterised as a gaining stream, while in another it is a losing stream. This interaction also differs in time depending on the instantaneous head difference between groundwater and stream.

After heavy rainfall, surface water levels tend to rise above groundwater, thereby, inferring a losing stream. During low stream flows, when groundwater head is higher, the stream becomes a gaining stream. Scanlon *et al.* (2002) stated that arid environments as compared to humid environments usually have deep groundwater levels, which make it more likely for streams to behave as losing streams, while humid environments with shallow groundwater usually have gaining streams.

Some recharge assessment methods that are discussed in Chapter 4, are based on the losing and gaining concepts to infer gaining streams through baseflow as *diffuse* recharge and a losing stream as *focused* recharge (Scanlon *et al.*, 2002; Healy, 2010).

3.3 Groundwater recharge mechanism in fractured crystalline rock aquifers

Crystalline rocks, also referred to as hard rocks, are characterised by very low primary porosity and permeability (Cook, 2003). The porosity and permeability of the hard rocks can, however, be significantly increased by secondary porosity through weathering and fracturing, leading to fractured aquifers (Cook, 2003; Adams *et al.*, 2004) and intergranular and fractured aquifers. In the absence of

secondary porosity, the matrix of the crystalline rocks cannot yield appreciable amounts of water alone and only enhance slow diffuse water movement (Freeze and Cherry, 1979; Cook, 2003; Abiye, 2011). The intergranular and fractured aquifers consist of the transmissive aquifer made of weathered zone also called regolith, which causes high yielding aquifers overlying the fractured bedrock system (Chilton and Foster, 1995). It has already been highlighted that within the UCRB, *fractured aquifers* and *intergranular and fractured* aquifers consist of igneous and metamorphic rocks such as granite, gneisses and quartzites (as explained in section 2.5.2 and 2.5.4) with negligible primary porosity.

The low primary porosity does not only affect the aquifer yields, but the recharge as well. There are various flow-paths through which recharge into the crystalline aquifer occurs. Figure 3.3 presents the different groundwater recharge mechanisms that may be representative of the UCRB. In Figure 3.3 (a), diffuse recharge occurs through the soil media down to the weathered and fractured material; in (b) recharge occurs rapidly and directly on the fractured bedrock outcrop; in (c) recharge also occurs rapidly and directly into the exposed weathered and fractured material, while (d) represents a zone of exchange between groundwater and surface water through a stream channel.

Based on the high evapotranspiration rate, which limits the amount of water that percolates past the unsaturated zone, scenario (a) could be least favourable in the UCRB. In addition to that, due to the insignificant permeability of the crystalline rocks, recharge from rainfall in this type of climatic and geological setting could bypass the unsaturated zone through scenario (b) and (c), while (d) would most likely occur underneath the surface water bodies.

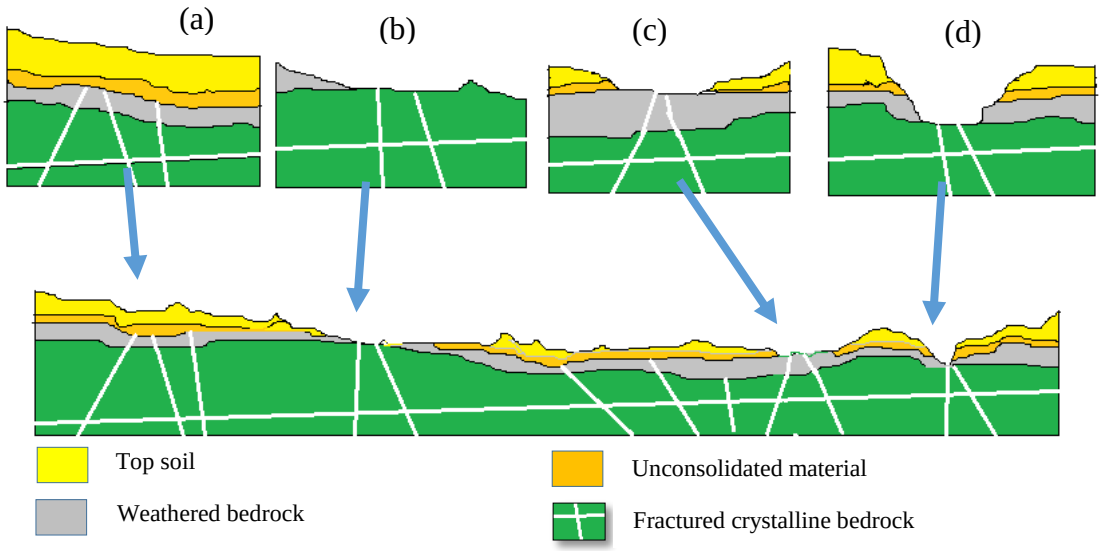

Figure 3.3: Conceptual representation of the unsaturated zone recharge and bypass flow through the weathered and fractured bedrock.

It takes much longer for the unsaturated pores of the rock to fill up during recharge and to drain during discharge because of the low permeability of the rock matrix (Healy and Cook, 2002; Healy, 2010). As a result of that, when recharge occurs in a fractured hard rock aquifer, the water tends to readily fill the fracture aperture yielding a sharp rise in water table, while the pores of the rock matrix remain unsaturated for some time. The water level is expected to then subside as water slowly diffuses from the fracture aperture into the rock matrix, leading to a saturated rock matrix.

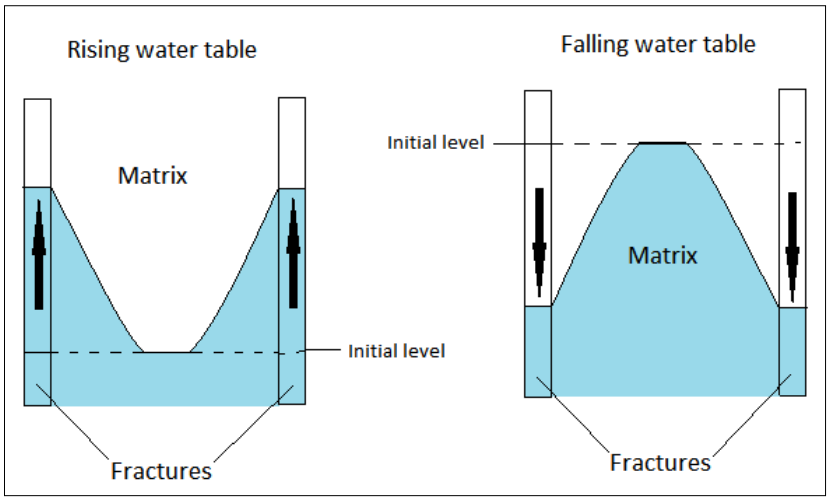

Figure 3.4: Schematic representation of saturation levels between fracture and matrix during both rising and falling water table. (Source: Healy (2010).

As a result, recharge in fractured rock aquifers of low permeability is often characterised by variations in groundwater levels (Healy, 2010) particularly after a rapid recharge event. The timing of water level measurement can, therefore, give an erroneous estimate. Also, because of the discontinuous and heterogeneous nature of the fractured hard rock aquifer, which is caused by an uneven distribution of fractures, it becomes challenging to determine the aquifer representative estimate of recharge (Daniel III, 1996; Chesnaux, 2013).

3.4 Summary of previous investigations in the UCRB

The majority of the groundwater assessments that were conducted in the UCRB placed focus on the dolomites of the Malmani Subgroup, mainly because of their high yields that contribute to economic growth in the area (Barnard, 2000; Holland and Witthüser, 2009). Holland and Witthüser (2009) undertook a multivariate statistical approach in combination with conventional geochemical and spatial analysis on groundwater and surface water to determine the hydrochemical impacts of anthropogenic sources. Different classes of water were observed, where one class was characterised by samples with traces of pollution from AMD and treated wastewater, while another one showed pristine dolomitic groundwater. This indicated that there is an interaction between groundwater and surface water in the dolomites.

Abiye (2011) and Abiye *et al.* (2011) applied hydrochemistry and environmental isotopes to assess the provenance of groundwater in Johannesburg area. In this study, mixing of fresh and polluted groundwater was observed at shallow depths within the weathered crystalline rocks and in the dissolution cavities of the dolomites in the Malmani Subgroup. The acidic environment that is caused by AMD is responsible for the dissolution of minerals and, hence, contributed to the evolution of minerals in groundwater. The low chloride and depleted $\delta^{18}O$ in the dolomitic aquifer were observed and deduced to be a result of low degree of water-rock interaction and lack of intensive evaporation due to rapid infiltration that occurred through the fractures and dissolution cavities, also indicating possibilities of high elevation recharge. The dominant groundwater circulation was found to be close to the surface at the depth of 40 m. The main mechanism of groundwater movement in the crystalline aquifer was deduced as a diffusive mechanism, mainly as a result of the limited fractures at deeper levels and possible sealing of the fractures by calcite precipitation. The study also stated that recharge is possibly occurring through the vertical fractures of the quartzites in the Witwatersrand Supergroup on the southern boundary of the UCRB.

Abiye *et al.* (2015) undertook a groundwater-surface water interaction study using environmental isotopes and stream discharge in the UCRB. The rationale behind the study was based on the potential pollution that can be caused by the interaction, particularly given the existence of AMD in the basin. In this study, it was observed that between 24 million m^3/yr and 29 million m^3/yr was seeped from mine water into the dolomitic aquifer. Environmental isotopes revealed that the decanting mine water has extensively interacted with shallow groundwater and surface water. It was observed that the streams are losing water into the dolomitic aquifer through sinkholes and fractures. The conclusion in this study was that groundwater and surface water in the dolomitic terrain are intimately connected.

Abiye (2016) gave a synopsis of recharge work done through the application of Water Table Fluctuation and Baseflow Separation methods in the Johannesburg dolomites and fractured quartzites. The recharge estimate of 118.2 mm/yr (17% of 697 mm rainfall) was obtained in the dolomite aquifer, while 98.9 mm/yr (14% of 697 mm rainfall) was obtained in the quartzite aquifer using the Water Table Fluctuation method. Using the Baseflow Separation method, a recharge value of 189.1 mm/yr (27.1% of MAP) was obtained. According to Abiye (2016), the baseflow amount was over estimated due to constant disposal of wastewater from the water treatment plants in the area. It was, therefore, recommended that for accurate estimations, wastewater should be deducted from stream flow.

In an explanation of a set of national groundwater maps, Vegter (1995) presented a combination of groundwater recharge values from different studies. The reported point recharge estimates assessed from the springs that appear in the UCRB are 11% from Pretoria Fountains in the eastern limb of the Malmani dolomite belt and 10.8% to 13.5% for the Steenkoppies springs in the western limb.

In summary, the previous investigations in the UCRB focused on the general groundwater assessment with a brief emphasis on groundwater recharge assessment. The following gaps were observed:

- No previous investigations assessed the sustainability of recharge under this dynamic climate and land use setting. This is a gap because, while the provided recharge estimates may be relevant for the period of assessment, they may not be achievable under different settings.
- The applications of tracer methods were successfully done to assess recharge, however, the assessment was mostly based on once off or limited groundwater and rainfall samples.
- No previous investigations gave a thorough characterisation of the environmental isotopes in Johannesburg rainfall, nor established the local meteoric water line for the Johannesburg area, which is most relevant given the possible recharge through the vertical quartzite fractures as deduced by Abiye (2011). The seasonality of rainfall brings about changes in isotopic signature of terrestrial water, which can be well captured by sampling over a hydrological year or several of them, to give a solid assessment of recharge.

In light of the above, this study attempts to undertake a holistic approach towards groundwater recharge assessment in the UCRB. In order to understand the isotopic signature trends in groundwater, rainfall as a source of recharge is thoroughly assessed. Groundwater samples are also collected for a longer period to capture the various recharge episodes and remove the possible bias brought by a single sample that could be representative of a specific recharge episode that had its unique signature. A quantitative assessment of recharge is also done through a combination of methods that supplement one another. The study does not only assess recharge, but also determines the spatial distribution of groundwater age and its flow path in the basin using carbon isotopes. The UCRB being affected by changes in climate and projected growth in urbanisation is likely to experience changes in its hydrological system. Therefore, over and above the recharge estimate for the assessed period, the predictive models are run to assess the potential effects of the changes in

temperature and rainfall on groundwater recharge. Eventually, the recommendations on the best practices in water resources management are made given the high volumes of wastewater from urban return flows that are an addition into the UCRB from the Vaal Catchment.

3.5 Conceptualised recharge processes in the UCRB

Having discussed the physiographic nature and literature related to groundwater recharge in the previous sections, it now becomes possible to develop a conceptual model of recharge processes in the UCRB by describing the probable location, timing, and likely recharge mechanisms. This conceptual understanding also influences the selection of methods.

- Being a catchment with high MAE, focused recharge is most likely to occur from the surface water bodies and localised recharge through the fractures than diffuse recharge through the soil.
- Because of higher rainfall in the southern elevated portion of the UCRB, recharge from rainfall could be occurring through the vertical fractures in the quartzite of the Witwatersrand Supergroup.
- Based on the seasonal pattern of rainfall, it can be assumed that recharge only occurs during the summer season, while the rest of the period is entirely for groundwater discharge.
- Because of the temperatures that increase from the southern portion to the northern portion, there could be more evapotranspiration in the north than in the south, resulting in more soil moisture losses and inferring less diffuse recharge in the northern part.
- Focused recharge could be occurring through fractures on the stream channel underlain by hard crystalline rocks and sink holes in streams underlain by karst aquifers. However, streams that are underlain by massive granites could only be enhancing interaction with the alluvial aquifer, which only has a limited lateral extent.
- The high volumes of wastewater discharge in the streams could be inducing focused recharge.
- The massive shallow underlying basement granites in the southern upper portion of the UCRB could be inducing interflow to nearest stream network.
- Hartbeespoort Dam could be contributing to groundwater recharge due to the inclined bedding planes in the quartzites of the Magaliesberg ridge and the two north south facing faults that cut across the Transvaal Supergroup into the Bushveld Igneous Complex.
- Diffuse recharge could be occurring due to intense irrigation from surface water, particularly in the northern part of the Magaliesberg range.
- There is low infiltration in the developed southern part of the UCRB than in the uncultivated open land in the north.

4 THEORETICAL BACKGROUND ON THE RECHARGE ASSESSMENT METHODS

4.1 Introduction

Xu and Beekman (2003b) stated that, there are as many methods for estimating recharge as there are different sources and processes of recharge and each of them has its own limitations in terms of applicability and reliability.

The recharge assessment methods can be classified through different criteria. In recharge assessment, some methods give a qualitative interpretation, which may be explaining: how is recharge occurring? Where in the watershed is it occurring? How long has it been since recharge occurred? On the other hand, some methods give a quantitative interpretation of recharge process, which explains how much recharge has occurred. These two can be used to supplement each other.

Some methods estimate actual recharge, while others only estimate potential recharge. Methods that use surface water and the unsaturated zone data mostly estimate potential recharge, while those that use groundwater data estimate actual recharge (Scanlon *et al.*, 2002).

The estimated values can also be classified as either point or integrated. Point estimates are those that represent a specific point in space and time, while integrated estimates refer to recharge values that are averaged over a large area or longer period (Healy, 2010).

In addressing these different aspects of recharge, the recharge assessment methods in this study are divided into the following classes based on their approach and domain of application:

- Chemical and isotope tracer methods
- Classical water balance methods
- Physical methods
    - Methods based on surface water data
    - Methods based on groundwater data
- Watershed modelling methods

4.2 Chemical and isotope tracer methods

The chemical and isotopic tracer methods have a wide application in hydrogeological studies in addressing both qualitative and quantitative questions. In groundwater recharge, they can help to identify the source and location of recharge, furthermore, the groundwater velocity and its subsurface residence time. The aquifer makeup along the flow path can also be determined given the chemical or isotopic traces found in groundwater (Marfia *et al.*, 2004; Karolytė *et al.*, 2017). Some tracers such as chloride can also be used to give a quantitative estimate of groundwater recharge (Eriksson and Khunakasem, 1969).

The characteristic property that makes tracers applicable in hydrogeological studies is their ability to move with water as it flows through the subsurface, particularly with concentrations or quantities that are detectable. They are generally chemical constituents of a water molecule (oxygen or hydrogen), chemical species that are dissolved in water (e.g. dyes, chloride), or the physical condition of water (e.g. temperature of water) (Scanlon *et al.*, 2002; Healy, 2010).

The tracers can be classified into natural environmental tracers, historical tracers, and applied tracers (Scanlon *et al.*, 2002). Natural environmental tracers are those that are generated or transported through natural processes in the environment. An example being chloride, which is mostly introduced into the atmosphere through spraying of water waves from the ocean, washed onto the land surface

through rainfall and dry deposition and introduced into the subsurface through infiltration. The isotopes that are constituents of a water molecule such as ^{16}O, ^{1}H, ^{18}O, ^{2}H and ^{3}H are also examples of natural tracers, though tritium can also be classified as an anthropogenic tracer due to its introduction into the atmosphere through atomic bombs in the 1950s (Clark and Fritz, 1997).

Historical tracers, sometimes referred to as anthropogenic tracers, are those that were introduced into the atmosphere through historic human activities, an example being tritium and isotopes of chloride (^{36}C) through the nuclear bomb activities (Gat, 2001). Applied tracers are those that are placed in the environment either intentionally to trace the movement of water or as an effect of other activities on earth, such as wastewater disposal and agricultural fertilisers.

The types of tracers that are applied in this study are environmental isotopes. These are used for the assessment of groundwater recharge mechanisms, groundwater age, travel time and flow path.

4.2.1 Environmental isotopes

Clark and Fritz (1997) defined *environmental* isotopes as the naturally occurring isotopes of elements found in abundance in the environment, such as hydrogen, carbon, nitrogen, oxygen and silicon. Isotopes can be classified as radioactive and stable isotopes. In hydrological studies, radioactive isotopes are mostly used for groundwater dating, while stable isotopes are used for assessing recharge processes, subsurface processes, geochemical reactions, reaction rates and for tracing groundwater provenance (Clark and Fritz, 1997).

The applicability of stable isotopes in hydrological studies is based on their ability to undergo fractionation, which has been defined by Urey (1947) as an exchange of isotopes (e.g. ^{18}O and ^{16}O) between any two molecular species or phases that are participating in a reaction. Fractionation alters the isotopic ratio of atoms that makeup a chemical specie. The different processes that cause fractionation are explained for each stable isotope in the following sections.

Stable isotope abundances in a sample are presented as a ratio of the heavier to the light isotopes, (e.g. $^{18}O/^{16}O$, $^{2}H/^{1}H$, $^{13}C/^{12}C$) and they are compared to the globally accepted standards using Equation 1. The stable isotopes that are used in this study, $^{18}O/^{16}O$ and $^{2}H/^{1}H$ are compared to Vienna Standard Mean Ocean Water (VSMOW), while the $^{13}C/^{12}C$ is compared to the VPDB, which is derived from the isotopic ratio of a fossil called Belemnitella americana from the calcareous Pee Dee Formation in South Carolina (Clark and Fritz, 1997; IAEA, 2000).

$$\delta_{sample}(‰) = \frac{R_{sample} - R_{standard}}{R_{sample}} \times 1000 \qquad \textit{(Equation 1)}$$

Where $\delta_{sample} = \delta^{18}O$, or $\delta^{2}H$ or $\delta^{13}C$ and where R is the ratio representing = $^{18}O/^{16}O$, or $^{2}H/^{1}H$ or $^{13}C/^{12}C$.

Because the abundance of heavier isotopes in a sample are extremely small compared to their lighter counterparts, and that fractionation process does not impart huge variations in isotope concentrations, the δ-values are expressed as part per thousand or permil (‰) (Clark and Fritz, 1997) as shown on Equation 1. If the value of δ is positive, then the sample is more enriched in heavy isotopes than the standard and if it is negative, then the sample is more depleted than the standard.

Radioactive isotopes, such as ^{3}H and ^{14}C, undergo natural decay, whereby their unstable nucleus is naturally transformed into a more stable nucleus through the loss of energy (IAEA, 2000). The decay of radioactive atoms occurs at a rate dictated by its characteristic half-life (Suckow *et al.*, 2013). This

means that the concentrations of the radioactive isotopes naturally decrease due to radioactive decay as water flows along the flow path. Because of this, if the concentration at recharge is known, radioactive isotopes can be used to estimate the Mean Residence Time (MRT) of groundwater, which is the time that groundwater has been isolated from the atmosphere (Gat, 2001). The applicability of the radioactive isotopes in hydrogeology is based on their ability to undergo radioactive decay.

Only the isotopes of carbon (^{12}C, ^{13}C and ^{14}C) and those of a water molecule (^{16}O, ^{18}O, ^{1}H, ^{2}H and ^{3}H) are applied in this study and are, therefore, explained in depth.

- *Stable isotopes of a water molecule ($\delta^{18}O$, $\delta^{2}H$)*

The stable isotope composition of natural meteoric water from different parts of the world were assessed by Craig (1961) who observed that there is a linear relationship between δ^2H and $\delta^{18}O$, which is represented by the equation $\delta^2H=8\delta^{18}O+10‰$, referred to as the Global Meteoric Water Line (GMWL). The GMWL is characterised by a slope of 8 and a deuterium excess (d-excess) of 10‰. However, the stable isotope composition in precipitation from different locations is dictated by the continental, temperature, seasonality, latitude, altitude and rainfall amount effects (Dansgaard, 1964; Clark and Fritz, 1997). These are well defined in literature in Clark and Fritz (1997) and Gat (2001), but can be briefly explained as thus:

Latitude effect: With increase in latitude, precipitation becomes more depleted, such that rainfall in the polar region is highly depleted and highly enriched towards the equator.
Temperature effect: Higher air temperatures lead to enriched rainfall, while lower temperatures cause depleted rainfall.
Altitude effect: As the moisture moves up a hill, the cloud mass becomes more and more depleted. Such that rainfall in the highlands is depleted while that in the lowlands is enriched.
Seasonality effects: Summer precipitation is more enriched than winter precipitation, because of temperature effect.
Continental effect: Coastal rainfall is enriched because it represents the first condensate of vapour from the ocean, while inland rainfall gets more depleted.
Amount effect: A high amount of rainfall is more depleted while a low amount is more enriched.

These isotopic effects cause the rainfall at a specific location to have its distinct isotopic signature due to its distinct climate, geomorphology and geographical setting. Therefore, the meteoric water line for a specific location will show deviation from the GMWL, giving its distinct $\delta^{18}O$ versus $\delta^{2}H$ regression line, which is referred to as a Local Meteoric Water Line (LMWL). Clark and Fritz (1997) stated that a LMWL is more appropriate to use in a local investigation because it represents the local climatic and geographical setting.

Since Craig (1961) released the landmark observation on isotopic variations in meteoric waters, subsequently Dansgaard (1964) on the air temperature and rainfall amount effects in precipitation, a lot of work has been done in understanding the isotopic compositions of rainfall from different parts of the world. For example, Schoch-fischer *et al.* (1983) assessed the hydrometeorological factors controlling the time variation of $\delta^{2}H$, $\delta^{18}O$ and ^{3}H in precipitation of Heidelberg Germany, Cracow Poland and Miami USA, Fritz *et al.* (1987) assessed the seasonal and air temperature effects on isotopic composition of precipitation in Canada. Apart from the intensive work on precipitation effects by Dansgaard (1964) and Gat (2001), which were done mostly in the northern hemisphere, Diamond and Harris (1997) and Harris *et al.* (2010) studied the controlling factors of isotopes in precipitation in the west coast of South Africa, where the four main factors were observed as

temperature, altitude, amount, and continental effect. However, there is no such record of work done in the central continental mid latitude (Johannesburg, South Africa) specifically looking at daily rainfall.

Dansgaard (1964) observed a linear relationship (Equation 2) between the mean annual air temperature and isotopic composition of the north Atlantic stations in the northern hemisphere. Gat (2001) also made a general assessment of the European and north Atlantic stations from GNIP database using monthly air temperatures and stable isotopes. The results by Gat (2001) gave rise to Equation 3, which compared reasonably well with the relationship given by Dansgaard (1964), which used annual air temperature values.

$$\delta^{18}O = 0.695T - 13.6‰ \qquad \textit{(Equation 2)}$$

Where "*T*" is the measured mean annual surface air temperature.

$$\delta^{18}O = (0.521 \pm 0.014)T - (14.96 \pm 0.21)‰ \qquad \textit{(Equation 3)}$$

Where "*T*" is the measured mean monthly surface air temperature.

It is worth noting that due to the decrease in air temperature with increase in altitude, the measured surface air temperatures during precipitation do not represent the in-cloud condensation temperature, which is responsible for stable isotope signature in precipitation (Clark and Fritz, 1997). However, Dansgaard (1964) observed that the mean surface air temperature correlates in a parallel way with the actual in-cloud condensation temperature. It is, therefore, deduced that the surface air temperature can be confidently used to assess the temperature effect in precipitation. It should also be noted that the Dansgaard (1964) work was done with the majority of sampling stations located in the northern hemisphere using the mean annual data and there was no representation of the Southern African precipitation.

Having emphasised the critical importance of stable isotopes and their effects in the local rainfall, it becomes important that prior to the application of stable isotopes signature for the assessment of groundwater recharge, there should be a good understanding of the isotopic signature in the local rainfall as a reference for groundwater. As per the above emphasis, the assessment should entail a thorough analysis to identify the stable isotope effects that play a major role in the isotopic signature of the local rainfall and to establish the suitable local meteoric water line.

It has been stated that stable isotopes are useful in hydrogeological studies because of their ability to undergo isotopic fractionation, which is actually a basis for groundwater provenance studies (Clark and Fritz, 1997). Through fractionation, the meteorological processes provide the rainfall with a characteristic finger print that helps to identify its origin (Clark and Fritz, 1997). Fractionation of stable isotopes of a water molecule ($\delta^{18}O$, $\delta^{2}H$) occurs during physical processes that result in a phase change, such as evaporation and condensation. Because of this, groundwater maintains the isotopic signature from the time and location of recharge as long as there are no phase changes in the subsurface, and provided that the water temperature does not exceed 60-80°C (Issar and Gat, 1981), a temperature above which rocks tend to leach out heavy isotopes into groundwater (Sami, 1992). However, recent studies have indicated that in aquifers with high CO_2 content, such as dolomitic aquifers, ^{18}O fractionation can occur between CO_2 and groundwater even under low temperatures (Karolytė *et al.*, 2017).

During evaporation from a surface water body, fractionation causes the light isotopes to preferentially vaporise, while the heavy isotopes tend to stay in the liquid phase. Fractionation during evaporation is based on the fact that more energy is required to break the stronger H-^{18}O bond than the weaker H-^{16}O bond in order to form vapour (Clark and Fritz, 1997). The difference in bond strengths also cause H-^{16}O to have more vapour pressure than H-^{18}O making it easier for $H_2{}^{16}O$ to vaporise than $H_2{}^{18}O$ (Clark and Fritz, 1997). With time, as vaporisation of light isotopes continues, the isotopic signature of the residual water body tends to get more enriched in heavy isotopes, thereby leading to a regression line with a smaller slope compared to the LMWL, called a Local Evaporation Line (LEL), which is illustrated in Figure 4.1.

It is because of this phenomenon that stable isotopes of a water molecule are useful for assessing groundwater recharge mechanisms (Sami, 1992). Focused recharge mechanism from a surface water body is often characterised by highly enriched groundwater that has similar isotopic signature to the surface water body usually plotting near the surface water evaporation line. On the other hand, aquifers that are recharged from rainfall through rapid and diffuse mechanism will have the same isotopic signature as the rainfall (Issar and Gat, 1981). It would also be expected that diffuse recharge that occurs after some degree of soil moisture evaporation, may also show some enrichment compared to the local rainfall, i.e. LMWL. Therefore, rainfall isotopic signature and surface water isotopic signature can be used as references for groundwater to assess diffuse and focused recharge mechanisms.

Stable isotopes of water have been widely used as environmental tracers to answer a range of hydrological questions: for example, in groundwater studies (Herczeg *et al.* (1992); Sami (1992); Harris *et al.* (1998); Abiye (2011); Abiye *et al.* (2011)), soil water (Allison and Hughes (1983); Selaolo (1998); Soderberg *et al.* (2012); Isokangas *et al.* (2017) interaction of surface water and groundwater (Herczeg *et al.* (1992); Leketa (2011); Abiye *et al.* (2015), dependency of vegetation on groundwater (Evaristo and McDonnell (2017); Shakhane *et al.* (2017) and isotopic characterisation of spring water (Harris *et al.*, 1998; Karolytė *et al.*, 2017). Stable isotopes of a water molecule have also been successfully used in various other studies, specifically, to assess groundwater recharge (Nkotagu, 1996; Abiye, 2011; Abiye *et al.*, 2011; Ayadi *et al.*, 2018). Moreover, they have been confirmed useful in the assessment of water resources in South(ern) Africa as documented in Abiye (2013b). Specifically, Abiye (2013a) successfully assessed the groundwater and surface water interaction dynamics in the UCRB using stable isotopes.

- *Deuterium excess (d-excess)*

Froehlich *et al.* (2002) defined deuterium excess as the measure of the relative proportions of $\delta^{18}O$ and $\delta^{2}H$ in water, which can be visualised as an index of deviation from the GMWL of d-excess = 10‰. In mathematical terms, d-excess is a y-intercept of the meteoric water line (MWL) representing a point at which the MWL intersects the vertical $\delta^{2}H$ line in a $\delta^{18}O$ versus $\delta^{2}H$ plot.

Dansgaard (1964) first computed the d-excess amount for rainfall samples using the equation $d\text{-}excess = \delta^{2}H - 8\delta^{18}O$, obtained from the GMWL. The computation of d-excess for a sample indicates a point along the vertical $\delta^{2}H$ line at which the sample would cross if a line that is parallel to the meteoric water line could be drawn. This is well illustrated in Figure 4.1 below (Froehlich *et al.*, 2002).

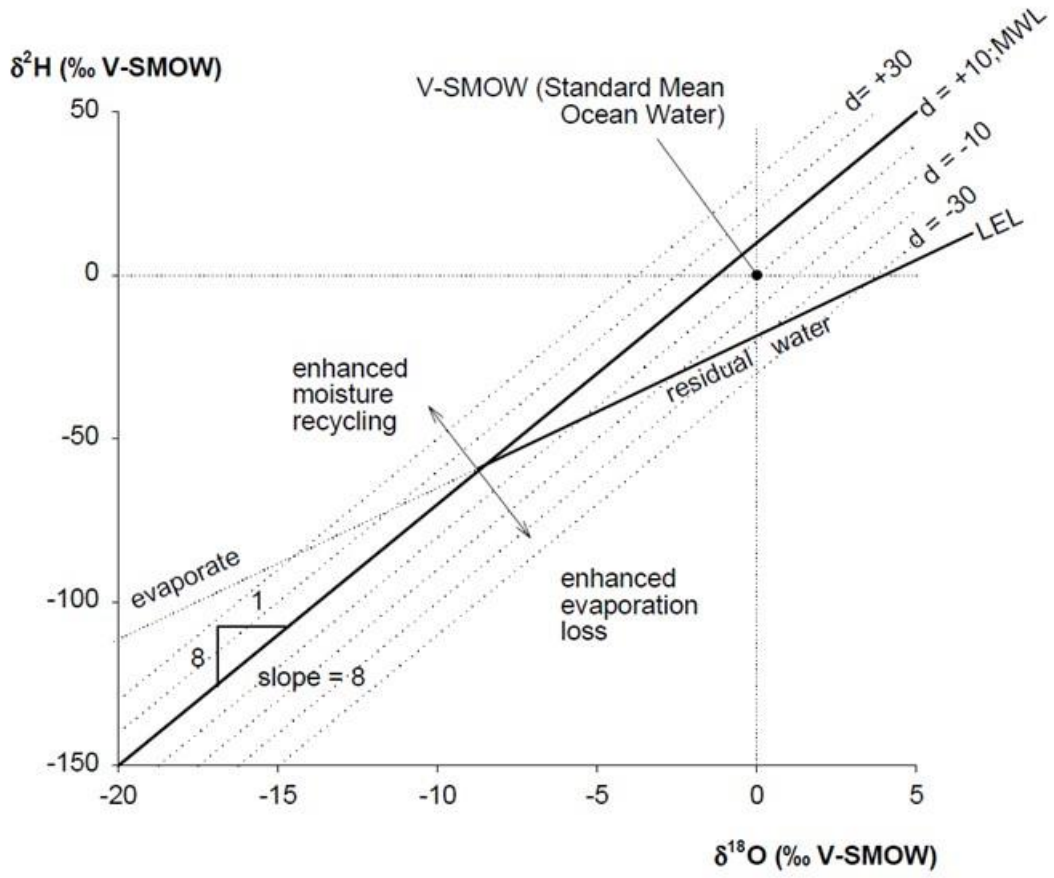

Figure 4.1: A schematic diagram of $\delta^{18}O$ versus $\delta^{2}H$ illustrating the global meteoric water line, the evaporation line (LEL), and the different d-excess values (adapted from Froehlich *et al.* (2002).

Clark and Fritz (1997) expressed that varying d-excess values present a range of rainfall types that were generated at different vapour humidity, air temperature conditions and different rain source air masses. This indicates that the d-excess value can be used to characterise the physical conditions of the rainfall moisture source (Froehlich *et al.*, 2002; Harris *et al.*, 2010). Evaporation occurs because of the difference in humidity between the liquid and the vapour phases.

Humidity is also a function of temperature because an increase in temperature leads to an increase in the water carrying capacity of moisture (Clark and Fritz, 1997). In hypothetical 100% humidity, the physical conditions between the vapour and liquid are similar, and therefore, equilibrium conditions prevail, such that there is movement of moisture between the two phases while there is no net isotopic exchange i.e. no fractionation. Meaning that the vapour phase will have the same isotopic signature as the liquid, and the first rainfall from that vapour will have the same signature as the liquid (Clark and Fritz, 1997). Therefore, evaporation at high humidity conditions close to 100%, occurs with minimal fractionation. Similarly, the increase in temperature causes an exponential increase in the moisture carrying capacity of the air (humidity), thereby, invoking formation of enriched vapour with low d-excess value (Clark and Fritz, 1997). Under low temperature and low humidity, non-equilibrium conditions prevail such that the movement of moisture into the vapour phase gets dominated by the light isotopes because of their higher vapour pressure and diffusivity (Clark and Fritz, 1997).

The d-excess can also be used to determine the recycling of moisture as a result of repeated evaporation and condensation (Froehlich *et al.*, 2002). This means that the more multiple recycling

of moisture from the ocean, the more depleted it becomes and, therefore, attaining higher d-excess value. If groundwater has been determined to have recharged via diffuse mechanisms without altering its isotopic signature prior to recharge, then d-excess for the groundwater sample can be used to assess the moisture source of the rainfall that generated the recharge.

Relative to the UCRB, the regions that are potential sources of moisture are the warmer Indian Ocean, cooler Atlantic Ocean, the cold Antarctica at high latitudes and the local terrestrial evapotranspiration. The low d-excess rainfall may be affiliated to the Antarctic region or regional air circulation. The high d-excess rainfall may be affiliated to the Indian Ocean and the local surface water bodies that have experienced extreme evaporation besides moisture recycling and moisture from terrestrial evapotranspiration.

- *Radioactive Tritium (^{3}H)*

Tritium (^{3}H) is a radioactive isotope of hydrogen with a half-life of 12.43 years mostly used to date young groundwater (Clark and Fritz, 1997). It is naturally formed in the atmosphere through cosmic ray bombardment of ^{14}N and is then integrated into the water molecule (Clark and Fritz, 1997; Gat, 2001; Gat, 2010). This is illustrated in the following chemical reaction:

$^{14}N + n \rightarrow {}^{12}C + {}^{3}H$ (IAEA (2000)

However, in the 1950s, the thermonuclear bomb tests generated anthropogenic tritium, creating a pulse that overshadowed the natural cosmic production (Clark and Fritz, 1997). This pulse, however, was most significant in the northern hemisphere where the tests were done, while the global air mass circulation into the southern hemisphere was retarded by the equatorial barrier (Gat, 2001). The 1950s thermonuclear bomb tests provided the tritium input signal that defined modern water (Clark and Fritz, 1997). Considering the initial average 1950s tritium pulse and its half-life, Clark and Fritz (1997) defined modern water as that which had a significant amount of tritium in the mid-1990s, deducing that it was recharged at least within the 45 years. While, sub-modern or old water was defined as that with no tritium content (Clark and Fritz, 1997). In the mid-1990, the groundwater that recharged prior to the 1950s could easily be identified with low tritium levels, while that which recharged afterwards was observed by high tritium levels.

However, apart from the atmospheric cosmic radiation and the 1950 bomb tritium pulse, there are other continuous geogenic subsurface sources and anthropogenic land surface sources of tritium, which could be incorporated into groundwater, thereby, increasing the tritium levels. The anthropogenic sources may include production of neutron fluxes through the nuclear reactors from power plants and nuclear research centres, while the geogenic sources may be a result of the fission of radioactive species such as Uranium and Thorium (Gascoyne and Kotzer, 1995; Clark and Fritz, 1997). If a rock has an appreciable amount of Lithium, the generated neutron flux then bombards the Lithium (^{6}Li) to form ^{3}H, which is then incorporated directly into groundwater at a rate that depends on the amount of Lithium and porosity of the host rock (Gascoyne and Kotzer, 1995). In most cases, however, geogenic sources of tritium are negligible and lower than the cosmogenic production (Gascoyne and Kotzer, 1995; Clark and Fritz, 1997), while the anthropogenic sources may be significant depending on the intensity of production.

Therefore, the more the number of tritium sources in a study area, the more complex it becomes to assess the input tritium at recharge and, therefore, difficult to determine the groundwater MRT. If tritium in water at the time of recharge is known, then tritium in groundwater and a half-life of 12.43 years can be used to estimate the MRT of water in the subsurface using Equation 4 (Clark and Fritz,

1997). In a piston groundwater flow system, the application of Equation 4 becomes more meaningful, while more complexity is brought by the diffusive type of flow characterised by mixing of new and old water along the groundwater flow path, thereby inducing lack of certainty on the estimated MRT.

$$t = t_{1/2} In \left(\frac{A_{t0}}{A_{t1}}\right)/In2 \qquad \textit{(Equation 4)}$$

Can also be presented as thus:

$$t = -17.93 \ ln\left(\frac{A_{t1}}{A_{t0}}\right)$$

Where "t" is MRT in years, "$t_{1/2}$" is half-life. "A_{t0}" is the input tritium and "A_{t1}" is tritium in groundwater all in units of "T.U".

- *Carbon isotopes in hydrogeological studies (^{14}C, ^{12}C and ^{13}C)*

Radiocarbon (^{14}C) is a radioactive isotope of carbon with a half-life of 5730 years, which is used to date old groundwater because of its long half-life (Clark and Fritz, 1997; Suckow *et al.*, 2013). ^{14}C is naturally produced in the atmosphere by the nuclear bombardment of nitrogen (^{14}N) to give ^{14}C (Libby *et al.*, 1949; Suckow *et al.*, 2013). This is illustrated in the following nuclear reaction:

$^{14}_{7}N + n \rightarrow {}^{14}_{6}C + p$ where, n=neutron and p= proton.

Atmospheric carbon, including both the stable (^{12}C, ^{13}C) and radioactive (^{14}C) isotopes of carbon, are oxidised to form CO_2 ($^{12}CO_2$, $^{13}CO_2$ $^{14}CO_2$) , which is later assimilated into the plants through plant respiration (Clark and Fritz, 1997). During microbial degradation of dead plants and plant root respiration, CO_2 is released from the dead plant organic matter, thereby increasing the carbon dioxide partial pressure in the soil pores (Appelo and Postma, 2005). Because of the high partial pressure in the soil, as water infiltrates, it dissolves high concentrations of CO_2, much higher than the one dissolved from the atmosphere, thereby yielding high dissolved carbon in water (Clark and Fritz, 1997; Suckow *et al.*, 2013). In solution, radiocarbon unlike the stable carbon isotopes, undergoes radioactive decay, which reduces the amount of ^{14}C in dissolved carbon. Radioactive decay of ^{14}C occurs as follows:

$^{14}C \rightarrow {}^{14}N + \beta^-$

Using the half-life of 5730, ^{14}C is used to date old groundwater using Equation 5.

$$t = -8267 \ln\left(\frac{a_t \, {}^{14}C}{a_0 \, {}^{14}C}\right) \qquad \textit{(Equation 5)}$$

Where $a_t{}^{14}C$ is the carbon-14 value measured from a groundwater sample and $a_0{}^{14}C$ is an initial ^{14}C at recharge (Clark and Fritz, 1997; Suckow *et al.*, 2013).

The stable carbon isotopes ($\delta^{13}C$) are suitable for assessing groundwater evolution (despite the complex recharge processes and groundwater flow patterns) due to great variations of $\delta^{13}C$ values of different carbon reservoirs along the flow path (i.e. biomass, soil carbon dioxide and carbonate rocks) (Clark and Fritz, 1997; Marfia *et al.*, 2004; Appelo and Postma, 2005). The $\delta^{13}C$ in groundwater, therefore, resembles the $\delta^{13}C$ signature of the dissolved carbon source and fractionations among the carbonate species in the solution (Appelo and Postma, 2005).

Because of the high partial pressure of CO_2 in the soil from respiring roots and decomposition of dead plants, the amount of $\delta^{13}C$ is mainly influenced by the type of vegetation that formed the organic matter at the recharge area. The $\delta^{13}C$ values are approximately -26‰ and -13‰ for C3 and C4 plants,

respectively (Marfia *et al.*, 2004; Kohn, 2010). So the infiltrating water maintains the isotopic signature of -26‰ or -13‰ based on the type of vegetation. The openness of groundwater system to soil CO_2 and occurrence of carbonate dissolution influence the evolution of $\delta^{13}C$ in groundwater. In a fully open system, the $\delta^{13}C$ of dissolved inorganic carbon ($\delta^{13}C_{DIC}$) in groundwater is only controlled by the hydrolysis of soil CO_2 (Marfia *et al.*, 2004).

The CO_2 from C3 plants initiates carbon evolution with an approximate value of -26‰ and the hydrolysis process enriches the value with approximately 9‰ (Appelo and Postma, 2005) so that $\delta^{13}C$ in an open system would have an approximate value of -17‰ (Marfia *et al.*, 2004). In a closed system, soil CO_2 and dissolution of carbonates equally control the $\delta^{13}C$ in groundwater, such that dissolution leads to more positive $\delta^{13}C$ (‰) values (Clark and Fritz, 1997; Appelo and Postma, 2005). The carbonate rocks are richer in heavy carbon isotopes with an approximate value of 0‰ (Marfia *et al.*, 2004; Appelo and Postma, 2005). The final $\delta^{13}C$ (‰) value of groundwater in a closed system, therefore, depends on the $\delta^{13}C$‰ value before closure of the system to soil CO_2 and the extent of carbonate dissolution. This usually leads to a value of approximately -13‰ in closed system (Marfia *et al.*, 2004; Appelo and Postma, 2005). However, in a case that dissolution of dolomite occurs in the closed groundwater aquifer, more positive values of $\delta^{13}C$ are also observed (Marfia *et al.*, 2004).

Stable isotopes of carbon have also been applied in various studies for the similar purpose of groundwater flow conditions (Marfia *et al.*, 2004; Awad, 2014; Bhandary *et al.*, 2015).

4.3 Classical water balance approaches

A water budget is an account of water that flows into, out of and stored in a domain or control volume. The domain or control volume is a space of interest where a water budget is applied such as the atmosphere, a surface water body, soil zone either in-situ or in the laboratory, an aquifer, a watershed, etc. (Healy, 2010). The application of the water budget methods is based on the concept of conservation of mass and can be applied over any space and time scale (Healy *et al.*, 2007). Figure 4.2 shows a simplified schematic of a water budget for the soil zone, and Equation 6 (Gee and Hillel, 1988; Healy, 2010) is a mass balance equation for the estimation of drainage as an unknown. P is precipitation, ET is evapotranspiration, R_{off} is surface runoff, ΔS is change in storage and D is drainage, which can also be referred to as potential recharge. The individual components of a water budget equation have to be determined separately, and therefore, the reliability of the calculated recharge depends on the accuracy and precision with which each of the components were measured (Gee and Hillel, 1988).

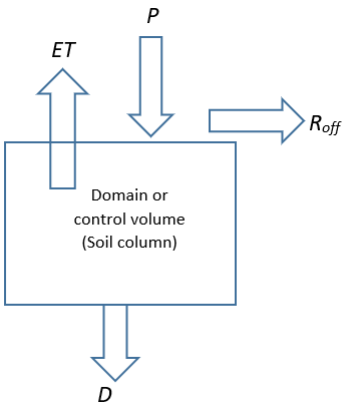

Figure 4.2: A schematic diagram showing a water balance of a water column (Adapted from Healy (2010)).

$$D = P - ET - R_{off} - \Delta S \qquad \textit{(Equation 6)}$$

This section discusses the classical water balance methods, which mainly utilise climate data at a watershed scale to deduce the component of precipitation that becomes groundwater recharge. The method is easy to apply because of easy access to rainfall, temperature and runoff data (Abiye, 2016). However, because of its surficial application, the estimate from classical water balance methods can be referred to as potential recharge rather than actual recharge. Also, since they do not consider the aquifer parameters, they can over or under estimate the recharge value, particularly in the arid and semi-arid areas (Abiye, 2016).

In this study, the Thornthwaite Monthly Water Balance Model by McCabe and Markstrom (2007) is applied to estimate potential recharge.

4.3.1 Thornthwaite Monthly Water Balance Model (TMWBM)

The Thornthwaite Monthly Water Balance Model (TMWBM) runs on a graphical user interface (GUI) by McCabe and Markstrom (2007). This GUI is a product of the United States Geological Survey and it can be obtained from https://wwwbrr.cr.usgs.gov/projects/SW_MoWS/Thornthwaite.html together with its documentation. It is simple to apply, as it only requires the mean monthly temperature in degrees Celsius and monthly total precipitation in millimetres. There are seven other input parameter that are used by the model and set on the GUI, which include runoff factor, direct runoff factor, soil-moisture storage capacity, latitude of the study area in decimal degrees, rain temperature threshold, snow temperature threshold, and maximum snow-melt rate of the snow storage (McCabe and Markstrom, 2007). These parameters are adjusted on the GUI window shown in Figure 4.3.

The monthly total precipitation data provides an input of water into the model, while the mean monthly temperature controls whether precipitation is in the form of snow or rainfall and provides the energy for some of the processes such as evapotranspiration. The components of the water balance that are computed by TMWBM are snow storage, direct runoff, evapotranspiration, soil-moisture storage and surplus. These are briefly described below and are computed monthly based on the parameters set on the GUI window and the data input.

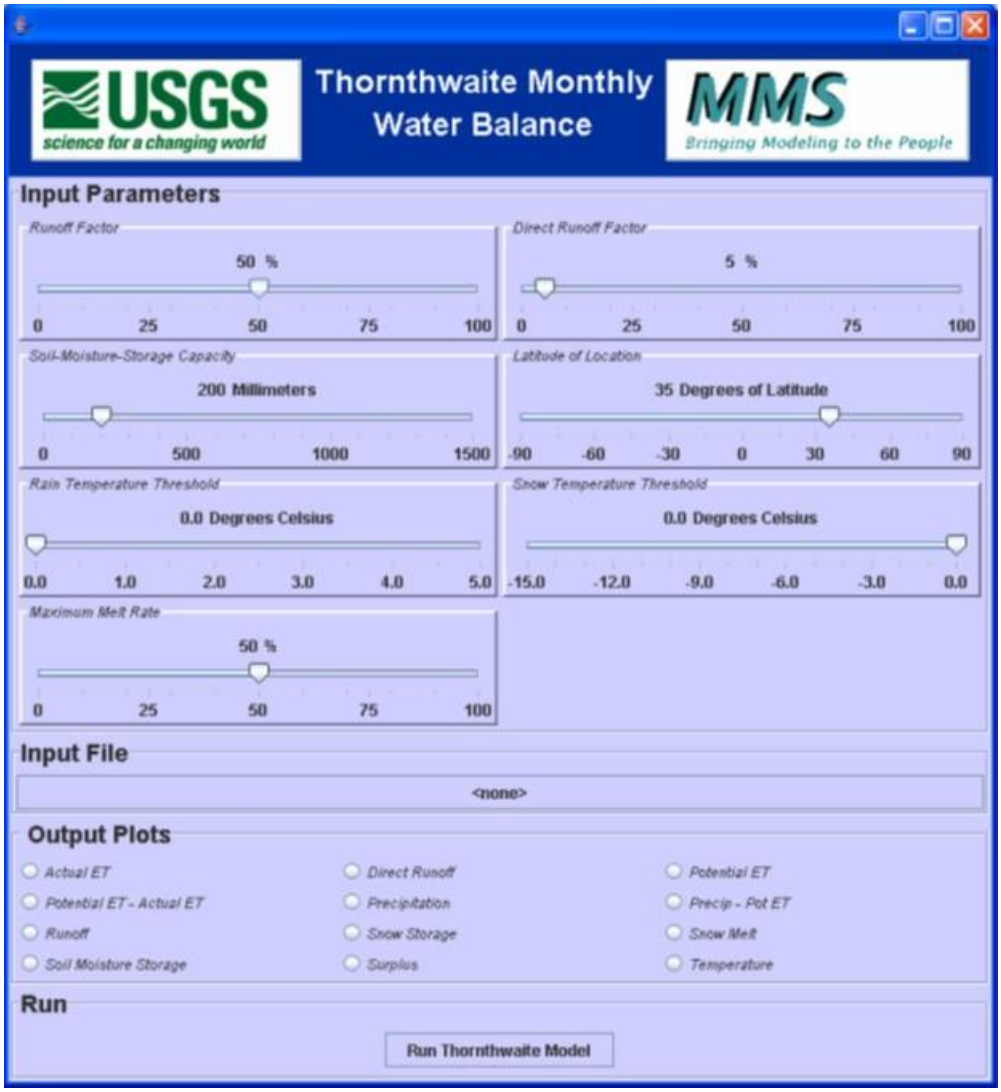

Figure 4.3: The Graphical User Interphase for TMWBM (Source: USGS).

TMWBM computes whether monthly precipitation is in the form of rain (P_{rain}) or in the form of snow (P_{snow}). The computation is based on the mean monthly temperature and the user specified values of rain temperature threshold (T_{rain}) and snow temperature threshold (T_{snow}). T_{rain} is the temperature above which all precipitation is rainfall, while T_{snow} is the temperature below which all precipitation is snow. Therefore, if the mean monthly temperature is less than T_{snow}, then precipitation is in the form of snow and if it is greater than T_{rain}, then precipitation is in the form of rain. The form of precipitation in the temperature range between T_{snow} and T_{rain} will change proportionally from 0% P_{rain} at T_{snow} to 100% P_{rain} at T_{rain}.

Once the form of precipitation has been set, direct runoff (DRO) is computed from $P_{rain,}$ while P_{snow} adds to snow storage (*snostor*), which has to go through further melting. DRO constitutes the amount of water that becomes runoff as a result of impervious surface or oversaturation of the soil. It constitutes an output from the model. The parameter direct runoff factor (*drofact*) represents the fraction of rainfall (P_{rain}) that becomes DRO, which is computed through this relationship; $DRO=P_{rain}$ *x drofact.* The *drofact* is computed separately for the catchment of study, however, some references have adopted the use of 5% (McCabe and Markstrom, 2007; Bakundukize *et al.*, 2011). From the computed DRO, the amount of water that remains in the model (P_{remain}) is computed by $P_{remain} = P_{rain} - DRO$.

From the computed *snostor*, the fraction of snow storage that melts per month (SMF) is computed using the mean monthly temperature (*T*) and the user-specified maximum melt rate (*meltmax*), which is often set to 0.5 (McCabe and Wolock, 1996). Then, the amount of snow that is melted in a month (SM) is computed as a product of SMF and the amount of snow storage (*snostor*). The SM is then added to the previously calculated P_{remain}, which together constitute a water input into the soil (P_{total}) through infiltration process.

TMWBM estimates Potential Evapotranspiration (PET) using the Harmon equation (Hamon, 1961) $PET_{hamon} = 13.97xdxD^2xW_t$, where *d* is the number of days in a month and *D* is the mean monthly hours of daylight in units of 12 hours. W_t is a saturated water vapour density term in grams per cubic meters calculated as $w_t = \frac{4.95xe^{0.062xT}}{100}$, where *T* is the mean monthly temperature in degrees Celsius. Thus, PET is the amount of water that would be lost through evapotranspiration if there was an unlimited supply of water, while Actual Evapotranspiration (AET) represents the actual water loss for the period.

Soil moisture storage represents the amount of water that is stored in the soil from the infiltrated P_{total} and it is computed based on the soil moisture storage capacity, which is the amount required for the soil to reach field capacity. If P_{total} for a given month is greater than *PET*, then the excess water is added to the soil moisture value of the previous month and if the soil reaches field capacity, then the excess water is converted to runoff and recharge. A deficit occurs when P_{total} is less than *PET*, indicating that there is no excess water and a surplus occurs when P_{total} is greater than PET indicating that there is an excess of water, at the time when the soil is at field capacity.

This method does not account for preferential flow because it assumes field capacity before potential recharge could occur, whereas preferential flow does not require field capacity to be satisfied. It is also biased towards precipitation being higher than PET for recharge to occur. However, recharge can still occur even if PET is greater than precipitation through what is called episodic recharge. Episodic recharge occurs during days of high-intensity precipitation where precipitation exceeds PET for that day (Van Wyk, 2010; Abiye, 2016). In such cases it is likely that precipitation will be greater than PET, while the overall monthly values indicate PET greater than precipitation, thereby wrongfully indicating zero recharge. Under preferential conditions, recharge can occur without the soil moisture being at field capacity, meaning that TMWBM may underestimate recharge in the crystalline and karst outcrops where recharge occurs through fractures and cavities.

The Harmon equation has been successfully applied to estimate PET in different studies. However, since the TMWBM does not use surface water data to calibrate for its parameters, this places a lot of dependency on the GUI input parameters such that their lack of accuracy leads to erroneous estimates of intermediate parameters such as DRO and the final potential recharge value.

4.4 Physical methods of estimating groundwater recharge

4.4.1 Methods based on surface water data

The primary target of the methods that use surface water data for recharge assessment is the quantification of the exchange between groundwater and surface water.

Some surface water methods such as the baseflow separation method segregate stream flow into baseflow and surface runoff (Rutledge, 1998; Healy, 2010). The baseflow is used as a proxy for the estimation of diffuse recharge in a catchment because a gaining stream is a result of diffuse recharge that occurred upstream of the discharge gauging station (Healy, 2010). The use of baseflow to

estimate diffuse recharge assumes that: 1) All groundwater that recharged in the watershed eventually discharges into the stream, 2) The low flows entirely consist of baseflow, 3) The discharge that is measured at the watershed outlet constitutes water that recharged within the boundaries of that watershed, such that there is no trans-basin groundwater flow. It, therefore, means that the accuracy of the recharge estimate depends on the validity of the above assumptions for the study area.

In areas underlain by shallow crystalline bedrock, assessment of baseflow as a proxy for recharge should be done with caution since discharge into the stream may actually be dominated by interflow. This is illustrated in Figure 4.4 (a) where groundwater from the saturated zone flows into the stream channel as baseflow and (b) showing interflow from a patched aquifer flowing laterally into the stream channel.

The release of water from the riparian bank storage could also lead to errors because the flow is a result of short-term fluctuations in surface water that is not from the main terrestrial aquifer (Scanlon *et al.*, 2002). The amount of interflow in this case could be erroneously interpreted as baseflow.

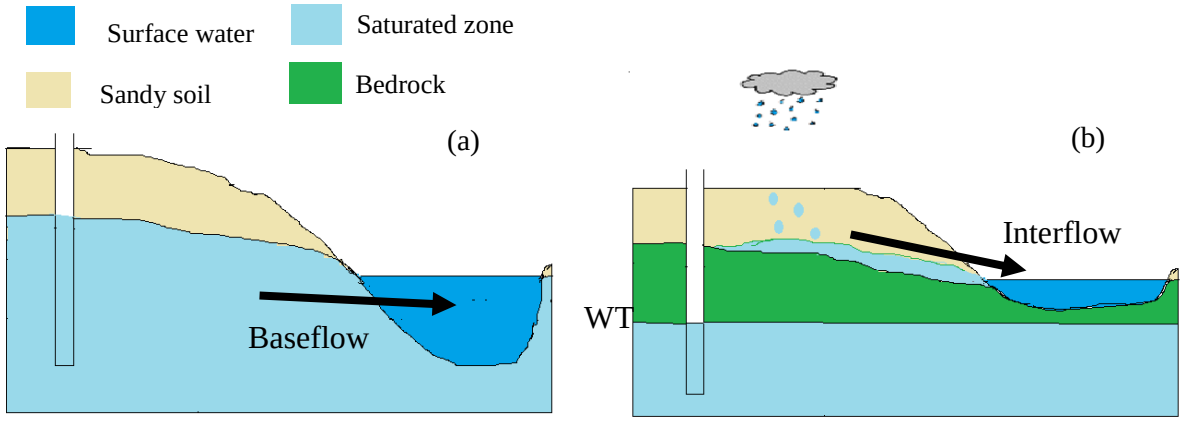

Figure 4.4: An illustration of baseflow and interflow into the stream channel (WT: Water table).

Some surface water methods such as stream segment water budget and reservoir water budget are based on the water budget approach, where the exchange between surface water and groundwater is the only unknown, while the amount of rainfall, evaporation, surface water inflow and outflow are known (Healy, 2010). Such an approach gives an estimate that is integrated in space and time because at any time or space, the surface water body may be losing or gaining, as a result, the integrated estimate gives only the net flux between groundwater and surface water. However, point estimates can be obtained by constructing a water budget on a more specific portion of the water body, for example, a shorter stream segment. The cylinder seepage meters by Lee (1977), can also be applied on a small area in the sediments to determine the net exchange between groundwater and surface water over an area as small as 0.25 m^2 (Rosenberry *et al.*, 2008). Rosenberry and LaBaugh (2008) discussed the different surface water based field techniques that can be used to estimate the exchange between groundwater and surface water. This exchange may not be quantitatively used as an estimate of recharge, but it is an estimate of the net difference between gains and losses in the given period (Richard Healy, personal communication, 9 April 2018).

Surface water methods are, however, said to be more applicable in the humid and sub-humid areas mainly because of the availability of surface water data. Surface water data are often scarce and too short term in the arid and semi-arid areas because groundwater levels are often deep, such that there

is not much baseflow and streams are predominantly losing and ephemeral. It is evident, therefore, that if there is no surface water, then the use of surface water methods is pointless and if the stream flow is too short term, estimation of focused recharge is also too temporal and almost impossible.

4.4.2 Methods based on the saturated zone/groundwater data

Groundwater level data is commonly included in groundwater monitoring activities, as a result, this type of data is often available making the use of groundwater methods for recharge estimation much more common (Healy and Cook, 2002; Healy, 2010).

As it has been discussed in section 3.1, recharge is the addition of water into groundwater storage. Therefore, following a rainfall event, the rise of a groundwater level in a monitoring well can be an indication that groundwater recharge has occurred. The methods that use groundwater level data estimate recharge based on the rise in groundwater levels with time. If a groundwater level rise is measured from a single monitoring borehole, a point recharge estimate can be obtained, otherwise, an integrated estimate can be obtained if multiple monitoring boreholes that are distributed in an aquifer are used (Healy, 2010). However, Healy and Cook (2002) stated that because a rise or fall of a groundwater level in a monitoring borehole represents a water table behaviour for the larger area, a groundwater recharge estimate that is obtained from a single monitoring borehole can be regarded as more of an integrated estimate than a point estimate.

The use of these methods is challenging because groundwater levels may rise even if no recharge has occurred and recharge could still be occurring even when there is no resultant rise in water level (Meinzer, 1923; Healy and Cook, 2002; Crosbie *et al.*, 2005; Healy, 2010). The probable dynamics that cause a groundwater fluctuation must, therefore, be well understood prior to recharge assessment in order to establish a basis and reality of the underlying assumptions related to these methods.

If the rate of groundwater abstraction from the aquifer exceeds recharge, a rise in water level will not occur although recharge is occurring (Meinzer, 1923). Furthermore, if a prolonged pumping activity is terminated or the land use change that involves clearing of deep rooted trees is done, the groundwater level could be seen rising (Albhaisi *et al.*, 2013). Evapotranspiration may also cause diurnal and seasonal changes in groundwater level fluctuations. The lack of evapotranspiration at mid night leads to a rise in groundwater level, which is followed by a drop during day time. Similarly, the low evapotranspiration in winter may lead to a rise in water level, while the high evapotranspiration in summer leads to a decline in groundwater level, particularly at the time when there is no summer rainfall (Healy, 2010).

At high atmospheric pressure, groundwater levels in a borehole column may drop and rise at low pressure (Healy and Cook, 2002). Also, as water percolates rapidly through the fine textured unsaturated zone, the flux may form a saturated blanket that has entrapped air underneath it, giving a false risen water level, a condition known as the Lisse effect (Krul and Liefrinck, 1946). Or the rapid infiltration into crystalline aquifers may lead to the saturated rock fractures, while the primary pores of the rock matrix remain unsaturated giving a false elevated water table. Therefore, the ability to identify and quantify these causes of uncertainties, influences the accuracy of the recharge value.

The most commonly applied technique in the saturated zone is the Water Table Fluctuation method, which utilises the rise in water level and a specific yield of the aquifer material at the fluctuation depth (Rasmussen and Andreasen, 1959; Healy and Cook, 2002). Other methods combine groundwater level data with groundwater withdrawal such as a lumped parameter model EARTH (Van der Lee and Gehrels, 1990; Wang *et al.*, 2018), others combine with rainfall amount such as

Cumulative Rainfall Departure (CRD) (Bredenkamp *et al.*, 1995; Van Tonder and Xu, 2000) and others use Darcy equation such as Theis method (Theis, 1937).

- *Water Table Fluctuation method (WTF)*

The WTF method requires the measured rise in groundwater level and a specific yield value of the geological material (Meinzer, 1923; Rasmussen and Andreasen, 1959). The rise is the difference in depth between the peak of the groundwater hydrograph and the vertical point downwards on the antecedent recession curve (Healy, 2010) as shown in Figure 4.5.

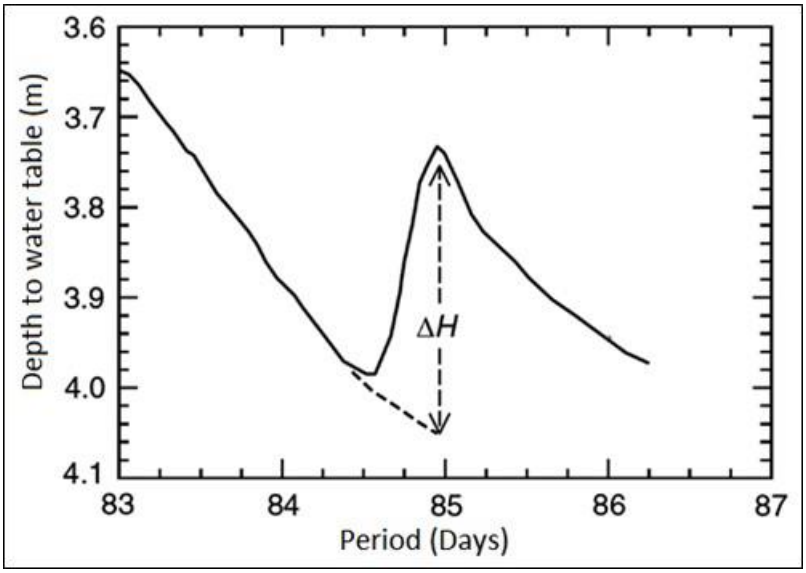

Figure 4.5: Hypothetical graph showing the magnitude of Δh measured from peak of the groundwater hydrograph to the point on the antecedent curve.

The antecedent recession curve is the trace that the hydrograph would have followed had there not been any rise in groundwater level (Rasmussen and Andreasen, 1959; Healy, 2010). The rise is measured from the antecedent curve so that the true recharge can be estimated, which accounts for the ongoing discharge of groundwater that is represented by a continuation of the recession curve (Rasmussen and Andreasen, 1959). Recharge can also be calculated for each rise in groundwater level. In order to arrive at a recharge value in units of depth (mm), the rise in water level is multiplied by the specific yield value (Rasmussen and Andreasen, 1959; Healy and Cook, 2002; Healy, 2010), as shown in Equation 7.

$$R = \Delta h/\Delta t * Sy \qquad (Equation\ 7)$$

Where, Sy is a unit-less specific yield, Δh is change in water level ($in\ mm$) and Δt is the period of water level increase.

In the application of WTF, caution should be taken to identify the appropriate geological material at the fluctuation depth so that an appropriate specific yield value can be used. Assuming that the geological material above the water table is at field capacity, then the recharge water that causes a rise of the water table occupies the effective porosity of the geological material. Effective porosity, also referred to as specific yield (Meinzer, 1923; Krešić, 2007), is the component of pore-water that can be drained due to gravity leaving behind retention porosity (field capacity) (Healy and Cook, 2002). Because different geological materials have different hydraulic parameters, in a multi-layered aquifer, the appropriate specific yield value is for the geological material at the depth where water

level rise took place. Figure 4.6 presents a schematic for a fluctuating water table in a multi-layered geological setting and the appropriate material at each water level rise.

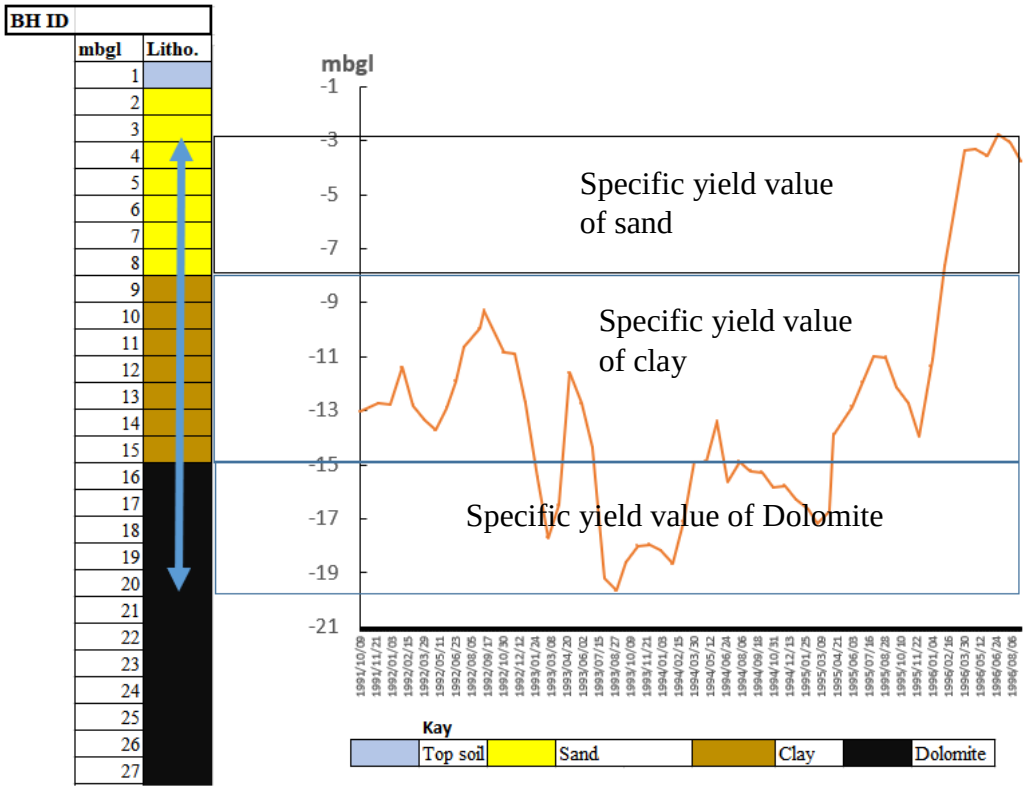

Figure 4.6: An illustration of a groundwater level fluctuation in a multi-layered geological setting.

The specific yield of an aquifer can be estimated through various methods that have been documented by Neuman (1987), Healy and Cook (2002) and Healy (2010). They include laboratory, theoretical and field pumping test methods. The accuracy of the WTF depends on the accurate estimations of specific yield, which is challenging to estimate (Cuthbert *et al.*, 2016) and is a major limitation in the application of WTF.

The advantage of the WTF method is that it is insensitive to the mechanism by which water moves through the unsaturated zone and it can be applied in aquifers that are recharged through preferential flow (Healy and Cook, 2002). Another advantage is that since the water level changes observed in a monitoring well are representative of a larger area, the recharge estimate obtained is not really a point estimate but it is more integrated in space compared to the unsaturated zone methods (Healy and Cook, 2002; Healy, 2010). Healy and Cook (2002) highlighted the following limitations of the method:

- The method is best suited for shallow water tables that display immediate water level rises and declines. However, the method has been applied with success in aquifers that only show seasonal water level fluctuations.
- It is challenging to identify the fluctuations that are a result of recharge.
- The method cannot account for the steady rate of recharge that is less than or equal to the drainage away from the aquifer leading to a declining or static water level.
- The method is very sensitive to the specific yield value and calculating the value is very challenging.

4.5 Watershed modelling methods

The principle that makes watershed models applicable in assessing groundwater recharge is that they are based on a water budget equation (Healy, 2010). They distribute precipitation falling on the land surface into interception, evapotranspiration, runoff, infiltration, recharge etc., depending on the prevailing climate variables and the user specified physical makeup of the land and sub-surface (Markstrom *et al.,* 2015). And, in order to improve the precision of the model and to ensure that the simulated fluxes are in agreement with reality, the watershed models often use all or any of the following measured variables; surface water discharge, solar radiation, potential evapotranspiration etc., to calibrate the model simulated values (Hay and Umemoto, 2007). If a model is well calibrated, then the component of recharge can be determined.

Predictive simulations can be run on a well calibrated model to assess how the hydrology of the catchment would be affected by the changes in climate and land cover by altering the precipitation, temperature and land cover in different scenarios. Healy (2010) identified the following watershed models as the most used; Soil and Water Assessment Tool-SWAT (Arnold *et al.,* 1998), Precipitation Runoff Modelling System-PRMS (Leavesley *et al.,* 1983), and MIKE-SHE (Graham *et al.,* 2006). The model used in this study is PRMS.

4.5.1 Precipitation Runoff Modelling System

The Precipitation-Runoff Modelling System (PRMS) is a modular, deterministic, distributed-parameter, physical-process-based hydrologic simulation code developed by the United States Geological Survey to evaluate the effects of various combinations of climate, physical characteristics, and simulation options on hydrologic response and water distribution at the watershed scale (Leavesley *et al.,* 1983; Markstrom *et al.,* 2015; Regan and LaFontaine, 2017). The previous versions of PRMS are documented in Leavesley *et al.* (1996), Markstrom *et al.* (2008), Markstrom *et al.* (2015) and Regan and LaFontaine (2017).

In PRMS, a watershed is spatially discretised (usually through a geographical information system (GIS) analysis (Markstrom *et al.,* 2015)) into smaller units called Hydrologic Response Units (HRU) of which each is assumed uniform and unique in the defined properties. HRU properties are defined by the user through a series of PRMS parameters, which specify the physical characteristics of the HRUs and computation coefficients to PRMS. Slope, aspect, land cover, soil type, elevation (z), latitude (y) and longitude (x) of the HRUs etc., are specified by the user in the Parameter File (parameter.dat) as well as the elevation, latitude and longitude of climate stations, flow and storage computation coefficients such as evapotranspiration, streamflow routing, soil water storage capacities, groundwater flow coefficients etc. The climate and stream flow data are specified in the Data File (data.dat), while the model execution information, simulation options and output variables are specified in the Control File (control.dat). These files are well documented in Markstrom *et al.* (2015).

PRMS distributes climate data (temperature and precipitation) from the climate stations to each HRU on daily basis. The amounts of distributed daily temperature and precipitation are decided by PRMS based on the geographical parameters (elevation, longitude, latitude etc.) of the HRUs relative to those of the climate stations. Once climate variables have been distributed, various amounts of water are apportioned into interception, through-fall, snowpack, evaporation, sublimation, snowmelt, runoff, infiltration, interflow, recharge, baseflow, etc., (Figure 4.7) based on climate conditions, antecedent storages and the various parameters that define the physical characteristics and computational coefficients of each HRU. After evapotranspiration and soil moisture storage, the

excess infiltration water will become groundwater recharge. A part of groundwater recharge will become baseflow into the stream network such that the surface runoff (Hortonian and Dunnian), interflow and baseflow will represent the PRMS simulated total daily stream discharge at the outlet of the catchment. All these processes and their interconnectedness are shown on Figure 4.7.

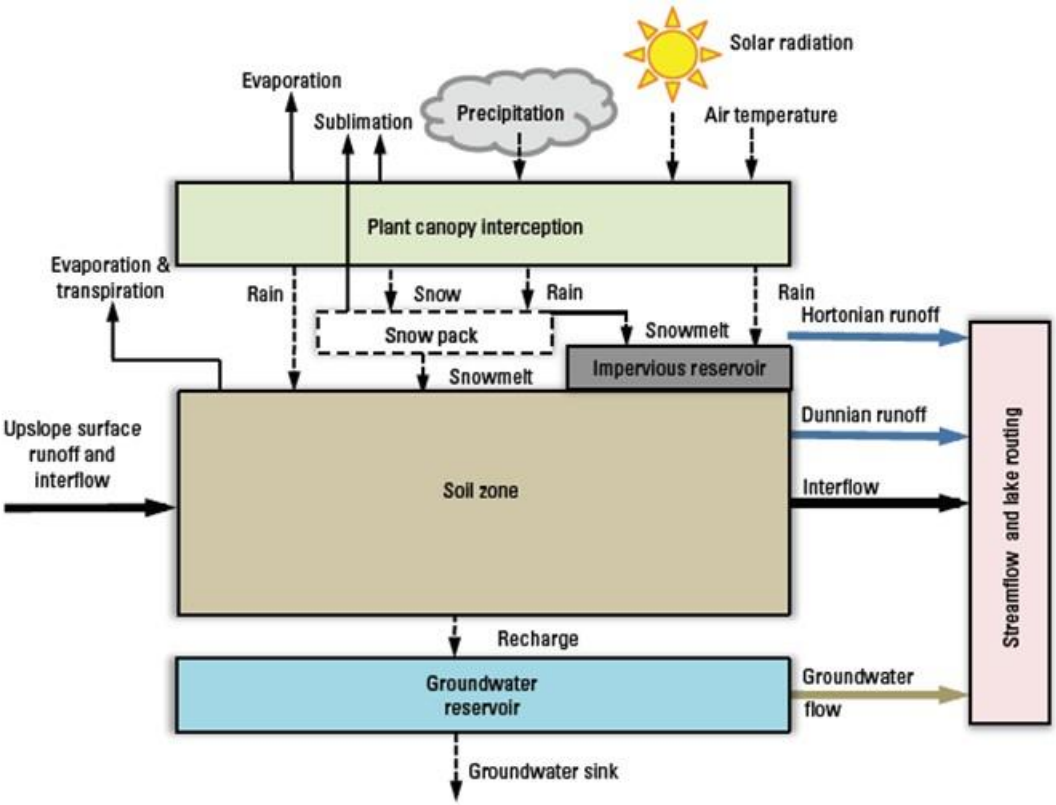

Figure 4.7: Hydrologic processes simulated by Precipitation-Runoff Modelling System (adapted from Markstrom *et al.* (2008) and Markstrom *et al.* (2015)).

In PRMS, simulated discharge can be used to calibrate the model against the measured discharge values (from the stream gauging station). The PRMS produces several output files including the statistic variable file, which shows the output variable fluxes and storages per day for the entire basin or for the user selected HRUs. More information on the software requirements and operation of PRMS is given in the user's manual (Markstrom *et al.*, 2015).

Since rainfall is a source for recharge and temperature is a major driver of evapotranspiration, groundwater recharge and baseflow simulations are expected to show sensitivity to changes in climate variables during a PRMS simulation. Because of this, PRMS has been applied and proven successful in simulating the catchment hydrological response to changes in climate variables in different parts of the world. Apart from the numerous applications of PRMS in the United States of America, PRMS has also been applied in the tropical West Africa, Ethiopian Rift Valley in the Meki River to determine the impacts and sensitivities of streamflow to changes in land use and climate (Legesse *et al.*, 2003; Legesse *et al.*, 2010a; Legesse *et al.*, 2010b) and the impacts of land use and climate on groundwater recharge (Abiye *et al.*, 2009). Different watershed modelling studies have been conducted in Southern African region (Schulze, 2000; Ncube and Taigbenu, 2008), but currently, there is no record of published work on the applications of the U.S. Geological Survey PRMS in the region.

5 RESEARCH METHODOLOGY EMPLOYED

5.1 Desktop review and data collection

The desktop study involved an inventory of available data sources for all existing hydrometeorological, hydrogeological and geological data within the UCRB. The hydrometeorological data consisting of precipitation and maximum and minimum air temperatures were obtained from the South African Weather Services (SAWS), while the pan-evaporation as well as the stream discharge data were downloaded from the Department of Water and Sanitation of South Africa (DWS), Hydrological Services. The hydrogeologocal data consisting of groundwater levels, borehole lithology and borehole construction data were obtained from the National Groundwater Archives (NGA) (http://www3.dwa.gov.za/NGANet/HomeForm.aspx). The shape-files for the geological maps were obtained from the Council for Geosciences (CGS), while the Digital Elevation Model (DEM) was obtained from the United States Geological Survey (USGS) Earth Explorer (https://earthexplorer.usgs.gov/).

5.2 Aquifer characterisation

The groundwater levels and borehole lithological logs were studied to classify aquifers as confined and unconfined and to determine the suitability of the WTF method. The confined aquifer was identified by the low permeability material at the upper boundary and the water level that rises above the top of the aquifer or the water level that is significantly higher than the water strike depth as a result of the piezometric pressure (Freeze and Cherry, 1979). On the other hand, the unconfined aquifer was observed by the water level resting at the water table within the aquifer material (Freeze and Cherry, 1979; Krešić, 2007). This analysis was done for the boreholes in the basement granites and in the dolomite aquifers.

The NGA lacked long-term groundwater level data for boreholes in the granites. For most boreholes, the NGA only had a single water level value that was measured after construction of the borehole. Because of this, the water level analysis was based on limited values, which likely created bias. As for the boreholes in the dolomites, the analysis of the groundwater level fluctuation, the lithology at fluctuation and the position of the water strike were integrated to classify the aquifer.

Figure 5.1 shows the locations of boreholes that were selected for aquifer characterisation in the granites.

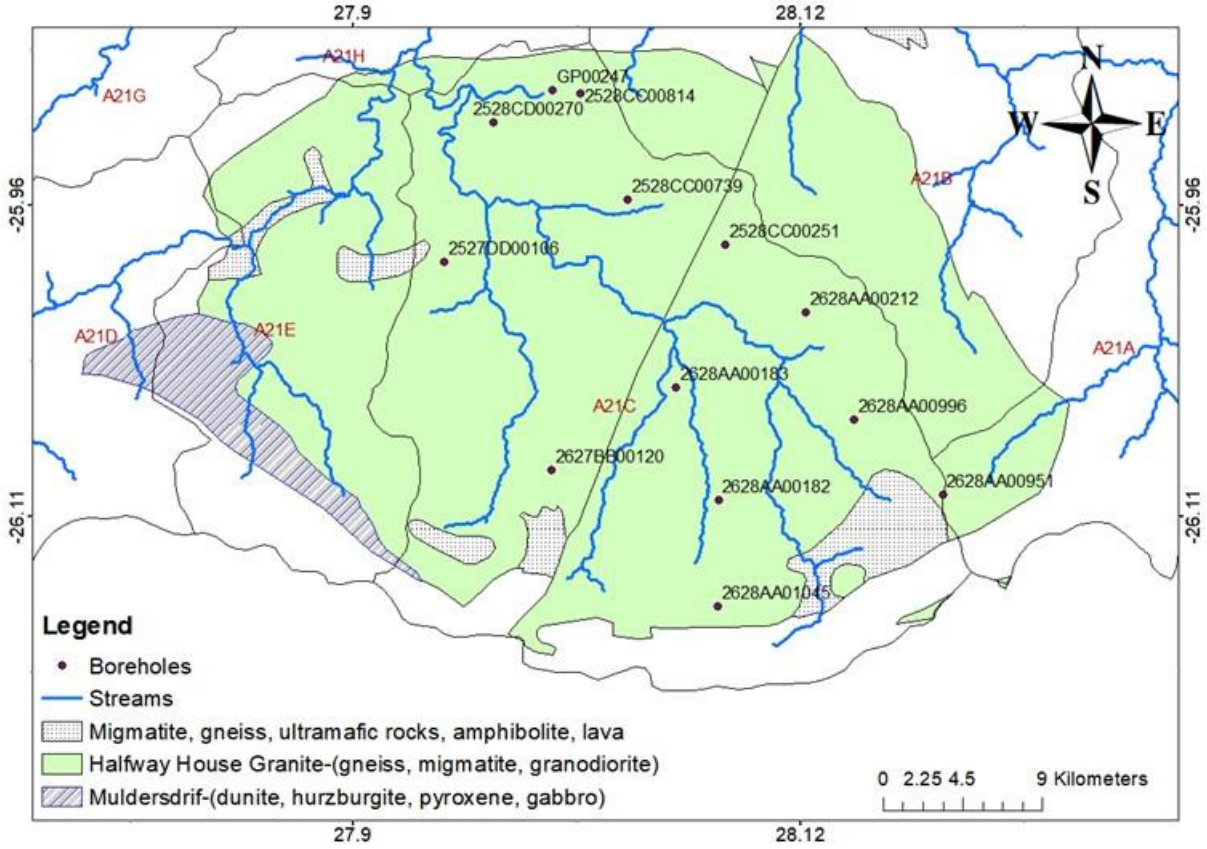

Figure 5.1: Locations of boreholes used for aquifer characterisation in the granites.

Healy and Cook (2002) emphasised that the WTF method disregards the path through which recharge occurs and stated that the method can be applied if the groundwater level responds to rainfall. Therefore, in addition to the lithology analysis, the hydrograph analysis also included assessing the response of groundwater levels to rainfall as a suitability measure for WTF (section 5.5.5).

5.3 Assessment of baseflow versus interflow occurrence in the streams that are underlain by the basement granites

5.3.1 Assessment using borehole information and stream channel elevation

In preparation for the application of surface water methods, an analysis of the hydraulic head difference between groundwater levels and surface water was done to determine the possibilities for baseflow versus interflow occurrence in the area that is underlain by the granites. The borehole elevation, groundwater level, depth to water strike and the top of the granite bedrock were compared with the elevation of the nearby adjacent stream channel. In a case that the borehole water level was more elevated than the stream channel, possibilities of baseflow occurrence were deduced, while the possibilities of stream loss were deduced where the stream channel is more elevated than the borehole water level. The possibilities of interflow were observed where the granite bedrock in the borehole is more elevated than both the groundwater level and the stream channel, indicating that infiltrating water may undergo lateral flow on the bedrock towards the stream channel. However, an assessment of structural lineaments between the borehole and the stream channel was not done. Anhaeusser (1973) indicated that the basement is intersected by numerous shear zones and dykes. If these lineaments exist between the borehole and the stream channel, then they could be responsible for diverting groundwater flow direction or creating a no-flow boundary, thereby, rendering the influence of water head difference insignificant.

Figure 5.2 shows the locations of the boreholes and the adjacent points along the surface water channels that were used in this analysis.

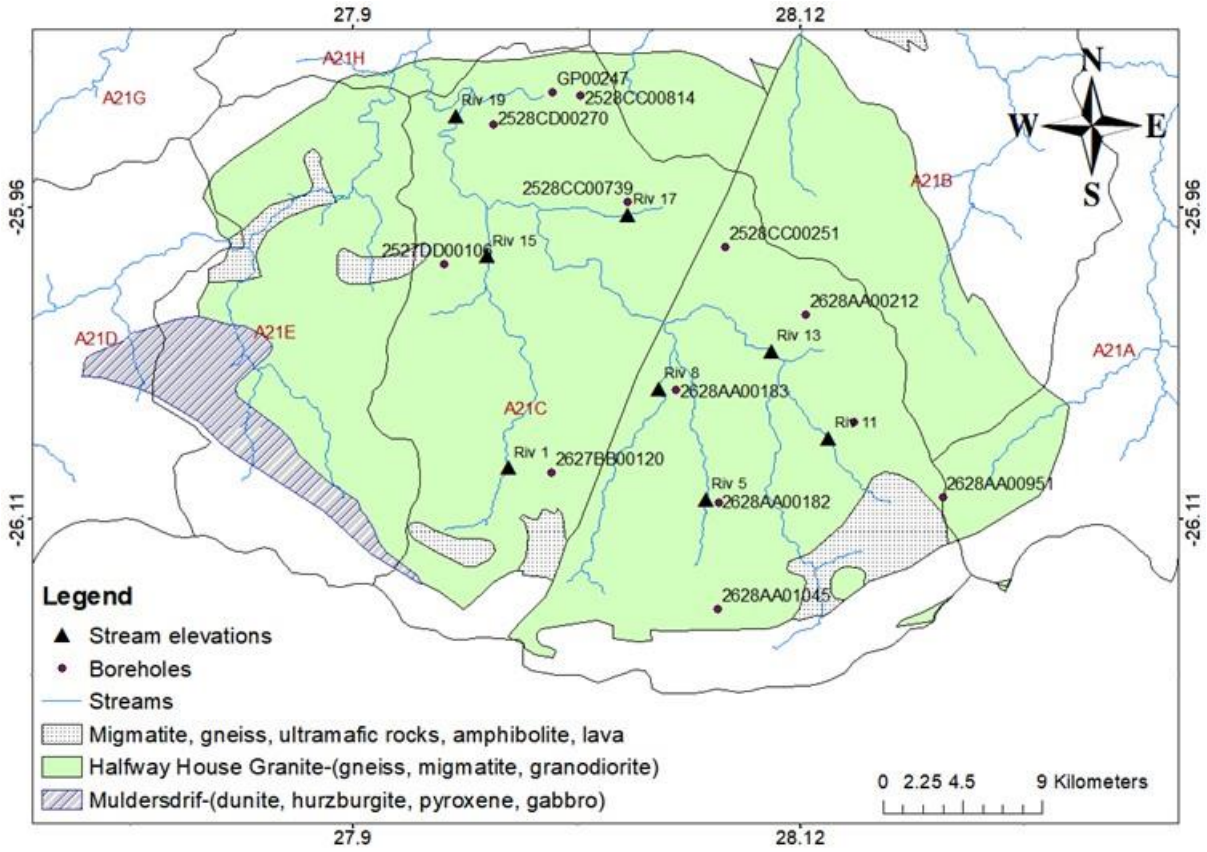

Figure 5.2: Locations of boreholes and adjacent river points.

5.3.2 Assessment using piezometers in the stream that is underlain by the granites

Two piezometers were constructed, one on the east and another on the west of the Montgomery stream that is underlain by the granites and flows towards the north direction, discharging into the Jukskei River. The water levels were measured in the piezometers and in the stream channel, in both cases using the height of the piezometers as a reference point (Figure 5.3). Measurements were done once a month between June 2016 and September 2016 and each time a 10 ml sample was collected for stable isotope analysis from the piezometers and the stream. This analysis was specifically done during the dry period because the focus was to determine if there is contribution of interflow to baseflow during dry periods also because wet seasons were prone to flooding that destroyed the piezometers and disrupted the monitoring program.

The stable isotope samples were analysed at the University of the Witwatersrand. The stable isotope data and the differences in water levels were used to determine the interaction between the piezometers and the stream, while additionally, the differences in water levels were also used to determine the direction of flow.

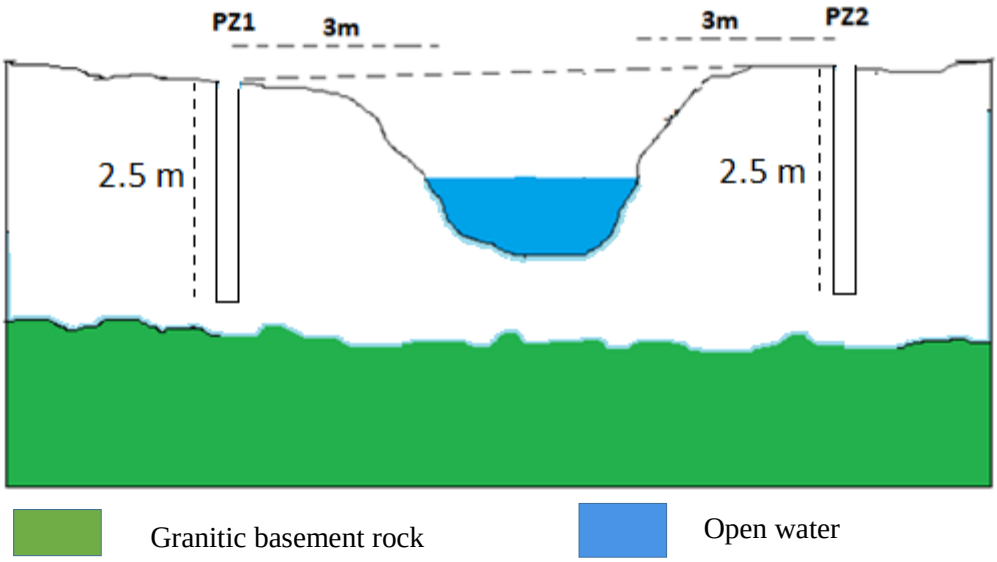

Figure 5.3: Construction of the piezometers across Montgomery stream (NB: not drawn to scale).

5.4 Applications of chemical and isotope tracer methods

5.4.1 Sampling and field work procedure

Daily rainfall was sampled for stable isotope analysis for three years at the two stations; one at the University of the Witwatersrand and another at Montgomery Park in Johannesburg, (Figure 5.4) using a graduated conventional rain gauge shown in Figure 5.5. Stable isotopes were collected in a 10 ml glass bottle. The daily rainfall samples were collected immediately after rainfall to avoid sample evaporation. The daily samples consisted of a composite of different rainfall events on days where multiple events took place. Two tritium samples from different rainfall events were also collected in 500 ml plastic bottles.

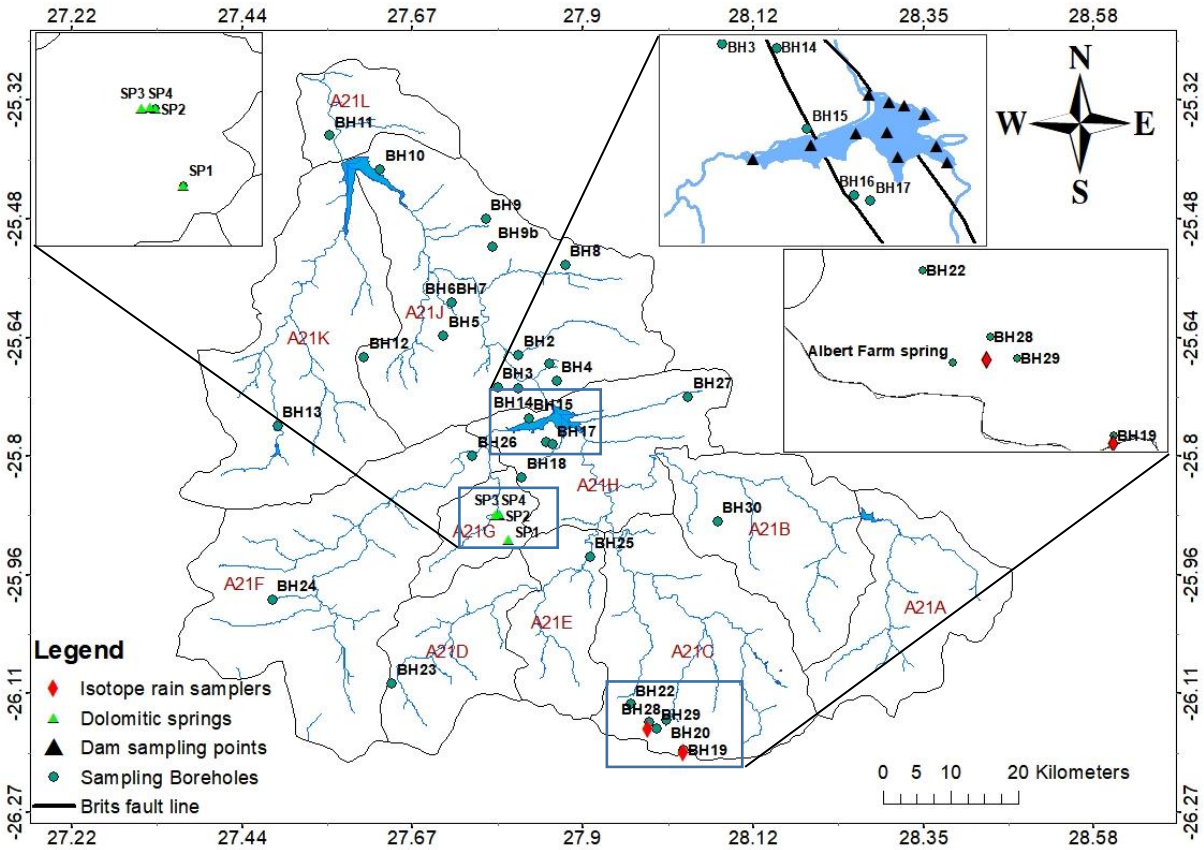

Figure 5.4: Locations of sampling points for groundwater, surface water and rainfall.



Figure 5.5: The type of rainfall sampler used in this study.

Groundwater samples were collected from privately owned boreholes within the UCRB for stable isotopes and tritium between June 2016 and February 2017, while the Albert Farm spring in Johannesburg was sampled for stable isotope analysis on monthly basis from June 2016 to June 2018. Sampling for carbon isotopes was also done at Albert Farm spring, at the Malmani dolomitic springs and at the 15 boreholes that were selected across the UCRB in the different lithological units. Surface water samples were also collected in 2016 for stable isotopes and tritium analysis from Hartbeespoort Dam, using a speed boat. The sampling points are all shown in Figure 5.4.

The discharge of the Albert Farm spring was monitored for a period of 14 months between February 2017 and May 2018 using a float method. Because of the hard rock nature of the underlying channel, only a maximum straight channel of 2 meters could be identified where the measurements were made. The width (w) of the 2-meter channel and the depth (d) of water were measured. Cross-sectional area (A) was obtained in m^2 as a product of channel width (w) and depth (d) across the flow. Two points were marked along a straight channel as the initial point (i) and final point (j), with their separation distance represented by the length of channel (l). The time (t) taken for a styrofoam piece to float from point "i" to "j" was measured using a stopwatch in six tries to minimise errors. The discharge (Q) was then determined as the product of cross-sectional area (A) and the length of channel (l) divided by the time of flow (t) (Equation 8). According to Shaw (2005), the discharge calculated from the velocity has to be adjusted by multiplying it with a correction factor in order to account for the roughness and size of the stream because the velocity is not uniform across the channel. The discharge was multiplied by the correction factor of 25%. The value for the correction factor was obtained from Hydromatch (https://www.hydromatch.com/sites/default/files/downloads/DIY-flow-measurement-guide.pdf) for a shallow rocky stream.

$$Q\ (m^3/s) = \frac{(w*d*l)}{t} \qquad \textit{(Equation 8)}$$

During sampling for ^{14}C and $\delta^{13}C$, the drum was filled with 50 L of sample water and carbonate free NaOH was added to raise the pH into alkaline media. A dash of phenolphthalein was added as a pH indicator to give the solution a pinkish colour ensuring that the pH remains alkaline. Barium chloride ($BaCl_2$) solution was prepared separately with sample water and poured into the drum to precipitate barium carbonate ($BaCO_3$). While all these are added, the drum was shaken to ensure homogeneity of the reagents. $BaCO_3$ precipitate was then separated from the supernatant, transferred into the 500 mL bottle and submitted for analysis at iThemba Laboratories, Johannesburg, South Africa. The sampling procedure is shown in Figure 5.6, where (a) shows the addition of $BaCl_2$ solution into the drum, (b) shows the shaking of the solution and (c) shows the draining of the supernatant from the precipitated $BaCO_3$. The detailed sampling procedure is provided in Appendix A.



Figure 5.6: Sampling procedure for ^{14}C and $\delta^{13}C$ using the drum method.

Stable isotopes of $\delta^{18}O$ and $\delta^{2}H$ were analysed at the University of the Witwatersrand using the Liquid Water Isotope Analyzer-model 45-EP. The instrument contains the laser analysis system, internal computer, liquid auto-sampler, a small membrane vacuum pump, and a room air intake line that passes air through a drierite column for moisture removal. 1 to 1.5 mL aliquot of a sample was pipetted into a 2 mL glass vial, which is capped with a Polytetrafluoroethylene (PTFE) septum cap. Hamilton microliter syringe was used to inject 0.75 µL of sample through a PTFE septum in the auto-sampler. The injection port of the auto-sampler was heated to 46°C to vaporize the sample under vacuum conditions immediately upon injection. The vapour was then passed down the transfer line into the pre-evacuated mirrored chamber for analysis. Five standards were used in the analysis procedure where the laser machine automatically calibrates itself and measures stable isotope values for each water sample. The laser machine is capable of providing accurate results with a precision of approximately 1‰ for $\delta^{2}H$ and 0.2‰ for $\delta^{18}O$ in liquid water samples of up to at least 1000 mg/L dissolved salt concentration.

Tritium samples were analysed at iThemba Labs in Johannesburg using electrolytic enrichment procedure. The 500 mL samples were distilled with sodium hydroxide (NaOH) and then enriched by electrolysis. This electrolysis enrichment was performed through application of 10-20 Amp electric current, which led to reduction of water volume to about 20 mL. Samples of standard known tritium concentrations called spikes were run together with the analysis samples to check the enrichment attained. Liquid scintillation counting was then conducted after mixing 10 mL of enriched sample with 11 mL of Ultima Gold and placed in the analyser. The analyser has 0.2 T.U detection limit.

5.4.2 Interpretation of environmental isotopes data

- *Stable isotopes in Johannesburg rainfall*

Using the stable isotope data from rainfall samples, the Johannesburg Local Meteoric Water Line (JLMWL) was constructed through the $\delta^{18}O$ versus $\delta^{2}H$ plots. The temperature and rainfall amount effects were assessed using the time series and regression analysis techniques for the two years (November 2016 to October 2018). The times series analysis was conducted to assess the effects in the individual rainfall events, while the regression analysis was done to quantify the temperature and amount effects in both the monthly and daily data through coefficient of determination (R^2).

From these regression analyses, the temperature-$\delta^{18}O$ relationship was established on a daily and monthly basis for Johannesburg rainfall and compared with the mean annual air temperature regression line proposed by Dansgaard (1964) (Equation 2) and the monthly temperature line proposed by Gat (2001) (Equation 3).

- *Characterisation of groundwater recharge and flow mechanisms*

The groundwater recharge mechanisms were determined by plotting the groundwater and surface water data on the $\delta^{18}O$ versus $\delta^{2}H$ plots against the JLMWL. The positions of the samples relative to the JLMWL and the surface water samples were used to identify the groundwater sources that are recharged through diffuse mechanism and those recharged through focused mechanisms. The Pretoria Local Meteoric Water Line and the Global Meteoric Water Line from the Global Network of Isotopes in Precipitation (GNIP) were also presented for comparison's sake because the JLMWL was first determined in this study and because other groundwater samples are located near Pretoria. Groundwater flow rate was also determined using tritium values in the dam and in groundwater for the samples that are recharged by focused mechanisms from Hartbeespoort Dam.

Deuterium excess (d-excess) was determined using the JLMWL for the boreholes that are recharged through diffuse mechanisms. The d-excess versus $\delta^{18}O$ plots were constructed for these groundwater samples to determine the moisture sources for the rainfall that generated the recharge.

Having identified the stable isotope effects in the Johannesburg rainfall, the traces of amount effect from rainfall were assessed in Albert Farm spring to determine the dependence of recharge amount on rainfall amount. This was done by plotting the spring discharge data versus the stable isotope data. The assessment was done on the basis that in some recharge areas, the amount of recharge mainly depends on the physical nature of the recharge area and the aquifer than the amount of rainfall in a rainfall event, while in other recharge areas, the amount of rainfall plays a more significant role for recharge to occur (Van Wyk, 2010).

Based on the temperature effect that was observed in rainfall, the air temperature at the time of recharge was also estimated using the temperature-$\delta^{18}O$ relationship established by Dansgaard (1964) and the one established for Johannesburg rainfall in this study.

The stable carbon isotope ($\delta^{13}C$) and radiocarbon (^{14}C) were used to assess the groundwater flow mechanisms, flow conditions and the groundwater MRT. Using the stable carbon isotopes, groundwater samples that receive dissolved carbon from the soil under open system conditions were identified from those that are under a closed system and those that additionally receive dissolved carbon from the carbonate rocks under closed system conditions. The radiocarbon age was also determined for the groundwater samples using Equation 5 where $a_0{}^{14}C$ is100 pMC. Based on the fact that there is a dry 2.2 km stretch in Grootvlei stream channel between the infiltration point

downstream of Nash Farm spring and the Nouklip spring, the hydrochemical and isotope analysis were done to assess whether the water at the infiltration point is the same one that re-appears at the Nouklip spring or if there is additional recharge. The environmental isotopes were also used to determine the groundwater flow path and velocity between the two points.

5.5 Applications of physical and water balance methods

Figure 5.7 presents the locations where the physical and water balance methods were applied.

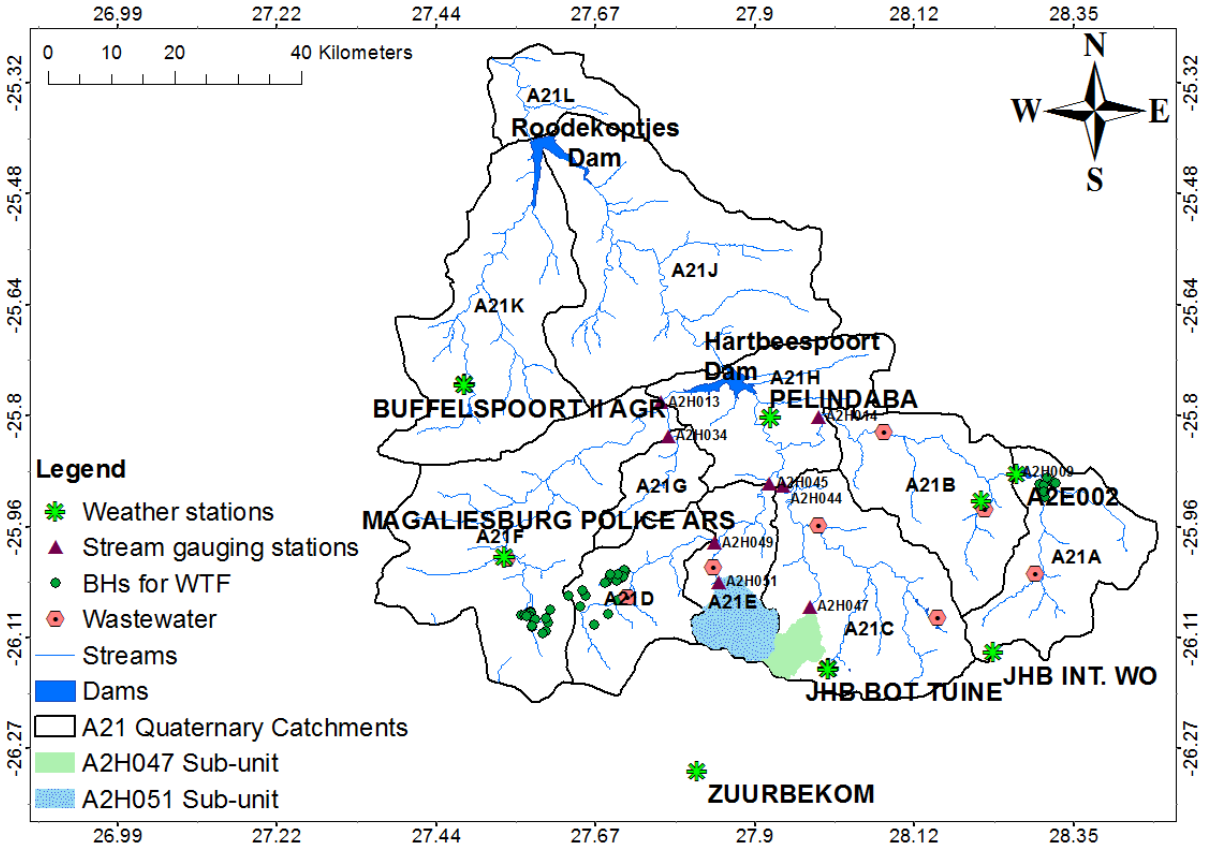

Figure 5.7: Location where the recharge methods were applied.

5.5.1 Thorthwaite Monthly Water Balance Model

The Thornthwaite Monthly Water Balance Model (TMWBM) by McCabe and Markstrom (2007) was constructed for the 10 year period from 1995 to 2004 to calculated the water balance components, which are used to estimate potential recharge.

The rainfall and temperature data were obtained from the JHB BOT Tuine, Pelindaba, Magaliesburg Police ARS and Buffelspoort II AGR climate stations that are shown in Figure 5.7. The separate models were constructed using data from each of the four climate stations to estimate potential recharge across the UCRB. The average monthly temperature and total monthly precipitation were populated into the TMWBM GUI according to the format presented in McCabe and Markstrom (2007). The monthly water balance components consisting of potential evapotranspiration, actual evapotranspiration, soil moisture storage, surplus/deficit etc., were added to give annual amounts from which annual potential recharge was determined.

5.5.2 Baseflow Separation Method

The Baseflow Separation (BFS) method was applied in the seven quaternary catchments (A21A to A21G) to estimate groundwater recharge across the UCRB. A21H was omitted because of Hartbeespoort Dam controlled exit flows. Quaternary catchments A21J, A21K and A21L were also omitted due to lack of adequate stream discharge and wastewater discharge data.

The wastewater discharge data was subtracted from the stream discharge so that computations can be made using only natural flows. Stream discharge from the upstream quaternary catchments was also deducted so that a computation can be done using only the stream flow components (runoff and baseflow) that are generated within the catchment of interest. The BFS results obtained from these catchments gave recharge estimates that are integrated across the quaternary catchment. The less integrated estimates were also obtained from the smaller sub-units of the quaternary catchments upstream of the gauging stations and wastewater disposal points. These are shown in Figure 5.7 as A2H047 and A2H051 sub-units.

The single parameter digital filter technique (Nathan and McMahon, 1990) was used for baseflow separation. The technique uses the following equation;

$$b_k = \alpha b_{k-1} + \frac{1-\alpha}{2}(y_k + y_{k-1}) \qquad \textit{(Equation 9)}$$

Where b_k and b_{k-1} are baseflow at time steps *k* and *k-1*, respectively. α is a dimensionless filter parameter. y_k and $y_{(k-1)}$ are total streamflow at the time steps *k* and *k-1*, respectively.

The single parameter digital filter method uses a filter parameter represented in Equation 9 as "α" to separate the high frequency flows associated with surface runoff from the low frequency flows associated with baseflow. The value used for the filter parameter in this study is 0.995 as confirmed suitable for South African baseflow by Smakhtin and Watkins (1997).

Computation of recharge was then conducted using baseflow as a proxy for recharge. This was achieved by dividing baseflow (in m^3/yr) with the area of the relevant catchment (in m^2) to obtain recharge (in m/yr, usually mm/yr). The annual rainfall (mm/yr) for the corresponding years was used to compute recharge as a percentage of rainfall.

5.5.3 Stream Segment Water Budget method

The Stream Segment Water-Budget method was applied between a minimum of two stream gauging stations (inflow and outflow) for the selected stream segments shown in Figure 5.8. This was done using data for the July month when there is no rainfall. These stream segments are underlain by various lithologies; granites (segment A), dolomites (segment B) and shales, quartzites and andesites (segment C).

Equation 10 was simplified to give Equation 11, where some components of the water budget were eliminated due to their zero or insignificant contribution, particularly because of the season of analysis and nature of the stream segment.

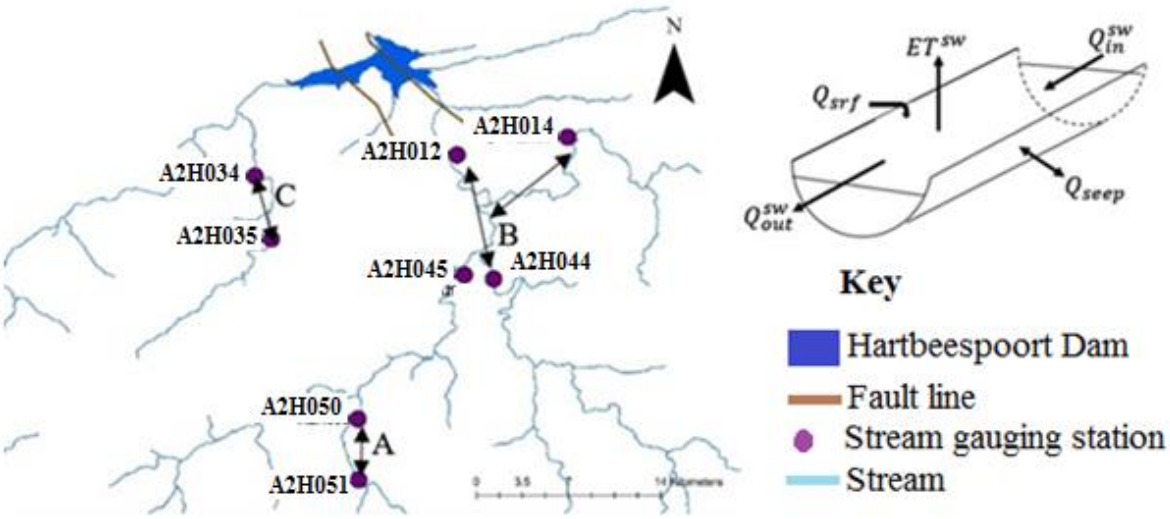

Figure 5.8: Location of gauging stations that were used in stream segment water-budget and a schematic of a water balance model.

$$Q_{out}^{sw} = Q_{in}^{sw} + QP^{sw} - ET^{sw} - \Delta S^{sw} + R_{off} + Q_{trib} + Q_{inter} + Q_{seep} - \boldsymbol{Q_{ab}} + \boldsymbol{Q_{wrf}} \quad \textit{(Equation 10)}$$

Where Q_{out}^{sw} and Q_{in}^{sw} represent flow at the downstream and upstream gauging stations, respectively. QP^{sw} is precipitation falling on the stream, ET^{sw} is evaporation directly from the stream, ΔS^{sw} is change in stream storage, R_{off} is surface runoff to the stream, Q_{trib} is stream flow addition from tributaries, Q_{inter} is interflow, which represents flow from the unsaturated zone (Q_{inter} is usually from infiltration of recent rainfall that never reached the water table (Freeze and Cherry, 1979; Shaw, 2005), and Q_{seep} represents an exchange of water between groundwater and surface water, which can either be negative or positive based on the losing or gaining nature of the stream segment. Q_{ab} represents abstraction and Q_{wrf} represents disposal of wastewater return flows that occurs between Q_{in}^{sw} and Q_{out}^{sw}. Q_{ab} and Q_{srf} have been introduced as a modification from Healy (2010) equation in order to suit the UCRB conditions.

The components QP^{sw} and R_{off} were eliminated because the assessment was conducted for the months of July when there is no rainfall. ΔS^{sw} was assumed zero because it was conceptualised as insignificant in a baseflow driven stream segment where there are no pulses of additional inflow and also that it is an insignificant amount relative to instream surface water measurement errors (Turco *et al.*, 2007; Healy, 2010). There were no tributaries that discharged into the segments, and therefore, Q_{trib} was zero. The studied catchments are characterised by agricultural activity with surface water and groundwater abstracted for irrigation. However, in the month of July, there is no intense agricultural activity in the selected area, and therefore, stream abstraction Q_{Ab} was assumed null. These alterations gave rise to Equation 11 with Q_{seep} as the residual to infer the groundwater surface water net exchange component.

$$Q_{seep} = Q_{out}^{sw} - Q_{in}^{sw} + ET^{sw} - Q_{srf} \quad \textit{(Equation 11)}$$

In Equation 11, $+Q_{seep}$ denotes a gaining stream while $-Q_{seep}$ denotes a losing stream. The value of Q_{seep} was then used to infer the dominant mode of recharge (diffuse or focused mechanisms) and the average net volume exchanged over the length of the segment.

5.5.4 Reservoir Water Budget

The Reservoir Water Budget method was applied on the Hartbeespoort Dam for the 15-year period 2000 to 2015 using a conceptual model shown in Figure 5.9. This was done to estimate the net exchange between groundwater and surface water in the review period.

Equation 12 is a modification of Equation 10, which has been altered to suit the Reservoir Water-Budget condition.

$$Q_{seep} = Q_{out}^{sw} - Q_{in}^{sw} - QP^{sw} + Q_{Ev} + \Delta S^{sw} + Q_{ab} \qquad \textit{(Equation 12)}$$

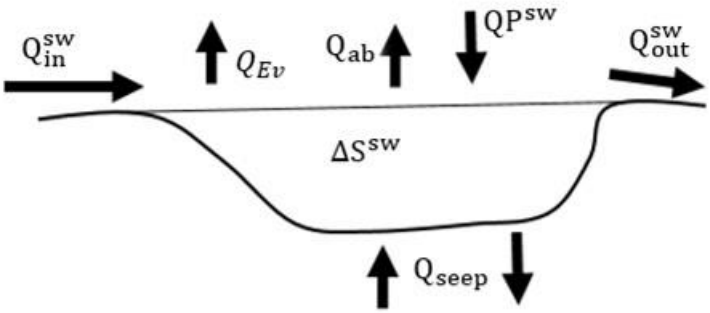

Figure 5.9: Schematic of a reservoir water balance.

The parameters maintain the same definitions as in Equation 10. Q_{in}^{sw} is a summation of all tributaries of the Hartbeespoort Dam, which includes Crocodile River, Magalies River, and Swartspruit (Table 5.1). Q_{out}^{sw} is discharge from the Crocodile River at the exit of the dam. ΔS^{sw} was calculated as a function of changing reservoir water level and surface area of the reservoir. ET^{sw} and QP^{sw} were calculated based on the contributions of evaporation and precipitation, respectively, on the reservoir surface area.

Table 5.1: Stations used for reservoir water budget calculations.

Component	**Station No.**	**Type of station**
Q_{in}^{sw}	A2H012 Crocodile River A2H058 Swartspruit A2H013 Magalies River	Stream gauging
QP^{sw}	A2E001	Climate Station: Precipitation
ET^{sw}	A2E001	Climate Station: Pan Evaporation
Q_{out}^{sw}	A2H001	Stream gauging

5.5.5 Water Table Fluctuation method

The boreholes with long term groundwater level data of several years and lithological logs were selected for this method. Furthermore, the boreholes that respond to rainfall were selected through the groundwater hydrograph analysis and rainfall, leading to 26 boreholes. On the selected boreholes,

the lithology at which each water level rise occurs was noted for selection of appropriate specific yield value.

During hydrograph analysis, the outlier points were identified by a sudden spike that is not related to a change in rainfall pattern and were replaced through interpolation. The examples of the outlier points are shown in Figure 5.10.

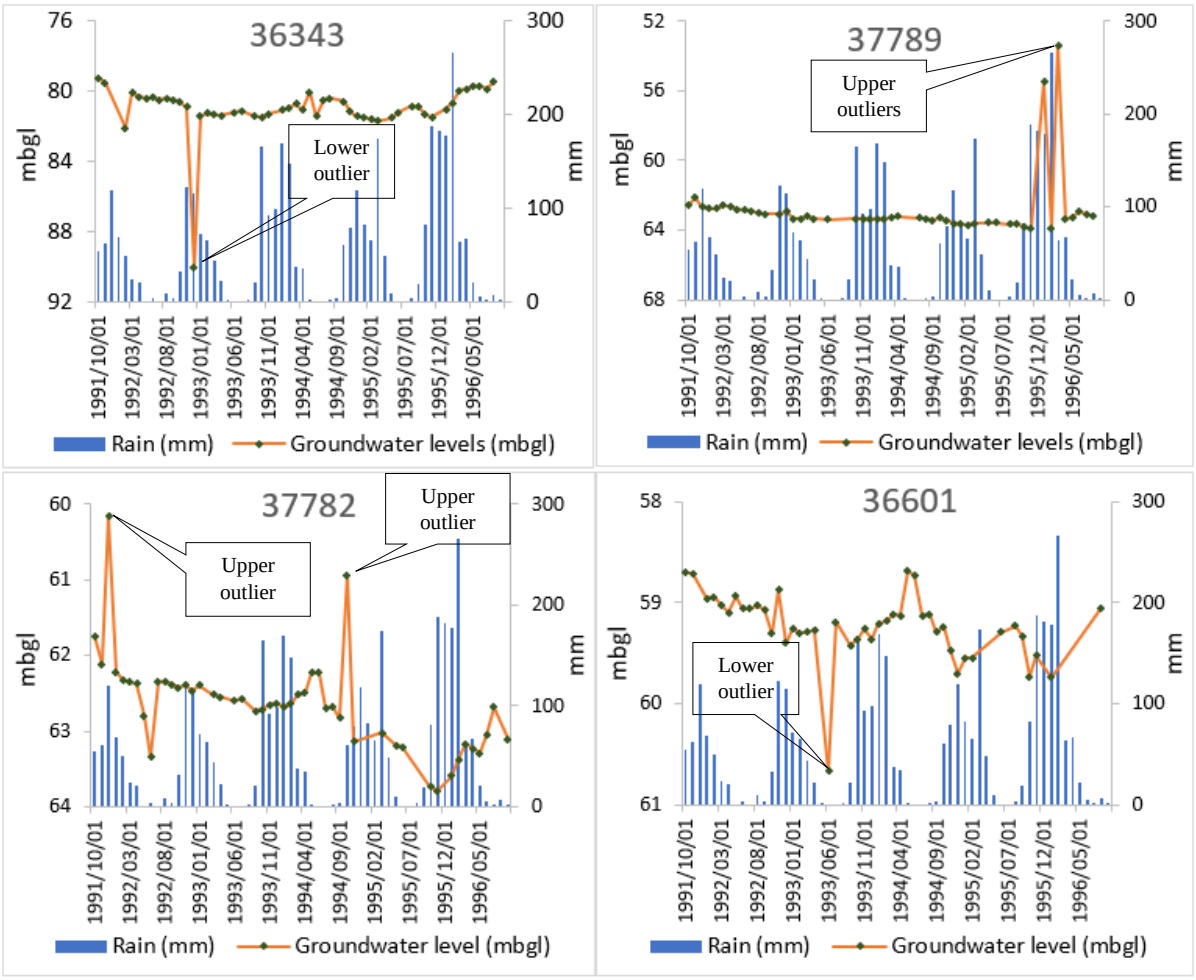

Figure 5.10: Examples of eliminated outlier points and boreholes with lack of response to rainfall.

In the NGA, the boreholes with the long-term groundwater level data are mainly in the dolomites of the Malmani Subgroup in the three quaternary catchments; A21A, A21D, and A21F. For this reason, the Water Table Fluctuation method was only applied in the Malmani Subgroup. Equation 7 was used for groundwater recharge estimation for each water level increase and the specific yield value of the geological material at the fluctuation depth. The annual recharge was then obtained as a total of the recharge events.

5.5 Precipitation Runoff Modelling System

5.5.1 Construction of the model

The PRMS model was constructed for the southern portion of the UCRB, which is gauged by the A2H012 station with a basin area of 2552 km^2. The model area is drained by Jukskei Stream from Johannesburg in the south of the UCRB and Hennops Stream from Pretoria in the south east. The elevation of the model area ranges from 1176 to 1843 masl. Figure 5.11 shows the location of the model area, the lithology and surface water resources that were described in Chapter 2.

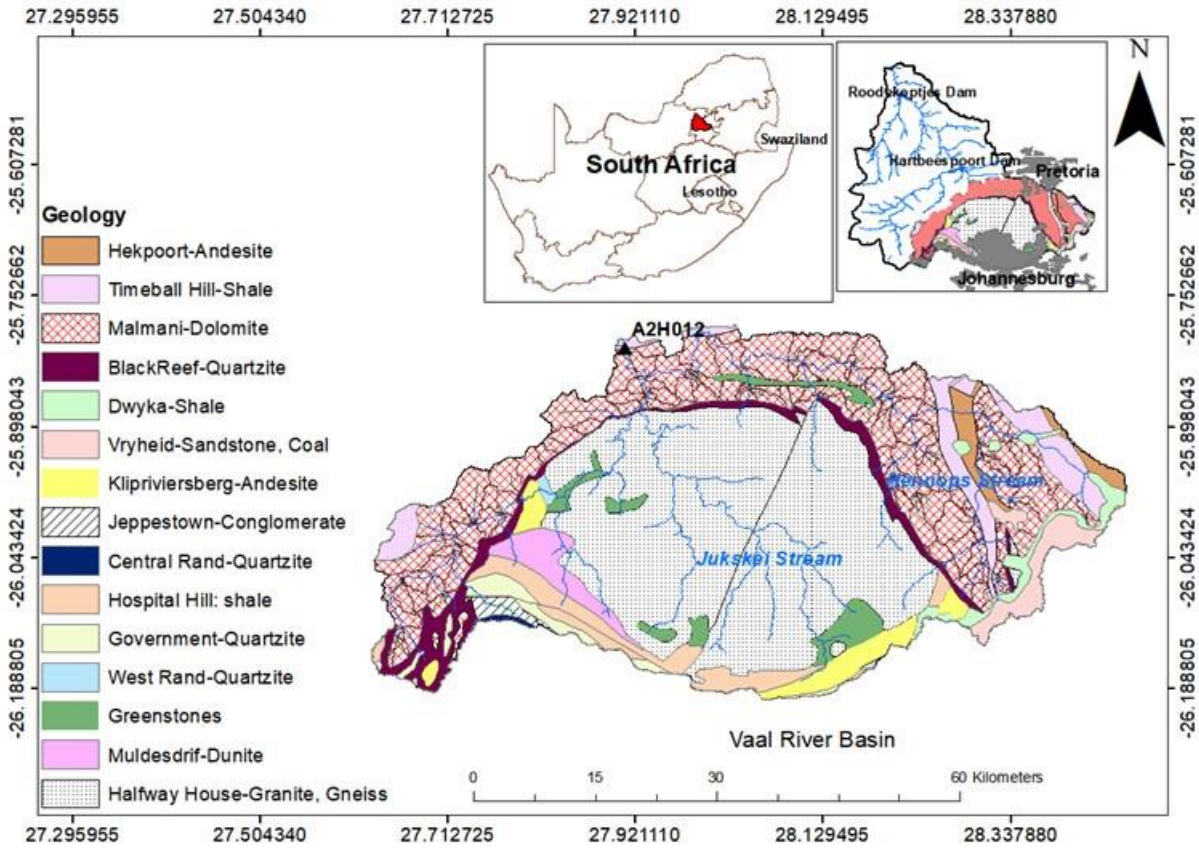

Figure 5.11: Combo map of the model area and its location in RSA map as insert (Source of Geological data: Council for Geosciences, South Africa).

The Digital Elevation Model (DEM) was used to generate the surface topography map of the model area. ArcGIS Terrain Processing was applied on the DEM to generate a map of 313 HRUs, which are in the form of watersheds (Figure 5.12). The slope and aspect maps were generated from the DEM using ArcGIS hydro-tools and the average slope and aspect values for each HRU were obtained using the zonal statistics tools under ArcGIS hydro-tools. The other properties of the HRUs were obtained by layering the HRU map over the individual maps such as geology, land use, vegetation, soil map etc., to obtain the properties of each HRU. In cases where an HRU was underlain by different properties, the dominant property within an HRU was assumed to represent the entire HRU. For example, an HRU with more surface area coverage of granite than dolomite was assumed to be entirely underlain by granite, therefore, the PRMS properties that are representative of granite were used.

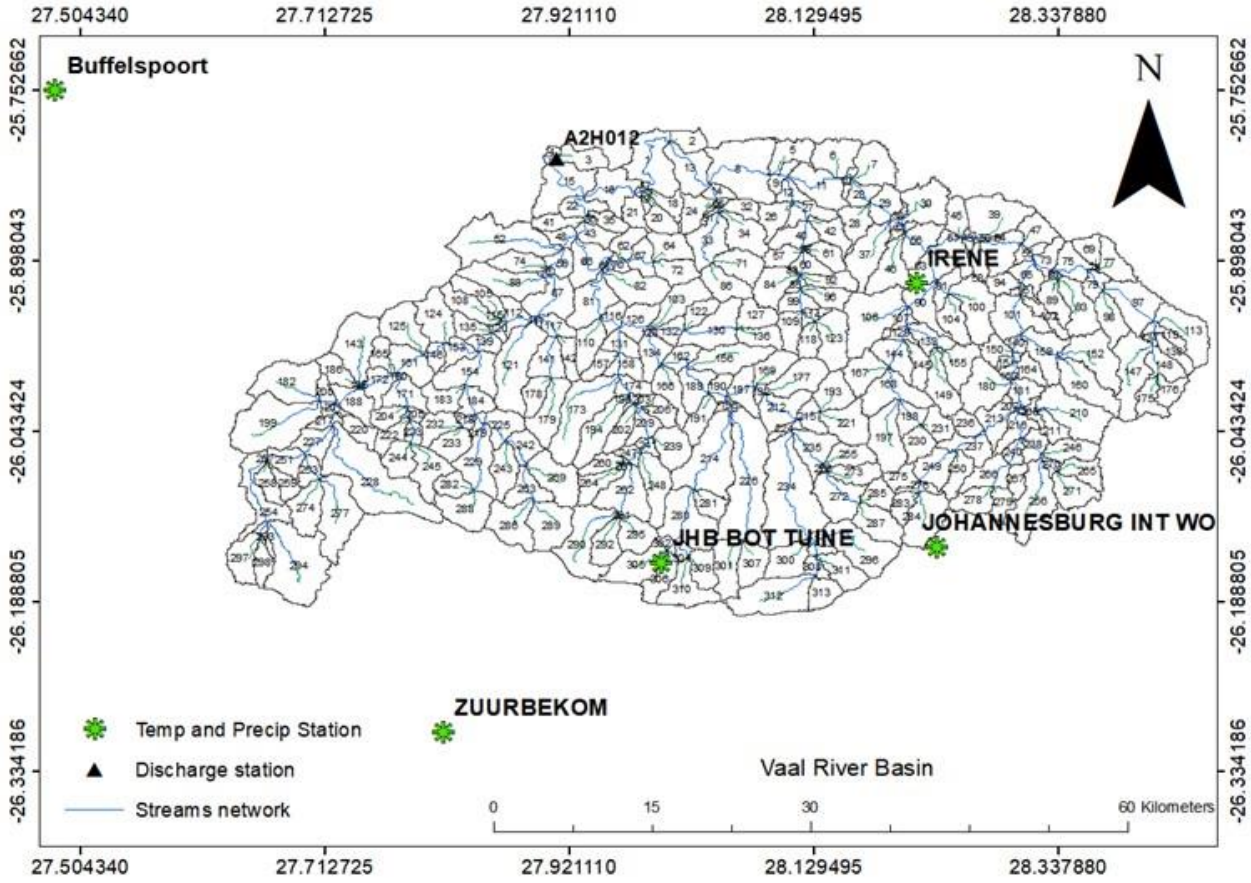

Figure 5.12: The constructed Hydrological Response Units (HRUs) in the UCRB with stream network, climate stations and a stream gauging station.

Figure 5.12 shows the generated HRUs, the locations of the stream gauging station and the selected climate stations. The daily maximum and minimum air temperature, precipitation and stream discharge data were obtained from the climate and gauging stations shown in Figure 5.12. The discharge of 5 m^3/s was deducted from the measured stream discharge to account for the wastewater of 400 000m^3/day that is being disposed upstream of the A2H012 station (Section 2.3).

The climate and stream discharge data were then inserted in the PRMS Data File. The description of the HRUs was specified in the PRMS Parameter File. The model execution information including model start and end date, locations of Data File and Parameter File, selection of PRMS modules and selection of variables to be written in the output files were specified in the Control File. The Data File, Parameter File and Control File were constructed according to Markstrom *et al.* (2015). Missing river discharge, air temperature and precipitation were specified with the value -19 in the Data File.

Table 5.2 shows the units that were set in the Parameter File for data input and output simulations, and the metric units that were converted for presentation in this work. Table 5.3 shows the modules that are used in this study and specified in the Control File.

Table 5.2: Input and output units in PRMS and the final unit conversions in this work.

Input variables	Output variables	PRMS Input and output units	Final unit conversions
Temperature	basin_temp	Degree Fahrenheit (°F)	Degree Celsius (°C)
Precipitation	basin_ppt	Inches/day (inch/day)	mm/day
Stream discharge	basin_cfs	Cubic feet/second (cfs)	Cubic meters/second (cms)
Baseflow	basin_gwflow_cfs	Cubic feet/second (cfs)	Cubic meters/second (cms)

Table 5.3: Names of modules used to build a PRMS model in this study.

Type of Module	Purpose	Specified module
Precipitation module (*precip_module*)	Distributes precipitation to each HRU per day	ide_dist
Temperature-Distribution module (*temp_module*)	Distributes temperature to each HRU per day	ide_dist
Solar radiation module (*solrad_module)*	Computes daily shortwave radiation for each HRU	ddsolrad
Transpiration period module (*transp_module*)	Determines the period of active transpiration	transp_tindex
Potential Evapotranspiration (PET) module (*et_module*)	Computes PET for each HRU	potet_jh
Interception module	Computes interception by plants and net precipitation	intcp
Surface runoff module (*srunoff_module*)	Computes surface runoff as an excess of infiltration and soil saturation	srunoff_smidx
Soil-zone module (soilzone)	Simulates the hydrologic processes in the soil zone	soil_zone
Groundwater-flow module (gwflow)	Simulates storage and inflow to and outflows from the groundwater reservoir	gwflow
Streamflow module (*streamflow_module*)	Computes stream flow leaving the model domain	muskingum

5.5.2 Assessment of baseflow and groundwater recharge

The discharge measured from the A2H012 station was used to estimate baseflow and recharge. The baseflow was estimated using a separate single filter parameter approach by Nathan and McMahon (1990) on a Web-based Hydrograph Analysis Tool (WHAT) (https://engineering.purdue.edu/mapserve/WHAT/; accessed July 22nd, 2018). The filter parameter value of 0.995 was used (Smakhtin and Watkins, 1997). The definition of WHAT has been provided by Lim *et al.* (2005).

Recharge was calculated for the 21 years by dividing annual baseflow (m^3/yr) by the area of the catchment (m^2) to give recharge in depth units per time (m/yr, usually mm/yr). The annual rainfall (mm/yr) for the corresponding years was then used to compute recharge as a percentage of rainfall. The recharge estimates were then calculated from baseflow obtained in each simulation.

5.5.3 Model sensitivity, calibration and validation

Model sensitivity analysis was conducted to identify the input parameters that have a significant effect on the simulated baseflow output variables (*basin_gwflow_cfs*) and the simulated stream flow output variable (*basin_cfs*). Numerous input parameters invoked sensitivity on the baseflow and stream

discharge. The parameters that showed significant sensitivity on baseflow were **gwstor_init**, which is groundwater storage at the beginning of a simulation and **gwflow_coef**, which is a coefficient that computes baseflow.

Since baseflow contributes to stream discharge, the simulated *basin_cfs* also showed significant sensitivity to parameter **gwflow_coef**. Over and above those two, **soil_moist_max** and the fast and slow shallow subsurface linear coefficients (**fastcoef_lin**, and **slowcoef_lin**) also invoked sensitivity on the **basin_cfs**. The **soil_moist_max** represents the soil water holding capacity for infiltrated water that is available for evapotranspiration and not for gravity flow as recharge or interflow. The fast and slow linear coefficients (**fastcoef_lin** and **slowcoef_lin**) affect the falling rate of simulated hydrograph limbs after the high flows. The parameter **jh_coef** seemed to affect the entire terrestrial moisture, which includes stream flow, baseflow and direct groundwater recharge. The **jh_coef** is the monthly (January to December) air temperature coefficient used in Jansen-Haise potential evapotranspiration computations. These parameters and variables are well defined in Markstrom *et al.* (2015).

Calibration of the PRMS model for the UCRB was done using both manual and automatic procedures. Manual calibration was mainly done to identify the acceptable ranges of model sensitive parameters, which were selected through sensitivity analysis. During manual calibration, the model sensitive parameters were adjusted for each consecutive simulation, until a good visual match was observed between the hydrograph of the simulated and measured streamflow and simulated and measured baseflow. The visual similarity of the hydrographs was assessed based on the following characteristics: rising limb slopes, the falling limb slopes, the timing of the peaks and the height of the hydrographs. The calibration data for stream flow were obtained from station A2H012.

Since one of the aims of PRMS in this study is to assess the impacts of changes in climate variables on the baseflow, the baseflow at A2H012 that was calculated in section 5.5.2 was also used to calibrate the PRMS model in order to ensure that PRMS is simulating realistic baseflow. This placed more certainty on the ability of the model to undertake scenario analysis for the baseflow response to changes in climate. Baseflow was calibrated manually by adjusting **gwflow_coef** and **gwstor_init**, while the streamflow component was further calibrated using automatic procedure as highlighted below.

The automatic calibration of streamflow was done to reduce possible uncertainties, which may have been brought by the user's subjectivity during manual calibration, and to ensure that the model closely simulates the hydrological processes of the catchment. This was done through a GUI called Luca (Let us calibrate). Luca is a stepwise, multiple objective calibration program, which was developed for calibration of the models compiled using the United States Geological Survey's Modular Modelling System such as PRMS (Hay and Umemoto, 2007). The calibration was done on seven years and seven months data (1st February 1996 to 30th September 2003). The first year of calibration (1st February1996 to 31st January 1997) was used for model initialization. The calibration period was selected because it had no data gaps in measured stream flows at station A2H012.

The validation period was selected between the 7th February 2007 and the 30th June 2017 mainly because it had a long record with no missing data. Model validation was done to see the accuracy and predictive capability of the model (Krešić, 2007) and to demonstrate that a given time specific calibrated model for the UCRB, can make accurate simulations in a different modelling period or different input data (Daggupati *et al.*, 2015). Konikow (1978) stated that the model is found to be

verified or valid, if its accuracy and predictive capability have been proven to lie within acceptable limits of error by tests independent of the calibration data, hence, a verification period was selected different from the calibration period in this study.

The statistical tools, in addition to the visual graphical analysis, were used to test the correlation between the observed and simulated discharge values in both calibration and validation periods. The used statistical tools are, coefficient of determination R^2 and Nash-Sutcliffe model-efficiency coefficient E_N (Nash and Sutcliffe, 1970). R^2 was obtained from excel plots, while E_N was calculated using a Web-based Hydrograph Analysis Tool (https://engineering.purdue.edu/mapserve/WHAT/; accessed July 24th, 2018).

The slope and intercept of the regression lines were also used in addition to the R^2 value as a measure of accuracy. This is because, Krause *et al.* (2005) indicated that a model, which systematically always over or under-predicts, can still have an acceptable R^2 value close to 1 even if all predictions are wrong. Therefore, for an acceptable correlation, an intercept should be close to 0, while the gradient should be close to 1 (Krause *et al.*, 2005). The E_N value should be between 1.0, and $-\infty$ (Krause *et al.*, 2005). For a perfect model fit, the E_N and R^2 values should be 1.0, however values above 0.5 are also accepted (Santhi *et al.*, 2001; Krause *et al.*, 2005).

5.5.4 Simulation of climate-based scenarios

As it was indicated in section 2.2, the prevailing annual trends for the period 1997 to 2016 indicated that there is an ongoing reduction in terrestrial moisture in the UCRB.

In this study, the simulations were run for the period 1996 to 2017 with an increase and decrease of 20% in rainfall and 1.5°C in temperature as shown in Table 5.4. Finally, a combined worst case scenario was run with a temperature increase of 1.5°C and rainfall decrease of 20%. The percentage change in baseflow and stream flow were calculated for each scenario. The Baseflow Index (BFI) was also assessed to study the contributions of baseflow to stream flow under each scenario.

Table 5.4: Scenarios used for PRMS simulations

Scenario	**Scenario input**
Scenario 1	+20% Rainfall
Scenario 2	-20% Rainfall
Scenario 3	+1.5°C Temperature
Scenario 4	-1.5°C Temperature
Scenario 5	-20% rainfall and +1.5°C temperature

A comparative analysis was also done to determine the number of occurrences (days), on which wastewater is more than streamflow (runoff and baseflow) and to determine how the occurrences change with changes in climate variables.

6 RESULTS AND DISCUSSIONS

6.1 Aquifer characterisation

6.1.1 Characterisation of aquifers in the basement granites

Table 6.1 presents the boreholes that were selected for aquifer characterisation in the granites and Figure 6.1 shows the lithological logs of some of the selected boreholes with water strike, water level depths and blow yield values shown relative to the different lithological units.

Table 6.1: Locations of boreholes and elevation information.

Boreholes	**Latitude**	**Longitude**	**Elevation (masl)**	**Water strike (masl)**	**Water level (masl)**	**Top of granite (masl)**	**Blow yield (L/s)**
2627BB00120	-26.08943	27.9955	1552	1524	1532	1533	1.10
2628AA00182	-26.10472	28.08026	1564	1534	1540	1537	0.4
2628AA00183	-26.04777	28.05859	1477	1460	1469	1463	0.76
2628AA00996	-26.06396	28.14886	1552	1538	1544	1535	0.15
2628AA00212	-26.00972	28.1247	1566	1541	1557	1565	0.38
2527DD00106	-25.98394	27.94135	1424	1393	1401	1389	2.13
2528CC00739	-25.95251	28.03439	1419	1403	1413	1412	1.51
2528CD00270	-25.91314	27.96632	1318	1300	1307	1316	0.11
2528CC00814	-25.89866	28.01027	1401	1390	1396	1401	2.7
GP00247	-25.89708	27.99613	1357	1332	1344	1338	0.2
2628AA01045	-26.15888	28.07998	1662	1648	1661	1622	1.8
2628AA00951	-26.10182	28.19388	1669	1635	1660	No granite	0.9
2528CC00251	-25.97561	28.08387	1523	1475	1501	1523	0.76

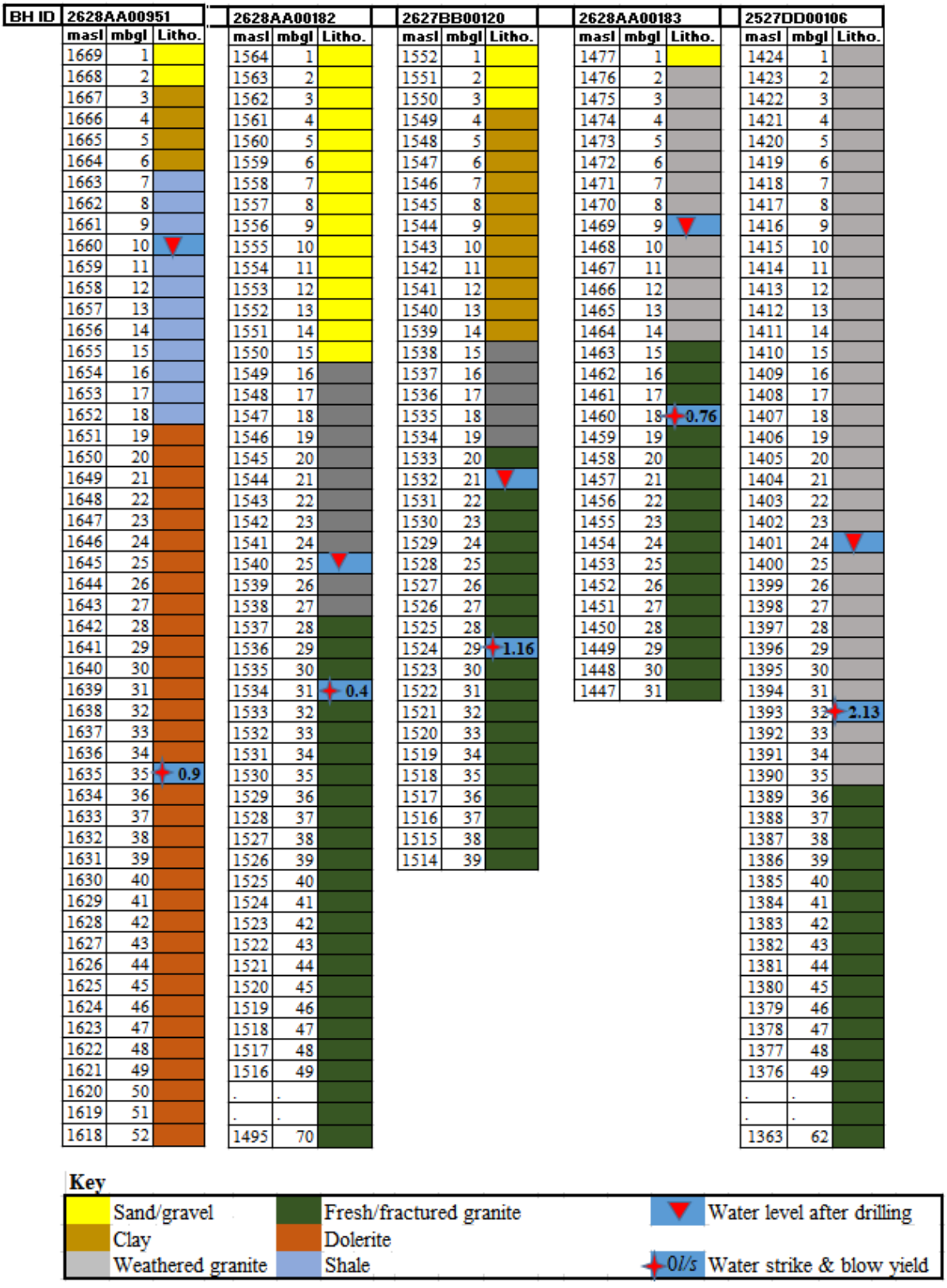

Figure 6.1: Lithology of the selected boreholes showing the positions of the water level, water strike and blow yield for each borehole (*mbgl is meters below ground level and masl is meters above sea level).*

It can be observed in Figure 6.1 that the borehole logs are generally of fresh bedrock overlain by weathered material, while some of the boreholes have sandy gravel material at shallow depths, saturated in part, ranging between 1 mbgl and 15 mbgl. The borehole logs indicate intergranular and fractured aquifers.

The raw data from the NGA mainly classified the granite as weathered or as just granite and seldom specified where there is fractured granite. However, based on the knowledge that granite has low primary porosity and permeability, it was deduced that the granite at which the water strike occurs must be fractured. In order to substantiate this assumption, the blow yield value is also presented for each water strike in Figure 6.1 to show just how unlikely it would be for the fresh granite to have that blow yield value unless it is fractured. The blow yield values for water strikes in the granite range from 0.9 L/s to 2.13 L/s for the boreholes presented in Figure 6.1.

The lithology above the weathered granite consists of sandy gravel and clay is observed in few boreholes indicating that it does not have much areal coverage. The water levels have generally risen from the water-strikes and they are generally within the aquifer material in the weathered granite or sandy gravel. Even though the water level has risen from the position of the water strike showing signs of confinement, in most boreholes, it is still within the aquifer material and not above the upper confining layer indicating limited piezometric pressure, thereby showing signs of unconfined to semi-confined aquifer.

6.1.2 Characterisation of aquifers in the Transvaal Supergroup

Table 6.2 presents the list of selected boreholes from A21A and A21D quaternary catchments that are underlain by the Transvaal Supergroup. Figure 6.2 shows the lithological logs for some of the selected boreholes with elevations of water strikes and the water level fluctuation range over the review period.

Table 6.2: Locations of boreholes and elevation information.

Boreholes	Other name	Latitude	Longitude	Elevation (masl)	Water strike (masl)	Highest Water level (masl)	Lowest Water level (masl)	Blow yield (L/s)
36349	(A2N0576)	-26.10025	27.64812	1594	1524	1567	1529	40
36337	(A2N0583)	-26.07921	27.68627	1601	1545	1558	1556	40
37794	(A2N0600)	-26.01792	27.71107	1470	1441	1451	1446	40
36334	(A2N0584)	-26.05843	27.69968	1502	1475	1483	1474	40
37027	(A2N0709)	-25.94443	28.31311	1449	1512	1516	1511	20
37811	(A2N0631)	-26.0171	28.28347	1575	1486	1569	1557	4.5
37329	(A2N0715)	-25.96866	28.33113	1576	1555	1558	1541	6
37815	(A2N0634)	-26.04535	28.3163	1594	1565	1590	1577	1

The lithological logs mainly consist of dolomite and chert overlain by shale, clay and sandy material and the water strikes mainly occur in the dolomite, while the water levels fluctuate in the unconsolidated material above the water strikes.

Considering the ranges in water levels, it can be deduced that the confined to semi-confined conditions occur in boreholes that show a significant rise in water level above the water strike, such as borehole 36329. The unconfined conditions are observed in the boreholes where the water level fluctuation interacts with the water strike, such as borehole 37815.

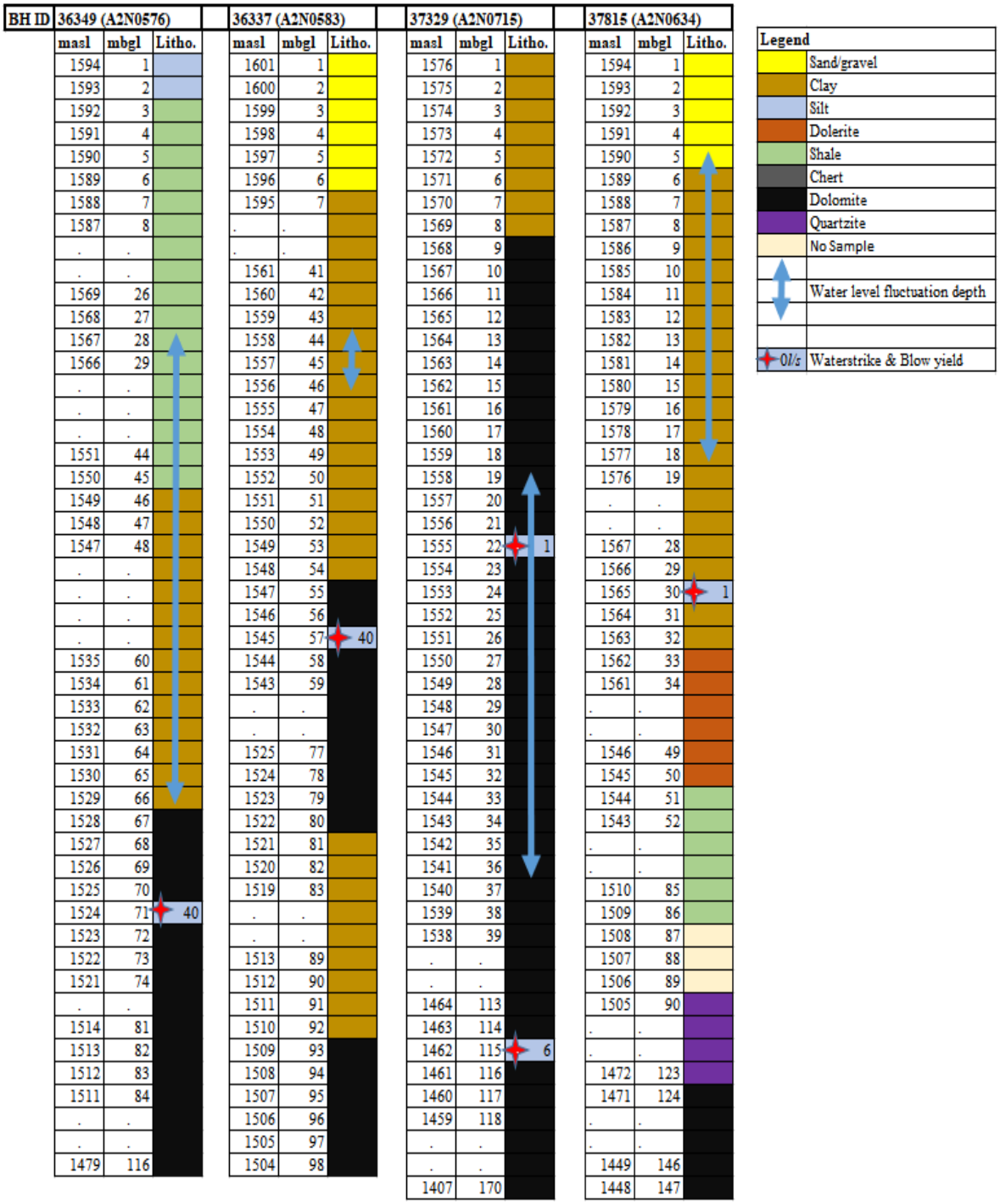

Figure 6.2: Lithology of the selected boreholes in the karst aquifers of the Malmani Sub-group showing the positions of the water strike and water level fluctuation depth for each borehole.

6.1.3 Assessment of groundwater level response to rainfall through hydrograph analysis

Figure 6.3 shows that in some borehole water levels fluctuate as deep as 71 mbgl while some as shallow as 5 mbgl. Regardless of the depth to water level, it can be observed that there are seasonal responses to rainfall periods, which make WTF method applicable. Healy and Cook (2002) stated that the method has been applied with success in aquifers that show seasonal fluctuations.

The selection led to 26 boreholes that are suitable for the WTF method. These are the boreholes that have lithological logs, long-term data and whose groundwater level responds to rainfall. The

hydrographs for some of the boreholes are presented in Figure 6.3, while the rest of the hydrographs for the selected boreholes are presented in Appendix B.

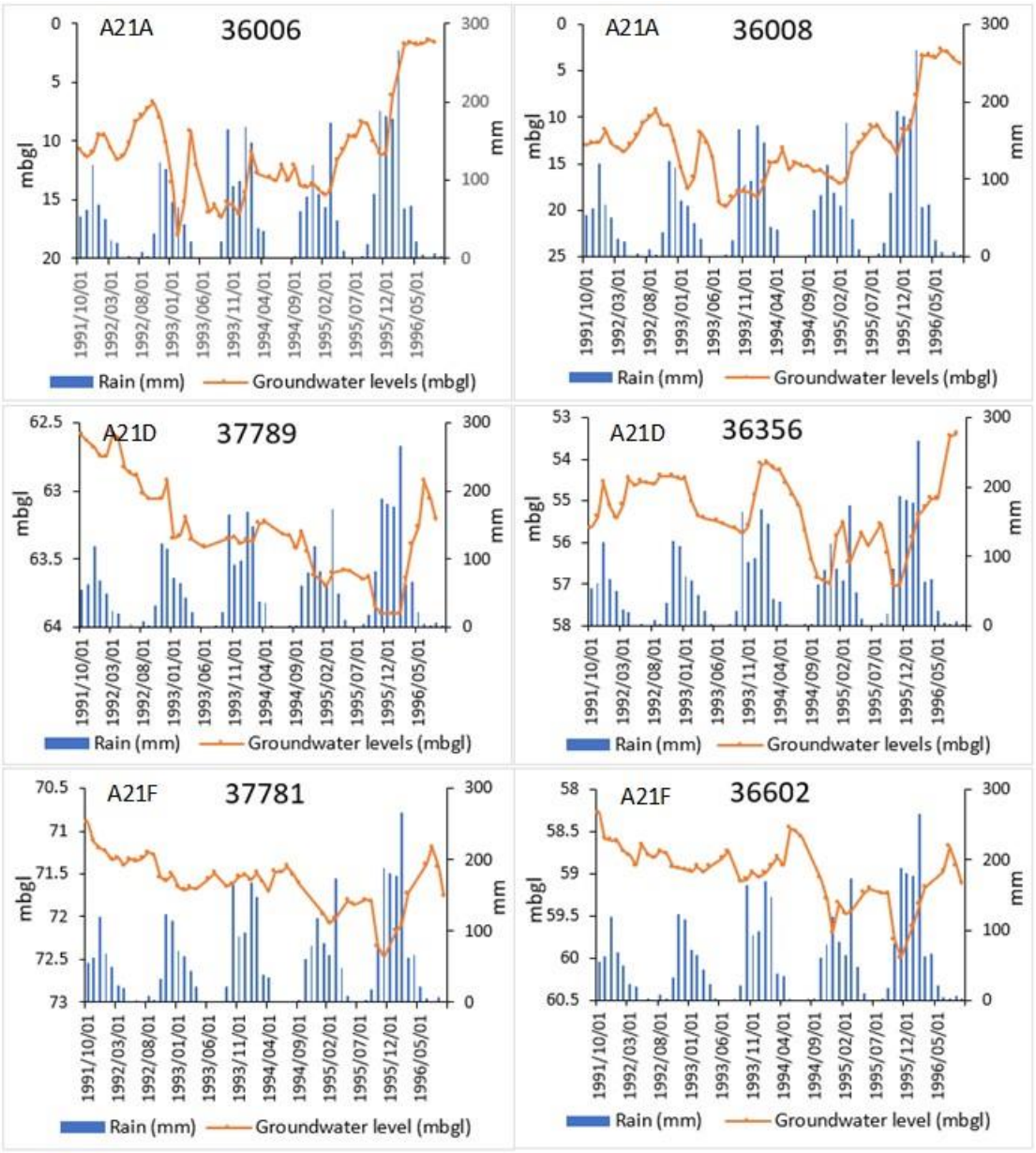

Figure 6.3: Monthly groundwater levels versus rainfall.

6.2 Assessing the possibilities for baseflow and interflow occurrence in streams underlain by the basement granites

6.2.1 Assessing the elevations of stream channel and borehole log components

Table 6.3 presents the elevations for the borehole water levels and the adjacent stream channels. Figure 6.4 presents the comparisons between the elevations of the borehole log components and the points along the adjacent stream channel.

Table 6.3: Location and elevation information for the stream channel points and boreholes water levels.

Stream point information				Borehole information	
River point	**Latitude**	**Longitude**	**Elevation (masl)**	**Borehole**	**Water level (masl)**
RIV 5	-26.102872	28.073983	1529	2628AA00182	1540
RIV 1	-26.086899	27.973346	1473	2627BB00120	1532
RIV 8	-26.046882	28.049853	1420	2628AA00183	1469
RIV 13	-26.028	28.107	1442	2628AA00212	1557
RIV 15	-25.979924	27.962174	1324	2527DD00106	1401
RIV 19	-25.908903	27.946536	1289	2528CD00270	1307
RIV 11	-26.072778	28.135169	1499	2628AA00996	1544
RIV 17	-25.958768	28.035234	1382	2528CC00739	1413

In Figure 6.4, it can be observed that the groundwater levels and water strikes are more elevated than the stream channel, which indicates possibilities for the occurrence of baseflow into the stream channel. In some boreholes such as 2528CD00270, the top of the granite material is more elevated than the groundwater level, indicating that the saturated zone is within the granite material. In such instances, it is possible that interflow is also contributing water into the stream channel through a lateral flow that is patched on the granite bedrock.

The perennial springs that discharge from the Witwatersrand quartzites (Albert Farm spring) and the Malmani Subgroup (dolomitic springs) also contribute baseflow in the UCRB.



Figure 6.4: Comparisons between groundwater level and the elevation of the nearby stream channel in meters above sea level.

6.2.2 Assessment of interflow in the stream underlain by the Basement Complex

Table 6.4 presents the water levels and stable isotope data for the two piezometers and the stream over the four months period.

Table 6.4: Stable isotope and water level data for the piezometers and the stream.

Site ID	Date	Water level (mbgl)	δ^2H (‰)	$\pm^2H$ StDev	$\delta^{18}O$ (‰)	$\pm^{18}O$ StDev
PZ1	06-Jun-16	1.12	-12.5	0.33	-3.00	0.06
PZ2	06-Jun-16	0.64	-68.5	0.13	-12.47	0.09
River head	06-Jun-16	0.72	-66.3	0	-12.27	0
PZ1	13-Jul-16	1.12	-17.8	0	-5.36	0
PZ2	13-Jul-16	0.52	-16.3	0	-5.04	0
River head	13-Jul-16	0.75	-9.8	0	-3.88	0
PZ1	12-Aug-16	1.17	-12.4	0.22	-3.05	0.05
PZ2	12-Aug-16	0.58	-12.3	0.16	-2.85	0.07
River head	12-Aug-16	0.72	-4.9	0.24	-1.59	0.06
PZ1	06-Sep-16	PZ dry no sample	PZ dry no sample	PZ dry no sample	PZ dry no sample	PZ dry no sample
PZ2	06-Sep-16	0.66	-1.7	0.22	-0.45	0.05
Stream head	06-Sep-16	0.92	-9.5	0.65	-1.83	0.02
PZ1 -26.149247 Lat, 27.997857 Long, 1593 masl Elev, 1.2mbgl PZ depth PZ2 -26.149333 Lat, 27.997868 Long, 1593 masl Elev, 2.15mbgl PZ depth						

Table 6.4 shows that PZ2 consistently has a higher water level compared to both PZ1 and the stream. It is evident from this observation that the stream gains from the eastern side and loses to the western side as shown in Figure 6.5, which presents the average water levels over the period of review.

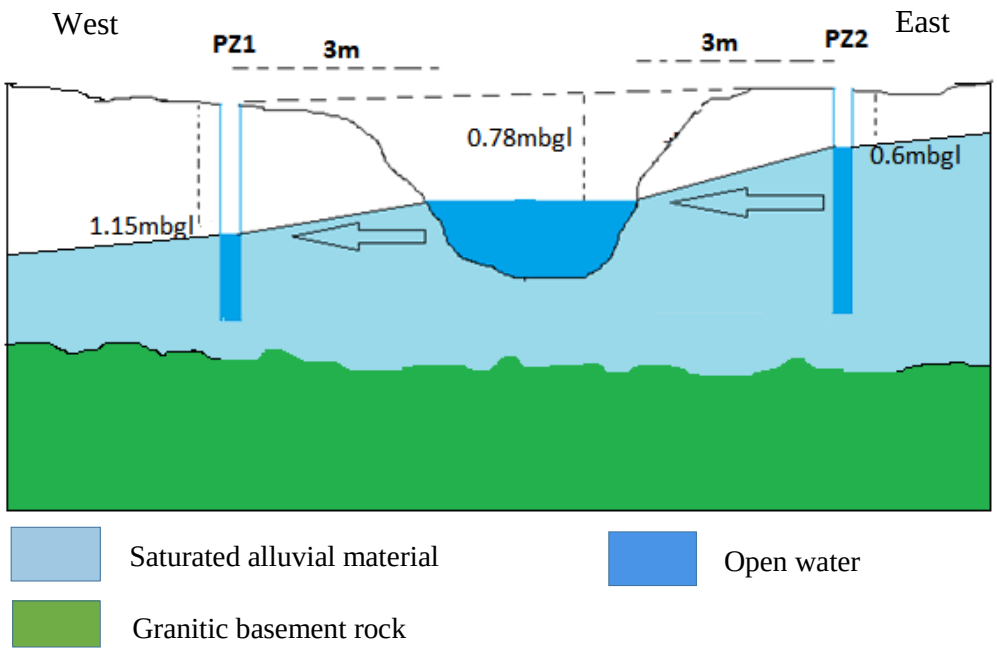

Figure 6.5: Schematic of stream gain and stream loss at Montgomery Stream, which is underlain by the granites (NB: not drawn to scale).

Figure 6.6 shows the four months stable isotope ($\delta^{18}O$ versus δ^2H) plot for piezometers and stream samples against the Johannesburg Local Meteoric Water Line (presented in section 6.3.1). It can be observed from this plot that there is a loss and a gain of water from the stream. With time, the samples seem to be generally shifting towards the most enriched part of the plot. The June samples are

generally most depleted getting more enriched towards September. The main sources of water for the stream are the springs such as the Albert Farm spring. Since there was no rainfall in that period, this behaviour shows a water source that is constantly being exposed to evaporation, thereby continuously getting enriched. This indicates that the source of water for the piezometers could be related to an open upstream water body such as a wetland or surface reservoir. The water is released as subsurface leakage patched on the granite bedrock flowing downslope towards the piezometers, which further seeps into the Montgomery stream.

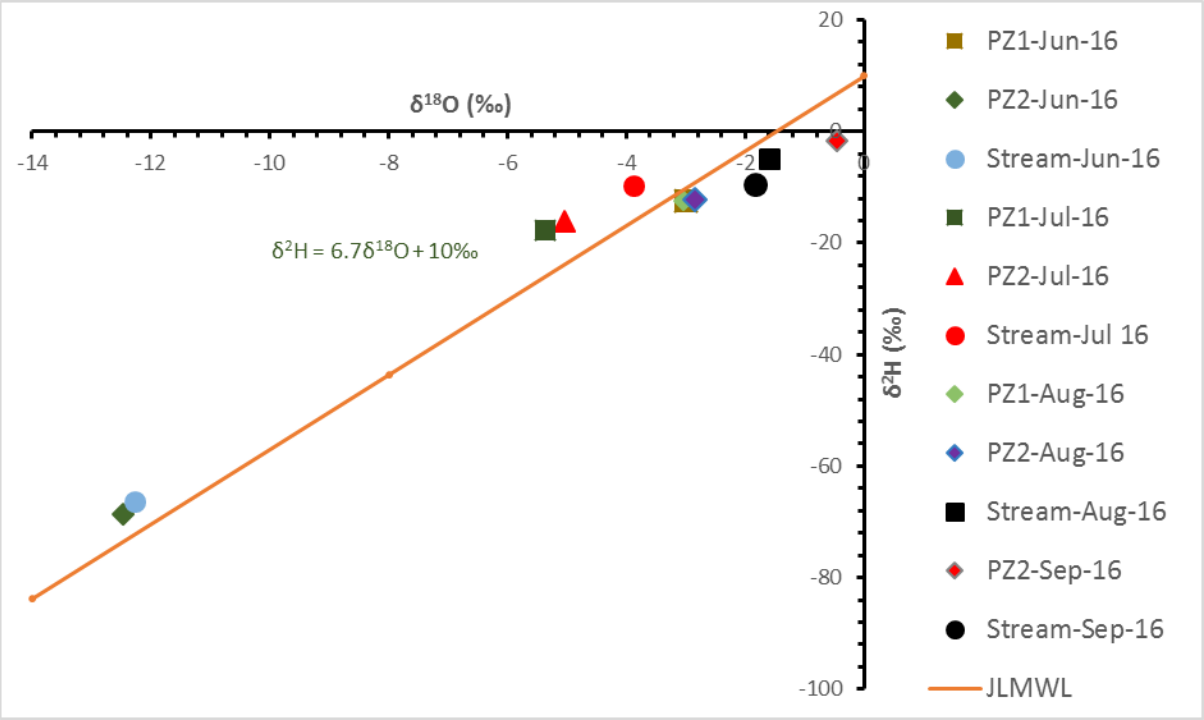

Figure 6.6: Stable isotope plot of piezometers and stream water plotted against the Johannesburg Local Meteoric Water Line.

Both the water levels and stable isotope interpretations revealed that there is interaction between the stream and the piezometers. This analysis indicates possibilities of interflow deducing that caution should be taken in the application of surface water methods. The recharge estimated from Baseflow Separation method in the area underlain by granites may include interflow even in dry seasons long after rainfall has occurred.

6.3 Application of chemical and isotope tracer methods

6.3.1 Stable isotope composition of Johannesburg rainfall

The Johannesburg Local Meteoric Water Line (JLMWL) of $\delta^2H=6.7\delta^{18}O+10‰$ was constructed from the three-year daily rainfall sampled at the University of the Witwatersrand and Montgomery Park. The data consisted of 260 rainfall events that gave a coefficient of determination, R^2 of 0.92 on a $\delta^{18}O$ versus δ^2H space.

Plotting the Johannesburg rainfall collected over a period of 3 years for the two stations, the most depleted rainfall sample had δ^2H and $\delta^{18}O$ values of -131.6‰ and -17.82‰, respectively, while the most enriched rainfall had 51.4‰ and 7.03‰, respectively. The most depleted rainfall, which was also extremely out of the range of pre-existing data, was received on the 14th May 2017 (winter rainfall).

From this range, rainfall seasonality and moisture source variations were observed. It is worth noting that the varying rainfall isotope signature in Johannesburg makes it challenging to inversely model the original rainfall that led to a particular groundwater signature during recharge characterisation. This is because, considering the $\delta^{18}O$ range, any water type from the most depleted -17.82‰ to most enriched 7.03‰ could be responsible for recharging the groundwater. In this case then, a high depletion in groundwater may not necessarily mean recharge from high elevation, high rainfall amount, or low temperature fractionation but could mean different moisture sources i.e. from Antarctica or Indian Ocean. The above emphasis calls for a thorough analysis of temperature and amount effects in rainfall so as to gain clarity on the controlling factors of isotopic signature in the Johannesburg rainfall and the predominant influencers of isotopic signature in groundwater.

Figure 6.7 shows the time series of rainfall amount, isotope signature in rainfall and the daily air temperature for the period November 2016 to October 2018 from the station positioned at Montgomery Park. Amount and temperature effects have been observed. The high amount of rainfall observed in arrows- **b**, **c**, and **j** correspond well with depletion in stable isotopes. On the other hand, a low rainfall amount shown by arrows- **g** and **h** correspond well with enrichment in the stable isotopes. Arrow-**f** shows the influence of temperature effect in that the lowest temperature recorded in the year also had the most depleted stable isotope signature. Arrows **h**, **k**, **n** and "**o**" show a combination of temperature and amount effect. Although it represented the highest temperature record, arrow-**a** does not show the highest enrichment in the year. This could be attributed to contribution from amount effect and heavy isotope washing off during a rainfall event. Within the "**a**" rainfall series with almost consistent air temperature, the rainfall became more depleted with time, a condition that is attributed to washing out of heavy isotopes from the cloud mass. Arrows-**d** and "**e**" clearly show an amount effect in that the temperature is constant but there is a variation in $\delta^{18}O$ and $\delta^{2}H$ between the two. Enrichment is observed in "**d**" of low rainfall and depletion in "**e**" of higher rainfall amount. At "**m**", both temperature and rainfall are low, thereby neutralising the amount and temperature effects leading the isotopic signature to average values.

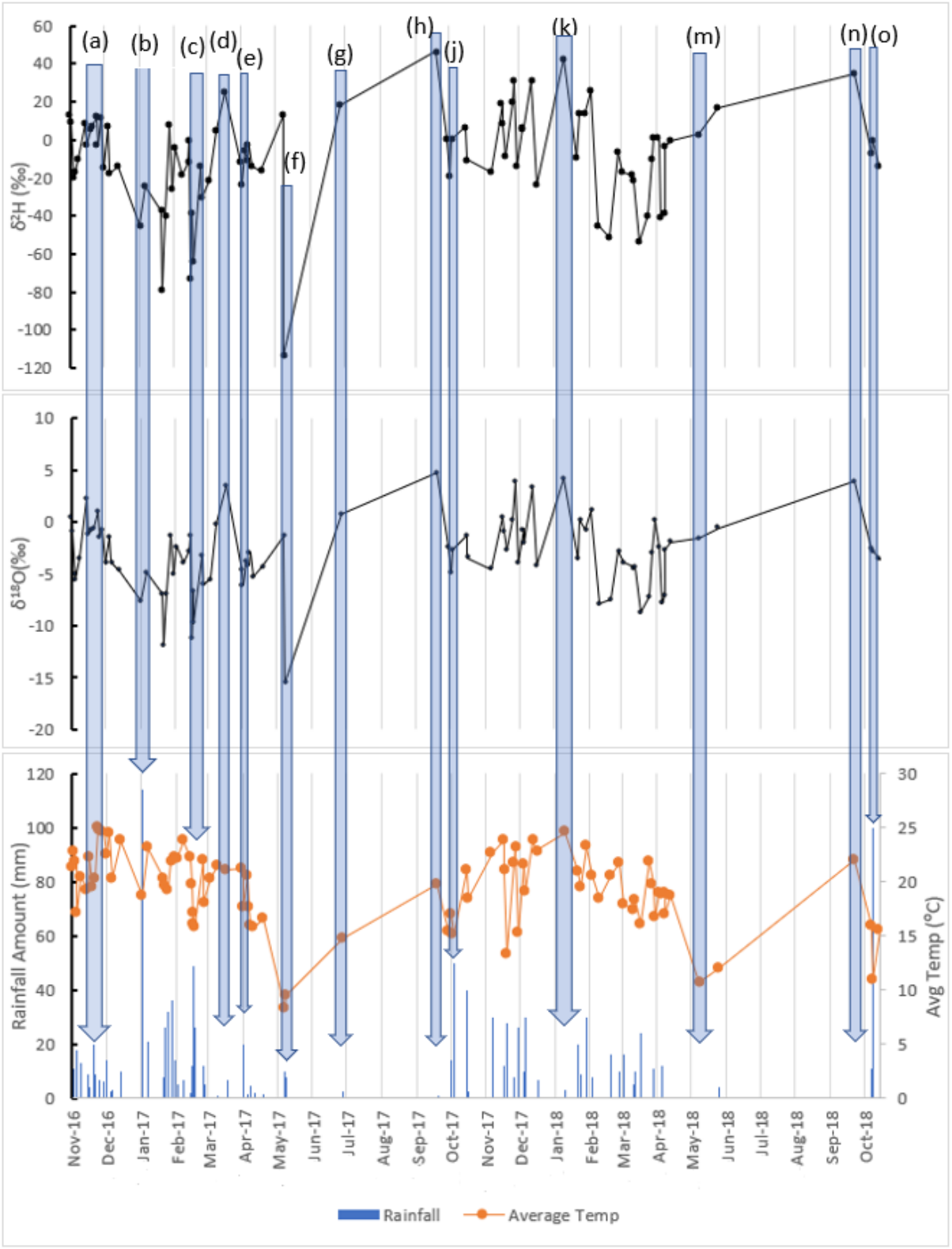

Figure 6.7: Time series of daily air temperature, amount of rainfall and stable isotopes in rainfall sampled at Montgomery Park rain sampling station during the period between November 2016 and November 2018.

The above analysis indicates that there is amount and temperature effect in the Johannesburg rainfall. In order to further characterise the temperature effect, Figure 6.8 (a) and (b) display $\delta^{18}O$ variation with daily air temperature and monthly air temperature, respectively. The two plots in Figure 6.8

show scattered points with poor correlation. However, a closer linearity is observed on the daily plot, which has a R^2 value of 0.21 compared to the monthly plot, which has a value of 0.0006.

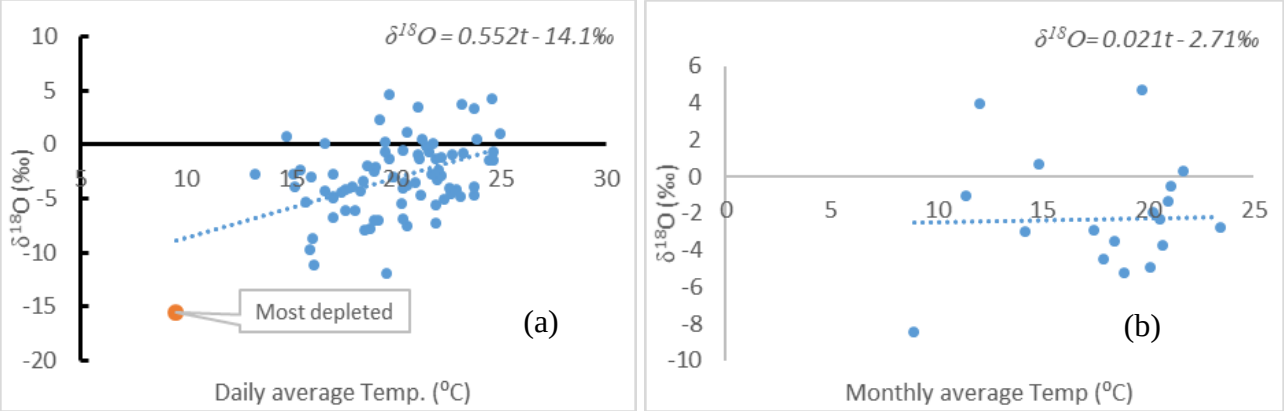

Figure 6.8: $\delta^{18}O$ variation with daily air temperature (a) and average monthly air temperature (b) for two years.

Equation 13 and Equation 14 are the established Johannesburg air temperature-$\delta^{18}O$ relationships for the daily and monthly, respectively (Figure 6.8).

$\delta^{18}O = 0.552t - 14.1‰$ *(R^2=0.21)* *(Equation 13)*

$\delta^{18}O = 0.021t - 2.71‰$ *(R^2=0.0006)* *(Equation 14)*

Despite the poor correlation in both regression equations, the trend lines have positive slopes, indicating some influence of temperature effect. However, the slope and $\delta^{18}O$-intecept obtained on a daily plot (0.552 and -14.1‰, respectively) are slightly lower compared to the ranges proposed by Gat (2001) using monthly data (0.521±0.014 slope and -14.96±0.21‰ intercept) (Equation 15). The slope from the Johannesburg monthly plot (0.021) diverges far below, and the $\delta^{18}O$-intecept (-2.71‰) is far above the Gat (2001) proposed intercept ranges. The monthly $\delta^{18}O$-intecept value that is higher than the value proposed by Gat (2001), means that the rainfall at 0°C is more enriched in Johannesburg than in the Northern Hemisphere where Gat (2001) undertook the majority of the study. The variation could be due to the location of the area in sub-tropical climatic setting, which is warmer than the European and north Atlantic stations where the previous studies were conducted.

Amount effect was also observed in the plots of $\delta^{18}O$ and $\delta^{2}H$ versus rainfall amount as shown in Figure 6.9. However, the enriched rainfall seems to obey amount effect more than the depleted one. The enriched rainfall could be a result of evaporation from highly enriched terrestrial water bodies or moisture source from the warmer Indian Ocean, while the depleted rainfall, which also vaguely obeys the amount effect could be a result of influence from cyclonic cold moisture source such as from the Antarctic region. The two water types that deviate from linearity are encircled in Figure 6.9. The most depleted rainfall as shown in Figure 6.8 and Figure 6.9 seems to obey temperature effect than amount effect. It has low temperature, which tallies well with temperature effect but it has a low rain amount, which contradicts amount effect. This could be an indication that the moisture was coming from the cold high latitude source in winter season (May 2017-Figure 6.7) when the local air temperatures were also low. However, the assessment of the isotopic ranges of the different moisture sources is beyond the scope of this study, but the study only deduces the likely moisture sources based on depletion or enrichment among the possible moisture sources for the UCRB.

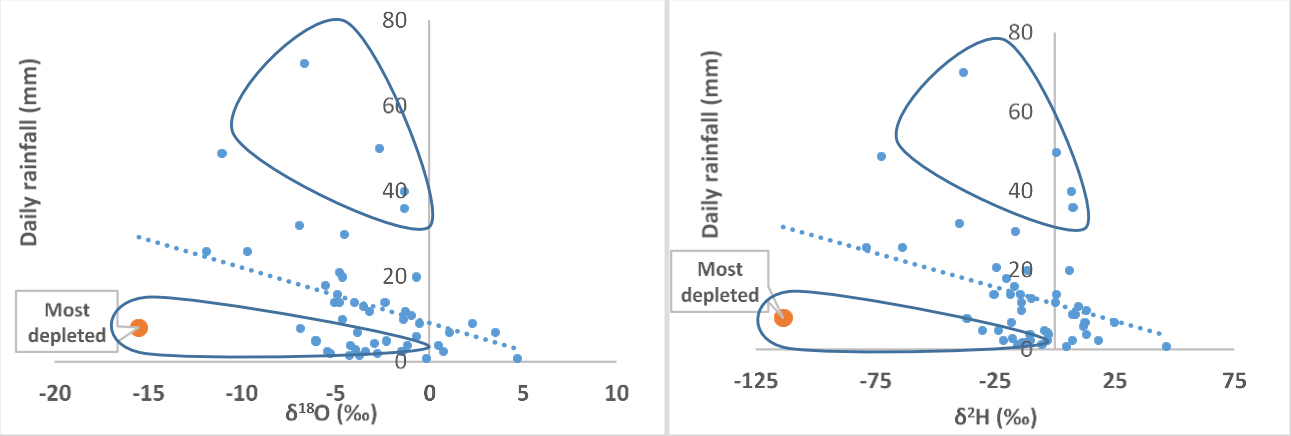

Figure 6.9: Stable isotopes ($\delta^{18}O$, $\delta^{2}H$) plotted against precipitation to assess traces of amount effect in Johannesburg daily rainfall. The water types that show extreme deviation from linearity are encircled.

6.3.2 Characterising groundwater recharge mechanisms using stable and non-stable isotopes of the water molecule ($\delta^{2}H$, $\delta^{18}O$, ^{3}H).

Table 6.5 shows the environmental isotope results for the Albert Farm spring, which was sampled monthly from June 2016 to June 2018. Table 6.6 also shows the environmental isotope results for groundwater and surface water sampled once between June 2016 and February 2017. The d-excess values computed from the JLMWL for each sample are also shown on the tables.

Table 6.5: The environmental isotope results for the Albert Farm spring sampled monthly from June 2016 to June 2018

ID	$\delta^{2}H$ (‰)	^{2}H StDev (‰)	$\delta^{18}O$ (‰)	^{18}O StDev (‰)	d-excess (‰)	^{3}H (T.U)	Error
Jun 2016	-19.29	0.23	-5.27	0.1	16.02	-	-
Jul 2016	-21.6	0.28	-6.01	0.09	18.67	-	-
Aug 2016	-19.08	0.14	-4.3	0.05	9.73	-	-
Sept 2016	-14.5	0	-2.86	0	4.66	-	-
Oct 2016	-13.71	1.28	-3.79	0.13	11.67	-	-
Nov 2016	-15.97	0.28	-3.78	0.12	9.37	2.3	±0.3
Dec 2016	-14.3	0.06	-3.57	0.10	9.61	-	-
Jan 2017	-12.5	0.53	-3.09	0.03	8.25	-	-
Feb-2017	-15.0	0.8	-3.43	0.0	8.00	-	-
Mar-2017	-16.4	0.6	-3.67	0.1	8.23	-	-
Apr-2017	-15.2	0.7	-4.13	0.2	12.43	-	-
May-2017	-12.3	0.5	-3.11	0.1	8.59	-	-
Jun 2017	-14.9	0.4	-3.46	0.0	8.27	-	-
Jul 2017	-16.3	1.2	-3.92	0.2	9.96	-	-
Aug 2017	-15.2	0.3	-3.05	0.1	5.24	-	-
Sept 2017	-18.3	0.3	-3.72	0.1	6.62	-	-
Oct 2017	-20.3	0.3	-4.12	0.1	7.30	-	-
Nov 2017	-12.0	0.4	-2.28	0.1	3.23	2.0	±0.3
Dec 2017	-11.7	1.5	-2.81	0.1	7.09	-	-
Jan 2018	-10.5	2.2	-2.79	0.2	8.20	1.9	±0.3
Feb-2018	-14.2	0.5	-2.86	0.1	4.94	-	-
Mar-2018	-16.0	1.3	-3.45	0.1	7.12	-	-
Apr-2018	-12.9	0.8	-3.10	0.1	7.86	-	-
May-2018	-12.3	2.8	-3.13	0.4	8.68	-	-
Jun 2018	-12.9	1.1	-2.85	0.1	6.27	-	-

Table 6.6: Environmental isotope data for groundwater and surface water.

ID	Latitude	Longitude	δ^2H (‰)	^2H StDev (‰)	$\delta^{18}O$ (‰)	^{18}O StDev (‰)	d-excess (‰)	^3H (T.U)	Error	Water Source
BH1	-25.67378	27.85107	-6.5	0.6	-1.39	0.1	4.55	5.3	±0.4	Borehole
BH2	-25.66243	27.81031	-6.8	1.0	-1.11	0.2	2.05	6.3	±0.5	Borehole
BH3	-25.70531	27.78251	-5.0	0.6	-0.89	0.1	2.07	1.7	±0.3	Borehole
BH4	-25.69700	27.86117	-18.1	1.6	-3.96	0.2	13.59	3.2	±0.4	Borehole
BH5	-25.63700	27.71011	-9.9	0.6	-1.94	0.1	5.60	2.8	±0.3	Borehole
BH6	-25.59320	27.72135	-26.5	0.12	-4.79	0.04	11.80	6.7	±0.5	Borehole
BH7	-25.59300	27.72135	-19.4	1.1	-4.09	0.1	13.32	5.9	±0.4	Borehole
BH8	-25.54250	27.87209	-9.6	0.5	-2.01	0.3	6.48	4.2	±0.4	Borehole
BH9	-25.48145	27.76628	-17.8	0.8	-3.05	0.1	6.65	2.3	±0.3	Borehole
BH10	-25.41614	27.62571	-17.1	1.4	-3.00	0.2	6.97	3.7	±0.4	Borehole
BH11	-25.37080	27.55919	-10.1	2.3	-1.71	0.3	3.55	3.8	±0.4	Borehole
BH12	-25.66576	27.60464	-14.4	0.6	-3.12	0.1	10.52	3.3	±0.4	Borehole
BH13	-25.75739	27.48989	-13.0	0.3	-2.14	0.1	4.14	2.2	±0.3	Borehole
BH14	-25.70753	27.80922	-0.9	1.5	-0.35	0.2	1.96	1.3	±0.3	Borehole
BH15	-25.74678	27.82403	-6.88	0.34	1.58	0.03	-19.52	4.8	±0.4	Borehole
BH16	-25.77922	27.84744	-39.3	0.4	-12.65	0.1	61.86	3.3	±0.4	Borehole
BH17	-25.78192	27.85511	-38.2	0.12	-13.47	0.03	69.58	1.3	±0.3	Borehole
BH18	-25.82533	27.81450	-32.8	0.07	-9.76	0.04	45.32	1.9	±0.3	Borehole
BH19	-26.18844	28.02931	-12.3	0.3	-2.23	0.1	5.56	1.4	±0.3	Borehole
BH20	-26.14838	28.00663	-12.4	0	-3.52	0	15.75	2.8	±0.3	Borehole
BH22	-26.12743	27.95913	-15.8	0.7	-3.55	0.1	12.56	1.9	±0.3	Borehole
BH23	-26.09973	27.64191	-12.5	3.5	-2.62	0.3	8.50	1.5	±0.3	Borehole
BH24	-25.98829	27.48239	-22.5	0.5	-5.08	0.4	18.15	1.2	±0.3	Borehole
BH25	-25.93074	27.90525	-21.6	0.4	-4.32	0.1	12.94	3.4	±0.4	Borehole
BH26	-25.79705	27.74881	-16.7	0.3	-3.27	0.1	9.44	3.1	±0.3	Borehole
BH27	-25.71812	28.03547	-15.0	0.7	-3.18	0.1	10.37	2.6	±0.3	Borehole
BH28	-26.15190	27.98402	-17.3	1.0	-3.83	0.1	13.36	1.8	±0.3	Borehole
BH29	-26.15991	27.99385	-18.2	1.5	-3.83	0.2	12.49	0.5	±0.2	Borehole
BH30	-25.88426	28.07489	-25.3	0.4	-5.15	0.0	15.85	0.6	±0.2	Borehole
SP1	-25.90807	27.79756	-27.6	0.4	-4.97	0.1	12.21	1.3	±0.3	Spring
SP3	-25.87524	27.78584	-27.5	0.5	-5.11	0.1	13.35	1.5	±0.3	Spring
SP4	-25.87494	27.78365	-29.6	0.4	-5.28	0.1	12.61	0.9	±0.2	Spring
SP7	-25.87516	27.78002	-27.8	0.4	-4.77	0.1	10.37	0.9	±0.2	Spring
Hartbeespoort Dam										
SA14	-25.7298	27.8547	-2.82	0.03	2.71	0.1		5.8	±0.4	Dam
SA15	-25.7333	27.8643	-3.3	0.0	2.07	0.0		5.0	±0.4	Dam
SA16	-25.7353	27.8720	-5.12	0.03	-0.32	0.0		5.6	±0.4	Dam
SA17	-25.7393	27.8816	-2.9	0.16	2.88	0.05		6.0	±0.4	Dam
SA18	-25.7548	27.8877	-2.74	0.12	2.58	0.07		6.0	±0.4	Dam
SA19	-25.7630	27.8929	-4.49	0.0	-0.45	0.0		6.1	±0.4	Dam
SA20	-25.7604	27.8688	-4.93	0.0	-0.37	0.0		5.6	±0.4	Dam
SA21	-25.7484	27.8636	-5.14	0.06	-0.5	0.12		6.6	±0.4	Dam
SA22	-25.7489	27.8482	-4.9	0.14	-0.66	0.04		6.2	±0.5	Dam
SA23	-25.7543	27.8264	-5.68	0.08	-0.69	0.02		5.4	±0.4	Dam
SA24	-25.7614	27.7978	-6.02	0.0	-0.4	0.0		6.5	±0.5	Dam

- *Stable isotopes (δ^2H versus $\delta^{18}O$) analysis*

The Albert Farm spring monthly isotope values ranges from -6.01‰ to -2.28‰ for $\delta^{18}O$ and from -21.6‰ to -10.48‰ for δ^2H with d-excess ranging from 3.23‰ to 18.7‰ for the review period. A variable isotopic signature is observed from the UCRB groundwater samples.

Figure 6.10 shows the stable isotope plot of all groundwater and surface water samples with respect to the Johannesburg Local Meteoric Water Line (JLMWL), Pretoria Local Meteoric Water Line (PLMWL) and the Global Meteoric Water Line (GMWL).

It can be observed in Figure 6.10 that surface water follows its distinct trend forming a surface water evaporation line, expectedly so, because of the evaporation exposure that leads to enrichment in heavy isotopes. On the other hand, all groundwater samples, with the exception of boreholes BH15, BH16, BH17 and BH18, seem to plot close to the meteoric water lines with various degrees of displacement. Generally, the most depleted samples are from the Transvaal Supergroup, including the boreholes BH16, BH17 and BH18, and the dolomitic springs (SP1, SP3, SP4 and SP7). Borehole BH15 is the most enriched groundwater sample and it plots along the surface water evaporation line. BH15 is located about 750 m to the north of Hartbeespoort Dam on the southern side of the Magaliesberg quartzite ridge.

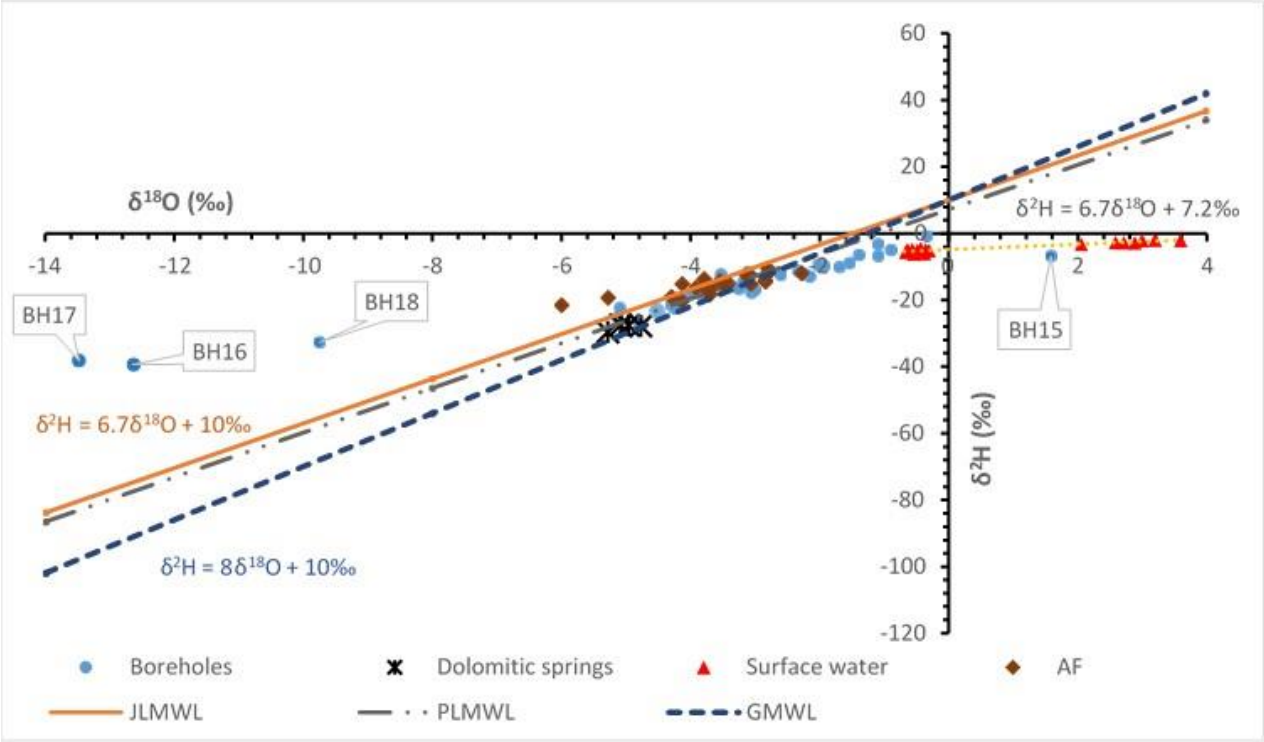

Figure 6.10: Stable isotopes of groundwater and surface water versus Johannesburg Local Meteoric Water Line (JLMWL), Pretoria Local Meteoric Water Line (PLMWL) and Global Meteoric Water Line (GMWL) (Craig, 1961).

Figure 6.11 is a zoomed version presenting a plot of all groundwater samples excluding the boreholes that plot on the two extremes of Figure 6.10, which are the most depleted BH16, BH17 and BH18 and the most enriched BH15. According to Figure 6.11, all boreholes plot along an evaporation line with a regression of $\delta^2H=4.7\delta^{18}O-0.96‰$ ($R^2=0.95$). Borehole BH24 occupies the depleted portion of the zoomed plot and, it is also underlain by the rocks of the Transvaal Supergroup. Surprisingly, boreholes BH25 and BH30, which are located on the periphery of the basement granitic gneiss near the Black Reef quartzites of the Transvaal Supergroup, also seem to trend towards the depleted Transvaal Supergroup groundwater samples.

Figure 6.11 also shows that boreholes BH1, BH2, BH3 and BH14, which are positioned on the northern side of the Magaliesberg Ridge (Hartbeespoort Dam) occupy the most enriched portion of the plot but still plot along the groundwater evaporation line. These boreholes trend towards the highly enriched BH15 and surface water samples. Figure 6.11 also shows the monthly samples for Albert Farm spring. It can be observed that the stable isotopes in Albert Farm spring are variable and

they all plot close to the JLMWL. Though Albert Farm spring samples were collected from a single sample location, its 24 months stable isotope record seems to cover more than half of the plot towards the depleted portion.

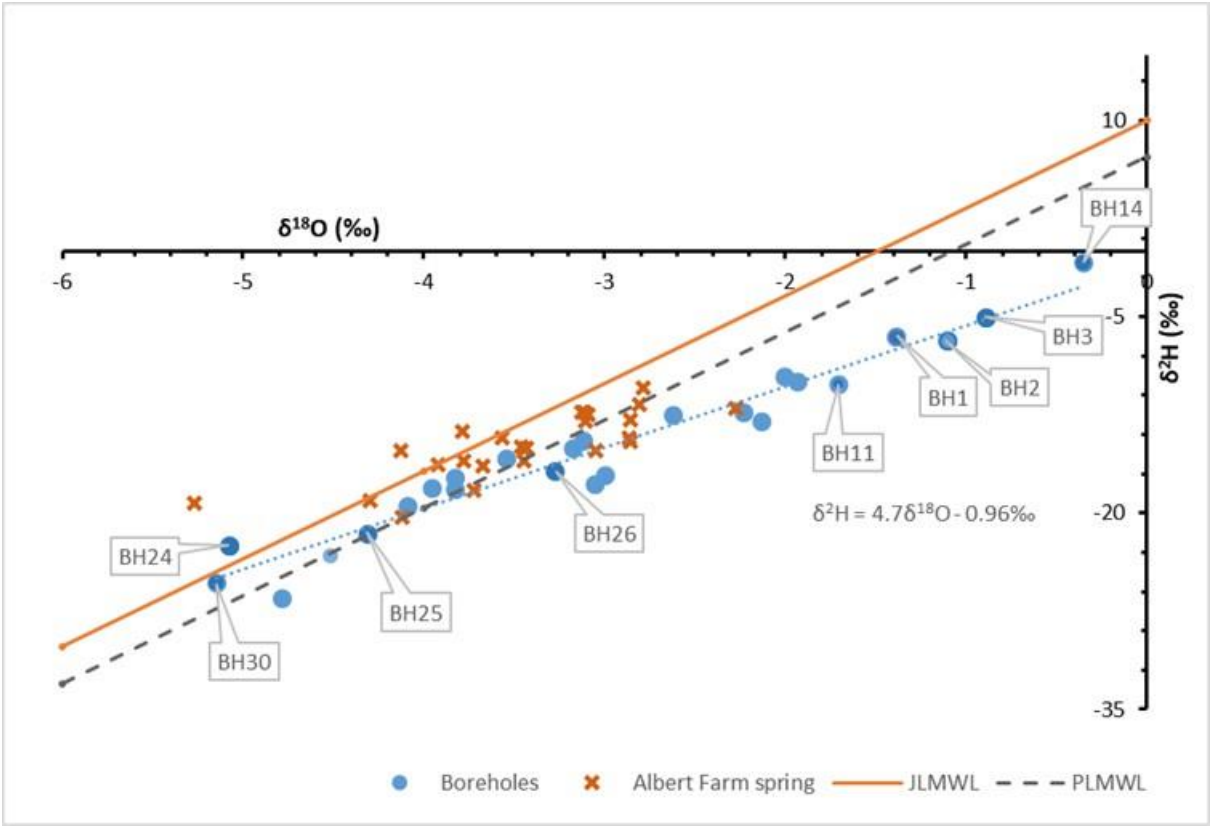

Figure 6.11: Zoomed in view of the boreholes plotted against the JLMWL (solid line $\delta^2H=6.7\delta^{18}O+10‰$) with borehole evaporation line shown as a dotted line.

The isotopic signature of borehole BH15 shows evidence of connectivity with surface water, which is not surprising seeing its close proximity with the Hartbeespoort Dam. This indicates that the aquifer that feeds borehole BH15 is recharged via focused mechanisms. There are possibilities of mixing between groundwater that recharged from focused mechanisms and diffuse recharge from rainfall. This is particularly observed in boreholes BH1, BH2, BH3 and BH14, which are located on the northern side of Hartbeespoort Dam. They plot towards the enriched part of the $\delta^{18}O$ versus δ^2H diagram at the intersection of the groundwater evaporation and the surface water evaporation lines. These boreholes could be engaging both diffuse recharge from precipitation, irrigation with surface water and focused recharge through the Brits fault lines and the bedding planes in the quartzites of the Magaliesberg Formation.

The alignment of the groundwater samples along the JLMWL with a slightly lower slope (Figure 6.11) shows recharge that occurred via diffuse mechanisms without prior exposure to extreme evaporation. The fractured nature of the rocks in the UCRB could also be contributing to rapid recharge from rainfall, particularly at the exposures along the catchment boundaries and the sinkholes and cavities of the dolomitic aquifers. In an assessment of the provenance of groundwater in the UCRB, Abiye (2011) indicated that the intensively fractured quartzite outcrops of the Witwatersrand Supergroup on the catchment boundary, provide a suitable condition for vertical recharge from precipitation. The observed high depletion of the Transvaal Supergroup samples could mean that effective recharge is not dominated by local rainfall but could be occurring elsewhere at higher

elevation through diffuse mechanisms without undergoing extreme evaporation prior to recharge. This high depletion can also be related to an exchange of oxygen between CO_2 and groundwater, particularly given that the Transvaal Supergroup consists of the Malmani Subgroup, which is represented by the dolomites. The high $\delta^{18}O$ depletion in groundwater was also reported as a common occurrence in natural CO_2 rich groundwater by Karolytė *et al.* (2017). Furthermore, the depletion of boreholes BH25 and BH30, which are positioned on the periphery of the basement granites could indicate influence of groundwater from the Transvaal Supergroup. Based on the presented results and observations, both focused and diffuse recharge mechanisms can be observed in the UCRB.

Figure 6.12 shows $\delta^{18}O$ versus d-excess plots of selected groundwater samples that were characterised from $\delta^{18}O$ versus $\delta^{2}H$ plots as having undergone diffuse recharge. The groundwater samples that were deduced to have recharged via focused mechanisms were excluded because they have been altered by evaporation in the surface water body prior to recharge. These samples do not represent the isotopic signature of precipitation and, therefore, the moisture source conditions of the precipitation may not be inferred with certainty. The d-excess values were used to assess the moisture source location and the humidity conditions at the source location.

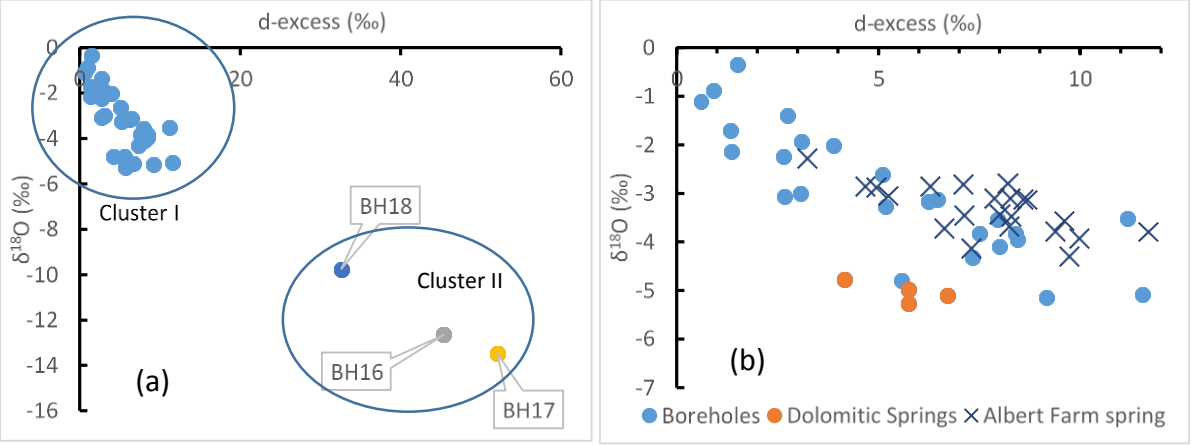

Figure 6.12: Plot of d-excess versus $\delta^{18}O$ for groundwater samples in the UCRB.

A varying signature in d-excess is observed among the groundwater samples. The variation in the $\delta^{18}O$ versus d-excess plots shows rainfall that has contributions from different moisture sources. Figure 6.12 (a) shows two clusters of groundwater samples with Cluster I having the majority of the groundwater samples that are further illustrated in Figure 6.12 (b) and Cluster II having the extremely depleted boreholes BH16, BH17 and BH18 with a high d-excess. Cluster II represents groundwater that recharged from rainfall whose moisture possibly evaporated under very low humidity and low temperature conditions, thereby, yielding highly depleted moisture. This is despite the possibilities of oxygen exchange between groundwater and CO_2.

Figure 6.12 (b) presents a zoomed in view of the boreholes, dolomitic springs, and the 24 months Albert Farm spring samples with exclusion of Cluster II boreholes. The Malmani dolomite springs are less scattered, and seem to form a cluster, suggesting that the aquifer is recharged from a similar moisture source or similar recharge episode, which is not surprising since the data represents a onetime sampling. The other borehole samples and the Albert Farm spring samples show variation across the plot. This indicates groundwater recharge by rainfall that was generated under different humidity conditions, different moisture source locations or mixture of different moisture sources i.e. the inland evaporation, warmer Indian Ocean, cooler Atlantic Ocean or the high latitude such as Antarctica. The samples with low d-excess could indicate groundwater that was recharged with

rainfall of moisture from inland evaporation source leading to convective rainfall or from the warmer region such as the Indian Ocean. The samples with high d-excess could indicate influence of frontal rainfall from the colder regions such as the Atlantic Ocean or the cold Antarctica region. It was stated in section 2.2 that the Johannesburg region occasionally receives convective rainfall and mainly frontal rainfall.

Having established that recharge in the UCRB occurs prior to extreme evaporation (recharge water was not isotopically altered prior to recharge), then groundwater resembles the isotopic signature of effective rainfall, which is also variable due to moisture source and climatic settings. The highly variable 24 months Albert Farm spring samples (Figure 6.11) could indicate the different recharge episodes of different rainfall that was generated at different moisture source locations. In that regard, the different isotopic signatures observed in the groundwater samples across the UCRB, could be a reflection of different recharge episodes rather than a spatial distribution of recharge mechanisms. Recharge rates and groundwater flow velocities vary in different lithologies, therefore, even though all other groundwater samples were collected at more or less the same period (February to April 2017), they most likely represented different recharge episodes of different isotopic signature.

This varying isotopic signature from a single sample location could be a good indication that in regions that receive rainfall of different isotopic signature, the use of a single groundwater sample to assess the mechanism of recharge may not be a good practice as this may erroneously yield biased interpretations.

A quasi-groundwater flow direction can be hypothesised based on stable isotope signatures of groundwater and surface water. Considering the four boreholes BH15, BH16, BH17 and BH26, which surround the Hartbeespoort Dam, groundwater flow direction can be deduced as northward. This is because, the south (BH16 and BH17) and western (BH26) boreholes show signs of depletion, while BH15, which is positioned on the northern side of the dam shows extreme enrichment similar to dam water, followed by the boreholes on the northern side of the Magaliesberg quartzite ridge (BH1, BH2, BH3, BH14). The two main semi parallel faults (Brits faults) that cut across the reservoir of the Hartbeespoort Dam in the north west-south east direction, could also be contributing to focused recharge, seeing that the enriched boreholes BH15 and BH14 are positioned on the western fault line.

- *Tritium analysis*

The tritium results in Johannesburg rainfall, just like the stable isotopes, are also variable. The tritium values for the two rainfall samples are 1.4±0.3 T.U collected in February 2017 and 3.5±0.4 T.U in October 2017. Abiye *et al.* (2015) also reported tritium values between 4.3±0.4 T.U and 8.0±0.5 T.U as shown in Table 6.7. The average tritium is then calculated as 3.4 ±0.4 T.U.

Tritium in groundwater ranges between 0.5±0.2 T.U and 6.7±0.5 T.U (Table 6.5 and Table 6.6), with the dolomitic springs having low tritium content and the boreholes on the northern side of the Hartbeespoort Dam generally having high tritium content. On the other hand, tritium values in Hartbeespoort Dam samples range between 5±0.4 T.U and 6.6±0.4 T.U and are significantly higher than all upstream groundwater samples, which range between 1.2±0.3 T.U and 3.4±0.4 T.U. Hartbeespoort Dam samples are almost in the same range as the boreholes in the northern side of the dam, which range between 1.3±0.5 T.U and 6.7±0.3 T.U. Similarly, Nkosi (2016) also obtained high tritium values in groundwater ranging between 3.5±0.4 and 7.1±0.5 T.U in the Brits area. The high tritium in the dam could come from the upstream industrial sources other than rainfall.

Table 6.7: Tritium in rainfall (*abstracted from Abiye *et al.* (2015)).

Date	**Tritium (T.U)**	
21-23 Feb 2017	1.4	±0.3
October 2017	3.5	±0.4
December 2010*	4.5	±0.4
January 2011*	4.3	±0.4
January 2012*	8.0	±0.5
Average	**3.34**	**±0.4**

Equation 4, ($t = t_{1/2} In ({}^{A_{t0}}/_{A_{t1}})/In2$), is often applied in hydrogeological studies to estimate the residence time of groundwater with the premise that precipitation is the sole source of tritium in groundwater. However, having a groundwater tritium content higher than precipitation indicate that there is an extra source of tritium into groundwater other than precipitation, thereby, presenting a challenge with the application of Equation 4. On a general basis, the low tritium content in the Malmani dolomite springs could indicate groundwater that spent a longer period since recharge, confirming what was deduced from the stable isotope interpretations.

Figure 6.13 (a) shows a schematic representation of the Hartbeespoort Dam with the two Brits fault lines. Shown in Figure 6.13 (b) is the Magaliesberg quartzite ridge dipping to the north and exposing the quartzite bedding planes onto the Hartbeespoort Dam to the south (right side on the image). Tritium values for borehole BH14 and BH15 are close to the Hartbeespoort Dam values and much higher than all other upstream boreholes. This supports the concept that groundwater flow direction is northwards such that the boreholes on the north of the Magaliesberg quartzite ridge are dominated by focused recharge from the dam. Considering that focused recharge occurs from the dam through the fault lines to feed boreholes BH14 and BH15, then the groundwater flow rate was estimated using Equation 4 and average tritium in the dam water as input, tritium in groundwater as output and a half-life of 12.43 years. The groundwater residence time and the flow rate for the boreholes are shown in Table 6.8.

Table 6.8: Estimated groundwater flow period and flow velocity.

Site	**T.U**	**Flow period (Yrs.)**	**Distance (m)**	**Flow velocity (m/Yr.)**
Reservoir	5.9	-	-	-
BH15	4.8	4	750	204
BH14	1.3	27	5400	199
Average				**202**

The average groundwater flow velocity is estimated at 202 m/yr. Irrigation with dam water also has a potential to increase tritium levels through diffuse recharge. If irrigation contribution is factored in, then the estimated flow rates are assumed to be the minimum flow rates.

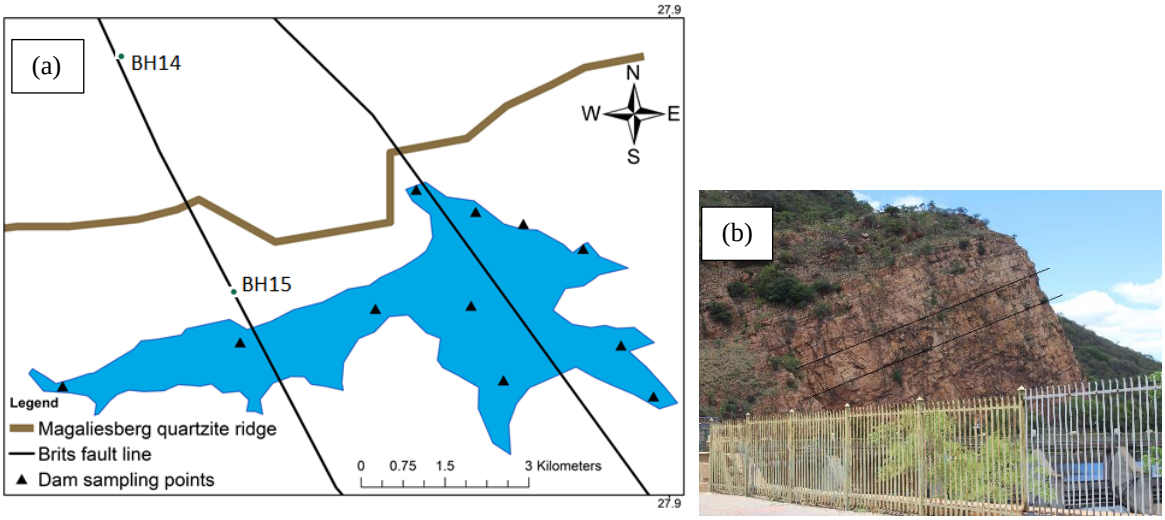

Figure 6.13: Schematic representation of Hartbeespoort Dam with the Brits fault lines (a) and north dipping quartzite bedding planes (b).

6.3.3 Using the amount and temperature effects to assess the groundwater recharge conditions

This section assesses the traces of amount and temperature effects in the discharge from the Albert Farm spring and tests the applicability of assessing the conditions of the rainfall from which groundwater recharge occurred. These conditions are rainfall amount, rainfall temperature, recharge mechanisms and groundwater flow mechanism.

- *Using spring discharge and stable isotope signature to assess the amount effect and the amount of effective rainfall*

It has been observed from the assessment of stable isotopes in precipitation that there are traces of amount and temperature effect in the Johannesburg rainfall. If the high rainfall amount is generally depleted and the low rainfall amount is enriched, then, having established from the $\delta^{18}O$ versus $\delta^{2}H$ plot (Figure 6.11) that groundwater in the Albert Farm spring is recharged by diffuse mechanisms prior to isotopic enrichment by evaporation, and assuming that the high amount of rainfall leads to high recharge and higher water table (and vice versa) then, it could be hypothesised that in a gravity fracture controlled spring where piston or preferential flow prevails, the high spring discharge is isotopically depleted and the low spring discharge is enriched.

Table 6.9 presents the 14 months stable isotope ($\delta^{18}O$, $\delta^{2}H$) and spring discharge data for the Albert Farm spring. Over this period, the discharge ranged between 0.66 L/s and 4.8 L/s.

Table 6.9: The stable isotope and spring discharge data from the Albert Farm spring.

Date	$\delta^{18}O$ (‰)	$\delta^{2}H$ (‰)	Spring discharge-Q (L/s)
Feb-17	-3.43	-15.0	3.2
Mar-17	-3.67	-16.4	3.9
Apr-17	-4.13	-15.2	4.8
May-17	-3.11	-12.3	2.2
Jun-17	-3.46	-14.9	3.6
Jul-17	-3.92	-16.3	3.8
Aug-17	-3.05	-15.2	1.4
Sep-17	-3.72	-18.3	1.4
Oct-17	-4.12	-20.3	1.9
Nov-17	-2.28	-12.0	0.66
Dec-17	-2.81	-11.7	1.3
Jan-18	-2.79	-10.5	1.3
Feb-18	-2.86	-14.2	1.2
Mar-18	-3.45	-16.0	2.3

Figure 6.14 shows the plots of spring yield versus stable isotopes with correlation values of 51% for yield versus $\delta^{18}O$ and a poor correlation of 8.7% between yield and $\delta^{2}H$. The figure shows that high flows are generally depleted, and low flows are enriched, which agrees well with the given hypothesis. The $\delta^{18}O$ versus yield correlation, however, seems to be most suitable at higher yield, while at low yield there seems to be an influence from more depleted water. This is observed by the outlier samples (encircled) that are both low yield and depleted. These samples have been deduced to be a result of low rainfall that came from a cold region with depleted stable isotope signature thereby, not fulfilling amount effect in rainfall. Figure 6.15 shows the plots of yield versus stable isotope signature with the outlier samples excluded. In these plots, a correlation of 91% is observed between the yield and $\delta^{18}O$, while $\delta^{2}H$ has a correlation of 47% with the regression lines shown on Equation 15 and 16.

These relationships confirm that the Witwatersrand quartzite aquifer that feeds Albert Farm spring is recharged from rainfall and also shows the dependence of recharge amount on the amount of rainfall.

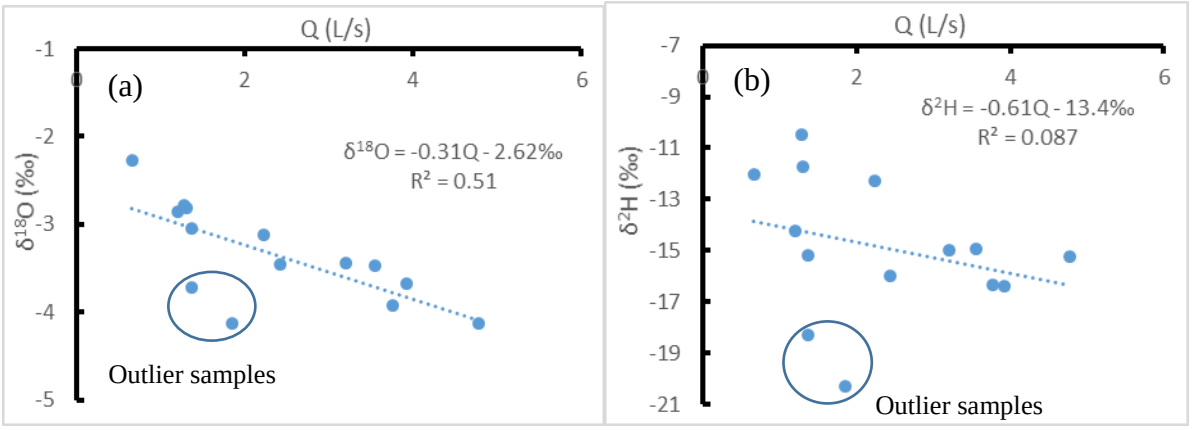

Figure 6.14: Plots of spring yield versus isotope signature at Albert Farm spring including the outlier points with (a) showing a correlation of 51% between yield and $\delta^{18}O$ and (b) showing no correlation between yield and $\delta^{2}H$.

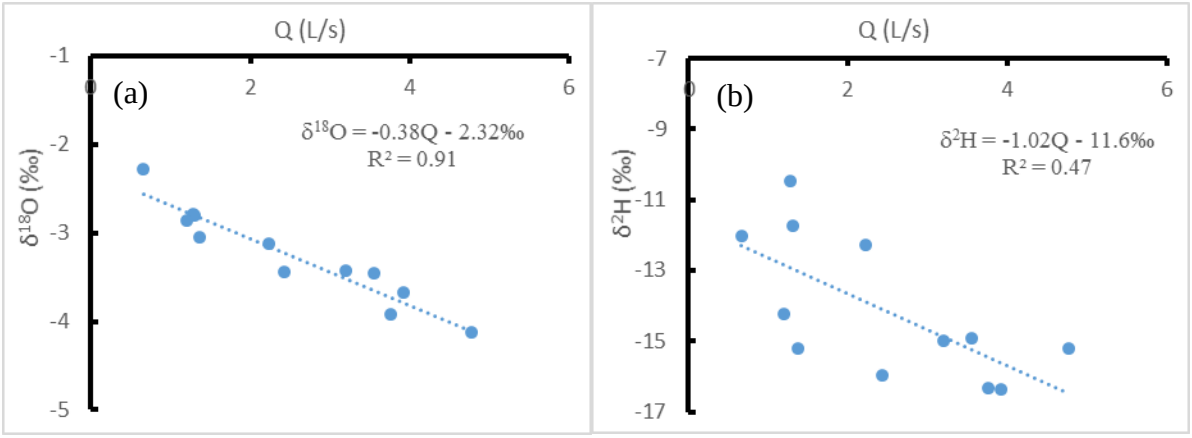

Figure 6.15: Plots of spring yield versus stable isotopes excluding outlier points with (a) showing a correlation of 91% between yield and $\delta^{18}O$ and (b) showing 47% between yield and $\delta^{2}H$.

$\delta^{18}O = -0.38Q - 2.32‰$, R^2=91% *(Equation 15)*

$\delta^{2}H = -1.02Q - 11.6‰$, R^2=47% *(Equation 16)*

Where Q is yield in L/s.

The regressions in Equation 15 and Equation 16 are also presented in Equation 17 and Equation 18, respectively using the SI units of m^3/s. It can be deduced that once the long-term spring yield versus $\delta^{18}O$ regression line has been established, a known spring discharge can be successfully used in Equation 17 and Equation 18 to estimate the stable isotope signature of the discharge and of the effective rainfall. The relationship could be improved with more long term stable isotope and discharge data.

$\delta^{18}O = -377Q - 2.32‰$ (*Equation 17*)

$\delta^{2}H = -1019.5Q - 11.6‰$ (*Equation 18*)

Where Q is yield in m^3/s.

- *Assessing the air temperature conditions at the time of recharge using the stable isotopes*

Based on the understanding that when diffuse-rapid recharge prevails, the isotopic signature of groundwater resembles that of effective rainfall, the temperature-$\delta^{18}O$ relationship ($\delta^{18}O=0.695T-13.6‰$; Equation 2) that was established by Dansgaard (1964) for rainfall was used to estimate the annual temperature at the time of recharge in the UCRB. Equation 13 ($\delta^{18}O=0.552T-14.1‰$), which was established from daily rainfall in this study, was also used to estimate the daily air temperature at the time of recharge. This was done using the $\delta^{18}O$ values (Table 6.5 and Table 6.6) of groundwater samples that were deduced through $\delta^{18}O$ versus $\delta^{2}H$ interpretations to have been recharged via diffuse mechanisms. The calculated annual and daily air temperatures are presented in Table 6.10 for the 24 months Albert Farm spring samples, the dolomitic springs and the selected boreholes.

Table 6.10: The estimated mean annual and daily air temperatures at the time of recharge.

Sample date	**Calculated Annual air Temp. (°C) on the year of recharge**	**Calculated daily air temperature during recharge (°C)**
Albert Farm spring		
Jun 2016	12.0	16.0
Jul 2016	10.9	14.7
Aug 2016	13.4	17.8
Sept 2016	15.5	20.4
Oct 2016	14.1	18.7
Nov 2016	14.1	18.7
Dec 2016	14.4	19.1
Jan 2017	15.1	19.9
Feb-2017	14.6	19.3
Mar-2017	14.3	18.9
Apr-2017	13.6	18.1
May-2017	15.1	19.9
Jun 2017	14.6	19.3
Jul 2017	13.9	18.4
Aug 2017	15.2	20.0
Sept 2017	14.2	18.8
Oct 2017	13.6	18.1
Nov 2017	16.3	21.4
Dec 2017	15.5	20.5
Jan 2018	15.6	20.5
Feb-2018	15.5	20.4
Mar-2018	14.6	19.3
Apr-2018	15.1	19.9
May-2018	15.1	19.9
Jun 2018	15.5	20.4
Average	**14.5**	**19.1**
MIN	**10.9**	**14.7**
MAX	**16.3**	**21.4**
Boreholes		
BH10	15.7	20.7
BH12	15.4	20.3
BH13	15.4	20.3
BH16	11.3	15.2
BH19	16.4	21.5
BH22	14.5	19.1
BH23	15.8	20.8

Sample date	Calculated Annual air Temp. (°C) on the year of recharge	Calculated daily air temperature during recharge (°C)
BH24	12.3	16.3
BH25	13.4	17.7
BH26	14.9	19.6
BH28	14.1	18.6
BH29	14.1	18.6
BH30	12.2	16.2
Dolomitic springs		
SP1 Nash Farm Spring	12.4	16.5
SP3 Nouklip Spring	12.2	16.3

The calculated surface air temperature for the year when the Albert Farm spring sample was recharged ranges between 10.9°C and 16.3°C, while the calculated daily air temperatures when the spring was recharged range between 14.7°C and 21.4°C. For the rest of the boreholes and dolomitic springs, the calculated annual surface air temperature ranges between 11.3°C and 17.6°C, while the daily calculated air temperatures range between 15.2°C and 21.5°C.

The calculated daily air temperatures on the day of rainfall for all groundwater samples are in the same range as the recent daily air temperatures measured between November 2016 and October 2018, which range between 15°C and 25°C (Figure 6.7). The calculated annual air temperatures have a slightly lower range compared to the present annual air temperatures that range between 15.5°C and 18.9°C (Figure 2.5) for the period 1997 to 2016 (JHB Bot Tuin weather stations).

The lower calculated annual air temperature could indicate two possibilities: 1) The Dansgaard (1964) equation is only applicable in the northern hemisphere stations where it was established and not applicable in the Johannesburg climate. 2) The Dansgaard (1964) is applicable in the Johannesburg climate, thereby meaning that at the time of recharge, the weather was characterised by annual temperatures that are colder than the present. On the other hand, the calculated daily air temperatures are still in agreement with the present air temperatures on the rainfall day. This could be explained by the fact that daily air temperature represents the actual temperature on the day of rainfall, which is assumed to be the temperature responsible for the fractionation (condensation in this case), while the annual temperature includes all days in a year even days without rainfall. It also indicates that, regardless of the change in climate, the physical temperature and humidity conditions that are suitable for condensation to occur are still the same, hence, there is agreement between the present measured daily air temperatures and the calculated daily temperatures at recharge.

6.3.4 Carbon isotopes to assess groundwater flow conditions and MRT

Table 6.11 shows the stable carbon ($\delta^{13}C$) and radiocarbon (^{14}C) data for the groundwater samples in the UCRB. The table also presents the MRT that was calculated for each sample using Equation 5. The table also shows the underlying lithology at each groundwater sample site.

Table 6.11: Isotope data for selected groundwater samples with radiocarbon data.

ID	**Lithology**	**$\delta^{13}C$ (‰)**	**^{14}C (pMC)**	**MRT (^{14}C years)**
BH1	Gabbro	-9.62	97.5 ± 2.6	209 ± 5
BH10	Lebowa Granite	-13.82	91.3 ± 2.6	752 ± 5
BH12	Gabbro/Norite	-10.27	98.5 ± 2.6	125± 5
BH13	Gabbro/Norite	-12.81	99.7 ± 2.6	25± 5
BH14	Gabbro, Norite, Anorthosite	-12.31	104.4 ± 2.7	0 ± 5
BH16	Shale/andesite	-17.35	88.2 ± 2.5	1038 ± 10
BH19	Quartzite/Shale	-15.22	95.7 ± 2.6	363 ± 5
BH22	Greenstones	-13.25	62.7 ± 2.3	3859 ± 10
BH23	Dolomite	-8.41	84.4 ± 2.5	1402 ± 10
BH24	Shale/andesite	-15.38	99.6 ± 2.6	33 ± 5
BH25	Granite/gneiss	-15.3	95.1 ± 2.6	415 ± 5
BH26	Shale	-15.07	101.5 ± 2.6	0 ± 5
BH28	Quartzite/Shale	-12.96	92.9 ± 2.6	609 ± 5
BH29	Granite/Gneiss	-12.29	98.1 ± 2.6	159 ± 5
BH30	Granite/Gneiss	-11.58	80.7 ± 2.5	1773 ± 10
SP1 Nash Farm Spring	Dolomite	-6.05	82 ± 2.5	1641 ± 10
SP3 Nouklip Spring	Dolomite	-5.64	79.9 ± 2.5	1855± 10
Albert Farm spring	Quartzite/Shale	-14.81	81.7 ± 2.5	1671± 10

- *Understanding groundwater flow conditions using the stable Carbon isotope ($\delta^{13}C$)*

As shown in Table 6.11, the $\delta^{13}C$ values range from the most depleted borehole BH16 with -17.35‰, which is underlain by the Silverton Formation and the Daspoort Formation of the Pretoria Group. On the other hand, the most enriched sample is the Nash Farm spring (SP1), which is hosted in the dolomites of the Malmani Subgroup with -5.64‰. Generally, all the Malmani Subgroup samples are represented by enriched values i.e., borehole BH23, Nash Farm spring and Nouklip spring. All other lithological units seem to show intermediate values.

Despite the intensive agricultural activities in the UCRB, the majority of land is uncultivated and consists of trees, grasses and shrub cover. This type of vegetation predominantly follows C3 photosynthesis (Clark and Fritz, 1997; Kohn, 2010). The dissolved inorganic carbon (DIC) evolution in groundwater of the UCRB is, therefore, assumed to be influenced by CO_2 from C3 vegetation, which has an average $\delta^{13}C$ value of -26‰ as reported by Marfia *et al.* (2004) and Kohn (2010). Therefore, further discussion assumes -26‰ as the initial $\delta^{13}C$ introduced into the deeper subsurface.

The depleted groundwater samples such as boreholes BH16, BH24 and BH26 from the Silverton Formation (shale) and Daspoort Formation (andesite); BH25 from the granites of the basement; borehole BH19 and Albert Farm spring from the quartzite of the Government Formation /shale of the Hospital Hill Formation indicate open system conditions deducing that the source of DIC is soil CO_2. The enriched Malmani dolomite samples, which include borehole BH23, Nash Farm spring and

Nouklip spring indicate carbonate dissolution that occurs in the aquifer under closed system conditions (Marfia *et al.*, 2004). The contribution of bicarbonate from the dolomites induces enriched $\delta^{13}C$ (‰) in groundwater.

While assessing the hydrochemistry of groundwater from the dolomites of the Malmani Subgroup, Barnard (2000) indicated that as infiltrating rainwater containing weak carbonic acid (H_2CO_3) percolates through the dolomitic terrain along the planes of weakness such as faults, fractures and joints, it causes dissolution of dolomite and increases bicarbonate concentration in groundwater as shown by the following chemical reaction:

$3CaCO_3.2MgCO_3+5H_2CO_3 \rightarrow 3Ca(HCO_3)_2 + 2Mg(HCO_3)_2$
Dolomite + Carbonic acid → Calcium-bicarbonate + Magnesium-bicarbonate.

The dolomite is enriched in ^{13}C, therefore, as the dolomite dissolves, it introduces an enriched $\delta^{13}C$ signature in the dissolved inorganic carbon, hence the enriched groundwater samples in the dolomites aquifer.

Groundwater samples that show intermediate values of $\delta^{13}C$‰ (-13.25‰ to-11.58‰) such as boreholes BH10, BH14, BH22, BH28, BH29 and BH30 suggest evolution from closed system condition to open system due to carbonate dissolution or mixing of water in an open system (such as from soil CO_2) and water that has undergone closed system carbonate dissolution along its flow path, particularly borehole BH30, which is positioned at the periphery of the basement granites near the Malmani dolomite aquifers. BH14 may also be expected to show high depletion due to its host rocks (gabbro, norite and anorthosite), which are rich in silicate minerals and poor in carbonate minerals (Judson *et al.*, 1976). However, its intermediate signature could be a result of influence of water from the Hartbeespoort Dam, which receives inflow from the rivers that are fed by the enriched dolomitic springs such as Nash Farm and Nouklip.

In the $\delta^{18}O$ versus $\delta^{2}H$ diagram, borehole BH16 and the Malmani dolomite springs showed extreme depletion, which indicated possibilities of recharge from the isotopically similar rainfall. However, in the stable carbon isotopes ($\delta^{13}C$ ‰) a high distinction is observed where by, the Malmani dolomite springs are highly enriched and BH16 is highly depleted. This indicates the differences in groundwater flow conditions and aquifer media. Borehole BH16 shows open system carbon evolution suggesting that it does not have interaction with the dolomitic aquifer, while the Malmani dolomite samples show closed system carbon evolution indicating a different groundwater flow path from BH16, which is underlain by shale and andesite. This indicates that in as much as they are recharged by similar rainfall, they undergo different groundwater flow paths.

- *Radiocarbon dating of groundwater*

As shown in Table 6.11 and Figure 6.16, carbon-14 data in percent modern carbon (pMC) ranges between 60 pMC and 100 pMC, with the majority ranging between 80 pMC and 100 pMC. Figure 6.16 (a) shows the plot of ^{14}C (pMC) versus $\delta^{18}O$ (‰), while Figure 6.16 (b) shows the plot of the ^{14}C age from present (MRT) versus the estimated annual temperature at the time of recharge. Though a poor correlation of 5% is observed between ^{14}C age and annual temperature, the regression line with an equation of $T(^0C) = 0.0004^{14}Cyears + 14.5^0C$ has a negative slope, indicating that the annual temperatures have generally been increasing over time.

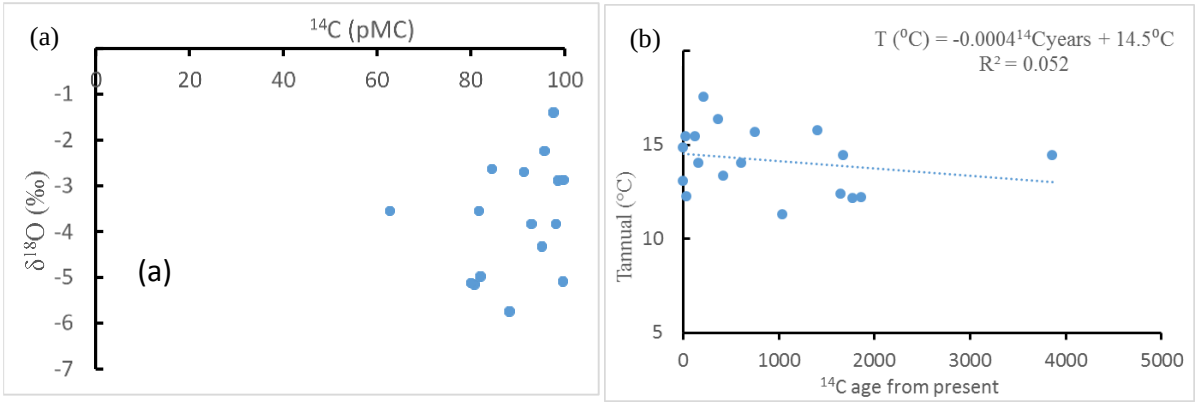

Figure 6.16: $\delta^{18}O$ versus ^{14}C (a) and calculated annual recharge temperatures (b) obtained from the Dansgaard (1964).

The radiocarbon data reveals that there is a vast MRT difference in groundwater found in the UCRB with the most recent in boreholes BH14 and BH26. BH14 is found on the northern side of the Hartbeespoort Dam, 5400 m downstream underlain by the rocks of the Bushveld Igneous Complex, while BH26 is in the western side of Hartbeespoort Dam on the flat topography underlain by the Silverton Formation. The highest MRT was found in borehole BH22 and BH30 underlain by greenstones and granitic gneiss of the basement, followed by the Malmani Subgroup samples represented by boreholes BH23, Nash Farm spring and Nouklip spring. The Malmani Subgroup aquifer is represented by the MRT ranging between 1855 years and 1402 years. Borehole BH30, which is found at the periphery of the basement towards the quartzites of the Black Reef Formation also showed the MRT of 1700 years. The ages of samples from other lithologies are not as distinct as the Malmani dolomites, meaning they are represented by different recharge episodes, possibly due to the heterogeneity of the aquifers. The Witwatersrand quartzite samples range from 1670 years in Albert Farm spring and 363 years in borehole BH19, both positioned on the southern boundary of the UCRB (Figure 5.4).

The old groundwater in the Malmani dolomite aquifer seems to be in agreement with the high depletion that was observed in the $\delta^{18}O$ versus $\delta^{2}H$ plots that has been attributed to the occurrence of high elevation recharge, which is possibly followed by long periods of deep circulation within the dolomitic aquifer. This also agrees with the stated possibilities of oxygen exchange between CO_2 and groundwater on the premise that such an exchange requires a long period of water rock interaction, particularly under cold temperatures. The stable isotope plots also indicated that borehole BH30 plots towards the depleted Transvaal Supergroup samples indicating possibilities of mixing. Therefore, the old age that is observed in BH30 could also confirm that there is mixing between the two aquifers. The recent age that is observed in boreholes BH14 and BH26 can be attributed to recharge from Hartbeespoort Dam as it was also deduced from stable isotope ($\delta^{18}O$ and $\delta^{2}H$) interpretations. Furthermore, the use of tritium as a tracer, estimated the travel time of 27 years between the reservoir and BH14, which is reasonably represented as recent based on the resolution of ^{14}C methods to recent waters.

Overall, out of 18 groundwater samples, 22% were recharged between recent and 100 years, collectively referred to as recent water, 78% between 100 and 3856 years referred to as old water. It

is deduced from these values that groundwater in the UCRB is dominated by old recharge episodes. Such diverse episodes could indicate the aquifer heterogeneity.

6.3.5 Hydrogeological characterisation of the dolomitic springs

Table 6.12 presents the hydrochemical data for the Malmani dolomite springs. The EC values range between 136.5 µS/cm and 220 µS/cm, pH ranges between 7.53 and 8.59, ORP ranges between -75.2 mV and 15.7 mV. Figure 6.17 presents the Stiff diagrams for the dolomitic springs. The Stiff diagrams were generated using the Windows Interpretation System for Hydrogeologists (WISH) computer program from the Institute for Groundwater Studies, University of the Free State. The figure shows that the major cations are Ca^{2+} and Mg^{2+}, while the major anion is HCO_3^-. Figure 6.18 and Figure 6.19 represent the changes in the physicochemical parameter along the flow path. It can be observed that there is a general decrease in EC and ORP and an increase in pH as water flows downslope to the lower reaches of the valley. These are observed by the slopes on the plots which are negative for EC and ORP and positive for pH.

Table 6.12: Hydrochemical data for the Malmani Dolomite springs.

Code	**Lat**	**Long**	**Elev.**	**EC**	**Temp.**	**pH**	**TDS**	**ORP**	**Ca^{2+}**	**Mg^{2+}**	**Na^{+}**	**K^{+}**	**HCO_3^{-}**	**CO_3^{2-}**	**Cl-**	**SO_4^{2-}**	**Electrical Balance**
			masl	µS/cm	°C		mg/L	mv	mg/L	mg/L	mg/L	mg/L	mg/L	mg/L	mg/L	mg/L	%
SP1-Nash Farm spring	-25.90806	27.79755	1450	181.4	22.1	7.53	116.2	-15.7	38	23	1.6	0.5	224	0	2.4	2.9	1.3
SP2	-25.90455	27.79596	1440	188.9	21.3	8.11	120.7	-64.5	32	24	1.5	0.2	207	1	2.4	2.4	1.7
SP3-Nouklip spring	-25.87515	27.78574	1323	220	21.6	7.65	140.2	-22.2	41	26	1.5	0.4	243	0	1.4	2.1	2.7
SP4	-25.87448	27.78378	1319	172.3	21.3	7.66	110	-31	38	24	1.5	0.3	226	2	1	0.6	2.1
SP5	-25.87471	27.7809	1320	-	21.5	7.77	-	-	-	-	-	-	-	-	-	-	
SP6	-25.87472	27.78048	1300	172.6	21.5	8.53	110.6	-73.2	34	24	1.3	0.3	221	4	1.4	1.9	-0.9
SP7	-25.87541	27.77959	1290	136.5	20.8	8.59	87.4	-75.2	31	20	1.8	0.4	219	5	2	1	-7.4
SP8	-25.87569	27.77913	-	-	21.10	8.52	-	-	-	-	-	-	-	-	-	-	
SP9	-25.87598	27.77968	-	-	19.20	8.38	-	-	-	-	-	-	-	-	-	-	

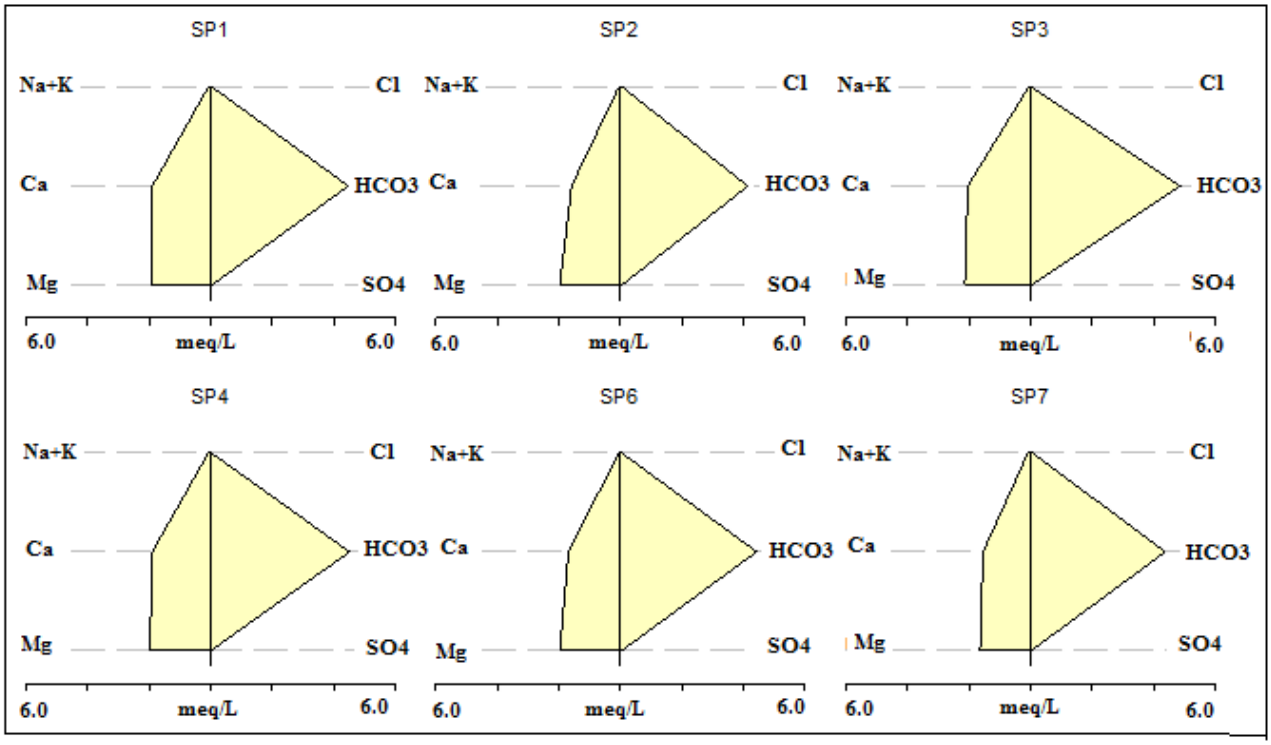

Figure 6.17: Stiff diagrams presenting the hydrochemistry of the dolomitic springs.

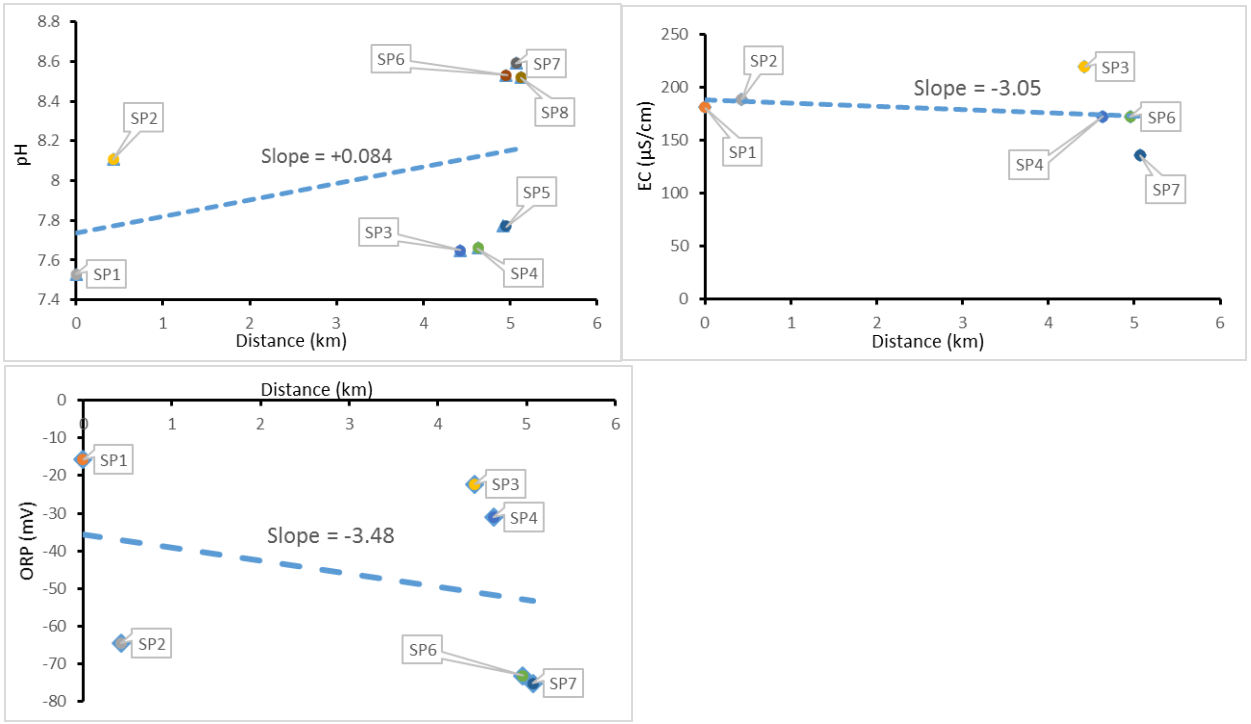

Figure 6.18: EC, pH and ORP variation along the flow path.

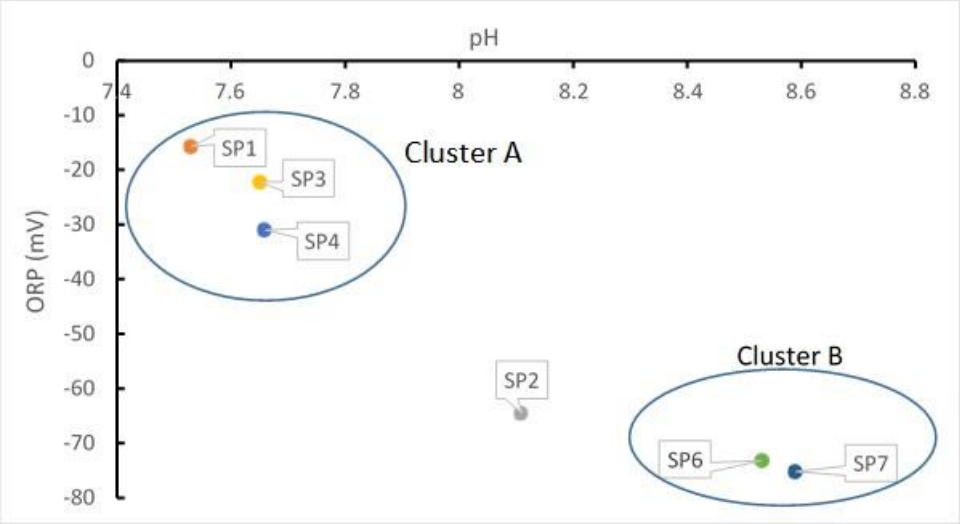

Figure 6.19: ORP and pH variation along the flow path.

The formation of travertine along the stream is possibly the cause of the evolving hydrochemistry. As water flows out of the SP3, it has a low pH and a higher carbon dioxide partial pressure (pCO_2). The CO_2 in solution begins to degas due to lower atmospheric pCO_2. As degassing continues, pH in water begins to increase. Since the solubility of carbonates decreases with an increase in pH (Appelo and Postma, 2005), as the pH increases, precipitation of calcium carbonate is induced thereby, forming rapids of travertine. The samples can be classified into two clusters as shown on Figure 6.19. Cluster A represents water at the sources where travertine has not precipitated, and cluster B represents water in the stream after the travertine deposition. The precipitation of carbonate minerals leads to a decrease in EC, ORP and TDS in the water, hence, the observed general trends along the flow path (Figure 6.18).

The long-term plot of Silica (Si) from Nouklip spring shown in Figure 6.20 shows that the silica concentrations vary between 4.2 and 6 mg/l. Silicates often react so sluggishly in water (Appelo and Postma, 2005) such that equilibrium is seldom reached within the residence time of water in a silicate aquifer (particularly at low temperatures). This means that for groundwater to have significant amount of dissolved Si, it may have had a significant residence time in a silicate rich aquifer. This could suggest that besides the dolomites, water may also be interacting with the overlying or the surrounding quartzite, shale, and chert layers possibly during recharge or along the groundwater flow path.

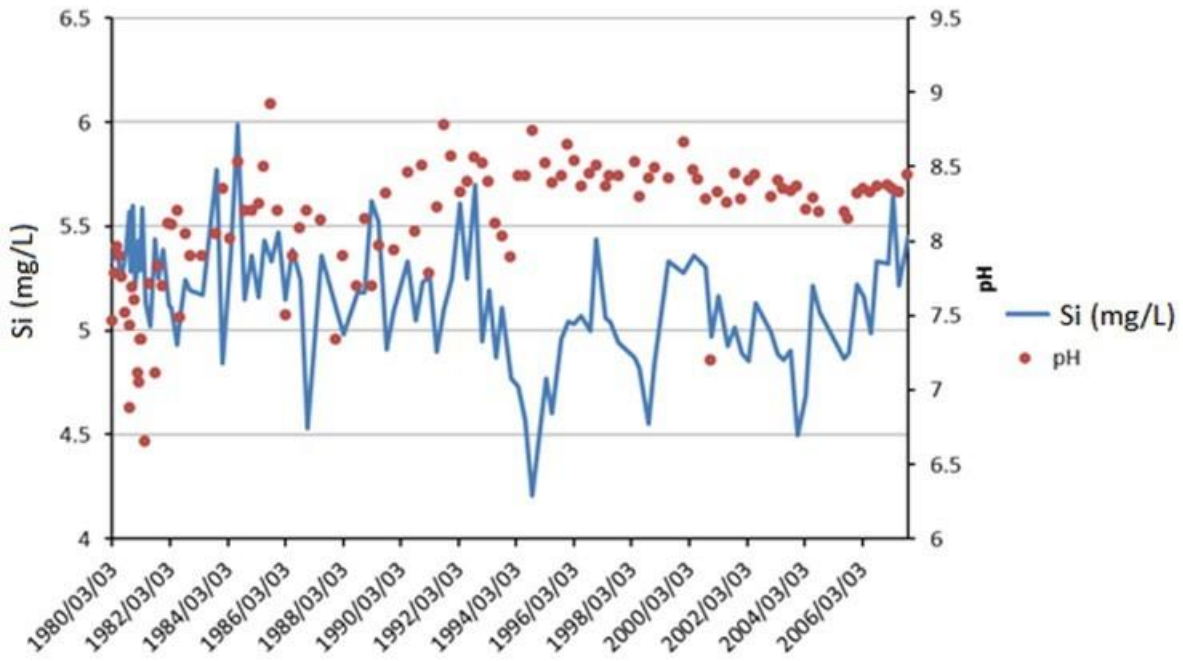

Figure 6.20: Temporal distribution of Si and pH in the Nouklip spring between 1980 and 2006 (Courtesy of Prof. Tamiru Abiye).

The ^{14}C ages for SP1 and SP3 were used to assess the approximate travel time and rate of circulation between the infiltration point downstream of SP1 and SP3 where water emerges. As shown in Table 6.11, SP1 and SP3 have residence times of 1641±10 years and 1855±10 years, respectively. Considering the separation distance of 2.2 km, and a residence time difference of 200 years, the rate of groundwater circulation in the aquifer was estimated as 11 m/year. In this assessment, the main assumption taken into consideration is that the seepage from SP1 travels through a preferential pathway within the dolomite. If a clear geometrical pattern or architecture of the fractures in the dolomites could be determined, the estimated rate could be improved. This rate could indicate the slow groundwater flow, which is possibly accompanied by a deeper circulation system.

6.4 Recharge assessment using classical and physical methods

6.4.1 Classical water balance methods

Table 6.13 presents the mean monthly components of the water balance for the ten-year period 1995 to 2004. From the table, it can be seen that the monthly precipitation ranges between 2.9 mm and 122 mm, potential evapotranspiration (PET) ranges between 33.5 mm and 105.4 mm while potential recharge ranges between 0 mm and 13 mm. Figure 6.21 shows the mean monthly trends for the potential evapotranspiration (PET), precipitation, direct runoff and potential recharge. From the figure, two distinct seasons in a year can be observed; the wet season observed by high precipitation between October and March and a dry season, which is observed by low rainfall between April and September. The highest mean monthly rainfall is observed in February, while the lowest is observed in July.

In the UCRB, the wet season includes the warm summer months, while the dry season includes the cold winter months. As a result of these seasonal temperature differences, the PET also seems to show seasonal variations, where the high PET is observed in the warm summer months and the low PET observed in the cold winter months. Potential recharge is observed in the wet summer season, while

none is observed in the low rainfall winter season. Potential recharge trend seems to reflect the mean monthly precipitation trend with February having both the highest mean precipitation and mean potential recharge with the values of 122 mm and 13 mm, respectively.

Table 6.13: Mean monthly components of the water balance.

Months	Precipitation (mm)	PET (mm)	Direct Runoff	P-PET (mm)	Potential Recharge (mm)	Recharge (%)
Jan	112.3	105.4	30.7	1.3	4.3	3.8
Feb	122.8	86.9	41.5	29.8	13.0	10.6
Mar	107.4	79.1	38.8	22.9	8.9	8.2
Apr	32.2	57.2	19.1	-26.6	0.0	0
May	23.8	42.6	12.4	-20.0	0.0	0
Jun	4.5	33.5	5.8	-29.2	0.0	0
Jul	2.9	34.9	2.9	-32.1	0.0	0
Aug	7.4	46.4	1.8	-39.4	0.0	0
Sep	20.1	62.1	1.7	-43.0	0.0	0
Oct	68.2	83.2	4.1	-18.4	0.0	0
Nov	100.1	93.8	6.4	1.2	0.4	0.4
Dec	107.0	104.0	8.8	-2.4	1.6	1.5
Annual	708.7	829.1	19.3	-155.8	28.2	4.0
Max	107.0	104.0	8.8	1.2	1.6	11
Min	68.2	83.2	4.1	-18.4	0.0	0.0

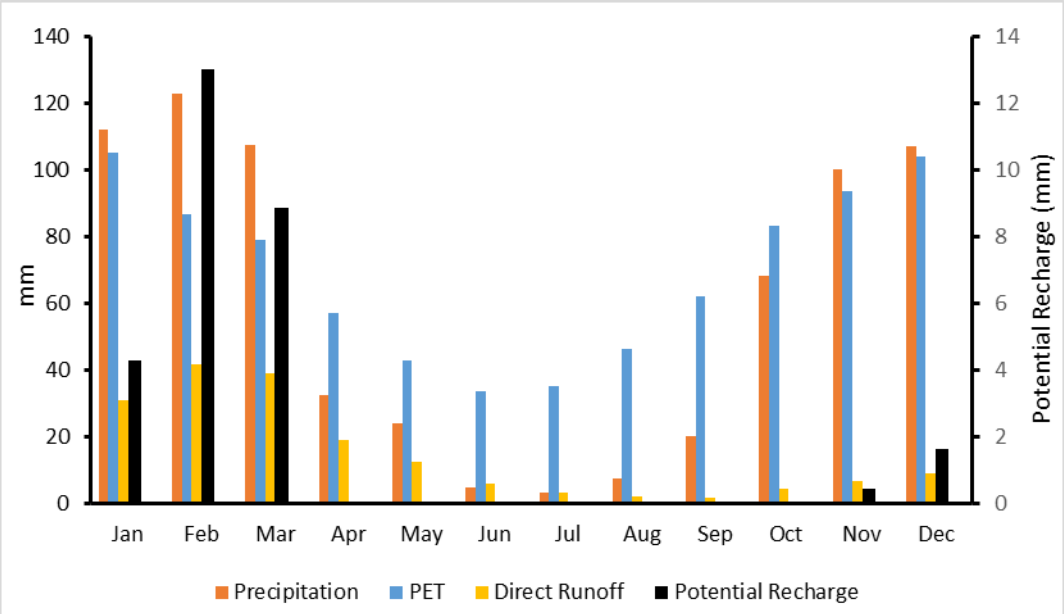

Figure 6.21: Mean monthly water balance components.

Potential recharge seems to be occurring during the summer months when precipitation is exceeding PET. This is because, when precipitation exceeds PET, there is a surplus of water and due to frequent rainfall events, the soil moisture is often at field capacity such that the subsequent rainfall has more potential to become recharge. On the other hand, in the winter months, PET is higher than precipitation leading to a water deficit.

In the ten year review period, annual precipitation ranges between 372 mm and 1072 mm, PET ranges between 792 mm and 887 mm, while potential recharge ranges between 0 mm and 91 mm (8.6%). It can be observed that the years (1996 and 1997) that had the highest precipitation also had the highest potential recharge. Figure 6.22 shows the annual amounts of precipitation, PET and potential recharge

for each year in the review period. It is observed that while precipitation has been fluctuating throughout the years, PET has been almost constant. Despite recharge having occurred for all the years, except 2002 and 2003, it seems that more significant recharge is observed during the years where precipitation is more than PET. In the years 1996, 1997 and 2000 when annual precipitation was more than PET, the amount of recharge was substantially higher than the years on which PET was greater than precipitation.

The drought conditions are observed in the years 2002 and 2003. These years have the lowest recorded precipitation and the highest recorded PET. Due to this condition, no recharge was observed. This could be related to the water deficit that occurs as a result of higher PET than precipitation that leads to soil water being below field capacity such that precipitation is not enough to satisfy the field capacity and recharge.

Table 6.14: The annual components of the water balance.

Months	**Precipitation (mm)**	**PET (mm)**	**Direct Runoff**	**P-PET (mm)**	**Potential Recharge (mm)**	**Recharge (%)**
1995	654.8	837.6	81.7	-215.5	5.7	0.87
1996	1072.5	791.5	364.2	227.4	79.5	7.42
1997	1051.9	804.8	404.8	194.5	90.5	8.60
1998	566.3	855.7	90.6	-317.7	7.0	1.24
1999	605.1	831.5	58.0	-256.7	0.7	0.11
2000	885.3	806.5	360.4	34.5	71.1	8.03
2001	640.0	826.5	64.7	-218.5	2.8	0.44
2002	572.0	835.8	58.5	-292.5	0.0	0.00
2003	372.3	886.7	47.9	-533.0	0.0	0.00
2004	667.2	814.4	209.3	-180.6	24.6	3.69
Average	708.7	829.1	174.0	-155.8	28.2	3.89
Max	1072.5	886.7	404.8	227.4	90.5	8.60
Min	372.3	791.5	47.9	-533.0	0.0	0.00

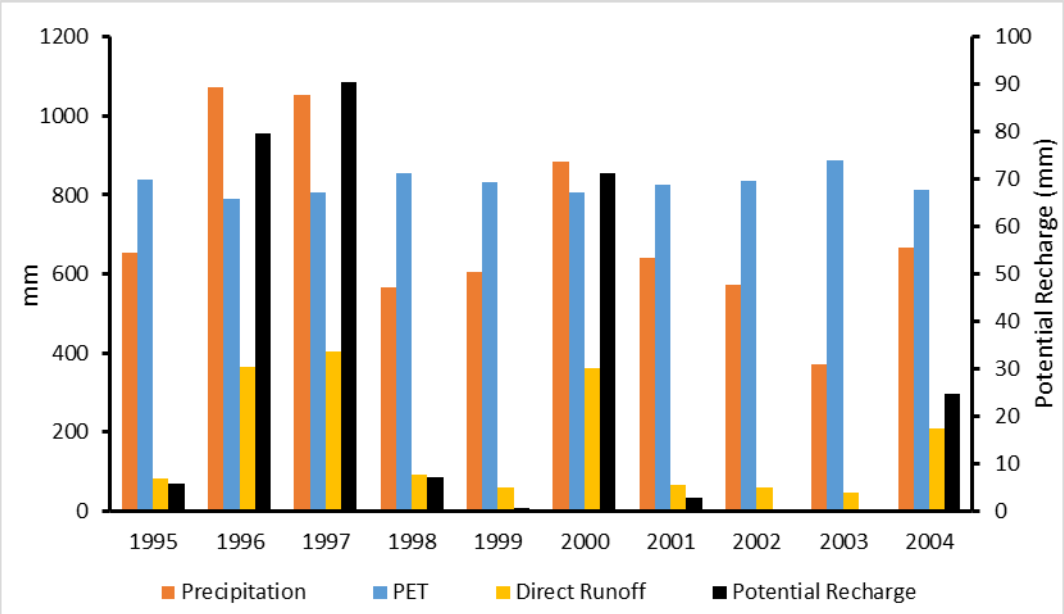

Figure 6.22: Time series of the annual components of the water balance.

It is observed in this study that potential recharge depends on the amount of excess precipitation over PET for both monthly and annual components. However, recharge can still occur through preferential flow even if PET is higher than precipitation. Van Wyk (2010) undertook an assessment of episodic recharge in South Africa and observed that during high intensive rainfall events, precipitation can still exceed PET and, therefore, recharge can occur through preferential flow without the soil moisture reaching field capacity. This has been termed episodic recharge (Van Wyk, 2010; Abiye, 2016). Also, since the TMWBM uses monthly average values, during the hot summer months, the precipitation can exceed PET in a few days while the monthly values indicate higher PET than precipitation. In such a case, TMWMB would still indicate that no recharge has occurred. TMWBM may therefore, underestimate recharge.

The stable isotope interpretations revealed that diffuse recharge seems to dominate in the study area and indicated that there is little evaporation occurring prior to recharge further indicating that recharge is most probably occurring though the fractures as preferential flow. This could, therefore, indicate that, while the TMWBM only regards recharge occurring through the soil zone, recharge in the UCRB may actually be higher than the average estimated 4% indicating that most recharge may actually be occurring through preferential flow.

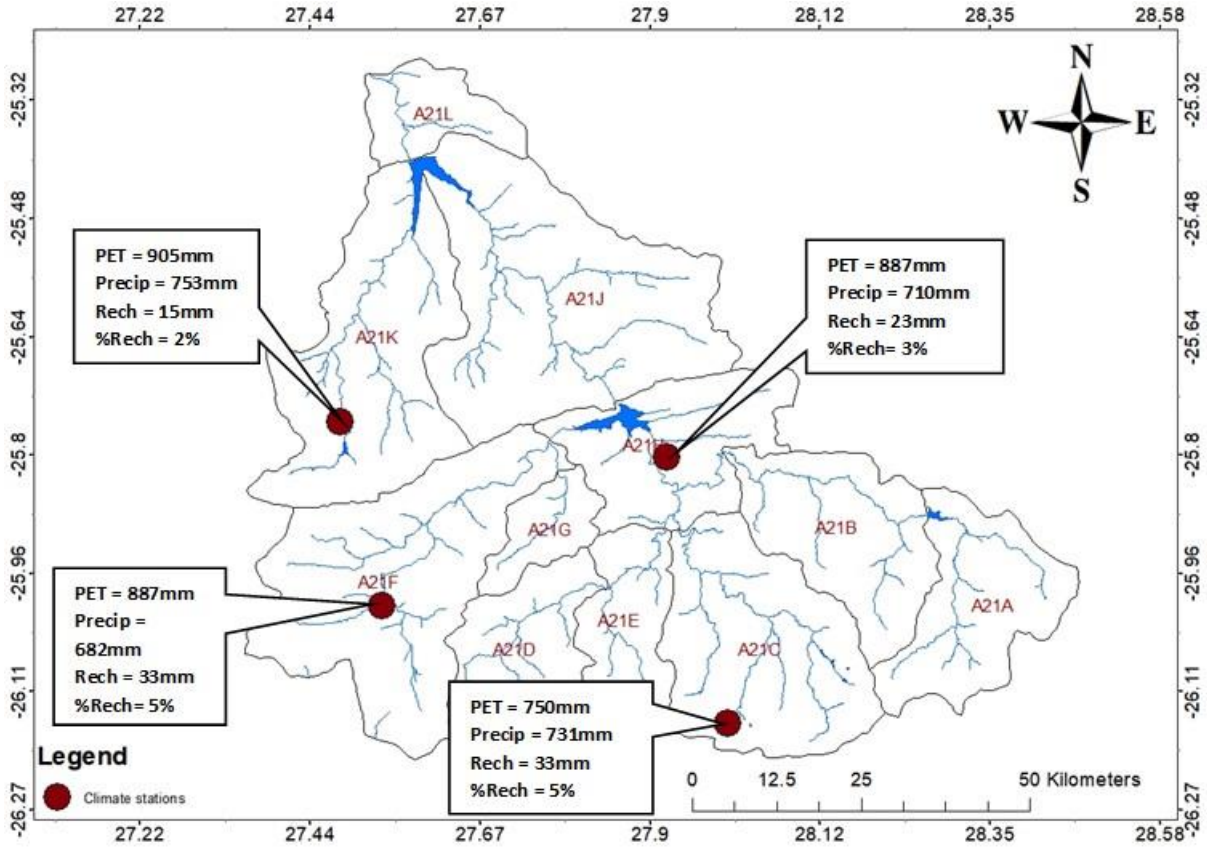

Figure 6.23: Spatial distribution of mean annual values of PET, precipitation and the estimated potential recharge.

It can be observed in Figure 6.23 that the potential evapotranspiration generally increases from the south to the north, possibly as a result of spatial distribution of mean annual temperature. Though there is a small range in recharge percentage (2-5%), there seems to be a higher potential for recharge

to occur in the south, possibly as a result of lower potential evapotranspiration and higher precipitation amount.

6.4.2 Baseflow Separation method

The recharge estimates obtained from Baseflow Separation method are shown in Table 6.15. The estimates range from 3.32% in A21C quaternary catchment to 22.07% in A21G. A21G has the smallest catchment size yet it has the highest recharge estimate among the UCRB quaternary catchments. A21A and A21G quaternary catchments are underlain predominantly by similar geology (Malmani dolomites as shown in Figure 2.7) despite the vast difference in recharge estimates i.e. 22.07% in A21G catchment and 5.5% in A21A. Table 6.15 also shows the average recharge estimates for the area as 6.67%, which is obtained as weighted fractions of the catchment areas to the total area. This value is significantly lower than the value of 27.1% where Abiye (2016) was emphasising the need to deduct wastewater during baseflow separation.

In order to get estimates that are distributed in space, baseflow was assessed in smaller sub-units upstream of the wastewater discharge stations in A21C and A21E. A21C quaternary catchment, which had an estimate of 5.5%, now had 7.2% in its sub-unit. A21E quaternary catchment had 14.9% recharge, while its smaller sub-unit gave a recharge value of 9.9% over the same period.

Table 6.15: Recharge estimations obtained through Baseflow Separation method.

Catchment	**Discharge station**	**Recharge (mm)**	**Area (km^2)**	**Sub-units: Recharge (%)**	**Recharge (%)**
A21A	A2H090	33.8	451	-	5.48
A21B	A2H014	57.4	527	-	8.50
A21C	A2H044	25	761	(A2H047) 7.2% on granites	3.32
A21D	A2H049	34.8	372	-	6.71
A21E	A2H045	99.8	282	(A2H051) 9.9% on granite and dunite	14.19
A21F	A2H013	24.1	1 001	-	4.23
A21G	A2H034	108.7	160	-	22.07
Weighted recharge average					6.67

A21G with 22% baseflow, hosts the high yielding dolomitic perennial springs such as Nash Farm and Nouklip that yield 130 L/s and 143 L/s (Hobbs, 2011), which explains the observed high baseflow.. The high yielding springs in the A21G could be a result of inter-basin movement of groundwater from the south west resulting to increased baseflow in A21G. A21A is also underlain by dolomites but positioned on the head waters of the dolomitic aquifer's eastern limb. This could indicate that, unlike the A21G, there is no significant contribution of inter-basin groundwater movement from the eastern catchments outside of the UCRB. Land cover is mostly impermeable in A21A due to urban development and as a result, it enhances more runoff than recharge. The reason for low baseflow in A21A could also be that A21A is a recharge point, which undertakes deeper circulation to discharge in the A21B at lower elevation, hence a higher baseflow of 8.5% in A21B quaternary catchment.

A21C quaternary catchment, which hosts Johannesburg, is covered with impermeable surfaces leading to a low recharge value of 3.32%. Low baseflow in A21C can also be attributed to its underlying geology, which is crystalline hard rocks composed of granites with low permeability. A21E quaternary catchment, which is completely underlain by hard rocks such as quartzite, granitic gneiss and dunite has a high recharge value of 14.9%.

Apart from the fact that the sub-units may be presenting recharge estimates at the sub-unit level, the different recharge estimates may also be a result of inaccurate wastewater discharge data leading to erroneous baseflow values.

6.4.3 Stream Segment Water Balance method

Table 6.16 shows the components of the stream segment water budget for the streams underlain by the granites, Malmani dolomites and the Pretoria Group rocks. Q_{seep} represents the net volume exchange in million cubic meters (Mm^3) between groundwater and surface water for the review period. Table 6.16 also shows the *seepage percentage of total flow* [$Q_{seep}/ (Q_{in}^{sw}+Q_{out}^{sw})$], which indicates the measure of the reliability of the estimated Q_{seep} values (Donato, 1998; Turco *et al.*, 2007; Healy, 2010). Healy (2010) stated that the reliability of the Q_{seep} value increases with increase in seepage percentage of total flow. During measurement of stream water budget components (e.g. evaporation and stream discharge), some errors are incurred and may be erroneously reflected as part of Q_{seep} during stream water-budget computation. Rantz (1982) also indicated that discharge determined from a stage-discharge rating equation (the same measurement methods applied by DWS), is within 5% of actual stream discharge. Therefore, 5% is considered as an acceptability minimum such that the value of Q_{seep} in Equation 11, has to be substantially larger in magnitude than 5% of the sum of Q_{in}^{sw} and Q_{out}^{sw} in order to provide confidence in Q_{seep} value (Healy, 2010). The percentage water flux (*%W Flux*) is also given as a percentage of Q_{seep}/ Q_{in}^{sw} in the case of losing conditions and Q_{seep}/Q_{out}^{sw} in gaining conditions. Therefore, a negative *%W Flux* denotes losing conditions, while a positive *%W Flux* denotes gaining conditions.

Table 6.16: Components of the July stream segment water-budget obtained through Equation 11.

Geology	**Inflow stations**	**Outflow station**	**Segment Length (m)**	**ET^{sw} (Mm^3)**	**Q_{in}^{sw} (Mm^3)**	**Q_{out}^{sw} (Mm^3)**	**Q_{seep} (Mm^3)**	**$[Q_{seep}/ (Q_{in}^{sw}+ Q_{out}^{sw})]$**	**%W Flux**
basement granites	A2H051	A2H050	5000	0.0012	0.39	0.47	0.085	9.9%	18%
Malmani dolomite	A2H014 A2H044 A2H045	A2H012	26000	0.0072	11	12.8	1.81	7.6%	14%
Pretoria group-shale, quartzite, andesite	A2H035	A2H034	6300m	0.0016	1.175	1.02	-0.154	7.0%	-13%
ET^{sw}=Evaporation Flux, Q_{in}^{sw}= Surface Inflow, Q_{out}^{sw}=Surface Outflow, Q_{seep}=Exchange, %W Flux =Percent water flux									

As seen in Table 6.16, the calculated Q_{seep} values are higher than the stated acceptability minimum amount of 5%. The basement granite rocks show more confidence with the excess of 4.9%, while the Pretoria Group rocks show the least confidence with an excess of 2%. The results for the water budget are also presented as a time series for the lithologies (Figure 6.24, Figure 6.25 and Figure 6.26). Despite the reported 18% stream segment gain in the granites (Table 6.16 and Figure 6.24), there was actually a gain and a loss in different July months. The average monthly stream loss was 2.4%, while the average stream gain was 25%, which together yielded an average net flux of 18%.

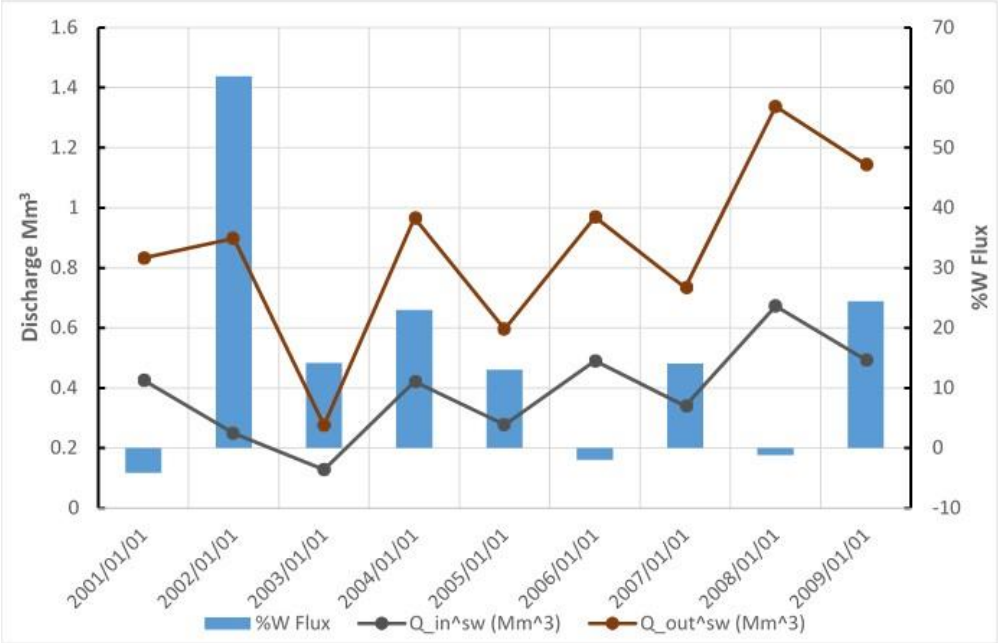

Figure 6.24: Components of a stream segment water budget underlain by the basement granites.

Figure 6.25 shows that throughout the review period, the stream that is underlain by the Malmani dolomite is gaining, while Figure 6.26 shows that the stream that is underlain by the Pretoria Group loses water each month.

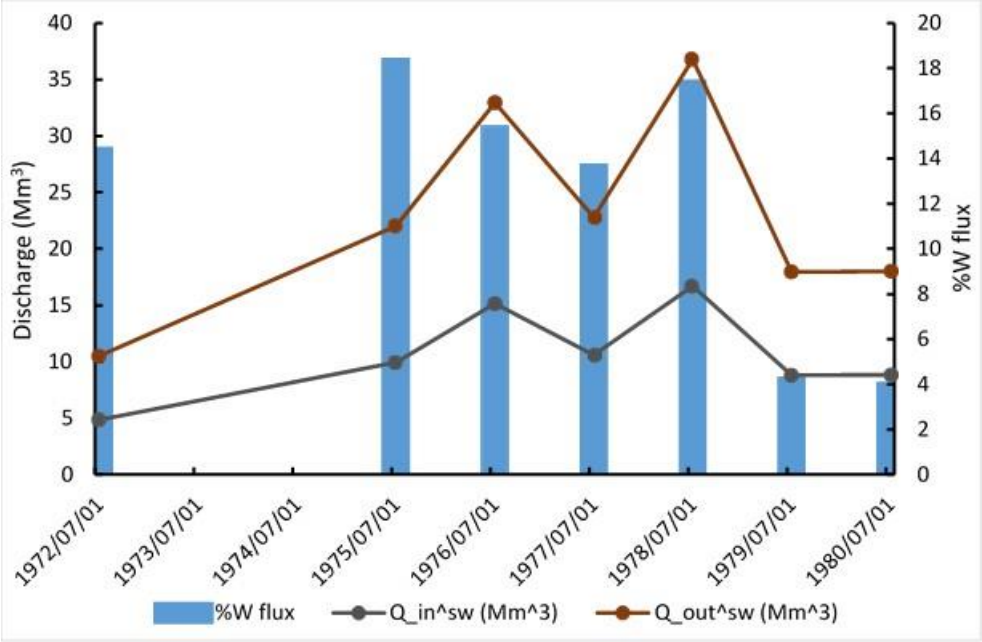

Figure 6.25: Components of Malmani dolomite stream segment water-budget.

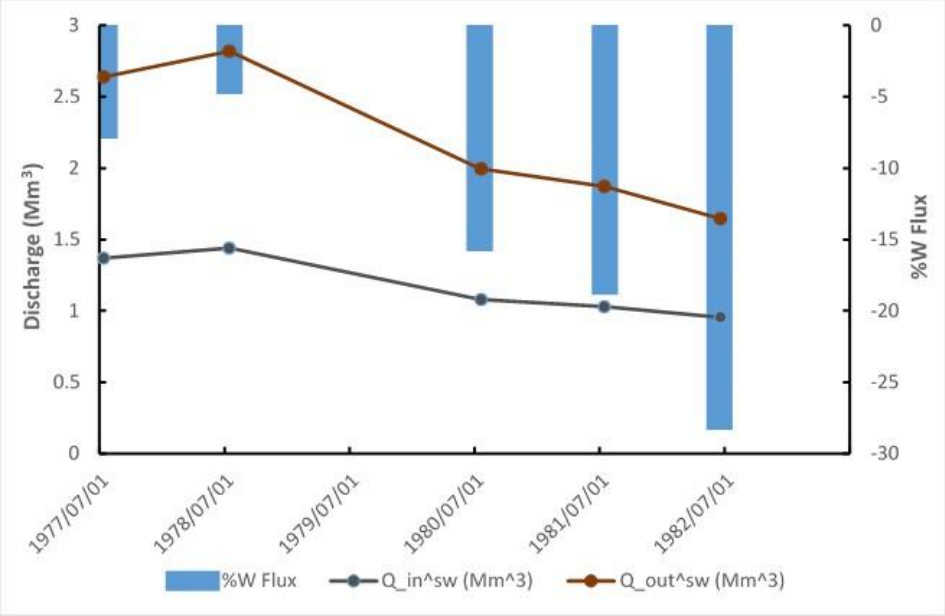

Figure 6.26: Components of a stream segment water-budget model in the Pretoria Group.

The Stream Segment Water Budget applications revealed the presence of both diffuse and focused recharge in the selected stream segments within the review periods. The stream segments that are underlain by the basement granites and Malmani dolomites show a gaining stream condition, which enhances the baseflow. Baseflow is an indication of diffuse recharge that occurs upstream of the stream segment (Healy, 2010). Since the assessment was done during the dry winter month of July, the gaining condition might be due to stream head that is lower than the water table thereby inducing flow direction to the stream. Because of the underlying massive nature of the bedrock, groundwater that percolated during the rainy season could be flowing laterally to the stream network as interflow instead of baseflow. The opposite could be occurring in the stream segment that is underlain by Pretoria Group aquifer, where stream loss conditions are observed. The losing stream is attributed to focused recharge occurring through the stream bed.

The riparian area of the stream segment underlain by Pretoria Group is vegetated with large trees that could be drawing shallow groundwater, thereby provoking an influx of stream water into groundwater. White (1932) indicated that phreatophytes along the riparian zones can extract significant volumes of water from the water table. Shakhane *et al.* (2017) undertook a groundwater and surface water interaction study in a typical semi-arid area in Free State Province of South Africa. It was observed through stable isotope analysis and tree stem heat tracer methods that deep rooted trees are capable of tapping water from the saturated riparian zone in quantities ranging from 60 to 350 litres/day per tree.

The Q_{seep} values computed are only integrated in space (along the stream segment) and time (Rosenberry and LaBaugh, 2008). At any particular point within the sub-reaches of the stream segment, there may be gaining dominating losing conditions or vice versa. Also, due to diurnal variations in evapotranspiration, particularly in losing streams (Pretoria Group segment), the stream might be dominated by either of the two, at different times of the day. Sophocleous (2002) expressed that the dynamic nature of the interaction depends on the geomorphology, biota and climatic setting of the sub-reaches. Therefore, the recharge and discharge estimated in each segment is only the net volume exchange (difference) which does not really give a quantity of the amount gained or lost. The

estimated flux in this study may not necessarily indicate interaction between the stream and groundwater but may actually refer to interaction of the stream with the unsaturated zone through interflow.

6.4.4 Reservoir Water Budget method

Figure 6.27 shows the monthly net groundwater surface water exchange from the Reservoir Water Budget method on the Hartbeespoort Dam.

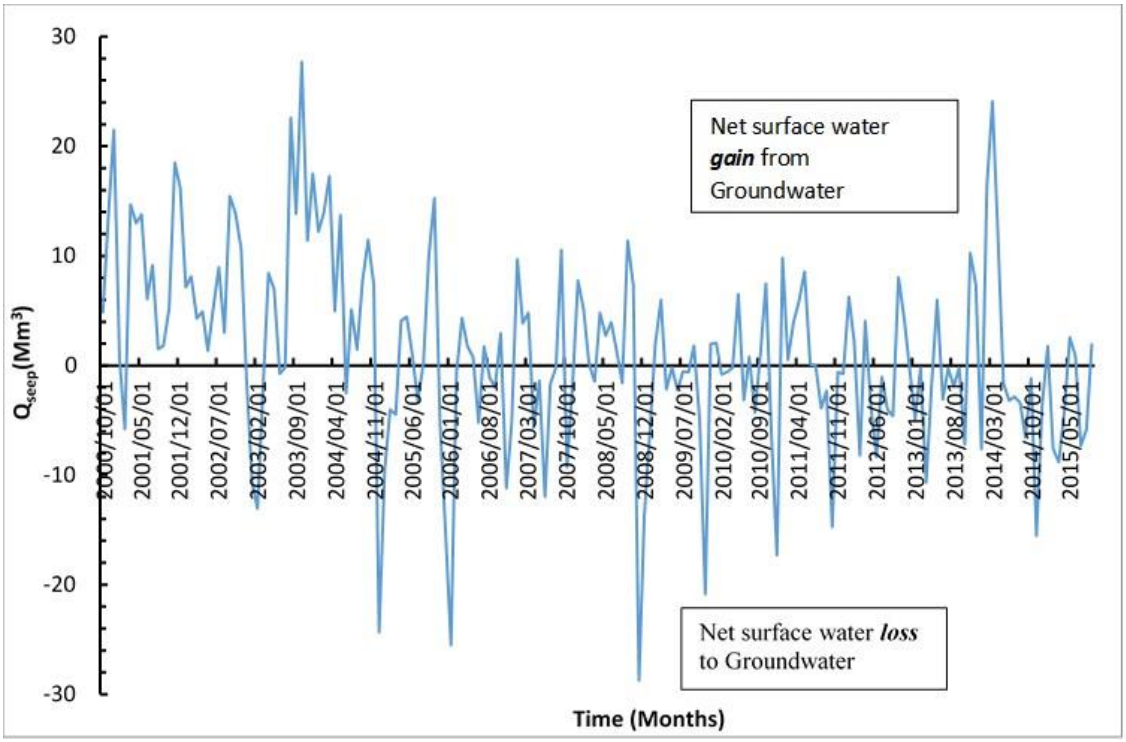

Figure 6.27: Monthly net groundwater and surface water exchange (Q_{seep}) for the 15-year review period.

Both net gain and net loss are observed over the 15-year review period, where $+Q_{seep}$ denotes gaining, while $-Q_{seep}$ denotes losing conditions. Figure 6.28 shows a conceptual water budget model for Hartbeespoort Dam with mean annual volumes for the water budget components shown in Equation 12. On average, the reservoir gains 3 213 378 m^3 groundwater, which constitutes 16% of Q_{out}^{sw}, while 7% of Q_{in}^{sw} is lost to groundwater constituting an average volume of 2 084 131m^3 per annum.

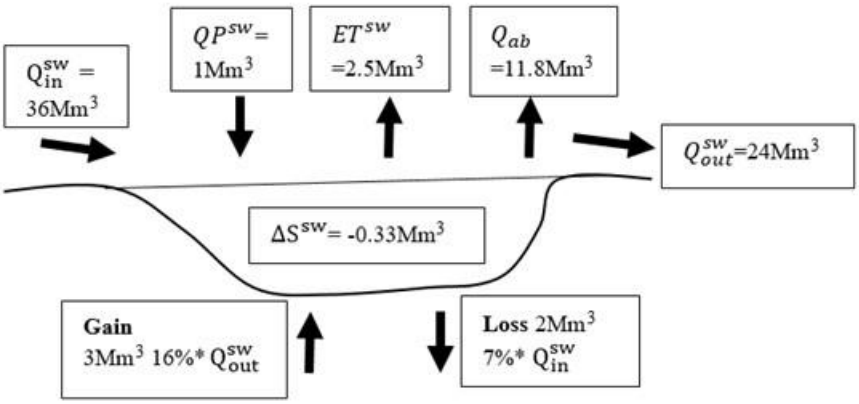

Figure 6.28: Schematic of the reservoir water budget components for Hartbeespoort Dam.

The monthly net volume exchange indicates a temporal variability in losing and gaining conditions of the dam. The time variability could be a result of the seasonal difference between water-table and surface water elevations (Rosenberry and LaBaugh, 2008). Considering a net loss to groundwater as an excess amount related to focused recharge and net gain as an excess indicating diffuse recharge, the Reservoir Water Budget method applied at the Hartbeespoort Dam indicates more of diffuse recharge that potentially occurred up stream of the UCRB. The estimated net volume of 2 084 131 m^3, which is lost into groundwater (focused recharge), potentially occurs as a result of the Brits fault lines or the Magaliesberg quartzite bedding planes that form the Hartbeespoort Dam wall.

6.4.5 Water table fluctuation method

The analysis of borehole lithology and the water levels indicated that the fluctuations occur in the clay, sandy top soil, shale and dolomite. The specific yield values for these materials are shown on Table 6.17 with their sources. The specific yield values for the dolomite were obtained from Eslin and Kriel (1968) who carried out a water balance study for the karst aquifer that was being dewatered for mining purposes in the Far West Rand in Johannesburg.

Table 6.17: Specific yield values used in this study and the relevant geological material.

Geological material	**Specific yield**	**Literature Source**
Clay	0.02	(Johnson, 1967)
Sand	0.21	(Johnson, 1967)
Shale	0.08	(Johnson, 1967)
Dolomite (0-61 mbgl)	0.091	Pumping test
Dolomite (62-76 mbgl)	0.055	Pumping test
Dolomite (77-107 mbgl)	0.026	Pumping test
Dolomite (108-126mbgl)	0.02	Pumping test
Dolomite (127-146 mbgl)	0.013	Pumping test

The recharge results for the 26 boreholes are presented in Table 6.18 with the relevant lithology at fluctuation and specific yield values. The mean annual recharge (MAR) ranges between 2.1% (12.8 mm/yr) and 36.8% (197.7 mm/yr), with the average as 11.4% (67.5 mm/yr) for the Malmani dolomite aquifer.

Table 6.18: The recharge result for the water table fluctuation method.

Boreholes	Latitude	Longitude	lithology at fluctuation	MAR(mm)	MAP (mm)	Recharge % of MAP
035730	-25.9131	28.3075	Unconsolidated Clay	25.7	726	4.5
036006	-25.9042	28.3166	Unconsolidated Clay	132.3	726	22.8
036056	-25.9053	28.3051	Unconsolidated Clay	56.8	726	8.4
036322	-26.0231	27.69918	Unconsolidated Clay	27.8	669	4.9
036325	-26.0350	27.6821	shale & dolomite	38.6	669	6.4
036334	-26.0584	27.6997	Unconsolidated Clay	14.2	669	2.4
036341	-26.0460	27.6492	Shale	155.1	669	28.5
036337	-26.0792	27.6863	Unconsolidated Clay	35.9	669	6.3
036342	-26.0523	27.6542	Dolomite	197.7	669	36.8
036343	-26.0530	27.6292	Shale	80.8	669	14.1
036356	-26.0948	27.6654	Dolomite	176.7	669	26.2
037783	-26.1058	27.5932	Unconsolidated Clay	12.8	669	2.2
037786	-26.0277	27.7051	Dolomite	65.0	669	10.7
037788	-26.0260	27.6910	Dolomite	46.2	669	7.7
037789	-26.0288	27.6876	Chert/Dolomite	71.3	669	12.5
037792	-26.0325	27.6843	Chert/Dolomite	91.2	669	17.1
037794	-26.0179	27.7111	Chert/Dolomite	174.7	669	26.0
036350	-26.0733	27.6034	Unconsolidated Clay	20.5	669	3.4
036352	-26.0913	27.6004	Chert/dolomite	15.1	669	2.6
036599	-26.0978	27.5774	Chert/dolomite	40.6	669	6.4
036601	-26.0764	27.5747	Dolomite	64.0	669	11.1
036602	-26.0766	27.5765	Dolomite	74.8	669	12.8
036603	-26.0771	27.5765	Dolomite	64.9	669	10.1
037779	-26.0871	27.5820	Shale	60.5	669	9.2
037781	-26.0855	27.5977	Unconsolidated Clay	13.0	669	2.1
037782	-26.0963	27.5783	Dolomite	44.6	669	7.9

Over and above the recharge estimates that are obtained from the groundwater levels, the recharge paths are also deduced. The different timing and magnitude of groundwater level response to rainfall can be seen in Figure 6.29 for two boreholes in each quaternary catchment. It is observed on these figures that there are highly variable fluctuations within the quaternary catchments. The water level in boreholes 036353A, 36350 and 37772 showed the least fluctuations for the period not exceeding 3 m. Boreholes 36008 and 36349 showed a significant fluctuation with a maximum of 20 m observed in borehole 36349. This varying nature of groundwater level response in different boreholes could suggest different recharge paths, which are attributed to the makeup of the recharge area rather than the depth of water table seeing that the borehole water levels are within the same depth ranges (Figure 6.29 (a) to (c)).

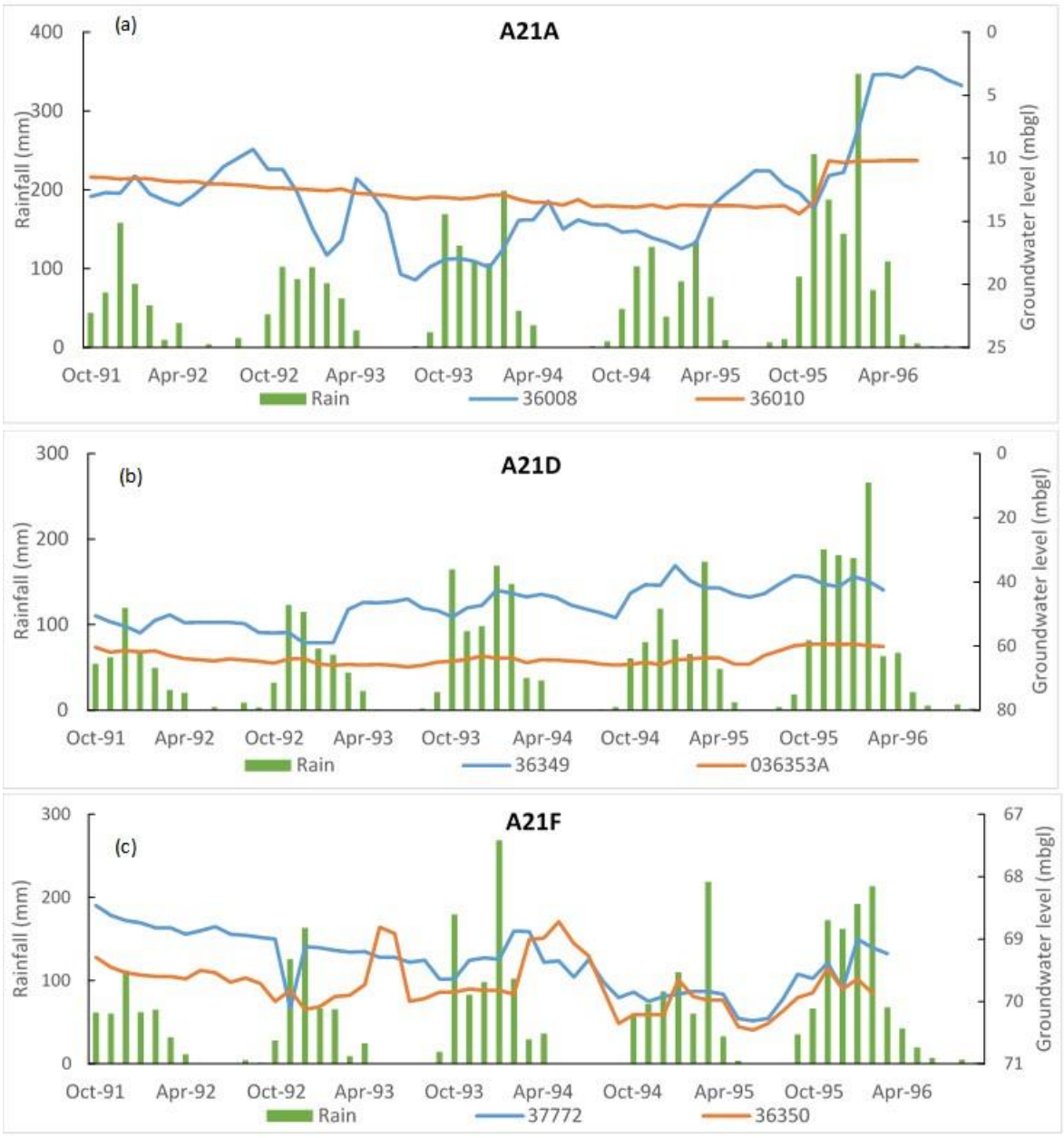

Figure 6.29: Groundwater level fluctuations for the selected boreholes within the sub-catchment A21A, A21D and A21F indicating that there are different groundwater recharge mechanisms.

6.5 Simulating the impacts of changes in climate variables on the stream flow using PRMS

6.5.1 Model calibration

Calibration of the PRMS model in the UCRB gave a correlation value of 0.89 for both R^2 and E_N between the simulated and measured stream flow at A2H012. Figure 6.30 presents a regression line, which shows the correlation between measured and simulated discharge values for the calibration period. The correlation values present a characteristic feature of a model that is able to replicate measured data. Santhi *et al.* (2001) and Krause *et al.* (2005) stated that for a good model, the values of R^2 and E_N should be close to 1. The gradient of the regression line is 1.0, while the intercept is 0.71. The gradient is equal to the expected value of 1 and the intercept is close to the expected value of 0 for a perfect model as stipulated by Krause *et al.* (2005). Figure 6.31 presents a graphical correlation showing a good visual match between measured and simulated flows for the calibration

period. Both the graphical and statistical analysis show that the model is well able to simulate measured flows.

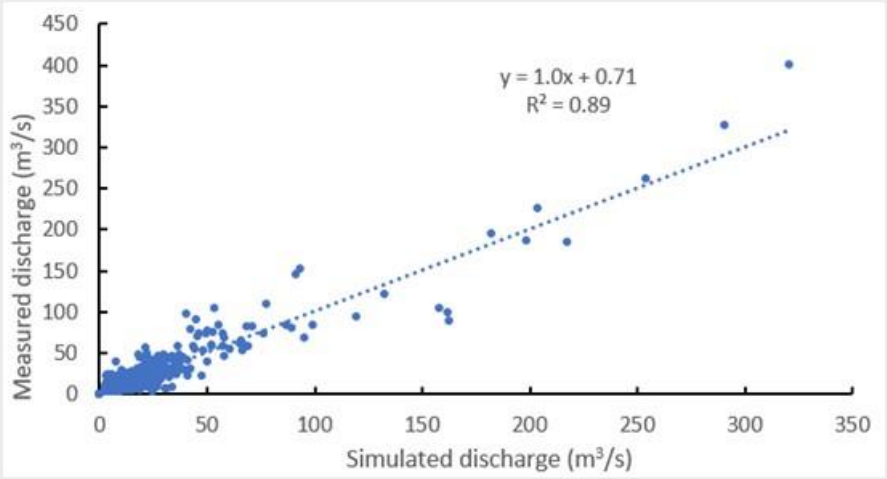

Figure 6.30: Correlation between simulated and measured annual flows for the station A2H012.

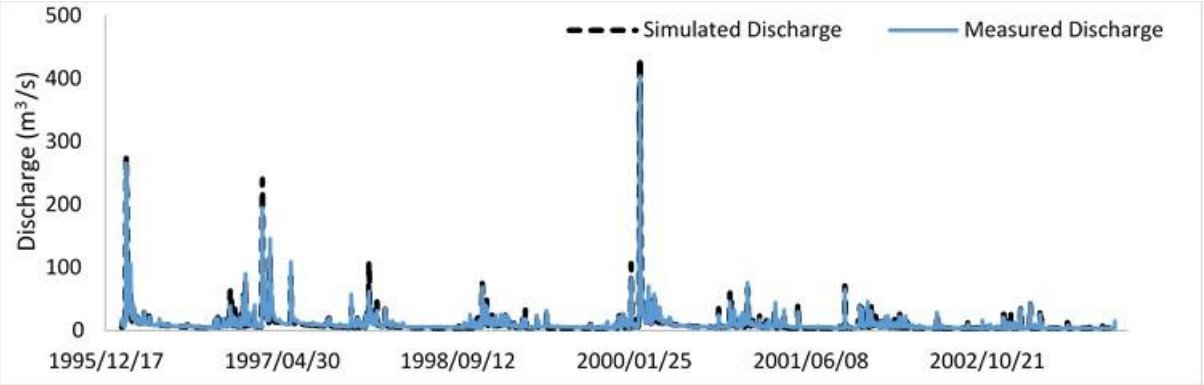

Figure 6.31: Daily measured and simulated time series discharge data of the A2H012 for model calibration period.

6.5.2 Validation periods

Model validation, which was done for the period between the 7th February 2007 and the 30th June 2017 yielded a R^2 value of 0.76 and E_N value of 0.56. Figure 6.32 presents a regression between measured and simulated discharge values for the validation period. As can be seen in Figure 6.33, the graphical analysis indicates that the model could not satisfactorily replicate the validation period, particularly the high flows. Despite the lower correlation statistical values compared to calibration period, the validation statistical values still fulfil the requirements for a successful model as stipulated by Santhi *et al.* (2001) that the correlation statistics (R^2 *and* E_N values) should at least be above 0.5. The gradient of the regression line is close to 1, while a bigger deviation is observed in the intercept. The higher value of the intercept means, where the simulated flow was 0 m^3/s, the measured flow was 3.6 m^3/s deducing that the model is underestimating the low flows. This parameter lowers the level of certainty for the validation period. While the intercept shows a bad correlation, the R^2, E_N and slope satisfy a good correlation and, therefore, mean that the model may be applied for scenario analysis.

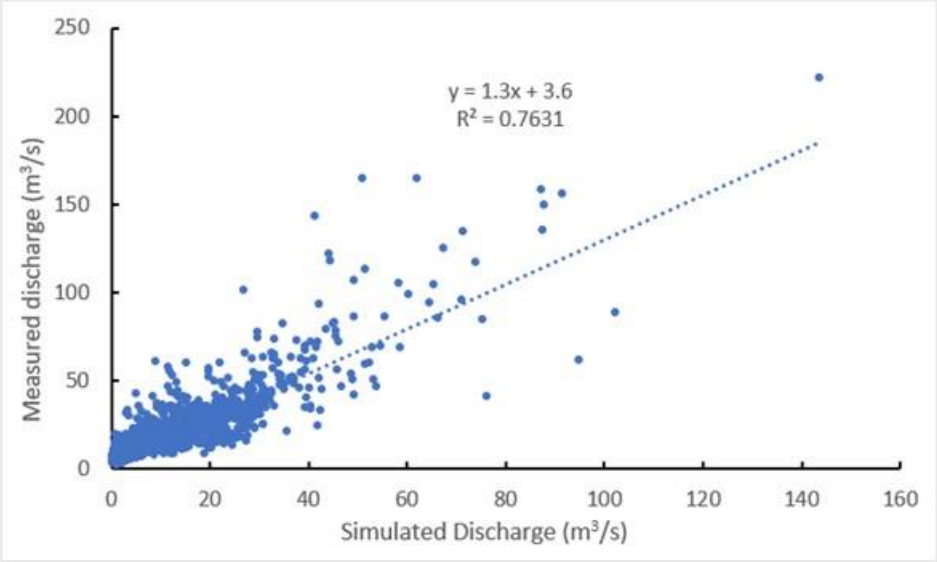

Figure 6.32: Correlation between simulated and measured daily stream discharge for the validation period 2007 to 2017.

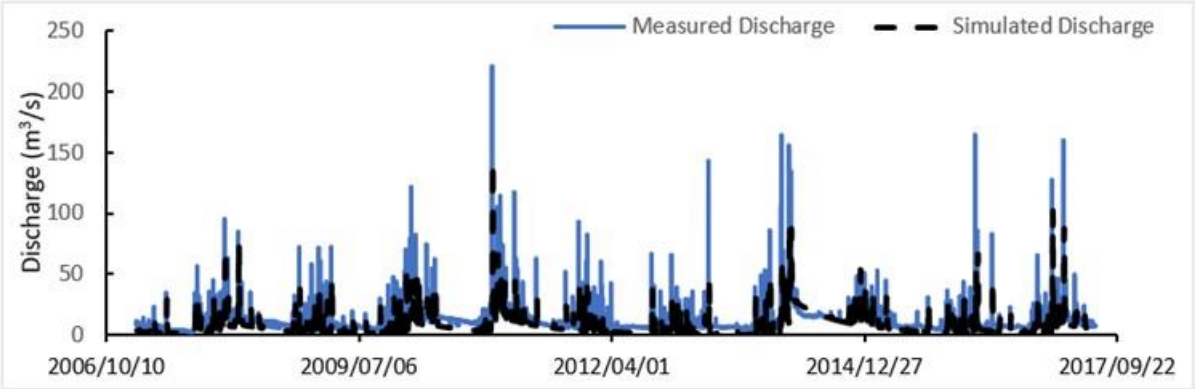

Figure 6.33: Daily measured and simulated time series discharge data of the A2H012 for model validation.

Table 6.19 shows the annual baseflow for the period 1997 to 2016 calculated using a separate single filter parameter technique (WHAT tool) and PRMS. Table 6.19 also shows the recharge estimates as percentages of annual precipitation. WHAT gave recharge estimates ranging from 5.2% to 12.5% with an average of 7.5%, while PRMS gave a range of 4.0% to 6.5% with an average of 5.3%, all as a percentage of total precipitation for the relevant year. The percentage values obtained in these two methods are in agreement with one another. Using the same single filter parameter in the application of Baseflow Separation method in section 6.4.2, a weighted average estimate of 6.5% was obtained, which is also in agreement with PRMS. Figure 6.34 shows the time series plot comparing baseflow estimated from PRMS and the one obtained using WHAT for the same daily discharge data. It shows that while PRMS simulates baseflow through a complex algorithm that incorporates data from climate, land use, land cover type etc., its capability to assess baseflow in the UCRB is in agreement with single parameter filter technique (Nathan and McMahon, 1990), which utilises only stream discharge data. The model is, therefore, assumed valid for scenario analysis on baseflow in the UCRB.

Table 6.19: Annual baseflow and recharge for the period of study from PRMS and WHAT.

	WHAT		PRMS	
Year	**Baseflow (m^3)**	**Recharge (%)**	**Baseflow (m^3)**	**Recharge (%)**
1997	255 408 701	7.0	237 342 097	6.5
1998	167 359 712	5.9	141 819 568	5.0
1999	149 916 846	8.1	115 091 358	6.2
2000	220 235 876	6.0	221 246 641	6.0
2001	142 983 118	5.2	117 869 811	4.3
2002	114 977 308	5.7	105 817 121	5.3
2003	-	-	-	-
2004	-	-	-	-
2005	-	-	-	-
2006	214 179 140	7.6	135 223 952	4.8
2007	-	-	-	-
2008	229 068 814	7.8	150 423 354	5.1
2009	174 887 205	5.9	123 637 152	4.2
2010	284 385 979	7.8	200 616 347	5.5
2011	291 499 335	8.9	191 274 331	5.8
2012	189 083 892	8.3	108 318 097	4.7
2013	177 831 436	7.2	106 186 603	4.3
2014	388 587 340	12.5	198 365 689	6.4
2015	196 155 577	10.4	119 420 901	6.3
2016	167 059 551	5.9	113 671 422	4.0
Average Recharge (%)		**7.5**		**5.3**

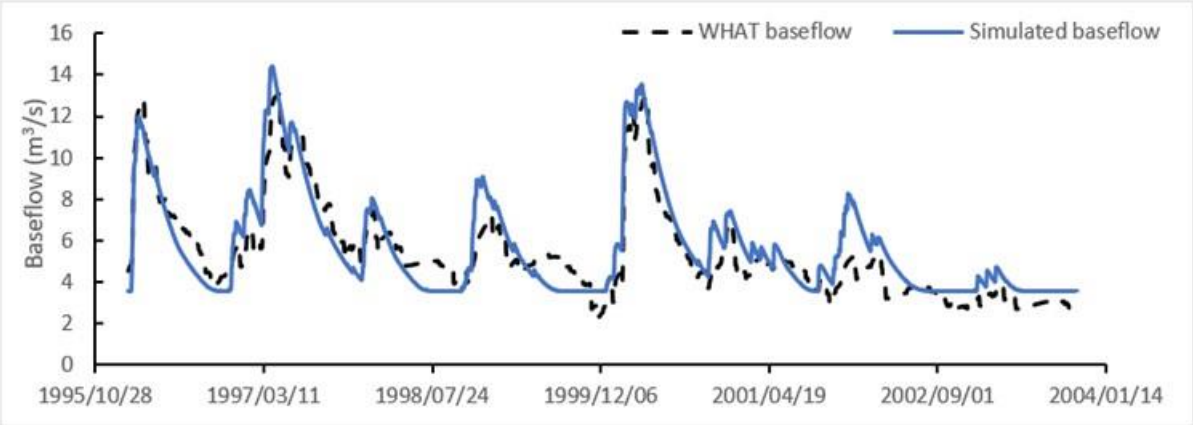

Figure 6.34: Time series plot of baseflow simulated from a PRMS model and externally in a web-based tool called WHAT for the calibration period.

6.5.3 Simulation of climate scenarios

Table 6.20 presents the results of climate simulations. Both baseflow and stream flow showed more sensitivity to an increase in rainfall than a decrease. Increasing rainfall by 20% caused an increase of 49% and 52% in baseflow and stream flow volumes, respectively. On the other hand, a reduction in rainfall with the same magnitude caused a reduction of 14% and 23% in baseflow and streamflow, respectively. Slightly more effect was observed in baseflow and streamflow as a result of an increase in temperature than a decrease. Increasing the temperature by 1.5°C reduced baseflow by 26% and streamflow by 27%, while reduction of temperature in the same magnitude increased baseflow by 23% and streamflow by 18%.

The recharge values were also calculated from the baseflow as a percentage of annual precipitation to give a recharge estimate in each simulation. The recharge values are shown in Table 6.20. Using the current baseflow estimates, the MAR value of 5.3% was obtained for the period between 1997 and 2016. Under the different climate scenarios, the following values are simulated. When rainfall is increased by 20%, recharge increases to 15.7% and decreases to 4.73% when rainfall is decreased by 20%. When temperature is increased by 1.5°C, recharge becomes 4.09%. It becomes 6.79% when temperature is decreased by 1.5°C. So, in all these scenarios, recharge ranges between 4.09% and 15.7%.

Table 6.20: Climate simulation results with impacts on baseflow and stream flow.

	Current	**+20% Rainfall**	**-20% Rainfall**	**+1.5°C Temp**	**-1.5°C Temp**	**-20% Rainfall & +1.5°C Temp**
Baseflow	-	49% more	14% less	26% less	23% more	28% less
Stream flow	-	52% more	23% less	27% less	18% more	39% less
BFI	0.55	0.54	0.61	0.571	0.569	0.65
Recharge (%)	5.3	15.7	4.73	4.09	6.79	4.97

Figure 6.35 shows a monthly time series of simulated baseflow and total streamflow under the changing rainfall scenarios, while Figure 6.36 shows the results of changing temperature scenarios.

Having observed that the simulations where temperature was increased and where rainfall was decreased caused a reduction in both streamflow and baseflow, a further combined simulation with reduced rainfall and increased temperature was run to assess the worst-case scenario. The result of the combined simulation was a 28% reduction in baseflow and a 39% reduction in streamflow. Figure 6.37 shows the results of a combined simulation. These show that there is less drought effect on baseflow compared to stream flow. The baseflow index analysis presented in Table 6.20 shows that the scenarios that invoke a reduction in terrestrial moisture such as reduced rainfall and increased temperature lead to a higher BFI. This is attributed to a delayed groundwater drought compared to surface water drought.

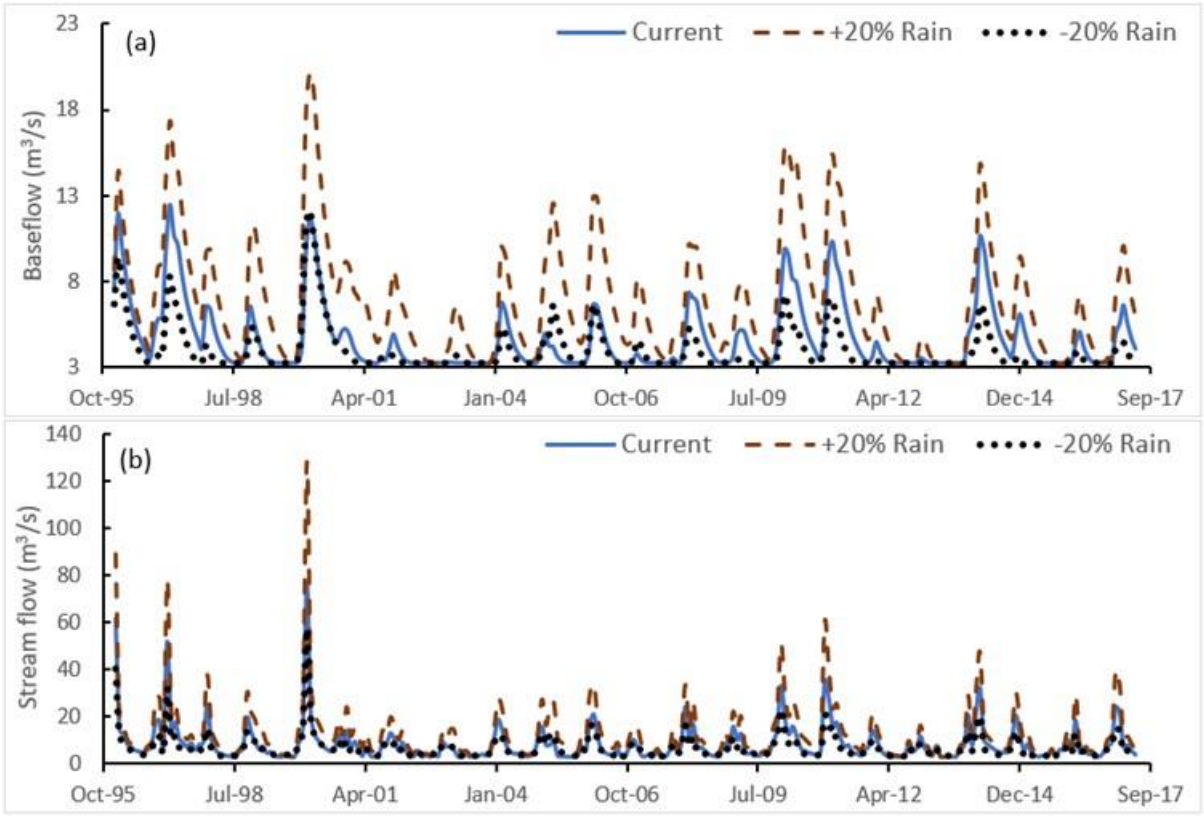

Figure 6.35: Scenario simulated for monthly average baseflow (a) and stream flow (b) with varying rainfall.

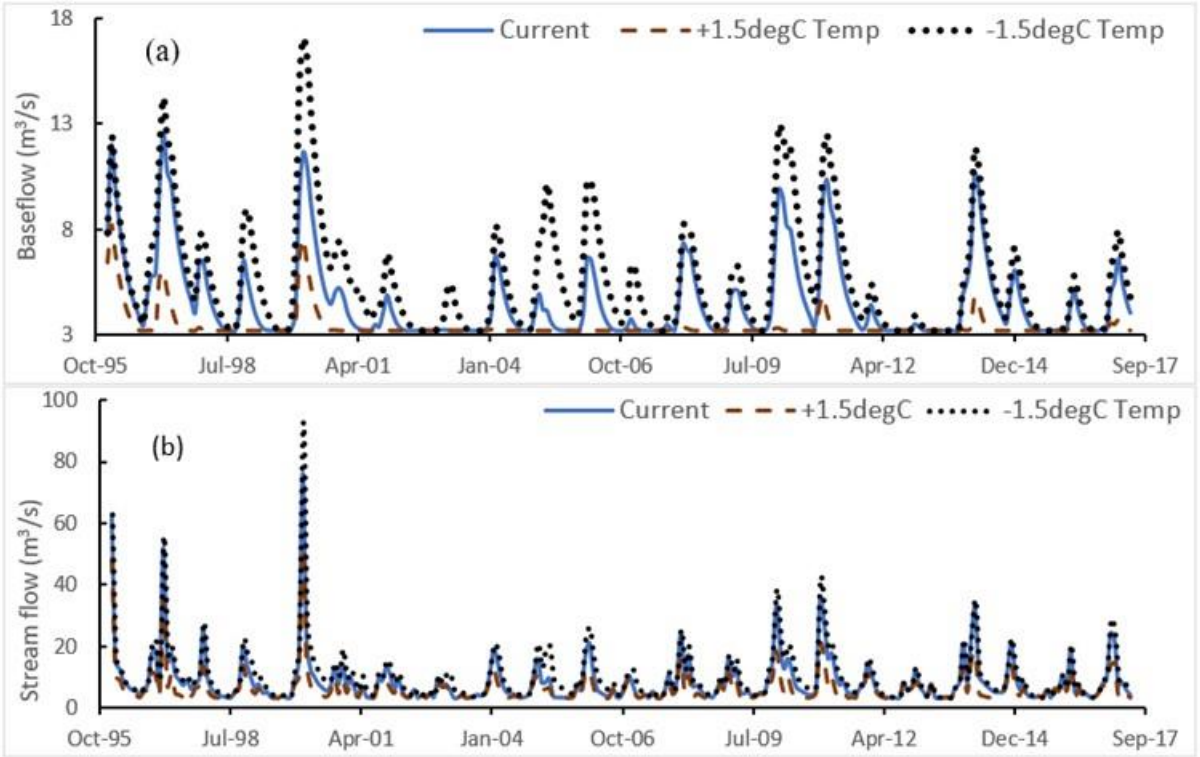

Figure 6.36: Scenario simulated for monthly average baseflow (a) and stream flow (b) with varying temperature.

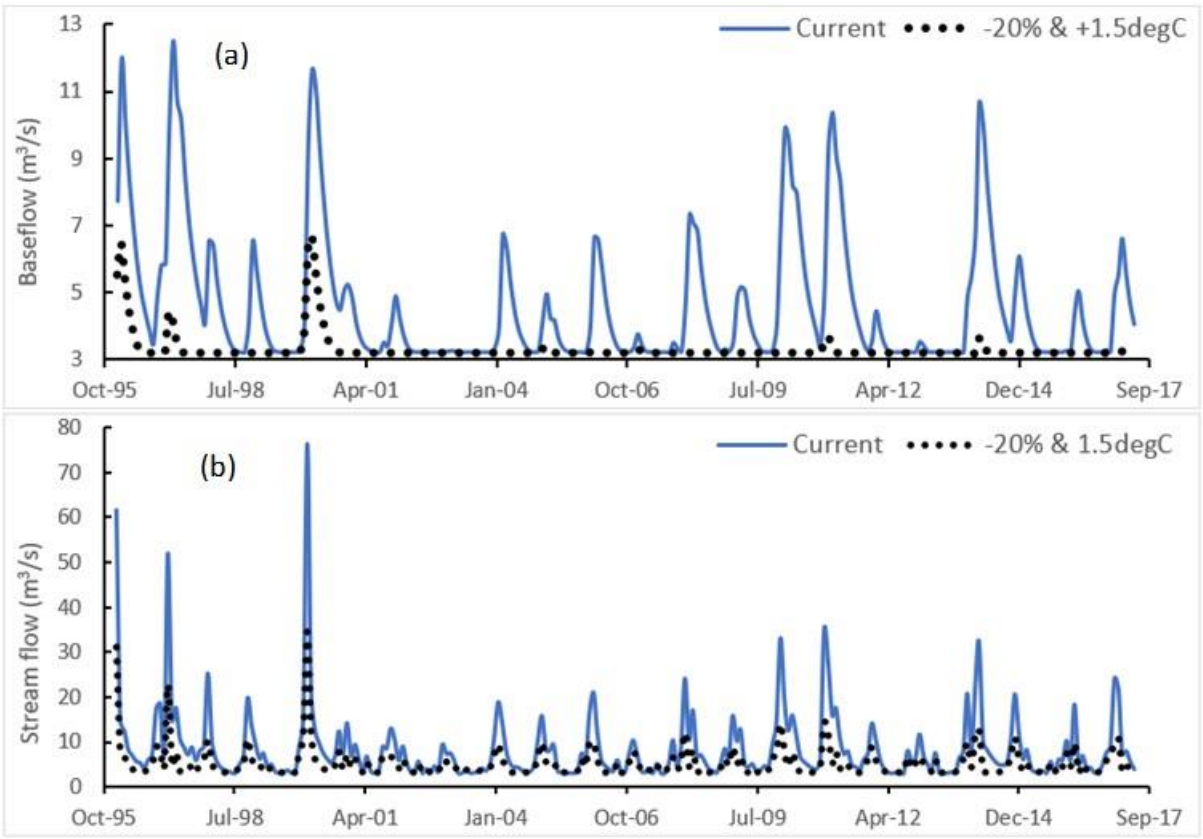

Figure 6.37: A Combined scenario simulated for monthly average baseflow (a) and stream flow (b) with increased temperature and reduced rainfall.

Table 6.21 presents the total number of days out of 7821 days of model review in which wastewater discharge ($5m^3/s$) is greater than daily stream flow. Currently, 54% of the model review period has wastewater exceeding streamflow. When rainfall is reduced by 20% and temperature increased by 1.5°C, wastewater exceeds streamflow 67% of the time and 75% of the time, respectively. As it was observed in Table 6.20, an increase in temperature causes more reduction in streamflow than a decrease in rainfall. Similarly, the number of occurrences on which wastewater exceeds streamflow is higher when temperature is increased than when rainfall is decreased. In the worst-case scenario, where rainfall is reduced and temperature increased, wastewater exceeds streamflow 80% of the time. This wastewater versus streamflow analysis indicates that as climate variables change, wastewater contribution in the UCRB is likely to dominate over natural streamflow.

Table 6.21: Shows the number of days on which stream flow is less than $5m^3/s$ out of 7821 days of modelling period.

	Current	**+20% Rainfall**	**-20% Rainfall**	**+1.5°C Temp**	**-1.5°C Temp**	**-20% Rainfall & +1.5°C Temp**
No. of days	4204	2149	5222	5883	3106	6292
% days < $5m^3/s$	54%	27%	67%	75%	40%	80%

6.6 Synthesis

6.6.1 Conceptual model of groundwater recharge and flow mechanisms in the UCRB

The recharge and groundwater flow mechanisms can be graphically presented as shown in Figure 6.38.

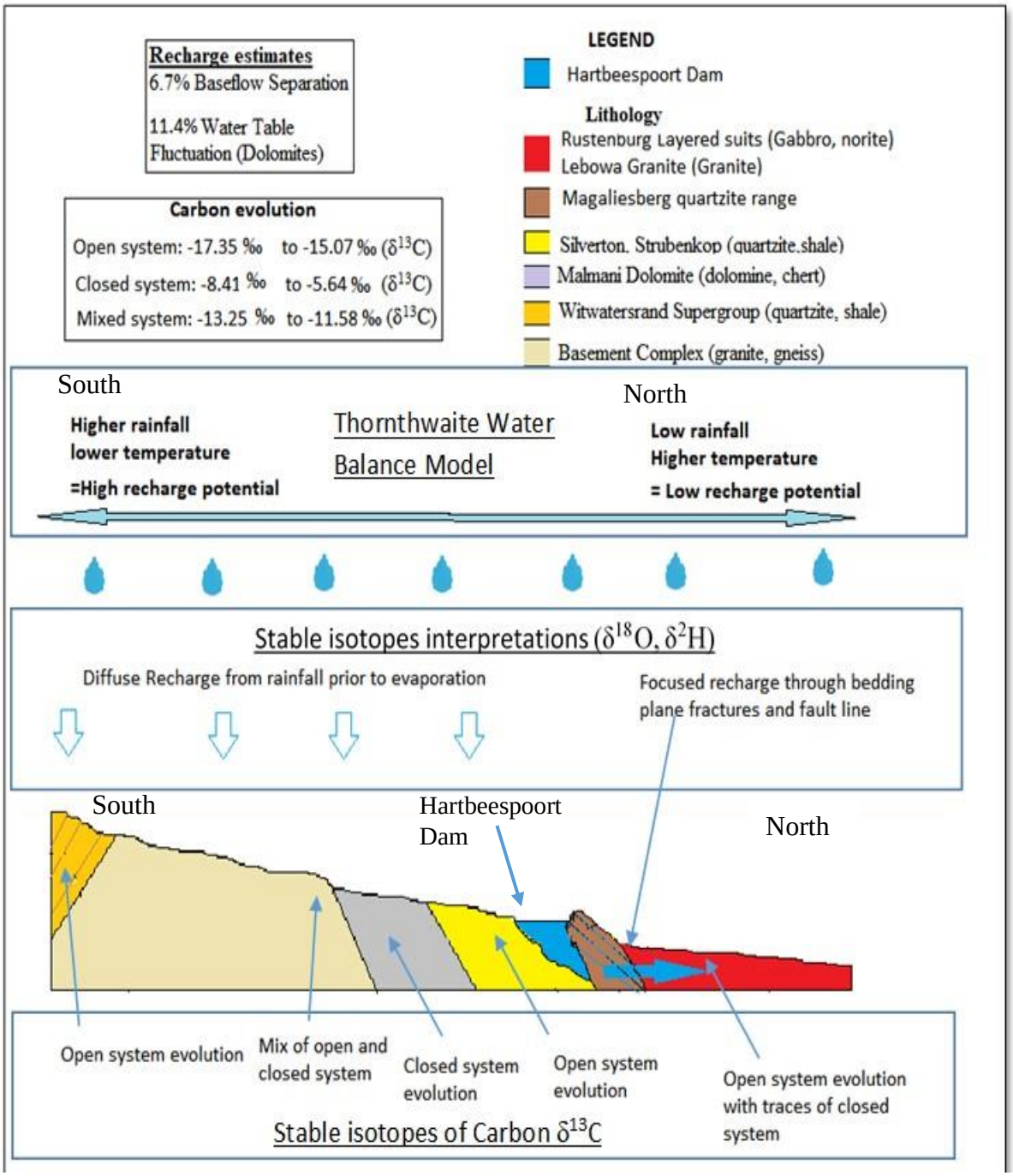

Figure 6.38: Graphical abstract for groundwater recharge in the UCRB.

6.1.1 The sustainability of groundwater in the UCRB

For the purposes of sustainable groundwater management, a percentage of groundwater use to the estimated recharge volume is also calculated to assess the extent of over or under abstraction. The results are presented in Table 6.22. Based on the spatial application of BFS method and, therefore, its representativeness of the entire area, the BFS recharge estimates were used for this comparison. From

the DWS, only the licensed groundwater use volumes could be obtained, which, however, exclude some unlicensed groundwater abstractions.

Table 6.22: Groundwater use as a percentage of recharge volume in the UCRB.

Quaternary Catchment	Discharge station	Recharge (mm)	Area (km^2)	MAP (mm)	Recharge (% MAP)	Annual recharge (Mm^3)	Groundwater usage (m^3)	% GW usage
A21A	A2H090	33.82	451	616.82	5.48	15.25	12 966 411	85.0
A21B	A2H014	57.44	527	616.82	8.50	30.27	33 662 463	111.2
A21C	A2H044	24.96	761	655.20	3.32	18.99	1 414 253	7.4
A21D	A2H049	34.76	372	542.07	6.71	12.93	1 856 423	14.4
A21E	A2H045	99.81	282	655.20	14.19	28.15	4 478 957	15.9
A21F	A2H013	24.07	1 001	542.07	4.23	24.09	3 780 223	15.7
A21G	A2H034	108.66	160	542.07	22.07	17.39	392 699	2.3
Weighted recharge average					**6.67**			

Groundwater use as a fraction of annual recharge ranges from 2.3% in A21G to 111.2% in A21B. The quaternary catchments with high groundwater use percentage are A21A and A21B, which indicate possibilities of groundwater over-abstraction. The estimates also indicate that groundwater is underutilised in A21G. These groundwater use percentage values have to be properly considered in the allocations of groundwater use licenses to avoid over-abstraction. The ^{14}C age indicated that 78% of groundwater samples in the UCRB have an MRT of more than 100 years. This indicates that groundwater in the UCRB is not sustainable and should, therefore, not be over abstracted because with changing climate variables, the scarcity of groundwater is expected to worsen as projected in the PRMS climate simulations.

7 CONCLUSION AND RECOMMENDATIONS

7.1 Conclusions

Using the three year stable isotope rainfall data, the Johannesburg Local Meteoric Water Line (JLMWL) was constructed as $\delta^2H=6.7\delta^{18}O+10‰$ (n = 260, $R^2 = 0.92$). The high variability in stable isotope signature of rainfall indicates that Johannesburg receives rainfall from different moisture sources. This variability is deduced to be a potential cause of uncertainties, which induce challenges when inversely modelling the original rainfall that led to an observed signature in groundwater. While a highly depleted groundwater sample could be interpreted as higher elevation recharge, high latitude moisture source, high rainfall amount or low temperature condensation, it could actually be a result of rainfall from different moisture sources. Similarly, an enriched groundwater sample may not be a result of exposure to evaporation prior to recharge but may be a result of rainfall that came from an enriched moisture source. The amount and temperature effects were observed in the Johannesburg rainfall and an analysis of the temperature effects in rainfall led to construction of the temperature-δ^{18}O regression line of $\delta^{18}O = 0.552t - 14.1‰$.

The stable isotopes indicated the occurrence of both focused and diffuse recharge in the UCRB. Focused recharge was observed in the groundwater samples that are located downstream of the Hartbeespoort Dam. It was deduced that the recharge occurs from the Hartbeespoort Dam through the Brits fault lines and the bedding planes of Magaliesberg quartzite ridge. The tritium analysis further indicated that focused recharge through the Brits fault lines occurs at an approximate rate of 202 m/year, while the water balance of the dam indicated a net flux of 2 084 131 m^3/year to groundwater, which equates to 7% of the dam's average annual inflow.

Diffuse recharge mechanism is also observed in various groundwater samples across the UCRB. Due to the isotopic signature of groundwater samples that is similar to that of rainfall, it was deduced that effective recharge occurs without prior exposure to extreme evaporation possibly through the vertical fractures in the crystalline rocks and through dissolution cavities in the dolomite aquifer. Considering that all the Malmani dolomite samples were highly depleted, it was deduced that recharge occurs at a similar location or the groundwater samples represent a similar recharge episode, which is followed by deeper groundwater circulation. This high depletion in the dolomites was also attributed to the possibilities of an exchange of oxygen from the dissolved CO_2 and groundwater. This also indicated long groundwater circulation under the premise that it takes a long period for oxygen exchange to occur between CO_2 and groundwater in cold conditions. The possibility of exchange should, however, be investigated further.

Analysis of deuterium excess in groundwater samples that are recharged by diffuse mechanisms indicated that recharge is derived from rainfall of different moisture sources and humidity condition, which are a result of the variability that was observed in rainfall samples. A high temporal variability in a single groundwater source (Albert Farm spring) indicated that the use of a single groundwater sample for recharge characterisation may not yield appropriate interpretations as that sample could be representing a unique recharge episode, which does not represent the long-term recharge mechanism.

The $\delta^{13}C‰$ analysis of the groundwater samples indicated that both open and closed system carbon evolution occur in the UCRB. Open system was observed mainly in shale and andesite of the Pretoria

Group, basement granites, quartzite of the Government Formation and the shale of Hospital Hill Formation, thereby, indicating that soil CO_2 is a dominant source of dissolved carbon. Enriched $\delta^{13}C$ values in the Malmani dolomite aquifers indicated that the predominant source of dissolved carbon is carbonate dissolution and, therefore, deduced that carbon evolution in Malmani dolomite aquifers occurs under closed system. The intermediate values of $\delta^{13}C‰$ indicated evolution from open to closed system conditions in the boreholes that are positioned at the periphery of the basement granites near the dolomites of the Malmani Subgroup. This was also attributed to a possibility of mixing of water from a closed system and that from an open system, thereby indicating that the boreholes on the periphery of the granites are tapping water from both the granite and the dolomite aquifers.

The radiocarbon analysis indicated that 78% of groundwater samples in the UCRB have ^{14}C ages between 100 and 3856 years. The diverse ^{14}C ages are said to be a result of the heterogeneity of the aquifers in the UCRB. Radiocarbon analysis along a flow path indicated a slow diffusive groundwater flow in the Malmani dolomite aquifer with a flow rate of about 11 m/yr. With this flow rate and the high spring yields, it is deduced that groundwater generally follows deeper circulation paths.

The Thornthwaite Monthly Water Balance Model indicated that there is more potential for recharge to occur in the southern than in the northern part of the UCRB indicating the influence of temperature on recharge. The TMWBM gave an average potential recharge estimate of 4.3%, which is deduced to occur through the unsaturated zone. The analysis of water levels in the piezometers and monitoring boreholes that are located on the granites, indicated that there is contribution of both interflow and baseflow in the UCRB streams. This indicates that caution should be taken while using surface water methods for recharge assessment because the estimated exchange may actually be interflow that is erroneously interpreted as baseflow.

The Stream Segment Water Budget methods indicated spatial and temporal net gain and net loss across the UCRB. Through application of the Baseflow Separation method in the quaternary catchments, an area weighted average recharge estimate of 6.7% was obtained for the UCRB. The Water Table Fluctuation method gave an average recharge estimate of 11.4% in the Malmani dolomite aquifers. Since the TMWBM estimates recharge that occurs through the unsaturated zone, the higher recharge estimates obtained from WTF and BFS, indicate the significance of the preferential or bypass flow. Meaning that if there was not fractures contribution, recharge would be much lower in the UCRB.

Using the temperature-$\delta^{18}O$ regression that was constructed for Johannesburg rainfall ($\delta^{18}O = 0.552t - 14.1‰$), the calculated daily air temperatures at the time of recharge were in the same range as the present air temperatures during rainfall. On the other hand, the calculated annual air temperatures (10.9°C and 17.6°C) are lower than the present annual air temperatures, which indicates that at the time of recharge the annual temperatures were lower than the present annual temperatures.

An interpretation of the stable isotopes in Albert Farm spring samples and the spring yields indicated that the high yields are generally depleted, and the low yields generally enriched. This observation was attributed to the amount effect that was observed in Johannesburg rainfall. Based on this observation, it was deduced that there is a high dependence of the amount of recharge on the rainfall amount in the quartzite aquifers of the Witwatersrand Supergroup. The dependence on rainfall amount also indicated that there are suitable land surface conditions for recharge to occur, i.e. the geological setting, such that recharge depends on rainfall amount. Furthermore, it was deduced that groundwater flow from the recharge point to the Albert Farm spring outlet, could be following piston

flow conditions with minimal mixing of different recharge episodes The isotopic signature versus yield relationship gave rise to the regression equations; $\delta^{18}O = -377Q - 2.32‰$ and $\delta^{2}H = -1019.5Q - 11.6‰$ where Q is in m^3/s, which can be used in the Albert Farm spring to estimate the isotopic signature when the yield is known or to estimate the yield when the isotopic signature is known. Over all, the analysis of stable isotopes indicate that assessing the traces of stable isotope effects in rainfall and in a gravity fed spring that is recharged directly by rainfall can be a useful tool to determine the dependence of recharge on rainfall amount and the existence of piston or preferential flow conditions

The climate simulations indicate a high significance of baseflow under drought conditions in the UCRB. It was also projected that as baseflow decreases due to changes in climate variables and wastewater increases due to growth in urbanisation, the amount of wastewater shall dominate baseflow up to 85% of the time in the UCRB leading to more polluted surface water.

7.2 Main contributions of the study

The main contributions of this PhD study are as follows:

- The construction of the Johannesburg Local Meteoric Water Line and the improved understanding of the stable isotopes in Johannesburg daily rainfall. This is an important contribution because the data from the nearest station in Pretoria (Pretoria Local Meteoric Water Line) does not have daily data and prior to this study, the characteristics of stable isotopes in daily rainfall for Johannesburg and Pretoria were unknown.
- Construction of the daily temperature-$\delta^{18}O$ relationship for Johannesburg rainfall and presentation of the relationship as a tool that can be used in groundwater that is recharged by rainfall to estimate the air temperature at the time of recharge. This is an important contribution because the previous temperature-$\delta^{18}O$ relationships by Dansgaard (1964) and Gat (2001) were determined for the annual and monthly data and were biased towards the northern hemisphere where the majority of the GNIP stations were located.
- An improved understanding and implications of the temporal variability in $\delta^{18}O/\delta^{2}H$ signature from one groundwater source. This is important because it implies that for groundwater recharge assessment in a sub-tropical region that receives rainfall from different moisture sources, it is necessary to collect multiple samples from each groundwater source possibly in different seasons rather than deducing interpretations from a single sample. This is because a single sample may represent a distinct outlier recharge episode causing bias during interpretation.
- Construction of the relationship between stable isotopes ($\delta^{18}O/\delta^{2}H$) and spring yields and an improved understanding of the traces of the rainfall amount effects in a spring regimen. This is important because it presents a technique that can be used to determine the dependence of recharge amount on the rainfall amount using spring data especially when dealing with old groundwater i.e. when the recent rainfall peak cannot be compared with the recent spring yield peak to deduce the dependence of rainfall amount on recharge.
- An improved understanding of the groundwater flow paths, mechanisms, age and interactions between the karst and crystalline aquifers using a combination of $\delta^{13}C$, $\delta^{18}O$, $\delta^{2}H$ and ^{14}C interpretations. This is important because it helps in the management of groundwater resources against pollution and over abstraction.

- An improved understanding of the effects of changes in climate variables on the baseflow/recharge and the relative contributions of natural streamflow and wastewater under a different climate. This is important because it emphasises a need to improve the quality of wastewater disposed into the UCRB at the time when baseflow is decreasing due to changes in climate variables and wastewater is increasing due to growth in industries.

7.3 Recommendations

The following are the recommendations to address the water resource challenges in the UCRB:

The high wastewater volume in the water stressed UCRB should be turned into good use to meet the high industrial processing water demands. This can be achieved by:

- Improving the quality of disposed wastewater in order to diversify options for re-use.
- Use treated wastewater for irrigation and industrial processing instead of portable water.
- Use treated wastewater for Managed Aquifer Recharge/Artificial recharge as a way to retain the water within the catchment and maintain higher water tables.

In addition to that, groundwater in the UCRB generally has a long mean residence time, indicating that it may not be sustainable and, therefore, requires cautious management.

- The historical groundwater pumping should be well managed through improved watershed management to avoid over abstraction.

The capacity of the authorities is often limited and centralized to certain aquifers of high economic importance. Perhaps the concept of *managing groundwater as it is used* should be implemented through decentralization of some DWS activities to the local farmers. This can be achieved by:

- Capacitating the farmers on personal small-scale groundwater management.
- Encouraging farmers to keep a record of groundwater use through installation of borehole meters.
- Improving the efforts to encourage farmers to monitor their own boreholes for groundwater levels and rainfall and watch over their trends. This will hold them accountable to proper management since they know the consequences that come with mismanagement.

REFERENCES

ABIYE, T. A., LEGESSE, D. & ABATE, H. 2009. The impact of climate change on groundwater recharge: a case study from the Ethiopian Rift. Groundwater and climate in Africa, June 2008 2009 Kampala, Uganda. International Association of Hydrogeologists, 7.

ABIYE, T. A. 2011. Provenance of groundwater in the crystalline aquifer of Johannesburg area, South Africa. *International Journal of Physical Sciences,* Vol. 6**,** pp. 98–111.

ABIYE, T. A., MENGISTU, H. & DEMLIE, M. B. 2011. Groundwater Resource in the Crystalline Rocks of the Johannesburg Area, South Africa. *Journal of Water Resource and Protection,* 03**,** 199–212.

ABIYE, T. A. 2013a. Surface water and groundwater interaction in the upper Crocodile River basin. *In:* ABIYE, T. A. (ed.) *The use of isotope hydrology to characterize and assess water resources in South(ern) Africa. WRC Report No TT 570/13.* Pretoria, South Africa: Water Research Commission.

ABIYE, T. A. (ed.) 2013b. *The use of isotopes hydrology to characterise and assess water resources in South(ern) Africa (WRC Report No TT 570/13)*: Water Research Commission.

ABIYE, T. A. 2014. MINE WATER FOOTPRINT IN THE JOHANNESBURG AREA, SOUTH AFRICA: ANALYSIS BASED ON EXISTING AND MEASURED DATA. *South African Journal of Geology,* 117**,** 87–96.

ABIYE, T. A., MENGISTU, H., MASINDI, K. & DEMLIE, M. 2015. Surface water and groundwater interaction in the Upper Crocodile River Basin, Johannesburg, South Africa: Environmental Isotope Approach. *South African Journal of Geology,* 118**,** pp. 109–118.

ABIYE, T. A. 2016. Synthesis on groundwater recharge in Southern Africa: A supporting tool for groundwater users. *Groundwater for Sustainable Development,* 2–3**,** pp. 182-189.

ADAMS, S., TITUS, R. & XU, Y. 2004. *Groundwater recharge assessment of the basement aquifers of Central Namaqualand: Report to the Water Research Commission,* Gezina, WRC.

ALBHAISI, M., BRENDONCK, L. & BATELAAN, O. 2013. Predicted impacts of land use change on groundwater recharge of the upper Berg catchment, South Africa. *Water SA,* 39**,** 211-220.

ALLANSON, B. R. & GIESKES, J. M. T. M. 1961. Part II An introduction to the limnology of Hartbeespoort Dam with special reference to the effect of industrial and domestic pollution. *Hydrobiologia,* 18**,** pp. 77–94.

ALLISON, G. B. & HUGHES, M. W. 1983. The use of natural tracers as indicators of soil-water movement in a temperate semi-arid region. *Journal of Hydrology,* 60**,** 157-173.

ALLISON, G. B. 1987. A review of some of the physical, chemical, and isotopic techniques available for estimating groundwater recharge. *In:* SIMMERS, I. (ed.) *Estimation of Natural Groundwater Recharge.* Dordrecht, Holland: D. Riedel.

ANHAEUSSER, C. R. 1971. The Geology and geochemistry of the archaean granites and gneisses of the Johannesburg-Pretoria dome. Economic Geology Research Unit University of the Witwatersrand Johannesburg.

ANHAEUSSER, C. R. 1973. The Evolution of the Early Precambrian Crust of Southern Africa. *Philosophical Transactions of the Royal Society of London. Series A, Mathematical and Physical Sciences,* 273**,** 359–388.

ANHAEUSSER, C. R. 1992. Archaean granite-greenstone relationships on the farm Zandspruit 191-IQ, North Riding area, Johannesburg Dome. *South African Journal of Geology***,** 94-101.

APPELO, C. A. & POSTMA, D. 2005. *Geochemistry, groundwater and pollution,* Leiden; New York, Balkema.

ARMSTRONG, R. A., COMPSTON, W., RETIEF, E. A., WILLIAMS, I. S. & WELKE, H. J. 1991. Zircon ion microprobe studies bearing on the age and evolution of the Witwatersrand triad. *Precambrian Research,* 53**,** 243–266.

ARNOLD, J. G., SRINIVASAN, R., MUTTIAH, R. S. & WILLIAMS, J. R. 1998. LARGE AREA HYDROLOGIC MODELING AND ASSESSMENT PART I: MODEL DEVELOPMENT1. *JAWRA Journal of the American Water Resources Association,* 34**,** 73-89.

ASSAF 2017. *First biennial report to cabinet on the state of climate change science technology in South Africa,* Academy of Science of South Africa (ASSAf).

AWAD, S. 2014. Analysing Groundwater Using the 13C Isotope. *8th International Conference on Material Sciences, CSM8-ISM5,* 55**,** 35–40.

AYADI, Y., MOKADEM, N., BESSER, H., KHELIFI, F., HARABI, S., HAMAD, A., BOYCE, A., LAOUAR, R. & HAMED, Y. 2018. Hydrochemistry and stable isotopes (δ18O and δ2H) tools applied to the study of karst aquifers in southern mediterranean basin (Teboursouk area, NW Tunisia). *Journal of African Earth Sciences,* 137**,** P 208–217.

BAKUNDUKIZE, C., VAN CAMP, M. & WALRAEVENS, K. 2011. Estimation of groundwater recharge in Bugesera region (Burundi) using soil moisture budget approach. *Geologica Belgica,* 14.

BARNARD, H. C. 2000. *An explanation of the 1:500 000 general hydrogeological map,* Pretoria, South Africa.

BHANDARY, H., AL-SENAFY, M. & MARZOUK, F. 2015. Usage of Carbon Isotopes in Characterizing Groundwater Age, Flow Direction, Flow Velocity and Recharge Area. *Procedia Environmental Sciences,* 25**,** 28-35.

BRANDL, G., CLOETE, M. & ANHAEUSSER, C. R. 2006. Archaean greenstone belts. *In:* JOHNSON, M. R., ANHAEUSSER, C. R. & THOMAS, R. J. (eds.) *The geology of South Africa.* Reprint ed. Johannesburg/Council for Geoscience, Pretoria,: The Geological Society of South Africa.

BRAUNE, E. & XU, Y. 2008. Groundwater management issues in Southern Africa- an IWRM perspective. *Water SA,* 34**,** 699-706.

BREDENKAMP, D. B., BOTHA, L. J., VAN TONDER, G. J. & VAN RENSBURG, H. J. 1995. *Manual on quantitative estimation of groundwater recharge and aquifer storativity: Based on practical hydro-logical methods,* Pretoria, Water Research Commission.

BRODIE, R., SUNDARAM, B., TOTTENHAM, R., HOSTETLER, S. & RANSLEY, T. 2007. An overview of tools for assessing groundwater -surface water connectivity. Bureau of RUral Sciences, Canberra.

CAWTHORN, R. G., EALES, H. V., WALRAVEN, F., UKEN, R. & WATKEYS, M. K. 2006. The Bushveld Complex. *In:* JOHNSON, M. R., ANHAEUSSER, C. R. & THOMAS, R. J. (eds.) *The geology of South Africa.* Reprint ed. Johannesburg/Council for Geosciences, Pretoria: The Geological Society of South Africa.

CHESNAUX, R. 2013. Regional recharge assessment in the crystalline bedrock aquifer of the Kenogami Uplands, Canada. *Hydrological Sciences Journal,* 58**,** 421–436.

CHILTON, P. J. & FOSTER, S. S. D. 1995. Hydrogeological Characterisation And Water-Supply Potential Of Basement Aquifers In Tropical Africa. *Hydrogeology Journal,* 3**,** 36-49.

CLARK, I. D. & FRITZ, P. 1997. *Environmental isotopes in hydrogeology,* Boca Raton, Fla., Lewis Publishers.

COOK, P. G. 2003. *A Guide to Regional Groundwater Flow in Fractured Rock Aquifers,* South Australia, CSIRO-Seaview Press.

CRAIG, H. 1961. Isotopic Variations in Meteoric Waters. *Science,* 133**,** 1702-1703.

CROSBIE, R. S., BINNING, P. & KALMA, J. D. 2005. A time series approach to inferring groundwater recharge using the water table fluctuation method. *Water Resources Research,* 41**,** n/a-n/a.

CUTHBERT, M. O., ACWORTH, R. I., ANDERSEN, M. S., LARSEN, J. R., MCCALLUM, A. M., RAU, G. C. & TELLAM, J. H. 2016. Understanding and quantifying focused, indirect

groundwater recharge from ephemeral streams using water table fluctuations. *Water Resources Research,* 52**,** 827-840.
DAGGUPATI, P., YEN, H., WHITE, M. J., SRINIVASAN, R., ARNOLD, J. G., KEITZER, C. S. & SOWA, S. P. 2015. Impact of model development, calibration and validation decisions on hydrological simulations in West Lake Erie Basin. *Hydrological Processes,* 29**,** pp. 5307-5320.
DANIEL III, C. C. 1996. Ground-water recharge to the regolith-fractured crystalline rock aquifer system, Orange County, North Carolina. *Water-Resources Investigations Report.*
DANSGAARD, W. 1964. Stable isotopes in precipitation. *Tellus,* 16**,** 436-468.
DE VRIES, J. J., SELAOLO, E. T. & BEEKMAN, H. E. 2000. Groundwater recharge in the Kalahari, with reference to paleo-hydrologic conditions. *Journal of Hydrology,* 238**,** 110–123.
DE VRIES, J. J. & SIMMERS, I. 2002. Groundwater recharge: An overview of processes and challenges. *Hydrogeology Journal,* 10**,** 5–17.
DEPARTMENT OF WATER AFFAIRS AND FORESTRY, S. A. 2004. Crocodile River (West) and Marico Water Management Area: Internal Strategic Perspective of the Crocodile River (West) catchment. *DWAF Report No. 03/000/00/0303.*
DEPARTMENT OF WATER AFFAIRS AND FORESTRY, S. A. 2008a. The Development of a reconciliation strategy for the Crocodile West Water Supply System Version 1: Water Resource Reconcilitation Strategy *In:* FORESTRY, W. A. A. (ed.) Version 1 ed. Pretoria, South Africa.
DEPARTMENT OF WATER AFFAIRS AND FORESTRY, S. A. 2008b. The Development of a Reconciliation Strategy for the Crocodile (West) Water Supply System: Summary of Previous and Current Studies. *In:* BKS (PTY) LTD & ARCUS GIBB (PTY) LTD (eds.) *Summary of Previous and Current Studies.* Pretoria, South Africa.
DEPARTMENT OF WATER AFFAIRS, S. A. 2010. Groundwater Strategy 2010. *In:* AFFAIRS, W. (ed.). Pretoria, South Africa.
DIAMOND, R. & HARRIS, C. 1997. Oxygen and hydrogen isotope composition of Western Cape meteoric water. *South African Journal of Science,* 93.
DONATO, M. M. 1998. Surface-water/ground-water relations in the Lemhi River Basin, east-central Idaho. *Water-Resources Investigations Report.* Reston, VA.
DOWER, S. 2003. Water Quality. *Water Wheel.* Pretoria South Africa.
ENGELBRECHT, F., ADEGOKE, J., BOPAPE, M.-J., NAIDOO, M., GARLAND, R., THATCHER, M., MCGREGOR, J., KATZFEY, J., WERNER, M., ICHOKU, C. & GATEBE, C. 2015. Projections of rapidly rising surface temperatures over Africa under low mitigation. *Environmental Research Letters,* 10**,** pp. 1-17.
ERIKSSON, E. & KHUNAKASEM, V. 1969. Chloride concentration in groundwater, recharge rate and rate of deposition of chloride in the Israel Coastal Plain. *Journal of Hydrology,* 7**,** 178–197.
ERIKSSON, P. G. & CLENDENIN, C. W. 1990. A review of the transvaal sequence, South Africa. *Journal of African Earth Sciences (and the Middle East),* 10**,** P 101–116.
ERIKSSON, P. G., HATTINGH, P. J. & ALTERMANN, W. 1995. An overview of the geology of the Transvaal Sequence and Bushveld Complex, South Africa. *Mineralium Deposita,* 30**,** 98-111.
ERIKSSON, P. G., ALTERMANN, W. & HARTZER., F. J. 2006. The Transvaal Supergroup and its Precursors. *In:* JOHNSON, M. R., ANHAEUSSER, C. R. & THOMAS, R. J. (eds.) *The geology of South Africa.* Reprint ed. Johannesburg/Council for Geosciences, Pretoria: The Geological Society of South Africa.
ESLIN, J. & KRIEL, J. The assessment and possible future use of the dolomitic ground water resources of the Far West Rand, Transvaal, Republic of South Africa. International

Conference on Water for Peace, 1967 May 23-31 1968 Washington DC, USA. Washington DC: US Government Printing Office, P 908-918.
EVARISTO, J. & MCDONNELL, J. J. 2017. Prevalence and magnitude of groundwater use by vegetation: a global stable isotope meta-analysis. *Scientific Reports,* 7**,** 44110 EP -.
FREEZE, R. A. & CHERRY, A. J. 1979. *Groundwater,* Englewood Cliffs; London, Prentice-Hall.
FRITZ, P., DRIMMIE, R. J., FRAPE, S. K. & O'SHEA, K. 1987. The Isotope composition of precipitation and groundwater in Canada. Proceedings of symposium, Vienna, 30 March-3 April 1987 organised by IAEA in co-operation with UNESCO, 30 March to 3 April 1987 1987 Vienna. Vienna, Austria: IAEA and UNESCO, 539-549.
FROEHLICH, K., GIBSON, J. J. & AGGARWAL, P. Deuterium excess in precipitation and its climatological significance. Proc. Int. Conf. on Study of Environmental Change Using Isotope Techniques: International conference held in Vienna, 23-27 April 2001 proceedings. C&S papers series, 2002 Vienna Austria. International Atomic Energy Agency, 531.
GASCOYNE, M. & KOTZER, T. 1995. Isotopic methods in hydrogeology and their application to the Underground Research Laboratory, Manitoba. Canada.
GAT, J. R. 2001. Environmentla Isotopes in the Hydrological Cycle-Principles and Applications Volume 2. *Environmentla Isotopes in the Hydrological Cycle.* Vienna Austria: International Atomic Energy Agency.
GAT, J. R. 2010. *Isotope hydrology: A study of the water cycle / Joel R. Gat,* London, Imperial College Press.
GEE, G. W. & HILLEL, D. 1988. Groundwater recharge in arid regions: Review and critique of estimation methods. *Hydrological Processes,* 2**,** 255-266.
GRAHAM, D. N., BUTTS, M. B. & FREVERT, D. K. 2006. Flexible integrated watershed modeling with MIKE-SHE. *In:* SINGH, V. P. & FREVERT, D. K. (eds.) *Watershed models.* Boca Raton, Florida: CRC Press.
HALL, A. L. & DU TOIT, A. L. 1923. On the section acoss the floor of the Bushveld Complex at the Hartbeesporrt Dam, West of Pretoria (Read 15th October, 1923). *Section across floor, bushveld complex.*
HAMON, H. R. 1961. Estimating potential evapotranspiration. *Journal of the Hydraulics Division,* 87**,** p.p 107-120.
HARRIS, C., OOM, B. & DIAMOND, R. 1998. A preliminary investigation of the oxygen and hydrogen isotope hydrology of the greater Cape Town area and an assessment of the potential for using stable isotopes as tracers. *Water SA,* 25.
HARRIS, C., BURGER, C., MILLER, J. & RAWOOT, F. 2010. O- and H-isotope record of Cape Town rainfall from 1991 to 2008, and its application to recharge studies of Table Mountain groundwater, South Africa. *South African Journal of Geology,* 113**,** 33–56.
HAY, L. E. & UMEMOTO, M. 2007. Multiple-Objective Stepwise Calibration Using Luca. *Open-File Report.*
HEALY, R. W. & COOK, P. G. 2002. Using groundwater levels to estimate recharge. *Hydrogeology Journal,* 10**,** 91-109.
HEALY, R. W., WINTER, T. C., LABAUGH, J. & FRANKE, L. O. 2007. Water budgets: foundations for effective water-resources and emvironmental management.
HEALY, R. W. 2010. *Estimating Groundwater Recharge,* United Kingdom, Cambridge University Press.
HERCZEG, A. L., BARNES, C. J., MACUMBER, P. G. & OLLEY, J. M. 1992. A stable isotope investigation of groundwater-surface water interactions at Lake Tyrrell, Victoria, Australia. *The Geochemistry of Acid Groundwater Systems,* 96**,** 19–32.
HOBBS, P. J. 2011. Situation assessment of the surface water and groundwater resource environments in the Cradle for Human Kind World Heritage Site. Report Prepared for the

Management Authority.: Department of Economic Development, Gauteng Province, South Africa.
HOLLAND, M. & WITTHÜSER, K. T. 2009. Geochemical characterization of karst groundwater in the cradle of humankind world heritage site, South Africa. *Environmental Geology,* 57**,** 513-524.
IAEA 2000. Environmental Isotopes in the hydrological cycle. *In:* MOOK, W. G. (ed.) *Principles and applications.* Paris/Vienna: International Atomica Energy Agency.
IPCC 2001. Climate change 2001: The scientific basis. Contribution of Working Group I to the Third Assessment Report of the Intergovernmental Panel on Climate Change. (eds) Houghton,J. T., Y. Ding, D.J. Griggs, M. Noguer, P.J. van der Linden,X. Dai, K. Maskel, and C.A. Johnson. Cambridge University Press, Cambridge, United Kingdom and New York. *Quarterly Journal of the Royal Meteorological Society,* 128**,** pp. 1038-1039.
ISOKANGAS, E., ROSSI, P. M., RONKANEN, A.-K., MARTTILA, H., ROZANSKI, K. & KLØVE, B. 2017. Quantifying spatial groundwater dependence in peatlands through a distributed isotope mass balance approach. *Water Resources Research,* 53**,** 2524-2541.
ISSAR, A. & GAT, J. 1981. Environmental Isotopes as a Tool in Hydrogeological Research in an Arid Basin. *Groundwater,* 19**,** 490-494.
JOHNSON, A. I. 1967. Specific yield: compilation of specific yields for various materials. *Water Supply Paper.* Washington, D.C.
JOHNSON, M. R., ANHAEUSSER, C. R. & THOMAS, R. J. 2006. *The geology of South Africa,* Pretoria; Johannesburg, Council for Geoscience; Geological Society of South Africa and Council for Geoscience.
JUDSON, S., DEFFEYES, K. S. & HARGRAVES, R. B. 1976. *Physical geology,* Englewood Cliffs; London, Prentice-Hall.
KAFRI, U. & FOSTER, M. B. J. 1989. Hydrogeology of the malmani dolomite in the Klip River and Natalspruit basins, South Africa. *Environmental Geology and Water Sciences,* 13**,** 153-166.
KAROLYTĖ, R., SERNO, S., JOHNSON, G. & GILFILLAN, S. M. V. 2017. The influence of oxygen isotope exchange between CO2 and H2O in natural CO2-rich spring waters: Implications for geothermometry. *Applied Geochemistry,* 84**,** 173-186.
KENT, L. E. C. 1980. *Stratigraphy of South Africa. Handbook 8, part 1, Lithostratigraphy of the Republic of South Africa, South West Africa,* Pretoria, Government Printer.
KOHN, M. J. 2010. Carbon isotope compositions of terrestrial C3 plants as indicators of (paleo)ecology and (paleo)climate. *Proceedings of the National Academy of Sciences of the United States of America,* 107**,** 19691–19695.
KONIKOW, L. F. 1978. Calibration of groundwater models. *Verification of mathematical and physical models in hydraulic engineering.* New York: American Society of Civil Engineers.
KRAUSE, P., BOYLE, D. P. & BÄSE, F. 2005. Comparison of different efficiency criteria for hydrological model assessment. *Advances in Geosciences,* 5**,** pp. 89–97.
KREŠIĆ, N. 2007. *Hydrogeology and groundwater modeling,* Boca Raton, Fla., CRC Press [London : Taylor & Francis.
KRUL, W. F. J. M. & LIEFRINCK, F. A. 1946. *Recent groundwater investigations in the Netherlands,* New York, Elsevier Pub. Co.
KUNIANSKY, E. L. 1989. Geohydrology and Simulation of Ground-Water Flow in the'400-Foot,"600-Foot,' and Adjacent Aquifers, Baton Rouge Area, Louisiana. *Water Resources Technical Report*.
LEAVESLEY, G. H., LICHTY, R. W., TROUTMAN, B. M. & SAINDON, L. G. 1983. Precipitation-runoff modeling system; user's manual. *Water-Resources Investigations Report.*

LEAVESLEY, G. H., RESTREPO, P. J., MARKSTROM, S. L., DIXON, M. & STANNARD, L. G. 1996. The Modular Modeling System (MMS): User's Manual. Denver, Colorado: United States Geological Survey in cooperation with the University of Colorado at Boulder, Center for Advanced Decision Support for Water and Environmental Systems (CADSWES).

LEE, D. R. 1977. A device for measuring seepage flux in lakes and estuaries1. *Limnology and Oceanography,* 22**,** 140-147.

LEGESSE, D., VALLET-COULOMB, C. & GASSE, F. 2003. Hydrological response of a catchment to climate and land use changes in Tropical Africa: case study South Central Ethiopia. *Journal of Hydrology,* 275**,** 67–85.

LEGESSE, D., ABIYE, T. A. & VALLET-COULOMB, C. 2010a. Modeling impacts of climate and land use changes on catchment hydrology: Meki River, Ethiopia. *Hydrology and Earth System Sciences Discussions,* 7**,** pp. 4535–4565.

LEGESSE, D., ABIYE, T. A., VALLET-COULOMB, C. & ABATE, H. 2010b. Streamflow sensitivity to climate and land cover changes: Meki River, Ethiopia. *Hydrology and Earth System Sciences,* 14**,** 2277–2287.

LEKETA, K. C. 2011. *Flow characteristics of groundwater systems: an investigation of hydraulic parameters* Master of Science in Hydrogeology, University of the Free State.

LERNER, D. N., ISSAR, A. S. & SIMMERS, I. 1990. *Groundwater recharge : a guide to understanding and estimating natural recharge,* Hannover, Heise.

LERNER, D. N. 2003. Surface water-Groundwater Interaction in the Context of Groundwater Resources. *In:* XU, Y. & BEEKMAN, H. E. (eds.) *Groundwater Recharge Estimation in Southern Africa.* Paris, France: UNESCO-IHP.

LIBBY, W. F., ANDERSON, E. C. & ARNOLD, J. R. 1949. Age Determination by Radiocarbon Content: World-Wide Assay of Natural Radiocarbon. *Science,* 109**,** 227-228.

LIM, K. J., ENGEL, B. A., TANG, Z., JOONGDAE, C., KI-SUNG, K., SURESH, M. & DIBYAJYOTI, T. 2005. AUTOMATED WEB GIS BASED HYDROGRAPH ANALYSIS TOOL, WHAT1. *JAWRA Journal of the American Water Resources Association,* 41**,** pp. 1407-1416.

LLOYD, J. W. 1986. A review of aridity and groundwater. *Hydrological Processes,* 1**,** 63-78.

MALIVA, R. & MISSIMER, T. M. 2012. *Arid lands water evaluation and management,* Berlin; New York, Springer.

MARFIA, A. M., KRISHNAMURTHY, R. V., ATEKWANA, E. A. & PANTON, W. F. 2004. Isotopic and geochemical evolution of ground and surface waters in a karst dominated geological setting: a case study from Belize, Central America. *Applied Geochemistry,* 19**,** P 937–946.

MARKSTROM, S. L., NISWONGER, R. G., REGAN, R. S., PRUDIC, D. E. & BARLOW, P. M. 2008. GSFLOW-Coupled ground-water and surface-water flow model based on the integration of the Precipitation-Runoff Modelling System (PMRS) and the Modular Ground-water Flow Model (MODFLOW-2005). *Section D, Groundwater/Surfacewater Book 6, Modeling Techniques and Methods.* United States Geological Survey.

MARKSTROM, S. L., REGAN, R. S., HAY, L. E., VIGER, R. J., WEBB, R. M. T., PAYN, R. A. & LAFONTAINE, J. H. 2015. PRMS-IV, the precipitation-runoff modelling system, version 4: U.S. Geological Survey Techniques and Methods, book 6, chap. B7, .

MCCABE, G. J. & WOLOCK, D. M. 1996. Effects of potential climatic change on annual runoff in the conterminous United States. *Journal of the American Water Resources Association,* 35**,** pp. 1341 - 1350.

MCCABE, G. J. & MARKSTROM, S. L. 2007. A Monthly Water-Balance Model Driven By a Graphical User Interface. *Open-File Report.* USGS.

MEINZER, O. E. 1923. The occurrence of ground water in the United States, with a discussion of principles. *Water Supply Paper.* Washington, DC.

MEYER, R. 2014. *Hydrogeology of groundwater: Report to the Water Research Commission,* Gezina, South Africa, Water Research Commission.
NASH, J. E. & SUTCLIFFE, J. V. 1970. River flow forecasting through conceptual models part I — A discussion of principles. *Journal of Hydrology,* 10**,** 282–290.
NATHAN, R. J. & MCMAHON, T. A. 1990. Evaluation of automated techniques for base flow and recession analyses. *Water Resources Research,* 26**,** pp. 1465-1473.
NCUBE, M. & TAIGBENU, A. 2008. Application of the SWAT model to assess the impact of land cover and land use on the hydrologic response in the Olifants Catchment. *8th WaterNet/WARFSA/GWP-SA Annual Symposium (31 October -2 November 2007).* Lusaka, Zambia: WaterNet.
NEUMAN, S. P. 1987. On Methods of Determining Specific Yield. *Ground Water,* 25**,** 679-684.
NKOSI, S. C. 2016. *Application of fate and transport models to evaluate the efficiency of a CR(VI) remediation pump and system.* Master of Science Partial fulfillment (Mini dissertation), University of the Witwatersrand.
NKOTAGU, H. 1996. Application of environmental isotopes to groundwater recharge studies in a semi-arid fractured crystalline basement area of Dodoma, Tanzania. *Hydrogeochemical Studies in Sub-Saharan Africa,* 22**,** P 443–457.
PITMAN, W. & VEGTER, J. 2003. Recharge and stream Flow. *In:* XU, Y. & BEEKMAN, H. E. (eds.) *Groundwater Recharge Estimation in South Africa.* Paris, France: UNESCO International Hydrologic Programme (IHP).
POUJOL, M. & ANHAEUSSER, C. R. 2001. The Johannesburg Dome, South Africa: new single zircon U–Pb isotopic evidence for early Archaean granite–greenstone development within the central Kaapvaal Craton. *Precambrian Research,* 108**,** 139–157.
PRETORIUS, D. A. 1964. Geology of South Rand Goldfield. Economic Geology Research Unit.
PRETORIUS, D. A. 1976. *The nature of the Witwatersrand gold-uranium deposits, ch 2,* Netherlands, Elsevier.
RANTZ , S. E. 1982. Measurement and computation of streamflow. *Geological Survey Water-supply Paper 2175.*
RASMUSSEN, W. C. & ANDREASEN, G. E. 1959. Hydrologic budget of the Beaverdam Creek basin, Maryland. *Water Supply Paper.*
REGAN, R. S. & LAFONTAINE, J. H. 2017. Documentation of the dynamic parameter, water-use, stream and lake flow routing, and two summary output modules and updates to surface-depression storage simulation and initial conditions specification options with the Precipitation-Runoff Modeling System (PRMS). *Techniques and Methods.* Reston, VA.
RIVARD, C., LEFEBVRE, R. & PARADIS, D. 2014. Regional recharge estimation using multiple methods: an application in the Annapolis Valley, Nova Scotia (Canada). *Environmental Earth Sciences,* 71**,** 1389-1408.
ROBB, L. J. & MEYER, F. M. 1995. The Witwatersrand Basin, South Africa: Geological framework and mineralization processes. *Ore Geology Reviews,* 10**,** 67–94.
ROSENBERRY, D. & LABAUGH, J. (eds.) 2008. *Field techniques for estimating water fluxes between surface water and ground water,* Reston, Virginia: United States Geological Survey.
ROSENBERRY, D., LABAUGH, J. & RANDALL, H. 2008. Use of Monitoring Wells, Portable Piezometers, and Seepage Meters to Quantify Flow Between Surface Water and Groundwater. *In:* ROSENBERRY, D. & LABAUGH, J. (eds.) *Field techniques for estimating water fluxes between surface water and ground water.* U.S Geological Survey.
RUTLEDGE, A. 1998. Computer programs for describing the recession of ground-water discharge and for estimating mean ground-water recharge and discharge from streamflow records-Update. Reston, Virginia USGS.

SAMI, K. 1992. Recharge mechanisms and geochemical processes in a semi-arid sedimentary basin, Eastern Cape, South Africa. *Journal of Hydrology,* 139**,** 27–48.
SANTHI, C., ARNOLD, J. G., WILLIAMS, J. R., DUGAS, W. A., SRINIVASAN, R. & HAUCK, L. M. 2001. VALIDATION OF THE SWAT MODEL ON A LARGE RWER BASIN WITH POINT AND NONPOINT SOURCES1. *JAWRA Journal of the American Water Resources Association,* 37**,** pp.1169-1188.
SCANLON, B. R., HEALY, R. W. & COOK, P. G. 2002. Choosing appropriate techniques for quantifying groundwater recharge. *Hydrogeology Journal,* 10**,** P 18-39.
SCANLON, B. R., KEESE, K. E., FLINT, A. L., FLINT, L. E., GAYE, C. B., EDMUNDS, W. M. & SIMMERS, I. 2006. Global synthesis of groundwater recharge in semiarid and arid regions. *Hydrological Processes,* 20**,** P 3335-3370.
SCHOCH-FISCHER, H., ROZANSKI, K., JACOB, H., SONNTAG, C., JOUZEL, I., OSTLUND, G. & GEYH, M. A. 1984. Hydrometeorological factors controlling the time variation of D, 18O and 3H in atmospheric water vapour and precipitation in the Northern Westwind Belt. Proceedings of a symposium Vienna, 12-16 Spetember 1983 organised by IAEA in co-operation with UNESCO, 12 to 16 March 1983 1983 Vienna, Austria. Vienna, Austria: IAEA and UNESCO, 3-30.
SCHULZE, R. E. 2000. Modelling Hydrological Responses to Land Use and Climate Change: A Southern African Perspective. *AMBIO: A Journal of the Human Environment,* 29**,** 12–22.
SELAOLO, E. T. 1998. *Tracer studies and groundwater recharge assessment in the eastern fringe of the Botswana Kalahari: The Letlhakeng-Botlhapatlou area.* PhD, Free University (Amsterdam).
SHAKHANE, T., FOURIE, F. D. & DU PREEZ, P. J. 2017. Mapping riparian vegetation and charactersing its groundwater dependency at the modder river government water scheme. *Groundwater for Sustainable Development,* 5**,** 216–228.
SHAW, E. M. 2005. *Hydrology in practice,* [Oxford, UK], Routledge.
SMAKHTIN, V. & WATKINS, D. 1997. Low flow estimation in South Africa. *Report to the Water Research Commission by the Institute for Water Research, Rhodes University.* Water Research Commission, Pretoria South Africa: Institute for Water Research, Rhodes University.
SODERBERG, K., GOOD, S. P., WANG, L. & CAYLOR, K. 2012. Stable Isotopes of Water Vapor in the Vadose Zone: A Review of Measurement and Modeling Techniques. *Vadose Zone Journal,* 11**,** 0.
SOPHOCLEOUS, M. 2002. Interactions between groundwater and surface water: the state of the science. *Hydrogeology Journal,* 10**,** 52-67.
SUCKOW, A., AGGARWAL, P. K. & ARAGUÁS ARAGUÁS, L. 2013. *Isotope methods for dating old groundwater,* Vienna, International Atomic Energy Agency.
SUN, X., XU, Y., JOVANOVIC, N., KAPANGAZIWIRI, E., BRENDOCK, L. & BUGAN, R. 2013. Application of the rainfall infiltration breakthrough (RIB) model for groundwater recharge estimation in west coastal South Africa. *Application of the rainfall infiltration breakthrough (RIB) model for groundwater recharge estimation in west coastal South Africa,* 39 10.
TESSEMA, A., MENGISTU, H., CHIRENJE, E., ABIYE, T. A. & DEMLIE, M. B. 2012. The relationship between lineaments and borehole yield in North West Province, South Africa: Results from geophysical studies. *Hydrogeology Journal,* 20**,** 351–368.
THEIS, C. V. 1937. Amount of ground-water recharge in the southern High Plains. *Eos, Transactions American Geophysical Union,* 18**,** 564-568.
TSOELOPELE-ENVIRONMENTAL 2006. Hartbeespoort Strategic Environmental Assessment. unpublished work: Tsoelopele Environmental (pty) Ltd.

TURCO, M. J., EAST, J. W. & MILBURN, M. S. 2007. Base flow (1966-2005) and streamflow gain and losses (2006) of the Brazos River, McLennan County to Fort Bend County, Texas. *U.S Geological Survey Scientific Investigations* Texas, USA: Unted States Geological Survey.

UREY, H. C. 1947. The thermodynamic properties of isotopic substances. *J. Chem. Soc.***,** 562–581.

VAN DER LEE, J. & GEHRELS, J. C. 1990. Modelling Aquifer Recharge, Introduction to the Lumped Parameter Model EARTH. 1-21.

VAN TONDER, G. J. & XU, Y. 2000. Estimation of recharge using a revised CRD method. *Water SA,* 27**,** 4.

VAN WYK, E. 2010. *ESTIMATION OF EPISODIC GROUNDWATER RECHARGE IN SEMI-ARID FRACTURED HARD ROCK AQUIFERS.* Doctor of Philosophy University of the Witwatersrand.

VANTONGEREN, J. A., MATHEZ, E. A. & KELEMEN, P. B. 2010. A Felsic End to Bushveld Differentiation. *Journal of Petrology,* 51**,** 1891–1912.

VEGTER, J. 1995. An explanation of a set of National Groundwater Maps. Pretoria, South Africa: Water Research Commission

WALRAVEN, F., ARMSTRONG, R. A. & KRUGER, F. J. 1990. A chronostratigraphic framework for the north-central Kaapvaal craton, the Bushveld Complex and the Vredefort structure. *Cryptoexplosions and catastrophes in the geological record, with a special focus on the Vredefort structure,* 171**,** 23–48.

WANG, Y., YOU, Y. & KULIE, M. 2018. Global Virga Precipitation Distribution Derived From Three Spaceborne Radars and Its Contribution to the False Radiometer Precipitation Detection. *Geophysical Research Letters,* 45**,** 4446-4455.

WATES, J., BRAUNE, E. & BREDENHANN, L. 2000. *Policy and strategy for groundwater quality management in South Africa,* Pretoria, Dept. of Water Affairs and Forestry.

WHITE, W. N. 1932. A method of estimating ground-water supplies based on discharge by plants and evaporation from soil: Results of investigations in Escalante Valley, Utah. *Water Supply Paper.* Washington, D.C.

WHO 2017. *Progress on Drinking Water, Sanitation and Hygiene: 2017 Update and SDG Baselines,* World Health Organization and the United Nations Children's Fund.

WINTER, T. C., JUDSON, H. W., FRANKE, L. O. & M, A. W. 1998. *Ground water and surface water: A single resource,* Denver Colo., U.S. Geological Survey.

WOODFORD, A. & CHEVALLIER, L. 2002. Hydrogeology of the Main Karoo Basin: Current Knowledge and Future Research Needs. South Africa: Water Research Commission.

XU, Y. & BEEKMAN, H. 2003a. *Groundwater Recharge Estimation in Southern Africa,* Paris, UNESCO.

XU, Y. & BEEKMAN, H. 2003b. Review of Groundwater Recharge Estimation in Arid and Semi-Arid Southern Africa. *In:* XU, Y. & BEEKMAN, H. (eds.) *Groundwater Recharge Estimation in Southern Africa.* Paris, France: UNESCO-IHP.

ZOHARY, T., JARVIS, A. C., CHUTTER, F. M., ASHTON, P. J. & ROBARTS, R. 1988. The Hartbeespoort Dam ecosystem programme - 1980-1988.

APPENDICES

A. Methodology on carbon14 sampling (Source is iThemba Labs, Johannesburg).

Environmental Isotope Laboratory, iThemba LABS (Gauteng)

Drum precipitation field method for collecting water samples for radiocarbon analysis

1. The object is to obtain enough carbon (minimum 2g) for a radiocarbon measurement. This will be ensured by precipitating the TDIC (total dissolved inorganic carbon) at a minimum of 2 meq/L (e.g. ~ 150 mg/L HCO_3) from 50 L of sample water.
2. If the TDIC is not known, do an alkalinity titration. If less than 120 mg/L, precipitate two drums.
3. The method using the drums provided is most efficient if the drums are kept on the field vehicle, where they can be both filled and emptied.
4. Empty a sachet of $BaCl_2$ powder into a bucket, pour in a few litres of sample water and stir until dissolved. NOTE: $BaCl_2$ is non-corrosive but poisonous (heavy metal). Avoid inhaling fine dust or ingesting and rinse hands on contact.
5. Rinse the drum well with sample water and fill. Whilst filling, add the following
   I. A dash of phenolphthalein solution (shake well before use)
   II. About 200 mL cleaned NaOH solution (**N.B**. **CAUSTIC**, wash hand immediately on contact).
   III. All of the $BaCl_2$ solution
6. The water will turn pink on addition of the NaOH solution and a cloud of precipitate will form when BaCl2 solution is added. These should mix by the swirl of the inflowing water. If needed, the contents of the drum may be stirred.
7. Fill the drum to close to the top and screw on cap. About 1 hour is required for the precipitate to collect on the bottom. Open cap and check if the liquid (which should still be visibly pink) is reasonable clear. If the pink colour has completely disappeared, add a little more NaOH. The precipitation can proceed whilst driving around in the vehicle.
8. The precipitate should now form a visible layer below the draining stopcock. Move the drum to the edge of the vehicle's loading platform, loosen the cap and open the stopcock to drain the clear supernatant onto the ground. Throttle if precipitate is entrained. Fill a 2-3 litre container with this clear liquid.
9. When the flow has reduced substantially, the drum may be tilted to extract more supernatant. Stop the draining process when precipitate appears.
10. Close the stopcock, swirl the contents of the drum and pour the precipitate slurry through a large funnel into a 2-3 litre container. If the remaining amount of slurry exceeds this volume, use a second container. Clearly mark these containers A & B. Top up with the reserved clear solution.
11. The next day, the precipitate will have compacted considerably. Pour off and keep most of the supernatant, swirl the precipitate and pour into 0.5 or 1 litre bottles. Top up with supernatant. If more than one bottle is required, repeat all information and mark A, B etc.
12. Although this is not critical, attempt to limit atmospheric exposure of the alkaline sample at every step of this procedure.

N.B. Take a 1 litre water sample from the same source for other isotopic measurements

B. Borehole hydrographs

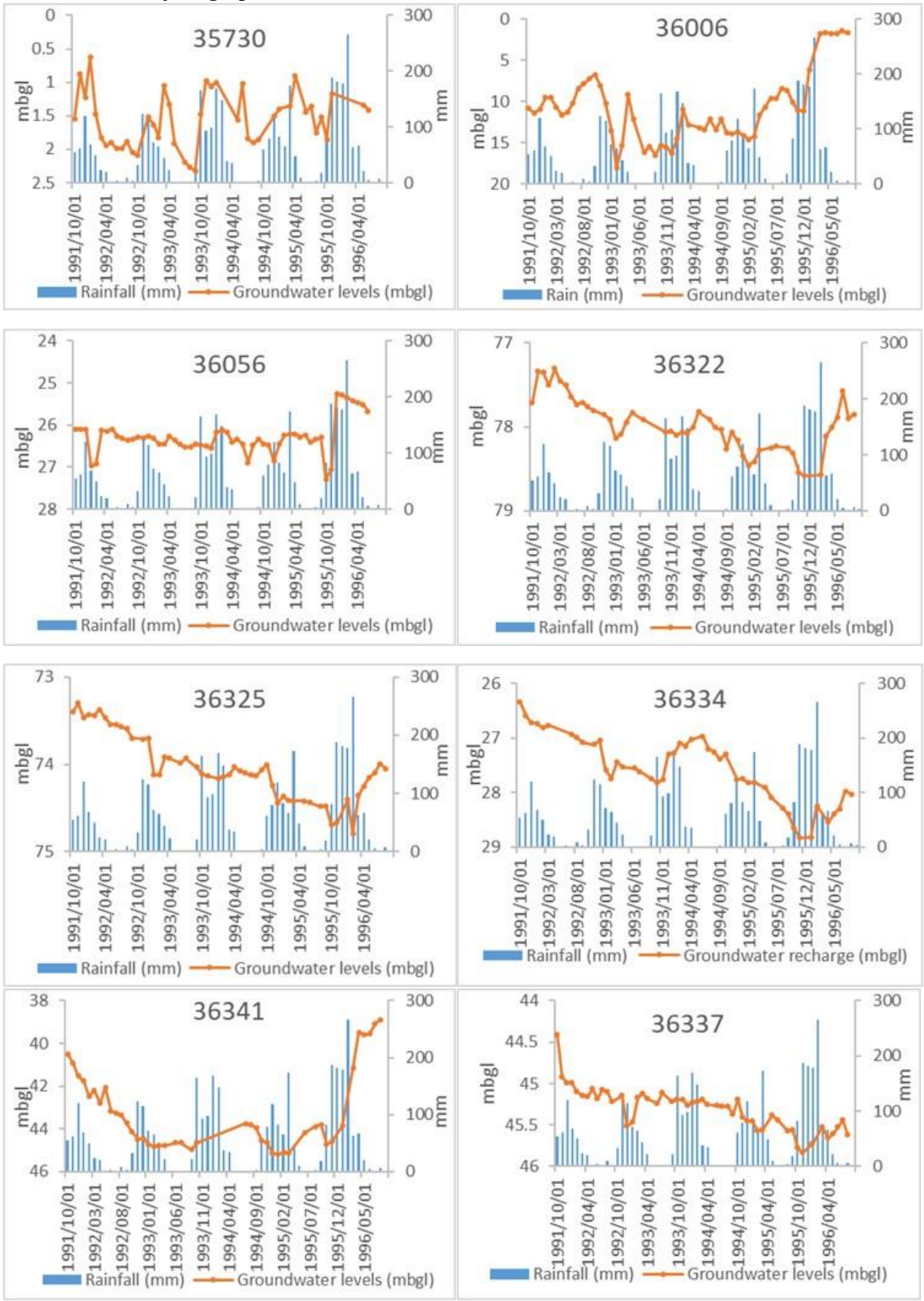

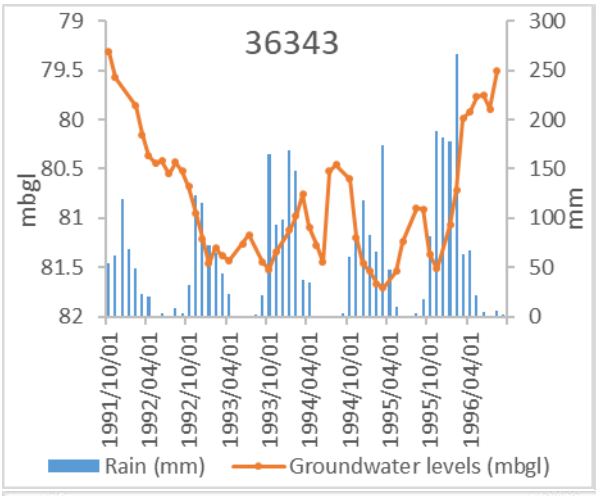
36343
mbgl
mm
Rain (mm)
Groundwater levels (mbgl)

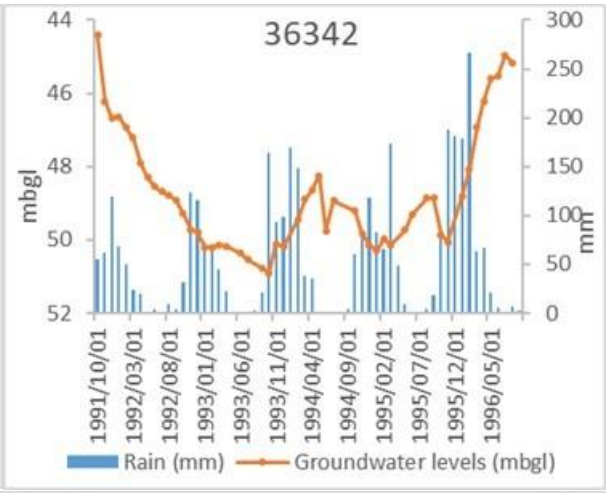
36342
mbgl
mm
Rain (mm)
Groundwater levels (mbgl)

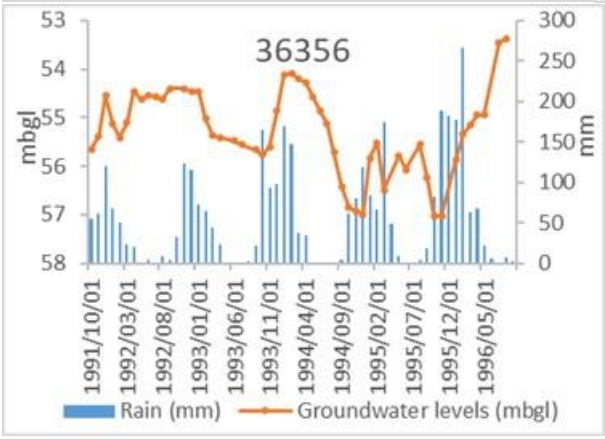
36356
mbgl
mm
Rain (mm)
Groundwater levels (mbgl)

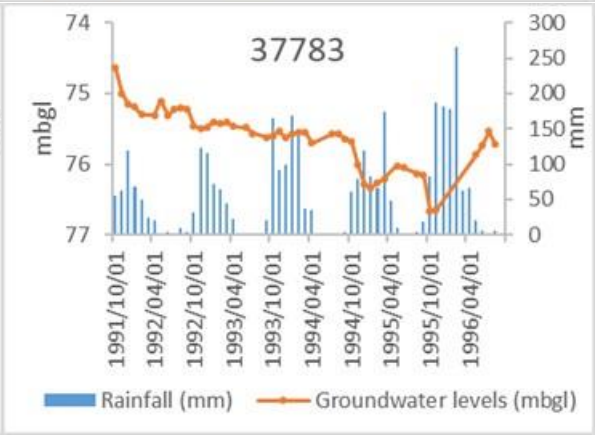
37783
mbgl
mm
Rainfall (mm)
Groundwater levels (mbgl)

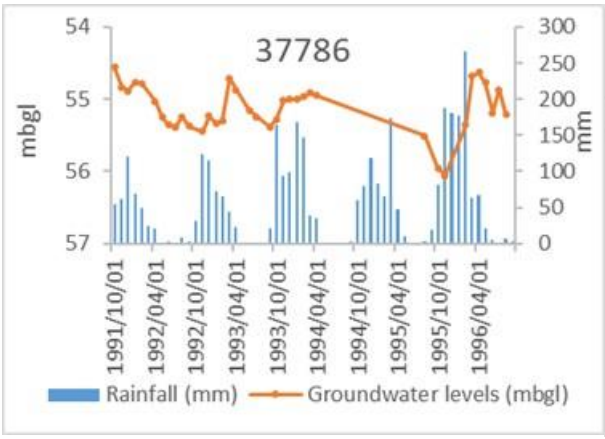
37786
mbgl
mm
Rainfall (mm)
Groundwater levels (mbgl)

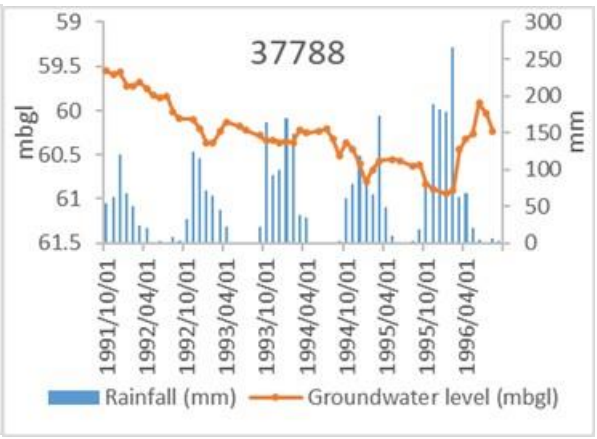
37788
mbgl
mm
Rainfall (mm)
Groundwater level (mbgl)

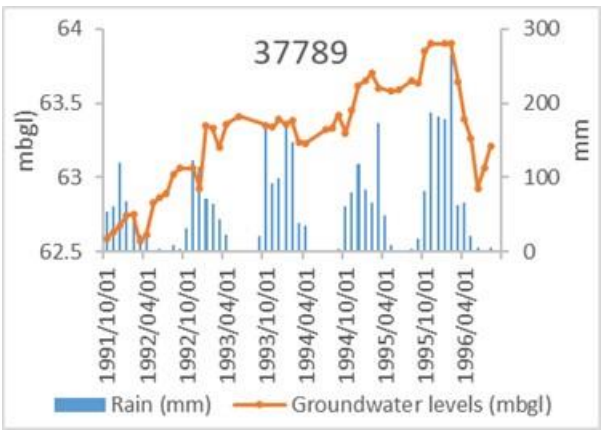
37789
mbgl)
mm
Rain (mm)
Groundwater levels (mbgl)

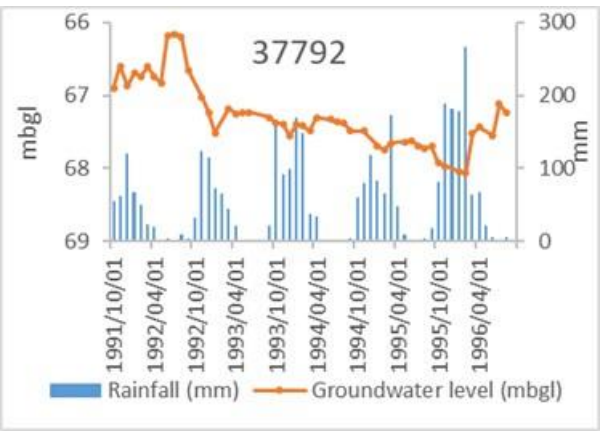
37792
mbgl
mm
Rainfall (mm)
Groundwater level (mbgl)

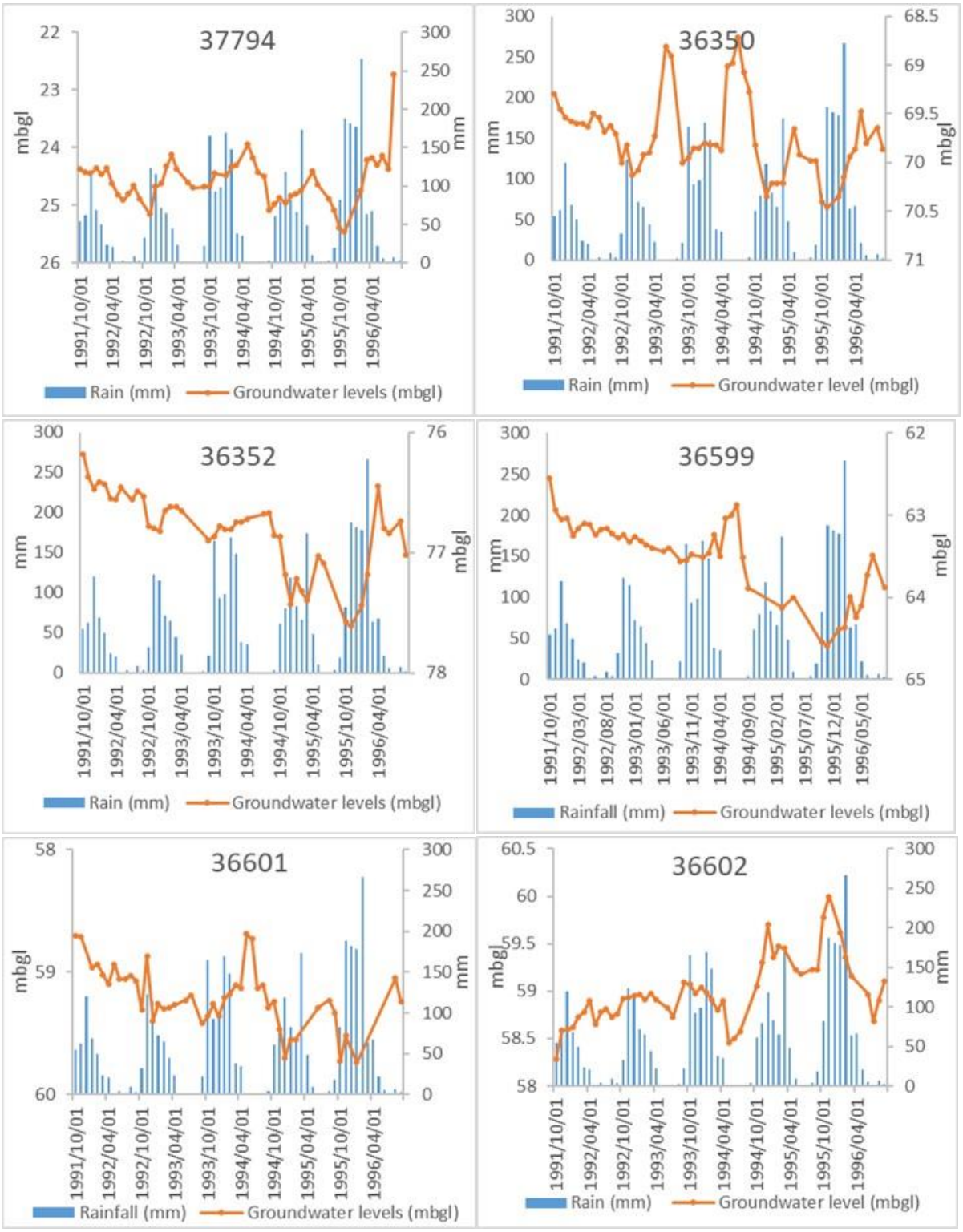
37794
mbgl
mm
Rain (mm)
Groundwater levels (mbgl)
36350
mm
mbgl
Rain (mm)
Groundwater level (mbgl)
36352
mm
mbgl
Rain (mm)
Groundwater levels (mbgl)
36599
mm
mbgl
Rainfall (mm)
Groundwater levels (mbgl)
36601
mbgl
mm
Rainfall (mm)
Groundwater levels (mbgl)
36602
mbgl
mm
Rain (mm)
Groundwater level (mbgl)

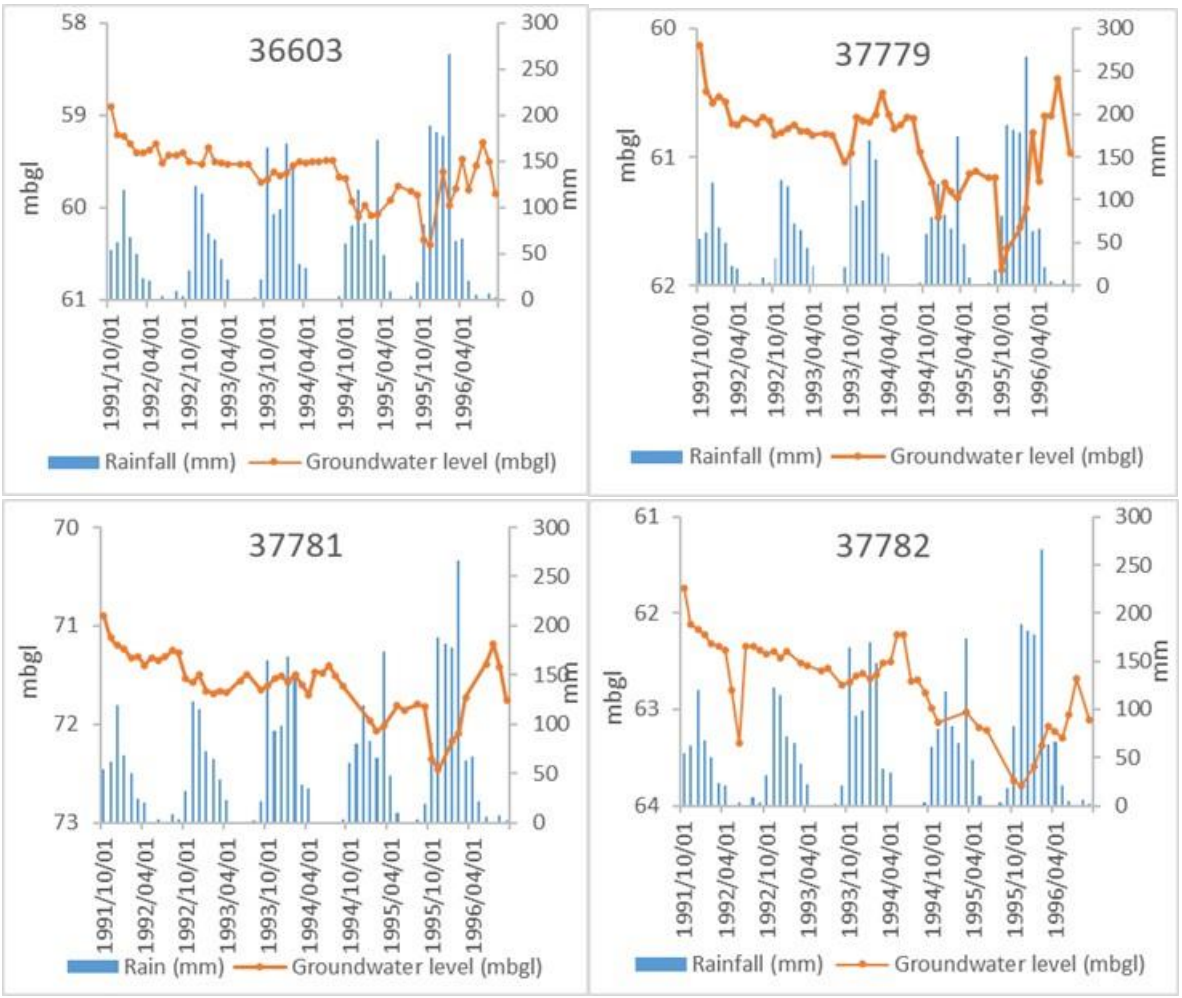

C. Publications

C.1. Publication 1-Journal of Groundwater for Sustainable Development

Leketa, K., Abiye T., Zondi, S. & Butler M. 2019. Assessing groundwater recharge in crystalline and karstic aquifers of the Upper Crocodile River Basin, Johannesburg, South Africa. Groundwater for Sustainable Development. 31-40. https://doi.org/10.1016/j.gsd.2018.08.002

Correction Note: On Table 5, the column "Annual recharge" is supposed to be in units of Million cubic meters (Mm^3) not cubic meters (m^3) as mistakenly written.

Groundwater for Sustainable Development 8 (2019) 31–40

Contents lists available at ScienceDirect

Groundwater for Sustainable Development

journal homepage: www.elsevier.com/locate/gsd

Research paper

Assessing groundwater recharge in crystalline and karstic aquifers of the Upper Crocodile River Basin, Johannesburg, South Africa

Khahliso Leketa[a,*], Tamiru Abiye[a], Silindile Zondi[a], Michael Butler[b]

[a] School of Geosciences, University of the Witwatersrand, Private Bag X3, P.O Box Wits 2050, Johannesburg, South Africa
[b] iThemba Labs, Private Bag 11, Wits 2050, Johannesburg, Gauteng, South Africa

ARTICLE INFO

Keywords:
Groundwater recharge
Stable isotopes of ^{18}O, ^{2}H and ^{13}C
Open carbon evolution
Closed carbon evolution
Johannesburg

ABSTRACT

Groundwater recharge and flow conditions were assessed in the Upper Crocodile River Basin, Johannesburg South Africa. This study revealed high elevation recharge from rainfall that is depleted in stable isotopes of water molecule ($\delta^{18}O$ and $\delta^{2}H$) occurring prior to extreme evaporation. The effective recharge occurs from rainfall of varying moisture source and humidity conditions. The $\delta^{13}C$ (‰) value in groundwater indicates both open and closed system carbon evolution. Open system was observed in shale, andesite and granitic gneiss aquifers indicating that soil CO_2 is a dominant source of carbon in bicarbonate. Enriched $\delta^{13}C$ observed in Malmani dolomite aquifers deduced the presence of carbonate dissolution, which indicates a closed system carbon evolution. Mixing of water from open and closed systems, or evolution from closed to open system is also observed in groundwater samples that had intermediate $\delta^{13}C$ (‰) values, particularly groundwater samples that are positioned at the periphery of the Basement Complex granitic gneiss near the Malmani dolomite aquifers. The integrated mean annual recharge estimates obtained from BFS for the UCRB is 6.7% while the distributed point recharge estimates in the Malmani dolomite obtained from application of WTF on 43 individual boreholes ranged between 2.5% and 39% with an average of 15% as a percentage of MAP. A comparison between estimated recharge and groundwater abstractions conducted for each sub-catchment revealed that there is an excess of groundwater recharge over groundwater use in most sub-catchments. The CMB point recharge estimates obtained from the Albert Farm spring and the Malmani dolomite springs are 2.5% and 27.8% of MAP, respectively. The low CMB recharge estimates in the shale and quartzite has been attributed to possible anthropogenic chloride sources such as leakage of chlorinated potable water in the pipelines of the city of Johannesburg, which elevate chloride concentrations in groundwater.

1. Introduction

In a region dominated by the semi-arid/arid climate, groundwater is usually the driving force behind economic development and the main source of water supply as the local surface water bodies are usually ephemeral (Scanlon et al., 2006; Manghi et al., 2009; Healy, 2010; Rivard et al., 2014; Abiye, 2016). The progressively changing climate setting, characterised by low rainfall and high temperatures leads to reduced terrestrial moisture (Engelbrecht et al., 2015; Assaf, 2017). This condition has invoked more groundwater dependence in South Africa, which already has 60–90% groundwater dependence (Braune and Xu, 2008).

The city of Johannesburg, which is the economic hub of South Africa, is supported by inter-basin surface water supply due to its water scarce nature (Department of water affairs and forestry, S.A., 2008). However, groundwater also plays a role in the socioeconomic development of the Johannesburg area, which is characterised as a semiarid climate (Abiye et al., 2018). The highly intensive farming, industrial and rural domestic activities in the area tend to rely more on groundwater abstractions from aquifers made of weathered and fractured crystalline rocks (basement granites and meta-sedimentary rocks) of low productivity, and the high yielding karstified meta-dolomites (Barnard, 2000). For groundwater to remain available as a sustainable source of water for economic development, there has to be a significant recharge to groundwater (Maliva and Missimer, 2012). In an event that the utilization of groundwater exceeds the recharge amount, the available groundwater resources may be depleted and therefore, fail to act as a source of water. This means that, during assessment of groundwater recharge in an aquifer that contributes to socioeconomic development, a balance must be established between the estimated

* Corresponding author.
E-mail address: 1436509@students.wits.ac.za (K. Leketa).

https://doi.org/10.1016/j.gsd.2018.08.002
Received 19 January 2018; Received in revised form 3 July 2018; Accepted 14 August 2018
Available online 24 August 2018
2352-801X/ © 2018 Published by Elsevier B.V.

groundwater recharge and groundwater usage in the aquifer, in order to establish the sustainability of the water source.

There are, however, several factors that contribute to recharge process and subsequent flow of groundwater to a designated aquifer from which abstraction is done. Therefore, equally important to the estimation of groundwater recharge in an area, is the attempt to further understand the recharge mechanism, groundwater fate and flow dynamics. It has been reported that streams in the West Rand region and shallow groundwater in the Malmani dolomite aquifer have been polluted by Acid Mine drainage from the abandoned Gold mines (Department of water affairs and forestry, S.A, 2008; Abiye et al., 2015). Also, the surface water courses that drain the city of Johannesburg are reported to be polluted due to constant discharge of partly treated waste water from the city. Since surface water resources are sources of focused recharge (Scanlon et al., 2002), polluted surface water resources may also be affecting groundwater quality. So, over and above the mere assessment of recharge estimates, it is important to understand where recharge occurs? How does it occur? And what are the dynamics and conditions that govern its flow path from the recharge area to the designated aquifer? This therefore calls for a need to assess recharge and groundwater flow dynamics in the Johannesburg area, which is located in the Upper Crocodile River Basin (UCRB), South Africa.

Due to their conservative nature, stable isotopes of water molecules ($\delta^{18}O$, $\delta^{2}H$) are suitable for understanding the recharge processes and predominant sources (Clark and Fritz, 1997). Moreover, stable isotopes have been confirmed useful in the assessment of water resources in South(ern) Africa as documented in Abiye (2013a). Specifically, Abiye (2013b) successfully assessed the groundwater and surface water interaction dynamics in the Upper Crocodile River Basin using stable isotopes. Stable isotopes of water molecule have also been successfully used in various other studies to assess groundwater recharge (Nkotagu, 1996; Abiye, 2011; Abiye et al., 2011; Ayadi et al., 2018). The stable carbon isotopes ($\delta^{13}C$) are also suitable for assessing groundwater flow path because various carbon sources (i.e. biomass, soil carbon dioxide and carbonate rocks) have distinct $\delta^{13}C$ signatures (Clark and Fritz, 1997; Marfia et al., 2004; Appelo and Postma, 2005). The $\delta^{13}C$ in groundwater, therefore, resembles the $\delta^{13}C$ signature of the dissolved carbon source and fractionations among the carbonate species in the solution (Appelo and Postma, 2005). This makes the use of $\delta^{13}C$ in groundwater suitable for tracing groundwater flow path despite the complex recharge processes and groundwater flow patterns. It has also been applied in various studies for the similar purpose of groundwater flow conditions (Marfia et al., 2004). Applications of the conventional chloride mass balance (CMB), groundwater and surface water hydrograph methods for groundwater recharge estimations, have also been proven useful in Southern Africa (Xu and Beekman, 2003).

In this study, groundwater recharge and flow dynamics are assessed in the Upper Crocodile River Basin, which is mainly underlain by the crystalline aquifers of the Basement Complex, meta-sedimentary aquifers of the Witwatersrand Supergroup and the karst aquifers of the Malmani dolomite. Chloride Mass Balance method, Water Table Fluctuation and Baseflow Separation Methods are applied to estimate recharge, while the environmental tracer methods are applied to understand the recharge process and the fate of groundwater in the UCRB aquifers.

2. Description of study area

The UCRB has a surface area of 4107 km^2 and extends with a northward general slope to Hartbeespoort Dam at about 85 km from the city of Johannesburg, which is located at the southern end of the catchment (Fig. 1). It is characterised by a semiarid climate with highly variable rainfall with a mean annual precipitation (MAP) of about 700 mm/year (Abiye, 2011). The available surface water resources in the catchment are mainly polluted due to disposal of partly treated waste water and industrial discharge into the surface water system, which renders surface water unsuitable for most uses. This is mostly observed in Hartbeespoort Dam which is a depository of all return flows from Johannesburg (Fig. 1) (Dower, 2003; Department of Water Affairs and Forestry, S.A, 2008). The UCRB catchment is made up of eight subcatchments; A21A to A21H that are identified as water management areas in South Africa (Fig. 1).

The geology of the Upper Crocodile River Basin is predominantly defined by the three major stratigraphic units which are; the Basement Complex, the Witwatersrand Supergroup and the Transvaal Supergroup rocks with a younging direction towards the north (Barnard, 2000; Johnson et al., 2006). Basement Complex is represented predominantly by the weathered and fractured Archaean Halfway House granitic bodies of similar age that differ slightly in their composition (granitic, granodioritic, gneissose or migmatitic) (Barnard, 2000). The Basement Complex is overlain by the Witwatersrand Supergroup, which is represented by the Government, Hospital Hill and Central Rand, which are mainly made of quartzite and shale forming the southern boundary of the UCRB (Fig. 1). The quartzite is vividly highly weathered and fractured having low yielding springs such as the Albert Farm spring (Fig. 1) emerging at the base of Government quartzites and acting as sources of small streams in the catchment. The northern part of the study area is covered by the Transvaal Supergroup, that includes the Black Reef and Malmani Formations of the Chuniespoort Group, which are represented by quartzite and dolomites. Overlying the Chuniespoort group is the Pretoria Group, which is represented by the following formations shown in Fig. 1; Timeball Hill, Hekpoort, Strubenkop, Daspoort, Silverton and Magaliesberg Formations. These formations are made of shale alternating with quartzites, interbedded basaltic-andesitic lava and subordinate conglomerate, which have all undergone low-grade metamorphism (Eriksson and Clendenin, 1990; Johnson et al., 2006).

The UCRB is characterised by four types of aquifers, which are, *Intergranular aquifers* made of unconsolidated alluvial sands and gravel, *Fractured crystalline aquifers* associated with fractures, fissures and joints of the granitic gneiss and quartzites, *Karstic aquifers* in the dolomites, and *Intergranular and fractured aquifers* that consist of a combination of hydraulically connected intergranular aquifers at the top and fractured aquifers at the bottom (Barnard, 2000; Abiye, 2011; Abiye et al., 2011, 2015). The aquifers are classified as hard rock aquifers with a modest groundwater productivity, whereas meta-dolomites with dissolution cavities yield large quantities of groundwater (Witthüser and Holland, 2008; Abiye et al., 2011). The abundant fractures and cavities in the meta-dolomites could act as good recharge zones, which eventually generate high yielding springs that are associated with dykes and tectonic depressions (Abiye et al., 2015). The high yields of about 30 l/s and 140 l/s for Nash Farm and Nouklip springs from the Malmani dolomite have been reported by Hobbs (2011).

The Malmani dolomite outcrop cuts across the UCRB in the east-west direction (Fig. 1), and can, therefore, easily allow groundwater movement across the water divide into the neighbouring catchments through the dissolution cavities and tectonic lineaments (Abiye et al., 2011). The intensively fractured quartzite outcrops of the Witwatersrand Supergroup that form the southern boundary of the UCRB may also provide a suitable media for vertical recharge on the catchment boundary (Abiye et al., 2011).

Groundwater recharge in the Johannesburg area was assessed and reported as 27.1% by Abiye (2016) through baseflow separation method (BFS). Abiye (2016) strongly expressed the need for deduction of waste water volumes from the estimated baseflow in order to come to a reliable recharge estimate.

3. Materials and methods

The mechanisms through which recharge predominantly occurs

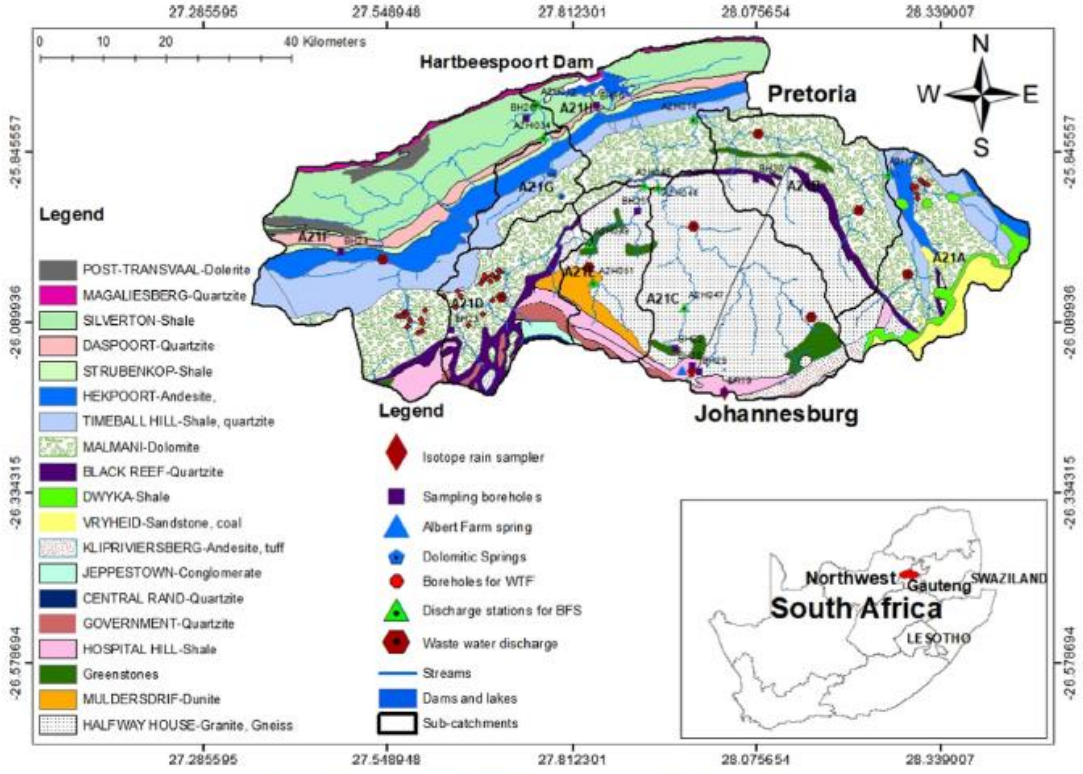

Fig. 1. Combo map of the UCRB and its location in RSA map as insert.

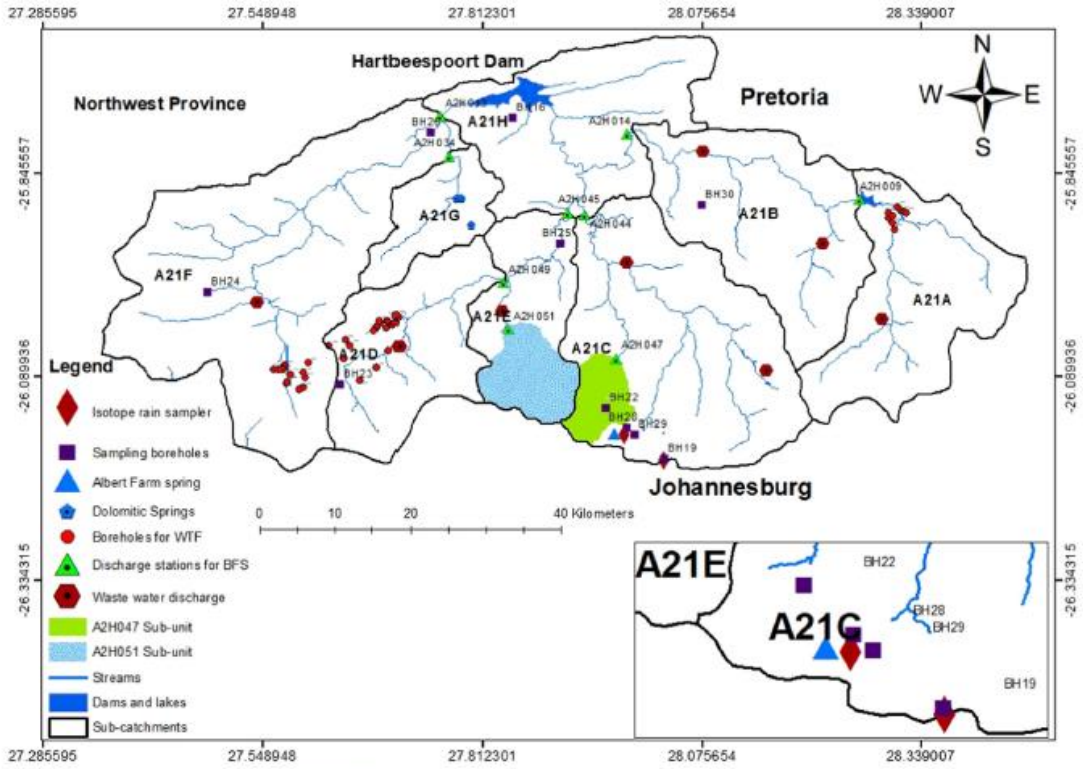

Fig. 2. Location where the recharge methods were applied.

Table 1
Specific yield values and their depths (where mbgl is meters below ground level).

Depth range (mbgl)	Specific yield (%)
Static water level to 61	9.1
62–76	5.5
77–107	2.6
108–126	2
127–146	1.3

were assessed using stable isotopes of water molecule ($\delta^{18}O$, $\delta^{2}H$), while the subsequent groundwater flow path dynamics were further investigated using stable carbon isotopes ($\delta^{13}C$). Chloride mass balance was applied at the Albert Farm spring and Malmani Dolomite springs to estimate recharge in the quartzite aquifer. Using Water Table Fluctuation method, groundwater recharge was estimated in the Malmani dolomite aquifer across the UCRB, while Baseflow Separation method was applied in the seven sub-catchments to estimate annual baseflow as a proxy for groundwater recharge. The CMB and WTF represented the point recharge estimates into the specific aquifer types, while the BFS gave an integrated recharge estimate, which is spatially distributed to the sub-catchments (Healy, 2010). Fig. 2 shows the locations of boreholes, spring sampling points and surface water discharge stations where the recharge methods were applied.

3.1. Environmental stable isotopes ($\delta^{18}O$, $\delta^{2}H$ and $\delta^{13}C$)

The Johannesburg Local Meteoric Water Line (JLMWL) of $\delta^{2}H = 6.7\delta^{18}O + 10‰$ was constructed from rainfall events that were sampled for three years at two stations: one at the University of the Witwatersrand and another at Montgomery Park in Johannesburg, South Africa (Fig. 2). The samples were collected with a 10 ml glass bottle immediately after rainfall to avoid sample evaporation. Samples were also collected for environmental isotope analysis from four Malmani dolomite springs, and twelve privately owned boreholes across the UCRB between February and April 2017, while the Albert Farm spring in Johannesburg, was sampled for stable isotope analysis on monthly basis from June 2016 to May 2017.

Stable isotopes of ^{18}O and ^{2}H were analysed at the University of the Witwatersrand, South Africa using the Liquid Water Isotope Analyser-model 45-EP. The precision for the machine is approximately 1‰ for $\delta^{2}H$ and 0.2‰ for $\delta^{18}O$ in liquid water samples of up to 1000 mg/L dissolved salt concentration. The analysis was done against five standards of different known isotopic signatures. A plot of groundwater samples versus the JLMWL was then used to understand the source and mechanism of recharge. The deuterium excess (d-excess) in groundwater samples was computed from the JLMWL and then used to infer the moisture source and humidity properties of the recharge rainfall (Clark and Fritz, 1997; Froehlich et al., 2002) using a plot of $\delta^{18}O$ versus d-excess.

Groundwater samples were collected from twelve boreholes, two dolomitic springs and Albert Farm spring for stable carbon isotopes ($\delta^{13}C$) analysis in April 2017. Albert Farm spring was also sampled in January 2018. The field sampling procedure involved filling the 30 l drum with sample water, followed by addition of carbonate free NaOH to raise the pH to alkaline and addition of a dash of phenolphthalein as a pH indicator. $BaCl_2$ was then added, from which Ba^{2+} would react with the CO_3^{2-} in solution to precipitate barium carbonate ($BaCO_3$). The $BaCO_3$ precipitate was then separated from the supernatant and stored in 500 ml bottles for laboratory analysis. The analysis was done using a Hewlett Packard TriCarb liquid scintillation spectrometer at iThemba Laboratories in Johannesburg, South Africa.

3.2. Chloride mass balance

Chloride samples were collected from rainfall events and Albert Farm spring and four Malmani dolomite springs in a 10 ml glass bottle. The chloride analysis was done at the University of the Witwatersrand using a colorimetric method with an analyser that has a 0.5 mg/l detection limit.

3.3. Water table fluctuation

Groundwater recharge was estimated from 43 boreholes that tap the Malmani dolomite aquifer, which are in the sub-catchments; A21A, A21D and A21F (Fig. 2). The data represented monthly water level time series for the period between 1993 and 1996 obtained from the National groundwater database. Eq. (1) was then used to estimate recharge from the water level change with time and specific yield that represents the Water Table fluctuation method (Rasmussen and Andreasen, 1959; Healy and Cook, 2002). The specific yield values were obtained from Eslin and Kriel (1968) who carried out a water balance study for the karst aquifer that was being dewatered for mining purposes in the Far West Rand, Johannesburg South Africa. From this study, it was observed that the specific yield values decreased with increasing depth from 9.1% to 1.3% as shown on Table 1.

$$R = \Delta h/\Delta t * Sy \quad (1)$$

where, Sy, is specific yield and Δh is change in water level (*in mm*) and Δt is the fluctuation period

A specific yield value was then used in Eq. (1) for each of the 43 UCRB boreholes depending on their range of water level fluctuation depth.

3.4. Baseflow separation

Baseflow separation (BFS) method was applied in the seven sub-catchments (A21A to A21G) to understand the spatial variability of recharge within the UCRB. The river discharge data was obtained from the Department of Water and Sanitation (DWS) while climate data were gathered from the South African Weather Services and DWS. The A21H sub-catchment was omitted because of Hartbeespoort Dam controlled exit flows (Fig. 2), which could result in erroneous estimations of baseflow. Stream discharge from the upstream sub-catchments were also deducted so that a computation can be done using only the stream flow components (runoff and baseflow) generated within the specific sub-catchment of interest. The BFS results obtained from the sub-catchments, gave recharge estimates that are integrated over a larger space. The less integrated estimates were also obtained from the smaller sub-units of the sub-catchments at the upstream of the discharge stations and waste water disposal locations as shown on Fig. 2. Wastewater discharged into the stream was subtracted from the estimated baseflow. The waste-water discharge data were obtained from the Johannesburg Water Authority and DWS.

Computation of recharge was then conducted by dividing baseflow (m^3/yr.) with the area of the sub-catchment (m^2) to obtain recharge (m/yr., usually mm/yr.). The annual rainfall (mm/yr.) for the corresponding years was used to compute recharge as a percentage of rainfall. For the benefit of water use planning purposes in the catchment, a percentage of groundwater use to recharge estimate was also determined to assess the sustainability of groundwater resource. Groundwater use data was obtained as licensed volumes from DWS.

According to Healy (2010), baseflow estimate is given as a proxy for recharge based on the following assumptions; 1) all groundwater that recharges in the catchment, ultimately discharges to a stream, 2) stream flow at dry low flows constitutes groundwater discharge. 3) Computation of recharge with baseflow (m^3/yr.) as a fraction of catchment area (m^2) to yield recharge (m/yr.), is done with the assumption that the

area of the aquifer that contributes to groundwater recharge is identical to the surface drainage area (Rutledge, 1998). Misrepresentation of the aquifer properties in light of the above assumptions, leads to erroneous recharge estimates.

In this study, BFS was applied using an excel based program called Timeplot, which is based on the single parameter digital filter method (Nathan and Mcmahon, 1990). Baseflow calculation using the single-parameter digital filter is done as follows;

$$b_k = \alpha b_{k-1} + \frac{1-\alpha}{2}(y_k + y_{k-1}) \quad (2)$$

Where b_k and b_{k-1} are baseflow at time steps *k* and *k-1*, respectively. α is a dimensionless filter parameter. y_k and $y_{k-1)}$ are total streamflow at the time steps *k* and *k-1*, respectively. Eq. (2) is applied on condition that $b_k \leq y_k$.

The single parameter digital filter method uses a filter parameter represented in Eq. (2) as "α" to separate the high frequency flows associated with surface runoff from the low frequency flows associated with baseflow. The value used for filter parameter in this study is 0.995 as confirmed suitable for South African baseflow by Smakhtin and Watkins (1997).

Abiye (2016) applied BFS in the UCRB and observed that the values obtained were over-estimated due to sewage return flows discharged into the streams, and therefore recommended its deduction for accurate results. In this study, the authors deducted waste water from the measured computed baseflow.

4. Results and discussions

4.1. Environmental stable isotopes ($\delta^{18}O$ and $\delta^{2}H$)

Table 1 presents stable isotope results for groundwater sampled from different boreholes and dolomitic springs in April 2017. The table also shows monthly stable isotope data for Albert Farm spring monitored over 12 months. The d-excess computed from the JLMWL for each sample is also shown. Albert Farm isotope monthly time series ranges from −6.01‰ to −2.86‰ for $\delta^{18}O$ and from −21.6‰ to −12.3‰ for $\delta^{2}H$ with d-excess ranging from 4.7‰ to 18.7‰ for the review period. A variable isotopic signature is observed from the UCRB groundwater samples (Table 2). The most depleted samples are represented by the Malmani dolomite springs and borehole BH16, while the most enriched sample is borehole BH19, which is underlain by the quartzite and shale of the Hospital Hill shale and Government quartzite (Barnard, 2000) as shown on Fig. 1.

Fig. 3 shows the stable isotope plot of the groundwater samples with respect to the Johannesburg Local Meteoric Water Line (JLMWL), Pretoria Local Meteoric Water Line (PLMWL) and the Global Meteoric Water Line (GMWL). The dolomitic springs and borehole BH16 are extremely depleted and positioned at the lower left portion of the plot. Borehole BH19 is the most enriched and positioned at the top right portion of the plot. Borehole BH19 is located at the elevated southern boundary of the UCRB while borehole BH16 which is at the low elevation near the Hartbeespoort Dam (Fig. 1) shows a high depletion. Fig. 3 also shows the monthly samples for Albert Farm spring to display the variable isotope signature over an annual cycle. Fig. 4 shows $\delta^{18}O$ plotted against d-excess of groundwater to assess the role of moisture source and humidity conditions during condensation of precipitation.

The position of groundwater samples along the JLMWL (Fig. 4) shows recharge that occurred rapidly prior to extreme evaporation. The fractured nature of rocks in the UCRB (Fig. 5) could be the one responsible for the rapid recharge from rainfall. This confirms what was said by Abiye et al. (2011) that, the intensively fractured quartzite outcrops of the Witwatersrand Supergroup provide a suitable condition for vertical recharge from precipitation on the catchment boundary. Based on the depleted nature of groundwater samples on Fig. 3, possibilities of focused recharge from surface water resources are not observed.

The monthly data for stable isotope signature of Albert Farm spring shows a variable behaviour that tends to maintain a regression line close to the JLMWL as shown on Fig. 3. Since stable isotopes reveal recharge occurring prior to extreme evaporation into the aquifer that feeds the Albert Farm spring, then the varying d-excess observed in Fig. 5, could indicate recharge that occurred as a result of rainfall events of different moisture source and condensation conditions (temperature or humidity), all of which are potentially due to varying seasonal or climatic setting. Naturally, stable isotope signatures in precipitation vary based on the moisture source, condensation temperature, humidity etc., so the same varying signature is reflected in monthly Albert Farm spring samples. Recharge into this aquifer is deduced to occurs preferentially through the fractures followed by piston groundwater flow of different recharge events.

A depletion and position along the JLMWL that is observed in dolomitic springs, could be a result of rapid recharge through the fractures and cavities. This possibly occurs via rapid infiltration of rainfall into groundwater, thereby avoiding exposure to extreme evaporation, hence close isotopic similarity with rainfall. The depletion shows the possibility of recharge at higher altitude from rainfall that is depleted in heavy isotopes due to altitude effect or colder climate. This suggests that recharge into the Malmani dolomites might be occurring elsewhere at higher altitude and flowing through the dissolution cavities to discharge at the springs. This could agree well with what was stated by Abiye et al. (2011) that, groundwater in dolomitic aquifers can easily flow across the water divides through the dissolution cavities. The depleted nature could also indicate groundwater that recharged from a rainfall event with low humidity in the vapour during condensation, or recharge from cold temperature rainfall or heavy rainfall. On a d-excess plot, the dolomitic springs are positioned towards the low d-excess relative to other groundwater samples. This condition indicates regional circulation from relatively high humidity moisture and their relative proximity to one another indicates that they are recharge from a similar recharge episode.

The stable isotope time series of Albert Farm spring represents a single sample location but shows temporal variability, which almost covers the entire range of other groundwater samples on a $\delta^{18}O$ and $\delta^{2}H$ plot (Fig. 3). Having established that recharge in the UCRB occurs prior to extreme evaporation (recharge water was not isotopically altered during recharge), then groundwater resembles the isotopic signature of effective rainfall, which is also variable due to moisture source and climatic settings. The different isotopic signatures observed in groundwater samples could be a reflection of different recharge episodes rather than a spatial distribution of recharge mechanisms. Recharge rates and groundwater flow velocities vary in different lithologies, therefore even though all other groundwater samples were collected at more or less the same period (February to April 2017), they most likely represented different recharge episodes of different isotopic signature. This may also explain why borehole BH16 (1220mamsl) at the low elevation is more depleted than borehole BH19 (1728mamsl) at the high elevation.

4.2. Stable carbon isotope ($\delta^{13}C$)

Table 3 shows the stable carbon ($\delta^{13}C$) data for groundwater samples. The table also presents the lithostratigraphy of the underlying aquifer for each borehole. The $\delta^{13}C$ values range from the most depleted borehole BH16 with −17.35‰, which is underlain by Silverton shale and Daspoort andesite of the Pretoria Group. On the other hand, the most enriched sample is the Nash Farm Spring (SP2), which is hosted in the Malmani dolomite aquifer with −5.64‰. Generally, all

Table 2
Stable isotopes in groundwater sampled from boreholes, Malmani Dolomite springs, and Albert Farm spring.

Sample ID	Lithology	Latitude	Longitude	Elevation (mamsl)	δ^2H (‰)	^2H StDev (±)	$\delta^{18}O$ (‰)	^{18}O StDev (±)	d-excess (‰)
BH16	Shale/andesite	− 25.7792	27.8474	1220	− 29.1	0.4	− 5.73	0.1	9.36
BH19	Quartzite	− 26.1884	28.0293	1728	− 12.3	0.3	− 2.23	0.1	2.66
BH22	Greenstone	− 26.1274	27.9591	1556	− 15.8	0.7	− 3.55	0.1	7.95
BH23	Dolomite	− 26.0997	27.6419	1594	− 12.5	3.5	− 2.62	0.3	5.09
BH24	Shale/andesite	− 25.9883	27.4824	1481	− 22.5	0.5	− 5.08	0.4	11.55
BH25	Granite/gneiss	− 25.9307	27.9053	1291	− 21.6	0.4	− 4.32	0.1	7.33
BH26	Shale	− 25.7971	27.7488	1198	− 16.7	0.3	− 3.27	0.1	5.18
BH28	Quartzite	− 26.1519	27.9840	1636	− 17.3	1.0	− 3.83	0.1	8.39
BH29	Granite/Gneiss	− 26.1599	27.9938	1640	− 18.2	1.5	− 3.83	0.2	7.51
BH30	Granite/gneiss	− 25.8843	28.0749	1482	− 25.3	0.4	− 5.15	0.0	9.16
SP1-Nash Farm	Dolomite	− 25.9081	27.7976	1460	− 27.6	0.4	− 4.97	0.1	5.70
SP2-Nouklip	Dolomite	− 25.8752	27.7858	1345	− 27.5	0.5	− 5.11	0.1	6.74
SP3	Dolomite	− 25.8749	27.7837	1324	− 29.6	0.4	− 5.28	0.1	5.75
SP4	Dolomite	− 25.8752	27.7800	1304	− 27.8	0.4	− 4.77	0.1	4.17
Average		− 26.1616	27.9703		**− 20.5**		**− 4.14**		**7.22**
Maximum					**− 12.3**		**− 2.23**		**11.55**
Minimum					**− 29.1**		**− 5.73**		**2.66**
Albert Farm spring data									
Sample ID		Latitude	Longitude	Elevation (mamsl)	δ^2H (‰)	^2H StDev (±)	$\delta^{18}O$(‰)	^{18}O StDev (±)	d-excess (‰)
06 Jun 2016	Quartzite	− 26.1616	27.9703	1655	− 19.29	0.23	− 5.27	0.1	16.0
06 Jul 2016	Quartzite	− 26.1616	27.9703	1655	− 21.6	0.28	− 6.01	0.09	18.7
06 Aug 2016	Quartzite	− 26.1616	27.9703	1655	− 19.08	0.14	− 4.3	0.05	9.7
06 Sept 2016	Quartzite	− 26.1616	27.9703	1655	− 14.5	0	− 2.86	0	4.7
06 Oct 2016	Quartzite	− 26.1616	27.9703	1655	− 13.71	1.28	− 3.79	0.13	11.7
06 Nov 2016	Quartzite	− 26.1616	27.9703	1655	− 15.97	0.28	− 3.78	0.12	9.4
06 Dec 2016	Quartzite	− 26.1616	27.9703	1655	− 14.3	0.06	− 3.57	0.10	9.6
06 Jan 2017	Quartzite	− 26.1616	27.9703	1655	− 12.5	0.53	− 3.09	0.03	8.3
02-Feb − 2017	Quartzite	− 26.1616	27.9703	1655	− 15.0	0.8	− 3.43	0.0	8.0
06-Mar − 2017	Quartzite	− 26.1616	27.9703	1655	− 16.4	0.6	− 3.67	0.1	8.2
06-Apr − 2017	Quartzite	− 26.1616	27.9703	1655	− 15.2	0.7	− 4.13	0.2	12.4
06-May − 2017	Quartzite	− 26.1616	27.9703	1655	− 12.3	0.5	− 3.11	0.1	8.6
Average					**− 15.8**		**− 3.92**		**10.4**
Maximum					**− 12.3**		**− 2.86**		**18.7**
Minimum					**− 21.6**		**− 6.01**		**4.7**

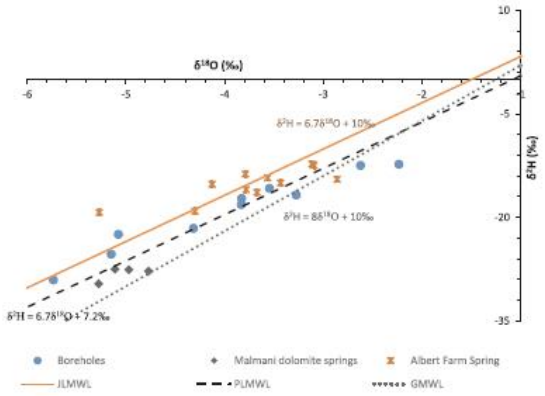

Fig. 3. Stable isotopes in groundwater versus Johannesburg Local Meteoric Water Line, Pretoria LMWL ($\delta^2H = 6.78\delta^{18}O + 7.2‰$ GNIP-IAEA) and Global MWL ($\delta^2H = 8\delta^{18}O + 10‰$ (Craig, 1961).

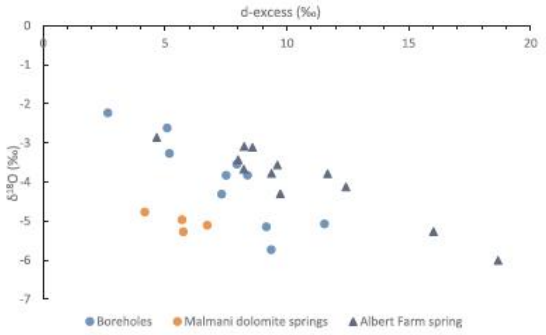

Fig. 4. Plot of d-excess versus $\delta^{18}O$ for groundwater samples in the UCRB.

the Malmani dolomite samples are represented by enriched values i.e. borehole BH23, Nash farm Spring and Nouklip Spring. All other lithostratigraphic units seem to show intermediate values with various magnitudes of depletion and enrichment.

Despite the intensive agricultural activities in the UCRB, the majority of land is uncultivated and consists of grasses and shrub vegetation cover. This type of vegetation predominantly follows C3 photosynthesis (Clark and Fritz, 1997; Kohn, 2010). The DIC evolution in groundwater of the UCRB is, therefore, assumed to be influenced by CO_2 from C3 vegetation, which has an average $\delta^{13}C$ value of − 26‰ as reported by Marfia et al. (2004) and Kohn (2010).



Fig. 5. The typical vertical fractures observed in the Witwatersrand quartzites that help in rainfall infiltration in Johannesburg, South Africa.

Table 3
Stable carbon isotope data and representative lithostratigraphy.

BH No	Stratigraphy	Lithology	$\delta^{13}C$ (‰)	Sampling Date
BH16	Silverton/Daspoort	Shale/andesite	− 17.35	April 2017
BH19	Government/Hospital Hill	Quartzite/Shale	− 15.22	April 2017
BH22	Basement Complex	Greenstones	− 13.25	April 2017
BH23	Malmani	Dolomite	− 8.41	April 2017
BH24	Hekpoort/Strubenkop	Shale/andesite	− 15.38	April 2017
BH25	Basement Complex	Granite/gneiss	− 15.30	April 2017
BH26	Silverton	Shale	− 15.07	April 2017
BH28	Government/Hospital Hill	Quartzite/Shale	− 12.96	April 2017
BH29	Basement Complex	Granite/Gneiss	− 12.26	April 2017
BH30	Basement Complex	Granite/gneiss	− 11.58	April 2017
Albert Farm	Government/Hospital Hill	Quartzite/Shale	− 14.81	January 2018
SP1-Nash farm Spring	Malmani	Dolomite	− 6.05	April 2017
SP2-Nouklip Spring	Malmani	Dolomite	− 5.64	April 2017

Table 4
Chloride concentrations and recharge estimates in Albert Farm and Malmani Dolomite springs.

Albert Farm spring		Rainfall		MAP	700 mm
Date	Cl (mg/l)	Date	Cl (mg/l)	Recharge (mm)	%
06 Jul 2017	20.7	06 Jul 2017	0.5 <	16.9	2.4
08 Aug 2017	20.1	22 Nov 2017	0.5 <	17.4	2.5
06 Sept 2017	17.8	–	–	19.7	2.8
06 Dec 17	20.6	–	–	17.0	2.4
28 Mar 18	22.7	–	–	15.4	2.2
Averages	**20.4**			**17.3**	2.5
Malmani dolomite spring					
SP1	2.4	April 2009		145.8	20.8
SP2	2.4	April 2009		145.8	20.8
SP3	1.4	April 2009		250.0	35.7
SP4	1	April 2009		350.0	50.0
Averages	**1.8**			**194.4**	**27.8**

In a fully open system, the $\delta^{13}C$ of dissolved inorganic carbon ($\delta^{13}C_{DIC}$) in groundwater is only controlled by the hydrolysis of soil CO_2 (Marfia et al., 2004). The CO_2 from C3 plants initiates carbon evolution with the value of approximately −26‰ of $\delta^{13}C$ (Marfia et al., 2004; Appelo and Postma, 2005). The hydrolysis process enriches $\delta^{13}C_{DIC}$ of infiltrating water with approximately 9‰ (Appelo and Postma, 2005), so that $\delta^{13}C$ in an open system with C3 vegetation landcover, would have an approximate value of −17‰ (Marfia et al., 2004). In a closed system, soil CO_2 and dissolution of carbonates equally control the $\delta^{13}C$ in groundwater, such that dissolution leads to more positive $\delta^{13}C$‰ values (Clark and Fritz, 1997). This is because, carbonate rocks are richer in heavy carbon isotopes with approximate values of 0‰ (Marfia et al., 2004; Appelo and Postma, 2005). The final $\delta^{13}C$‰ value of groundwater in a closed system, therefore, depends on the $\delta^{13}C$‰ value before closure of the system to soil CO_2 and the extent of carbonate dissolution. This usually leads to a value of approximately −13‰ in closed system (Marfia et al., 2004; Appelo and Postma, 2005). However, in a case that dissolution of dolomite occurs in the closed groundwater aquifer, more positive values of $\delta^{13}C$‰ are also observed (Marfia et al., 2004).

Therefore, the depleted groundwater samples such as; boreholes BH16, BH24 and BH26 from the Silverton shale and Daspoort andesite; BH25 from the granitic gneiss of the Basement Complex; borehole BH19 and Albert Farm spring from the government quartzite/Hospital Hill shale indicate open system condition deducing that the source of DIC is soil CO_2. The Malmani dolomite samples, which include borehole BH23, Nash Farm Spring and Nouklip Spring are the most enriched, possibly due to carbonate dissolution that occurs in the aquifer under closed system conditions (Marfia et al., 2004). The contribution of bicarbonate from dolomite, induces enriched $\delta^{13}C$ (‰) in groundwater within the Malmani dolomite aquifer. The deduced system agrees well with the expected behaviour of the dolomite aquifers. Bamard (2000) reported this about the hydrochemistry of the Malmani dolomite; as infiltrating rainwater containing weak carbonic acid (H_2CO_3) percolates through the dolomitic terrain along the planes of weakness such as faults, fractures and joints, it causes dissolution of dolomite and increases bicarbonate concentration in groundwater as shown by the following chemical reaction:

$$3CaCO_3.2MgCO_3 + 5H_2CO_3 \rightarrow 3Ca(HCO_3)_2 + 2Mg(HCO_3)_2$$

Dolomite + Carbonic acid → Calcium-bicarbonate + Magnesium-bicarbonate.

Groundwater samples that show intermediate values of $\delta^{13}C$‰ (−13.25‰ to −11.58‰) such as boreholes BH22, BH28, BH29 and BH30 suggest evolution from closed system condition to open system due to carbonate dissolution or mixing of open system water and water that has undergone closed system carbonate dissolution along its flow path, particularly borehole BH30, which is positioned at the periphery of the Basement Complex granitic gneiss near the Malmani dolomite aquifers.

Borehole BH16 and the Malmani dolomite springs both showed extreme depletion in stable isotopes of water molecule ($\delta^{18}O$ and $\delta^{2}H$), which indicated possibilities of recharge from the isotopically similar rainfall. However, a distinction that is observed in the stable carbon isotopes ($\delta^{13}C$‰) indicate the differences in groundwater flow conditions and aquifer media.

4.3. Chloride mass balance method

Table 4 below shows chloride concentrations in the Albert Farm spring sampled from July 2018 to March 2018. The table also shows Malmani dolomite springs sampled in April 2009 by Abiye et al. (2011). Chloride in Johannesburg rainfall sampled in July and November 2017 is also presented. The table also shows the computed recharge as a percentage of mean annual precipitation of 700 mm (Abiye, 2011) for the UCRB. The average recharge obtained in the Albert Farm is 2.5% while the Malmani dolomite springs gave 27.8%.

The presented chloride concentrations in rainfall consist of only two rainfall events from summer and winter season, which may not be representative of the long-term average chloride value in Johannesburg rainfall. The chloride concentrations in rainfall were below the detection limit of the colorimetric instrument (0.5 mg/l), therefore the computed recharge estimates for the quartzite aquifer may represent the maximum recharge values.

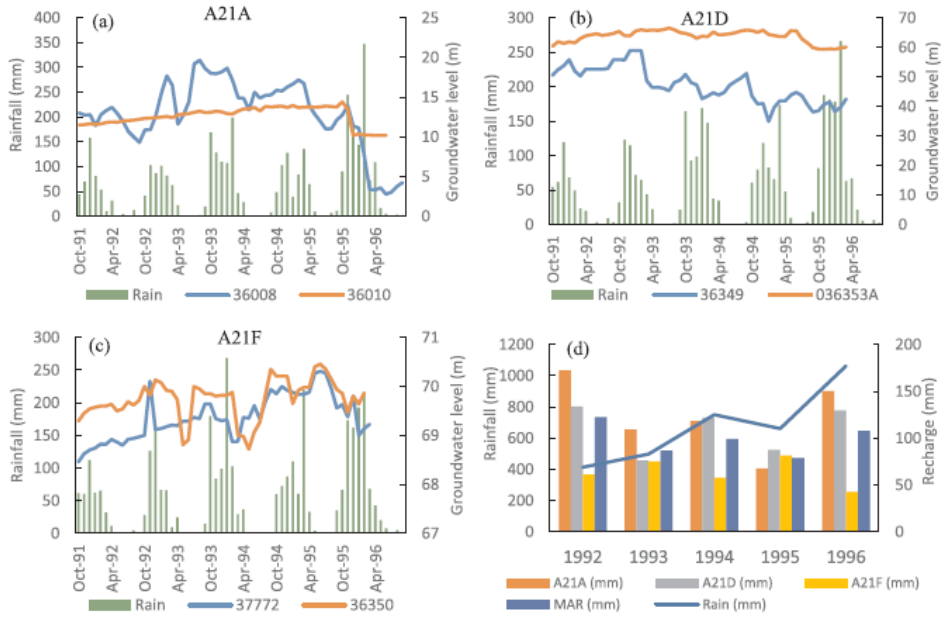

Fig. 6. Groundwater level fluctuations and groundwater recharge for selected boreholes within the sub-catchment A21A, A21D and A21F.

4.4. Water Table Fluctuation

Groundwater levels in different boreholes fluctuated at variable magnitude and timing of response to rainfall as shown on Fig. 6. The water level in boreholes 036353A, 36350 and 37772 showed the least fluctuations for the period with water level changes not exceeding 3 m. Boreholes 36008 and 36349 showed a significant fluctuation of maximum 20 m observed in borehole 36349. Each of the boreholes however, show that there is a response to rainfall which is a requirement for the application of water table fluctuation method (Healy and Cook, 2002). The varying nature of groundwater level response in different boreholes could suggest different recharge paths, which are attributed to the makeup of the recharge area rather than the depth of water table seeing that the borehole water levels are within the same depth ranges (Fig. 6(a) to (c)). Rapid responses could be attributed to recharge occurring through preferential flow possibly via sinkholes and fractures, while a more delayed increase could be attributed to a less permeable recharge area.

For the 43 boreholes considered for this study, where WTF was applied, the mean annual recharge (MAR) ranged between 2.5% (17.5 mm/yr.) and 39% (270 mm/yr.), with the average as 15% (104 mm/yr.) for the Malmani dolomite aquifer. Fig. 6(d) shows that there is a relationship between rainfall amount and recharge. Annual precipitation varies throughout the study period with a minimum of 413.5 mm in 1992 and a maximum of 1061.8 mm for the year 1996. The temporal and spatial variability of groundwater recharge are observed, in that, recharge amount increases with precipitation while it also varies spatially among the sub-catchments through the review period.

4.5. Baseflow separation

The recharge estimates obtained from Baseflow Separation method are shown on Table 5. Recharge is given as a fraction of mean annual precipitation (MAP) (column 7) and annual groundwater use as a fraction of recharge volume (column 10). Recharge estimates as a fraction of MAP range from 3.32% in A21C sub-catchment to 22.07% in A21G sub-catchment. A21G sub-catchment has the smallest surface area yet it has the highest recharge estimate compared to the other sub-catchments of the UCRB. A21A sub-catchment and A21G sub-catchment are underlain predominantly by similar geology (Malmani dolomites as shown by Fig. 1) despite the vast difference in recharge estimates i.e. 22.07% in A21G sub-catchment and 5.5% in A21A catchment. Table 5 also shows the average recharge estimates for the area as 6.67%, which is obtained as weighted fractions of sub-catchment areas to the total area.

A21G sub-catchment with 22% baseflow, hosts the high yielding dolomitic springs including the Nash Farm and Nouklip, which yield 30l/s and 140l/s, respectively (Hobbs, 2011). This could explain the observed high baseflow. Abiye et al. (2011) stated that the Transvaal dolomites allow movement of groundwater across the water divide through the dissolution cavities. The high yielding springs in the A21G sub-catchment could be a result of inter-basin movement of groundwater from the south west resulting to increased baseflow in A21G sub-catchment. A21A sub-catchment, which is underlain by dolomites is positioned on the head waters of the dolomitic aquifer's eastern limb and therefore no significant contribution of inter-basin groundwater movement is expected from the eastern catchments outside of the UCRB, hence, low baseflow in A21A catchment (5.48%), compared to A21G sub-catchment in the same lithology. Land cover is mostly impermeable in A21A sub-catchment due to urban development and therefore enhances more runoff than recharge. The reason for low base flow in A21A sub-catchment could also be that, A21A sub-catchment is a recharge point which undertakes deeper circulation to discharge in the A21B sub-catchment at lower elevation hence a higher baseflow of 8.5% in A21B sub-catchment. A21C sub-catchment, which hosts the city of Johannesburg is covered with impermeable surfaces leading to low recharge value of 3.32%. Low baseflow in A21C sub-catchment can also be attributed to its underlying geology which is crystalline hard granitic gneiss with low hydraulic properties. A21E sub-catchment, which is completely underlain by hard rocks such as quartzite, granitic gneiss and dunite has high recharge value of 14.9%. The more site-

Table 5
Recharge estimations obtained through Baseflow Separation method.

Catch.	Discharge station	Recharge (mm)	Area (km^2)	Subunits: Recharge (%)	MAP (mm)	Recharge (% MAP)	Groundwater usage (m^3)	Annual recharge (m^3)	% GW usage
A21A	A2H090	33.82	451	–	616.82	5.48	12,966,411	15.25	85.0
A21B	A2H014	57.44	527	–	616.82	8.50	33,662,463	30.27	111.2
A21C	A2H044	24.96	761	(A2H047) 7.2% on granites	655.20	3.32	1,414,253	18.99	7.4
A21D	A2H049	34.76	372	–	542.07	6.71	1,856,423	12.93	14.4
A21E	A2H045	99.81	282	(A2H051) 9.9% on granite and dunite	655.20	14.19	4,478,957	28.15	15.9
A21F	A2H013	24.07	1 001	–	542.07	4.23	3,780,223	24.09	15.7
A21G	A2H034	108.66	160	–	542.07	22.07	392,699	17.39	2.3
Weighted recharge average						**6.67**			

specific estimates determined from sub-units that are upstream of wastewater discharge stations, gave a lower estimate of 9.9% in a sub-unit within A21E sub-catchment. This is quite lower than the initial 14.9% from the entire A21E sub-catchment downstream of the sewage discharge stations. Similarly, 7.2% was obtained in the sub-unit within A21C sub-catchment where the initially 3.32% was obtained. Apart from the fact that the sub-units may be presenting recharge estimates at the sub-unit level, the different recharge estimates may also be a result of inaccurate values of the data on wastewater discharge leading to erroneous baseflow values.

In order to get estimates that are less integrated in space, baseflow was assessed in smaller sub-units upstream of the waste water discharge stations in A21C sub-catchment and A21E sub-catchment (Fig. 2). A21C sub-catchment, which had an estimate of 5.5%, now had 7.2% in its sub-unit. A21E sub-catchment had 14.9% recharge while the smaller sub-unit gave a recharge value of 9.9% over the same period. Compared to the BFS groundwater recharge value of 27.1%, where Abiye (2016) recommended deduction of waste water, a lower value of average of 6.7% is obtained in this study where wastewater volumes are deducted.

Groundwater use as a fraction of annual recharge ranges from 2.3% in A21G to 111.2% in A21B. The estimates reveal that, groundwater is underutilised in A21G, while A21B is over abstracted. The groundwater use volumes were however obtained from licensed groundwater abstraction volumes from the Department of Water and Sanitation of South Africa not actual abstracted volumes. The data may be excluding some unlicensed groundwater abstractions and therefore pose uncertainties in the estimated values.

The assumptions on which BFS is applied are not all satisfied in the UCRB. The assumption that the aquifer area is equal to catchment area may not apply in the A21G sub-catchment. The assumption that all low flows are baseflow, is partially valid since the wastewater volume has been deducted from stream discharge. The assumption that all recharge eventually discharges into a stream may not be valid, however, as an indication that the calculated baseflow only represents part of recharge, the estimated values can be referred to as minimum recharge as proposed by Pitman and Vegter (2003). Vegter (1995) compared recharge estimates from baseflow technique and other methods in various catchments in South Africa, and observed a 50% variance, which was highest in smaller baseflow streams, decreasing with increase in baseflow estimates.

5. Conclusions

This study revealed that recharge in the UCRB predominantly occurs from rainfall prior to extreme evaporation, possibly through the vertical fractures in the crystalline rocks and dissolution cavities of the Malmani dolomite rocks in the karstic aquifer. The stable isotope results indicated that, effective recharge into the Witwatersrand aquifers was derived from rainfall of different moisture source and humidity condition. In the Malmani dolomite aquifer, recharge occurs at high elevation where the rainfall is depleted due to altitude effect, prior to extreme evaporation, while its lack of variation in stable isotopes and d-excess suggests a similar recharge episode. The $\delta^{13}C‰$ value in groundwater indicates both open and closed system carbon evolution. Open system was observed mainly in shale and andesite of the Pretoria Group, some groundwater samples from the granitic gneiss aquifers of the Basement Complex and some Government quartzite and Hospital shale samples indicating that soil CO_2 is a dominant source of carbon. Enriched $\delta^{13}C$ observed in Malmani dolomite aquifers deduced the predominant source of dissolved carbon as carbonate dissolution, and therefore deduced that carbon evolution in Malmani dolomite aquifers occurs under closed system conditions. The possibilities of evolution from open to closed system conditions were also observed in groundwater samples that showed intermediate values of $\delta^{13}C‰$ (-13.25‰ to-11.58‰). This was also attributed to a possibility of mixing with water that has undergone closed system carbonate dissolution along its flow path, particularly borehole samples that are positioned at the periphery of the Basement Complex granitic gneiss near the Malmani dolomite aquifers.

The estimated mean annual recharge for the UCRB is 6.7% obtained from Baseflow Separation method as a percentage of MAP. This value has been referred to as a minimum recharge amount, because not all diffuse recharge in a catchment discharges to a stream network as baseflow, so the estimated value only represents a portion that discharge into the stream network. Point recharge estimates obtained through Water Table Fluctuation method from a distribution of boreholes in the Malmani dolomite ranged between 2.5% and 39% with an average of 15% of MAP. There are possibilities of groundwater over-abstraction in the sub-catchment A21A and A21B, where groundwater use percentage is high. These groundwater use percentages have to be properly considered in the allocations of groundwater use licenses to avoid over abstraction of groundwater. A point recharge estimates obtained through CMB in the Hospital Hill shale and Government quartzite of the Witwatersrand Supergroup is 2.5%, while 27.8% is observed in the Malmani dolomites. The low CMB recharge estimates in the Witwatersrand Supergroup could be a result of elevated chloride values from other chloride sources such as leakage of chlorinated potable water in the pipelines of the city of Johannesburg.

Acknowledgement

This study was funded in whole or part by the United States Agency for International Development (USAID) and the National Academies of Sciences, Engineering, and Medicine (NAS) through Partnership for Enhanced Engagement in Research (PEER) under cooperative agreement number AID-OAA-A-11-00012 Sub-Grant Number: 2000006304 and the Department of Science and Technology, South Africa (UID: 101594). This is where the GRECHLIM project entitled "Understanding recharge in the Limpopo River Basin, South Africa" has been implemented. Any opinions, findings, conclusions, of recommendations expressed in this article are those of the authors alone, and do not necessarily reflect the views of USAID or the NAS, and DST. We would like to thank the Department of Water and Sanitation, Johannesburg

Water Authority and South African Weather Services for providing us with different data. Many thanks to the School of Geosciences, University of the Witwatersrand for logistic support. The authors are also very grateful to the anonymous reviewers, whose constructive comments and recommendations helped to improve this work.

References

Abiye, T., Masindi, K., Mengistu, H., Demlie, M., 2018. Understanding the groundwater-level fluctuations for better management of groundwater resource: A case in the Johannesburg region. Groundw. Sustain. Dev. 7, 1–7. https://doi.org/10.1016/j.gsd.2018.02.004. (2352-801X).

Abiye, T.A., 2011. Provenance of groundwater in the crystalline aquifer of Johannesburg area, South Africa. Int. J. Phys. Sci. 6, 98–111. https://doi.org/10.5897/IJPS10.119.

Abiye, T.A., 2013b. Surface water and groundwater interaction in the upper Crocodile River basin (*WRC Report No TT 570/13*) In: Abiye, T.A. (Ed.), The use of isotope hydrology to characterize and assess water resources in South(ern) Africa. Water Research Commission, Pretoria, South Africa.

Abiye, T.A., 2016. Synthesis on groundwater recharge in Southern Africa: a supporting tool for groundwater users. Groundw. Sustain. Dev. 2–3, 182–189. https://doi.org/10.1016/j.gsd.2016.10.002.

Abiye, T.A., Mengistu, H., Demlie, M.B., 2011. Groundwater resource in the crystalline rocks of the Johannesburg Area, South Africa. J. Water Resour. Prot. 03, 199–212. https://doi.org/10.4236/jwarp.2011.34026.

Abiye, T.A., Mengistu, H., Masindi, K., Demlie, M., 2015. Surface water and groundwater interaction in the Upper Crocodile River Basin. South Afr. J. Geol. 118, 109–118. https://doi.org/10.2113/gssajg.118.2.109.

Abiye, T. A. (ed.) 2013a. The use of isotopes hydrology to characterise and assess water resources in South(ern) Africa (WRC Report No TT 570/13): Water Research Commission. p. 211. ISBN 978-1-4312-0480-9.

Appelo, C.A., Postma, D., 2005. Geochemistry, Groundwater and Pollution. Balkema, Leiden; New York (ISBN 0415364280).

Assaf, 2017. First biennial report to cabinet on the state of climate change science technology in South Africa. Acad. Sci. South Afr. (ASSAf) (ISBN 978-0-9947117-0-0).

Ayadi, Y., Mokadem, N., Besser, H., Khelifi, F., Hambi, S., Hamad, A., Boyce, A., Laouar, R., Hamed, Y., 2018. Hydrochemistry and stable isotopes (δ18O and δ2H) tools applied to the study of karst aquifers in southern mediterranean basin (Teboursouk area, NW Tunisia). J. Afr. Earth Sci. 137, 208–217. https://doi.org/10.1016/j.jafrearsci.2017.10.018. (1464-343X).

Barnard, H.C., 2000. An explanation of the 1:500 000 general hydrogeological map, Pretoria, South Africa.84. ISBN 0621299146.

Bmune, E., Xu, Y., 2008. Groundwater management issues in Southern Africa—an IWRM perspective. Water SA 34, 699–706 (ISSN 0378-4738).

Clark, I.D., Fritz, P., 1997. Environmental Isotopes in Hydrogeology 352 Lewis Publishers, Boca Raton, FL (ISBN 1-56670-249-6).

Craig, H., 1961. Isotopic variations in meteoric waters. Science 133, 1702–1703. https://doi.org/10.1126/science.133.3465.1702.

Department of water affairs and forestry, S. A, 2008. The Development of a Reconciliation Strategy for the Crocodile (West) Water Supply System: Summary of Previous and Current Studies. BKS (PTY) LTD & ARCUS GIBB (PTY) LTD (P WMA 03/000/00/3408).

Dower, S., 2003. Water quality. Water Wheel (Pretoria South Africa).

Engelbrecht, F., Adegoke, J., Bopape, M.-J., Naidoo, M., Garland, R., Thatcher, M., Mcgregor, J., Katzfey, J., Werner, M., Ichoku, C., Gatebe, C., 2015. Projections of rapidly rising surface temperatures over Africa under low mitigation. Environ. Res. Lett. 10, 1–17 (ISSN 1748-9326).

Eriksson, P.G., Clendenin, C.W., 1990. A review of the transvaal sequence, South Africa. J. Afr. Earth Sci. (Middle East) 10, 101–116. https://doi.org/10.1016/0899-5362(90)90049-k. (ISSN 0899-5362).

Eslin, J. & Kriel, J. 1967. The assessment and possible future use of the dolomitic ground water resources of the Far West Rand, Transvaal, Republic of South Africa. In: Proceedings of International Conference on Water for Peace, May 23-31 1968 Washington DC, USA. Washington DC: US Government Printing Office, pp. 908-918.

Froehlich, K., Gibson, J.J., Aggarwal, P., 2002. Deuterium excess in precipitation and its climatological significance. In: Proceedings International Conference on Study of Environmental Change Using Isotope Techniques International Conference held in Vienna, 23-27 April 2001 proceedings. C&S papers series Vienna Austria. International Atomic Energy Agency, 531.

Healy, R.W., 2010. Estimating Groundwater Recharge. Cambridge University Press, United Kingdom, pp. P245 (ISBN 978-0-521-86396-4).

Healy, R.W., Cook, P.G., 2002. Using groundwater levels to estimate recharge. Hydrogeol. J. 10, 91–109. https://doi.org/10.1007/s10040-001-0178-0. (1435-0157).

Hobbs, P.J., 2011. Situation Assessment of the Surface Water and Groundwater Resource Environments in the Cradle for Human Kind World Heritage Site. Department of Economic Development, Gauteng Province, South Africa.

Johnson, M.R., Anhaeusser, C.R., Thomas, R.J., 2006. *The geology of South Africa*, Pretoria; Johannesburg, Council for Geoscience; Geological Society of South Africa and Council for Geoscience.691. ISBN 1919908773.

Kohn, M.J., 2010. Carbon isotope compositions of terrestrial C3 plants as indicators of (paleo)ecology and (paleo)climate. Proc. Natl. Acad. Sci. USA 107, 19691–19695. https://doi.org/10.1073/pnas.1004933107. (ISSN 1091-6490).

Maliva, R., Missimer, T.M., 2012. Arid lands water evaluation and management. Springer, Berlin; New York (1 online resource. ISBN 978-3-642-29104-3).

Manghi, F., Mortazavi, B., Crother, C., Hamdi, M.R., 2009. Estimating regional groundwater recharge using a hydrological budget method. Water Resour. Manag. 23, 2475–2489. https://doi.org/10.1007/s11269-008-9391-0. (ISSN 0920-4741).

Marfia, A.M., Krishnamurthy, R.V., Atekwana, E.A., Panton, W.F., 2004. Isotopic and geochemical evolution of ground and surface waters in a karst dominated geological setting: a case study from Belize, Central America. Appl. Geochem. 19, 937–946. https://doi.org/10.1016/j.apgeochem.2003.10.013. (ISSN0883-2927).

Nathan, R.J., Mcmahon, T.A., 1990. Evaluation of automated techniques for base flow and recession analyses. Water Resour. Res. 26, 1465–1473. https://doi.org/10.1029/WR026i007p01465. (ISSN 1944-7973).

Nkotagu, H., 1996. Application of environmental isotopes to groundwater recharge studies in a semi-arid fractured crystalline basement area of Dodoma, Tanzania. Hydrogeochem. Stud. Sub-Sahar. Afr. 22, 443–457. https://doi.org/10.1016/0899-5362(96)00022-x. (ISSN 1464-343X).

Pitman, W., Vegter, J., 2003. Recharge and stream flow. In: Xu, Y., Beekman, H.E. (Eds.), Groundwater Recharge Estimation in South Africa. UNESCO International Hydrologic Programme (IHP), Paris, France, pp. 109–122 (ISBN 92-9220-000-3).

Rasmussen, W. C. & Andreasen, G. E. 1959. Hydrologic budget of the Beaverdam Creek basin, Maryland. Water Supply Paper.

Rivard, C., Lefebvre, R., Paradis, D., 2014. Regional recharge estimation using multiple methods: an application in the Annapolis Valley, Nova Scotia (Canada). Environ. Earth Sci. 71, 1389–1408. https://doi.org/10.1007/s12665-013-2545-2. (1866-6299).

Rutledge, A., 1998. Computer programs for describing the recession of ground-water discharge and for estimating mean ground-water recharge and discharge from streamflow records-Update.

Scanlon, B.R., Healy, R.W., Cook, P.G., 2002. Choosing appropriate techniques for quantifying groundwater recharge. Hydrogeol. J. 10, 18–39. https://doi.org/10.1007/s10040-001-0176-2. (ISSN 1435-0157).

Scanlon, B.R., Keese, K.E., Flint, A.L., Flint, L.E., Gaye, C.B., Edmunds, W.M., Simmers, I., 2006. Global synthesis of groundwater recharge in semiarid and arid regions. Hydrol. Process. 20, 3335–3370. https://doi.org/10.1002/hyp.6335. (ISSN 1099-1085).

Smakhtin, V., Watkins, D., 1997. Low flow estimation in South Africa. Report to the Water Research Commission by the Institute for Water Research. Institute for Water Research, Rhodes University.

Vegter, J., 1995. An Explanation of a Set of National Groundwater Maps. Water Research Commission, Pretoria, South Africa.

Witthüser, K., Holland, M., 2008. Hydrogeology of the Cradle of Humankind World Heritage Site, South Africa. In: Proceedings of the 12th International Conference of International Association for Computer Methods and Advances in Geomechanics (IACMAG). Goa, India.

Xu, Y., Beekman, H., 2003. Groundwater Recharge Estimation in Southern Africa. UNESCO, Paris (ii, 207. ISBN 92-9220-000-3).

C.2. Publication 2-Journal of Environmental Earth Sciences

Leketa, K., Abiye, T. & Butler, M. 2018. Characterisation of groundwater recharge conditions and flow mechanisms in bedrock aquifers of the Johannesburg area, South Africa. Environmental Earth Sciences, 77, 727. https://doi.org/10.1007/s12665-018-7911-7.

Environmental Earth Sciences (2018) 77:727
https://doi.org/10.1007/s12665-018-7911-7

ORIGINAL ARTICLE

Characterisation of groundwater recharge conditions and flow mechanisms in bedrock aquifers of the Johannesburg area, South Africa

Khahliso Leketa[1] · Tamiru Abiye[1] · Michael Butler[2]

Received: 20 January 2018 / Accepted: 20 October 2018
© Springer-Verlag GmbH Germany, part of Springer Nature 2018

Abstract
Groundwater is the major source of water and a critical resource for socioeconomic development in semi-arid environments like the Johannesburg area. Environmental isotopes are employed in this study to characterise groundwater recharge and flow mechanisms in the bedrock aquifers of Johannesburg, which is known for polluted surface water. With the exception of boreholes near the Hartbeespoort Dam, groundwater in the study area was derived from meteoric water that has undergone some degree of evaporation before recharge, possibly via diffuse mechanisms. Boreholes that tap groundwater from the Transvaal Supergroup Formation show depletion in $\delta^{18}O$ and $\delta^{2}H$ values. This is attributed to diffuse recharge through weathering fractures at high elevation that are undergoing deep circulation or recharge from depleted rainfall from the high-latitude moisture sources. The influence of focused recharge from the Hartbeespoort Dam was observed in the boreholes north of the dam, possibly as a result of the north–south trending fault lines and the north-dipping fractures in the bedding planes of quartzites. This is also supported by a reservoir water budget method which indicated a mean annual net flux of 2,084,131 m^3 from Hartbeespoort Dam recharging groundwater per annum. Using tritium in the dam and boreholes located at 750 m and 5400 m downstream, average groundwater flow velocity was estimated as 202 m/year. An open system was observed in shale, andesite and granitic-gneiss aquifers indicating soil CO_2 as a dominant source of carbon ($\delta^{13}C$) in groundwater. A closed system was also observed in dolomitic aquifers indicating carbonate dissolution as the predominant source of carbon.

Keywords Groundwater recharge · Crystalline aquifer · Open and closed carbon system · Focused recharge mechanism · Johannesburg

Introduction

Water has a significant contribution in the socioeconomic development of any community. Moreover, in regions with semi-arid or arid climates, groundwater in particular plays a central role in providing water supplies because local surface water bodies are usually ephemeral (Scanlon et al. 2006; Healy 2010; Rivard et al. 2014; Abiye 2016). Determining the recharge processes in a semi-arid environment is, therefore, important to ensure sustainable groundwater use and continuing socioeconomic development.

Groundwater is becoming increasingly important in the semi-arid Johannesburg area, the economic hub of South Africa. This is because surface water bodies in the region have become highly polluted due to the discharge of partly treated urban water return flows from urban areas and the effects of acid mine drainage from abandoned gold mines (Department of Water Affairs and Forestry 2008; Abiye et al. 2015). This has limited the use of surface water resources to mainly irrigation and recreational uses, particularly for water in the Hartbeespoort Dam and Crocodile River (Fig. 1) which are downstream of the city of Johannesburg. Highly intensive farming, industrial and rural domestic activities in the region are increasingly relying on groundwater abstraction from fractures in crystalline basement rocks which form localised aquifers with modest groundwater productivity, and high-yielding karstified meta-dolomites.

✉ Khahliso Leketa
kleketa@gmail.com

[1] School of Geosciences, University of the Witwatersrand, Private Bag X3, P.O Box Wits 2050, Johannesburg, South Africa

[2] iThemba Labs, Private Bag 11, Wits, 2050, Johannesburg, Gauteng, South Africa

Published online: 26 October 2018

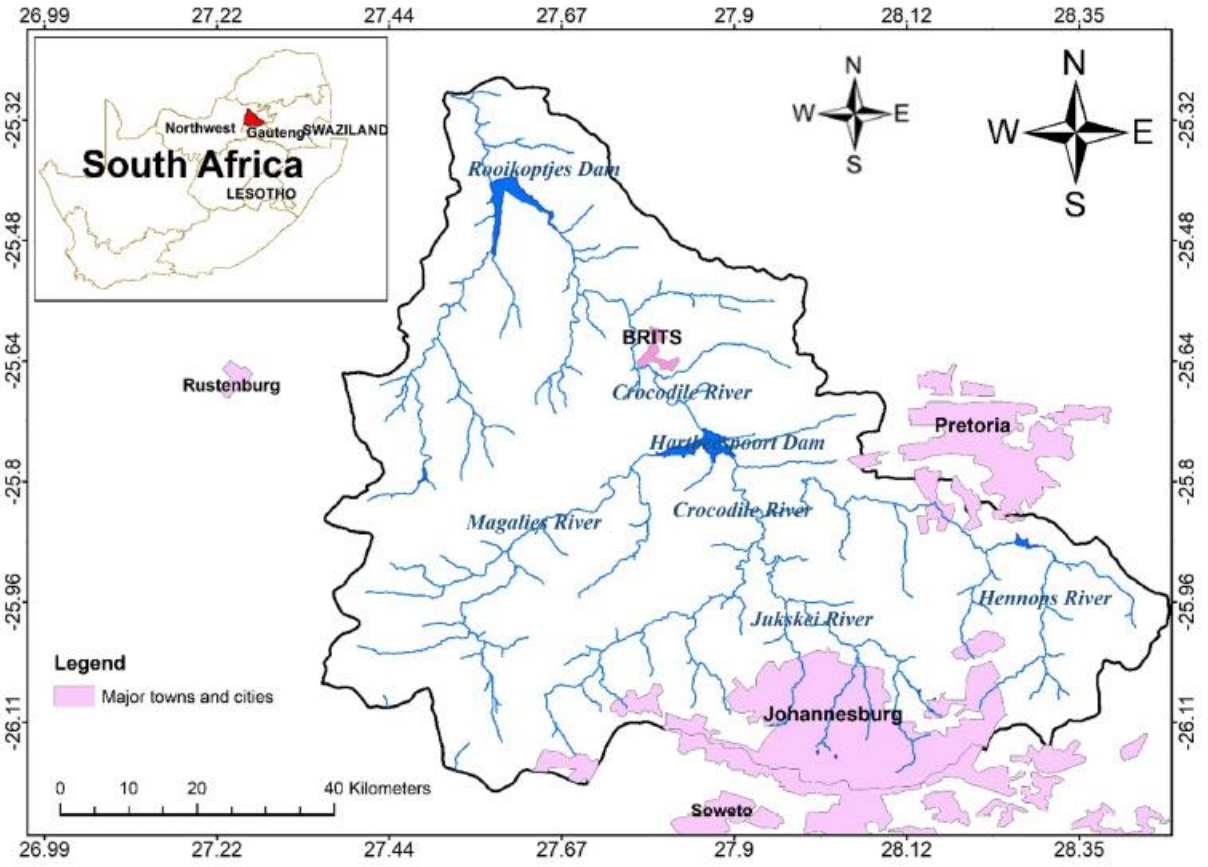

Fig. 1 Locality map of UCRB

Previous investigations have indicated that groundwater quality in the area has been impacted at shallow depths by mining wastes (Abiye 2011; Abiye et al. 2011, 2015). Abiye (2011) assessed the recharge dynamics and flow-paths of groundwater using hydrogeochemical characteristics and environmental isotopes in bedrock aquifers in the Johannesburg area. The study focused on the dolomite aquifers where it was observed that there was mixing of fresh and polluted shallow groundwater mainly from acid mine drainage in the weathered karstic dolomite.

Recharge from surface water bodies, often referred to as focused recharge, is more prevalent than diffuse recharge in regions with a semi-arid climate. This is due to the low precipitation and high rate of evapotranspiration which generally limits the extent to which diffuse recharge from precipitation can take place (Scanlon et al. 2006; Healy 2010). Healy (2010) defined focused recharge as the movement of water from a surface water body to an underlying aquifer, and diffuse recharge as the deep percolation of water through the unsaturated zone into groundwater that is distributed over large areas as a result of precipitation.

As Johannesburg is drained by polluted streams that have potential to provide focused recharge to the underlying aquifers, it is necessary to characterise groundwater recharge and flow mechanisms into various aquifers within the Upper Crocodile River Basin (UCRB) to understand the vulnerability of groundwater to contamination from this source. In semi-arid areas underlain by fractured rock aquifers, recharge characterisation may be difficult because of the complexity of surface water–groundwater interactions and the importance of preferred flow-paths in these aquifers (Scanlon et al. 2006; Tessema et al. 2012). The assessment of recharge in the area is further complicated by the use of surface water for intensive irrigation of crops in the area which generates diffuse recharge and causes mixing of different recharge water sources in groundwater.

Owing to their conservative nature, stable isotopes of water molecules ($\delta^{18}O$, $\delta^{2}H$) are suitable for determining the history of water before recharge and identifying the mixing of distinct water sources (Sami 1992; Clark and Fritz 1997). Radioactive tritium is suitable for determining groundwater age and travel time since it forms part of the water molecule

(Clark and Fritz 1997) and is only altered by radioactive decay through the flow-path in the absence of mixing. The stable isotope of carbon ($\delta^{13}C$) is also suitable for assessing groundwater movement along a flow-path because various carbon sources (i.e. biomass, soil carbon dioxide, and carbonate rocks) have distinct $\delta^{13}C$ signatures (Clark and Fritz 1997; Marfia et al. 2004; Appelo and Postma 2005). The $\delta^{13}C$ in groundwater, therefore, resembles the $\delta^{13}C$ signature of the dissolved carbon source and the extent to which this isotope is fractionated among the carbonate species in the solution (Appelo and Postma 2005). These make the use of $\delta^{13}C$ in groundwater suitable for tracing groundwater flow-paths even in situations where there are complex recharge processes.

In this study, environmental isotopes ($\delta^{18}O$, $\delta^{2}H$, ^{3}H and $\delta^{13}C$) are used to characterise groundwater recharge and flow mechanisms in the crystalline aquifers of the semi-arid Upper Crocodile River Basins (UCRB) in the Johannesburg area (Fig. 1). The recharge mechanisms and sources of recharge are determined using stable isotopes of water molecule ($\delta^{18}O$ and $\delta^{2}H$). The groundwater travel time from a recharge source to an aquifer is also determined using tritium (^{3}H), an isotope that has a half-life of 12.43 years (Clark and Fritz 1997; Appelo and Postma 2005). The stable isotope of carbon ($\delta^{13}C$) is used to trace groundwater evolution by determining the probable source of dissolved carbon in groundwater, which is also an indication of groundwater openness to soil carbon dioxide (Clark and Fritz 1997; Appelo and Postma 2005).

Description of study area

The UCRB, with a surface area of 6336 km^2, has a subtropical highland climate (Cwb in the Köppen climate classification system) with a highly variable low rainfall with a mean of about 700 mm/year (Abiye 2011). The UCRB is drained by the Jukskei and Hennops Rivers that converge to form the Crocodile River in the east and the Magalies River in the western part of the catchment. The Crocodile River contributes 90% of the Hartbeespoort Dam inflow (Tsoelopele-Environmental 2006) and further flows northwards into the Rooikoptjes Dam, eventually discharging into the Limpopo River.

Figure 2 shows the lithology of the UCRB. The catchment is underlain by the rocks of the Basement Complex, the Witwatersrand Supergroup, the Transvaal Supergroup and the Bushveld Igneous Complex rocks with a younging direction towards the north (Barnard 2000; Johnson et al. 2006).

The Witwatersrand Supergroup, which forms the southern boundary of the UCRB consists of a range or metasediments and interbedded lavas (Anhaeusser 1971; Barnard 2000). The Witwatersrand Supergroup overlies the Basement Complex, which is represented predominantly by weathered and fractured Archaean granitic bodies of similar age that differ slightly in their composition (granites, granodiorites, gneisses and migmatites) (Barnard 2000). The Transvaal Supergroup is stratigraphically younger than the Witwatersrand Supergroup and covers the middle portion of the area and consists of: Black Reef quartzites, Malmani dolomites and Pretoria Group; shales alternating with highly resistant protruding quartzites, interbedded basaltic-andesitic lava and subordinate conglomerate and carbonate rocks which have been subjected to low-grade metamorphism (Eriksson and Clendenin 1990; Johnson et al. 2006). Within the Pretoria Group, Magaliesberg Formation (quartzite) forms an elongated ridge that constitutes part of the Hartbeespoort Dam axis. Further north of the Magaliesberg Ridge is the Bushveld Igneous Complex which is dominantly represented by gabbros, norites, anorthosites and granitic rocks.

The hydrogeology of the UCRB is characterised by four types of aquifers which are: intergranular aquifers in areas covered by colluvium; fractured crystalline aquifers associated with fractures, fissures and joints in granitic gneisses and quartzites; karstic aquifers in the dolostones; and intergranular and fractured aquifers consisting of hydraulically connected colluvium aquifer at the top and fractured crystalline aquifer at the bottom (Barnard 2000; Abiye 2011; Abiye et al. 2011, 2015). The crystalline aquifers are classified as hard rock aquifers with a modest groundwater productivity, whereas meta-dolomites with dissolution cavities yield large quantities of groundwater (Witthüser and Holland 2008; Abiye et al. 2011). The abundant fractures and cavities in the meta-dolomites could act as good recharge zones, which eventually generate high-yielding aquifers that are associated with springs and tectonic depressions (Abiye et al. 2015). The high-yielding springs of about 30 l/s and 140 l/s for Nash Farm and Nouklip Springs discharge from dolomite aquifers (Hobbs 2011).

Since the meta-dolomite outcrop cuts across the catchment in an east–west direction (Fig. 2), groundwater can easily move across the water divide into the neighbouring catchments through the dissolution cavities and tectonic lineaments (Abiye et al. 2011). The intensively fractured quartzite outcrops of the Witwatersrand Supergroup that form the southern boundary of the UCRB could also provide recharge on the catchment boundary (Abiye et al. 2011). The aquifers across the Transvaal Supergroup and the Bushveld Complex are hydraulically interconnected by the two northwest southeast faults that create a graben at the middle of the Hartbeespoort Dam. These faults could also be contributing to focused recharge between the dam and its underlying aquifer (see the inset in Fig. 2 which displays the aerial view of the dam with the positions of the fault lines and a graben in the middle). This graben is characterised by a horizontal

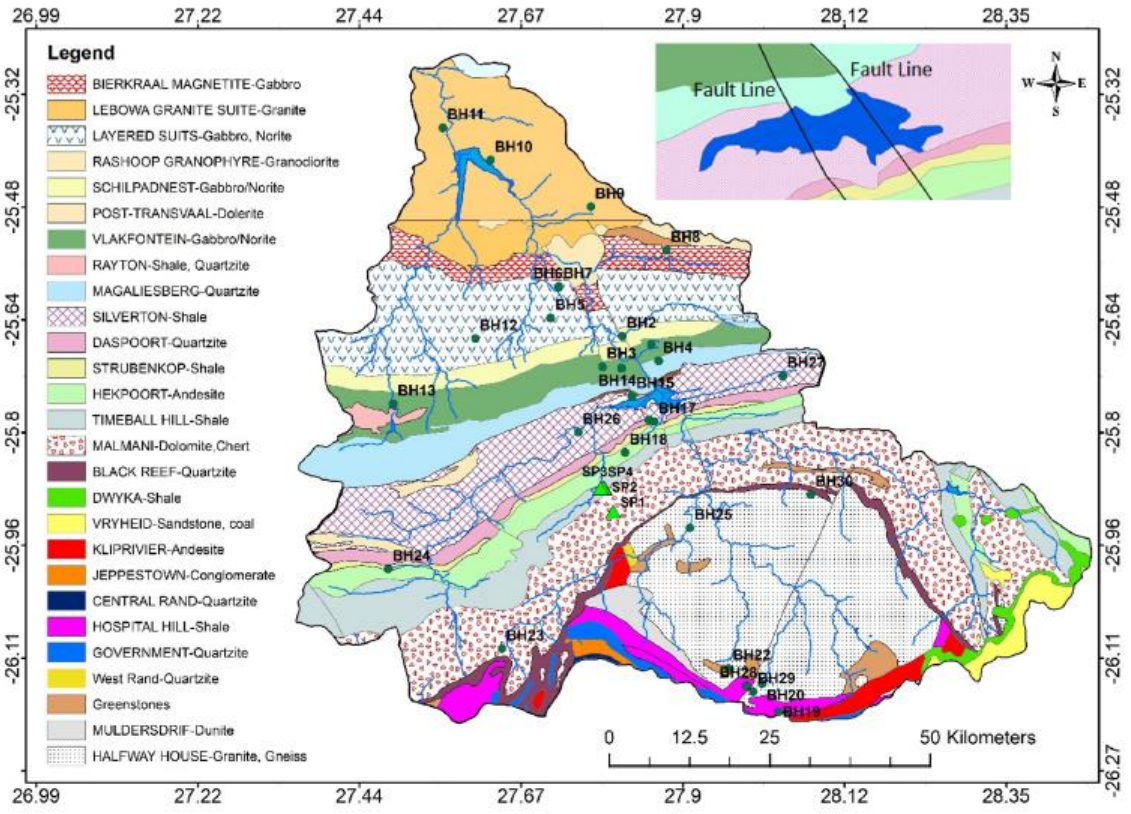

Fig. 2 Geological setting of the study area (source for geological data is Council for Geosciences)

displacement of approximately 1280 m to the south and a vertical displacement of 390 m (Hall and du Toit 1923).

Materials and methods

The Johannesburg Local Meteoric Water Line (JLMWL) was constructed from rainfall samples collected over 3 years at two stations for this work: one at the University of the Witwatersrand and another at Montgomery Park in Johannesburg, South Africa (Fig. 3). Water samples were collected with a 10 ml glass bottle immediately after rainfall to avoid sample evaporation. The samples represent individual rainfall events rather than rainfall totals over an extended period of time.

Groundwater samples were collected from privately owned boreholes within the UCRB between June 2016 and February 2017 (Fig. 3) and spatial sampling was carried out on the Hartbeespoort Dam using a speed boat on the dam. Selected borehole samples were collected for stable carbon isotope ($\delta^{13}C$) analysis.

Sampling for tritium was carried out with a 500 ml plastic bottle in the field. The field sampling procedure for carbon isotopes involved filling the 30 l drum with sample water, followed by addition of carbonate-free NaOH to raise the pH to an alkaline value and adding a dash of phenolphthalein as a pH indicator. $BaCl_2$ was then added, from which Ba^{2+} would react with the CO_3^{2-} in solution to precipitate barium carbonate ($BaCO_3$). The $BaCO_3$ precipitate was then separated from the supernatant and stored in 500 ml bottles.

Stable isotopes of ^{18}O and ^{2}H were analysed at the University of the Witwatersrand, South Africa using the Liquid Water Isotope Analyser-model 45-EP. The laser machine is capable of providing accurate results with a precision of approximately 1‰ for δ^2H and 0.2‰ for $\delta^{18}O$ in liquid water samples of up to 1000 mg/l dissolved salt concentration. The analysis was done against five standards of different known isotopic signatures. Tritium and carbon isotopes were analysed at iThemba Laboratories in Johannesburg, South Africa. Tritium was analysed using the electrolytic enrichment method with an analyser that has 0.2 T.U detection limit. The carbon isotopes on the other hand were

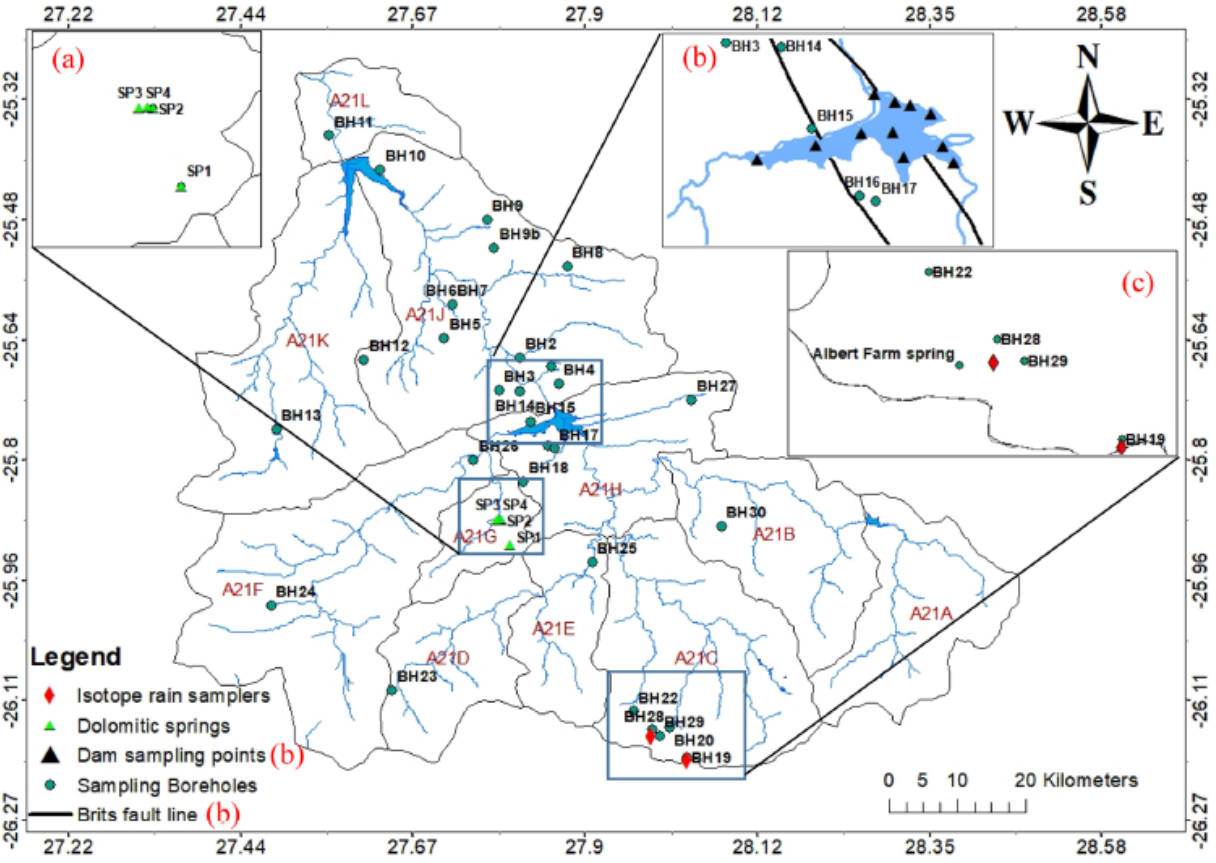

Fig. 3 Location of boreholes and rainfall samplers for environmental isotope

analysed using a Hewlett Packard TriCarb liquid scintillation spectrometer.

In a way to quantitatively assess the role of focused recharge from surface water bodies, a reservoir water budget method was tested from Hartbeespoort Dam, which had already been identified through environmental isotopes as a source of focused recharge. This was done using a conceptual model (for the 15 year period 2000–2015) shown on Eq. (1), where $Q_{\Delta G}$ is net groundwater flux, $Q_{\Delta S}$ is change in storage, Q_{Ev} is evaporation flux, $Q_{S\,\mathrm{out}}$ reservoir water outflow, Q_{Ab} reservoir abstractions, Q_P precipitation onto the reservoir, and $Q_{S\,\mathrm{in}}$ is reservoir inflow all in units of m^3.

$$Q_{\Delta G} = Q_{\Delta S} + Q_{\mathrm{Ev}} + Q_{S\,\mathrm{out}} + Q_{\mathrm{Ab}} - Q_P - Q_{S\,\mathrm{in}}\ (\mathrm{m}^3)\,. \quad (1)$$

Results and discussion

Using the Johannesburg rainfall data of 3 years, a local meteoric water line of regression $\delta^2\mathrm{H} = 6.7\delta^{18}\mathrm{O} + 10‰$ was constructed for use as a reference for groundwater in the UCRB. This regression line is first released in this work.

Table 1 below shows environmental isotope results for groundwater sampled between June 2016 and February 2017. All boreholes were sampled once. The table also shows *d*-excess values calculated from the JLMWL.

Figure 4 shows groundwater and surface water results from the study area plotted against the Johannesburg Local Meteoric Water Line (JLMWL), the Pretoria Local Meteoric Water Line (PLMWL) and the Global Meteoric Water Line (GMWL) to illustrate the deviation from the lines. From this figure, the influence of both focused and diffuse recharge can be observed. Surface water seems to follow a distinct trend along an evaporation line, expectedly so because of evaporation exposure that leads to enrichment in heavy isotopes. BH15 is highly enriched showing evidence of connectivity with surface water, which is not surprising because of its close proximity with the Hartbeespoort Dam on Fig. 3. It can, therefore, be deduced that the aquifer that feeds BH15 is dominated by focused recharge from the dam water.

On the other hand, BHs16, 17, and 18, which are also underlain by the Transvaal Supergroup are extremely depleted relative to the JLMWL and the PLMWL, which

Table 1 Environmental isotopes for groundwater sampled between June 2016 and February 2017

ID	Latitude	Longitude	δ^2H (‰)	^{2}H StDev (±)	δ^{18}O (‰)	^{18}O StDev (±)	*d*-excess (‰)	^{3}H (T.U)	^{3}H StDev (±)
BH1	−25.67378	27.85107	−6.5	0.6	−1.39	0.1	2.75	5.3	±0.4
BH2	−25.66243	27.81031	−6.8	1.0	−1.11	0.2	0.60	6.3	±0.5
BH3	−25.70531	27.78251	−5.0	0.6	−0.89	0.1	0.92	1.7	±0.3
BH4	−25.69700	27.86117	−18.1	1.6	−3.96	0.2	8.45	3.2	±0.4
BH5	−25.63700	27.71011	−9.9	0.6	−1.94	0.1	3.08	2.8	±0.3
BH6	−25.59320	27.72135	−26.5	0.12	−4.79	0.04	5.57	6.7	±0.5
BH7	−25.59300	27.72135	−19.4	1.1	−4.09	0.1	8.00	5.9	±0.4
BH8	−25.54250	27.87209	−9.6	0.5	−2.01	0.3	3.88	4.2	±0.4
BH9	−25.48145	27.76628	−17.8	0.8	−3.05	0.1	2.68	2.3	±0.3
BH10	−25.41614	27.62571	−17.1	1.4	−3.00	0.2	3.06	3.7	±0.4
BH11	−25.37080	27.55919	−10.1	2.3	−1.71	0.3	1.33	3.8	±0.4
BH12	−25.66576	27.60464	−14.4	0.6	−3.12	0.1	6.47	3.3	±0.4
BH13	−25.75739	27.48989	−13.0	0.3	−2.14	0.1	1.36	2.2	±0.3
BH14	−25.70753	27.80922	−0.9	1.5	−0.35	0.2	1.50	1.3	±0.3
BH15	−25.74678	27.82403	−6.88	0.34	1.58	0.03	−17.47	4.8	±0.4
BH16	−25.77922	27.84744	−39.3	0.4	−12.65	0.1	45.42	3.3	±0.4
BH17	−25.78192	27.85511	−38.2	0.12	−13.47	0.03	52.07	1.3	±0.3
BH18	−25.82533	27.81450	−32.8	0.07	−9.76	0.04	32.63	1.9	±0.3
BH19	−26.18844	28.02931	−12.3	0.3	−2.23	0.1	2.66	1.4	±0.3
BH20	−26.14838	28.00663	−12.4	0	−3.52	0	11.17	2.8	±0.3
BH22	−26.12743	27.95913	−15.8	0.7	−3.55	0.1	7.95	1.9	±0.3
BH23	−26.09973	27.64191	−12.5	3.5	−2.62	0.3	5.09	1.5	±0.3
BH24	−25.98829	27.48239	−22.5	0.5	−5.08	0.4	11.55	1.2	±0.3
BH25	−25.93074	27.90525	−21.6	0.4	−4.32	0.1	7.33	3.4	±0.4
BH26	−25.79705	27.74881	−16.7	0.3	−3.27	0.1	5.18	3.1	±0.3
BH27	−25.71812	28.03547	−15.0	0.7	−3.18	0.1	6.24	2.6	±0.3
BH28	−26.15190	27.98402	−17.3	1.0	−3.83	0.1	8.39	1.8	±0.3
BH29	−26.15991	27.99385	−18.2	1.5	−3.83	0.2	7.51	0.5	±0.2
BH30	−25.88426	28.07489	−25.3	0.4	−5.15	0.0	9.16	0.6	±0.2
SP1-Nashfarm spring	−25.90807	27.79756	−27.6	0.4	−4.97	0.1	5.74	1.3	±0.3
SP2-Nouklip spring	−25.87524	27.78584	−27.5	0.5	−5.11	0.1	6.71	1.5	±0.3
SP3-Spring at the picnic site	−25.87494	27.78365	−29.6	0.4	−5.28	0.1	5.75	0.9	±0.2
SP4	−25.87516	27.78002	−27.8	0.4	−4.77	0.1	4.17	0.9	±0.2

could mean that the recharge in the aquifers that host the boreholes was not dominated by the local rainfall. Moreover, the springs and boreholes in the dolomites, shale and andesite of the Transvaal Supergroup seem to dominate the depleted part of Fig. 4 i.e. the lower left portion. Surprisingly, BH 25 and BH 30, which according to Fig. 2 are near the periphery of granitic gneiss of the Basement Complex and Black Reef quartzite of the Transvaal Supergroup, also seem to have the same level of depletion as the Transvaal Supergroup groundwater (Fig. 5). With an exception of BHs16, 17, and 18, all groundwater samples including the dolomitic springs seem to plot semi-parallel to the JLMWL with slight deviations of enrichment. But to get a clearer look, Fig. 5 shows the zoomed-in view of groundwater samples versus the JLMWL, which shows the position of the majority of the samples below the line as an indication to the presence of progressive evaporation prior to recharge.

According to Fig. 5, all boreholes are plotted along an evaporation line with a regression of $\delta^2H = 4.78^{18}O - 0.96‰$. Figure 5 also shows that BHs 3, 14, 2 and 1, which are positioned on the northern side of the Magaliesberg quartzite ridge (Hartbeespoort Dam area) occupy the most enriched portion of the plot but still plot along the evaporation line. Not surprising is the fact that, according to Fig. 4, these boreholes trend towards the highly enriched surface water samples. This behaviour suggests that mixing of depleted groundwater and enriched surface water has taken place, possibly as a result of focussed recharge from the dam wall

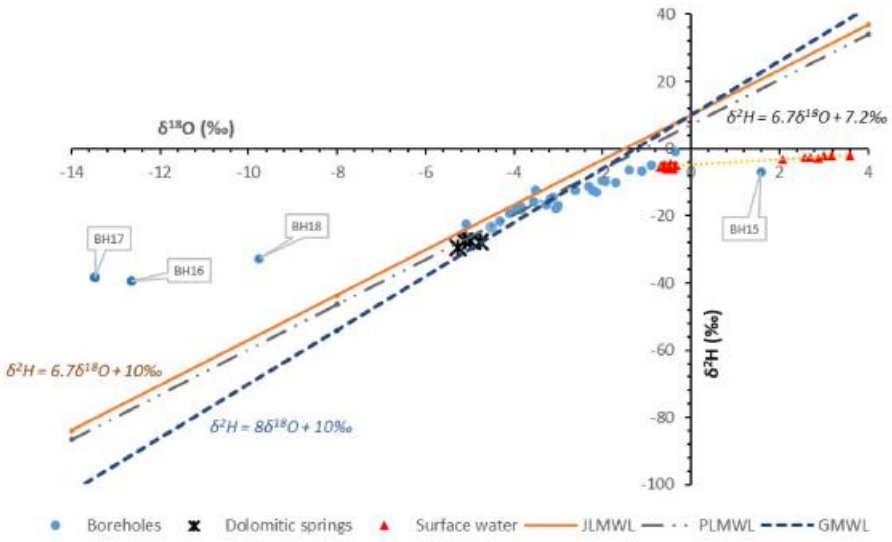

Fig. 4 Stable isotopes of groundwater and surface water versus Johannesburg Local Meteoric Water Line, Pretoria LMWL ($\delta^2H = 6.7\delta^{18}O + 7.2‰$ GNIP-IAEA) and global MWL ($\delta^2H = 8\delta^{18}O + 10‰$) (Craig 1961)

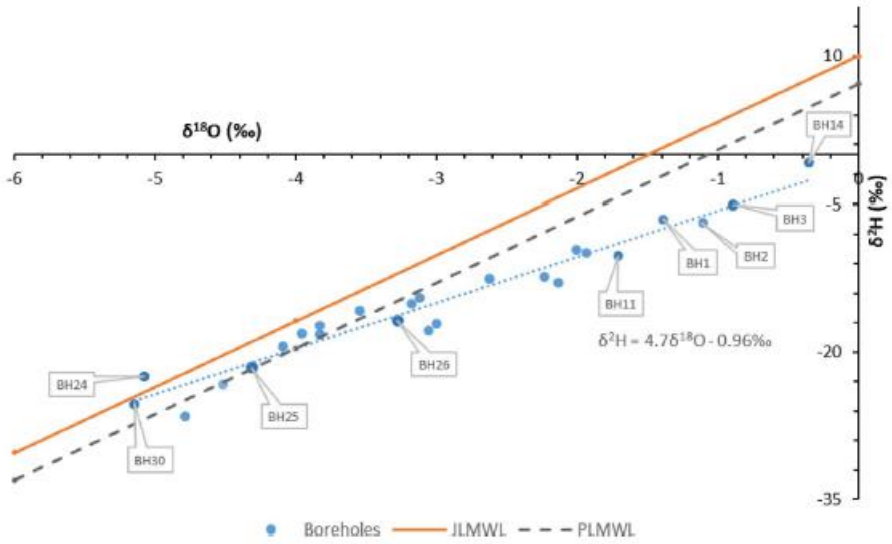

Fig. 5 Zoomed-in view of the boreholes plotted against the JLMWL (solid line $\delta^2H = 6.7\delta^{18}O + 10‰$) with a projected evaporation line for boreholes, shown as a dotted line

or diffuse recharge as a result of irrigation by water from the dam.

A quasi-groundwater flow direction can be hypothesised using stable isotope signatures of groundwater and surface water. Considering the four boreholes BHs 15, 16, 17 and 26, which surround the Hartbeespoort Dam, a quasi-groundwater flow direction has been deduced as northward. This is because, the south and western boreholes show signs of depletion while BH15 which is positioned on the northern side of the dam shows extreme enrichment similar to dam water followed by the boreholes on the northern side of the Magaliesberg quartzite ridge (BH3, BH14, etc.). The two main semi-parallel faults that cut across the Hartbeespoort Dam in the north west–south east direction (as shown in Fig. 2) could also be contributing to focused recharge seeing that BH15 and BH14 are positioned on the western fault line. BH15 could, however, be mainly recharged by the dam while BH14 shows signs of mixing between dam water and meteoric water, possibly from diffuse recharge.

Clark and Fritz (1997) indicated that varying *d*-excess values can be caused by different rainfall events generated under different vapour humidity conditions and different rain source air masses. The magnitude of the *d*-excess value gives an indication of the physical conditions of the oceanic moisture source area in terms of humidity, temperature and sea surface temperature (Froehlich et al. 2002; Harris et al. 2010). The deuterium excess values for the study area have been determined and are presented in Table 1. $\delta^{18}O$ was plotted against *d*-excess as shown in Fig. 6 in order to assess the impact of moisture source and humidity on groundwater

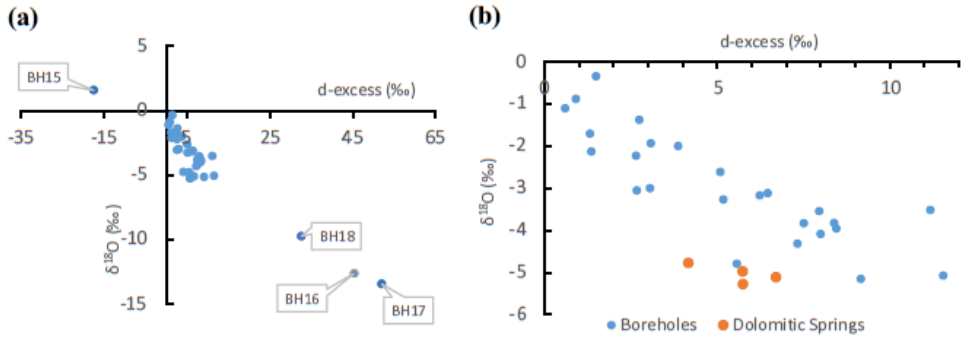

Fig. 6 Deuterium excess plotted against $\delta^{18}O$ for groundwater samples in the UCRB

isotope signature. The range of *d*-excess values is between − 17.47 and + 52.07‰.

Figure 6a, b shows varying signature in *d*-excess among the groundwater samples. Figure 6a shows three clusters of groundwater samples with the extremely depleted BH 16, 17 and 18 and the extremely enriched BH 15 showing distinct variance in *d*-excess. It has been established that BH 15 sample was isotopically altered due to evaporation from a surface water body prior to recharge, hence a low *d*-excess. Therefore, BH 15 does not give an indication of the moisture source conditions. The variance in the other samples shows the influence of both local and regional circulation of moisture. Groundwater samples with high *d*-excess are potentially recharged from rainfall whose moisture was formed under evaporation conditions of very low humidity and low temperature, thereby yielding highly depleted moisture (Clark and Fritz 1997). Figure 6b presents a zoomed-in view of the boreholes and dolomitic springs showing that the dolomitic springs have similar *d*-excess values, suggesting that they are recharged from a similar moisture source or similar recharge episode. A dynamic *d*-excess in groundwater samples is observed, which is potentially due to recharge by moisture of different sources, i.e. from air masses from the warmer Indian Ocean as distinct from air masses that have come from the cooler Atlantic Ocean and the cold high latitude near Antarctica. Air mass from the warmer Indian ocean is indicative of low *d*-excess moisture due to evaporation that occurs at higher temperature and higher humidity leading to relatively enriched moisture, unlike the higher *d*-excess values that are often expected in the colder high-latitude region and the Atlantic Ocean.

Figure 7a shows a bird's eye view schematic representation of the Hartbeespoort Dam with its two major semi-parallel northwest–southeast aligned fault lines (Brits fault lines). Also shown on Fig. 7b is the Magaliesberg quartzite ridge dipping to the north by exposing the quartzite bedding plane fractures on the Hartbeespoort Dam reservoir to the south (right side on the image). Environmental isotopes revealed that tritium is highest in the reservoir possibly from upstream industrial sources. Tritium values for BH 14 and BH 15 are close to the Hartbeespoort Dam values and much higher than all other upstream boreholes. This supported the conceptualisation that groundwater flow direction is northwards such that the boreholes on the north of the Magaliesberg quartzite ridge are dominated by focused recharge from the dam. The tritium residence time method was then applied to estimate groundwater flow period and velocity from the Hartbeespoort Dam to the northern boreholes (BH 15 and BH 14).

Equation 3, which is a simplified form of Eq. (2), was used to calculate groundwater travel time from the Hartbeespoort Dam using the average tritium content of the dam water and tritium in the groundwater. This was based on the premise of focused recharge from the dam through the fault line as deduced by stable isotope interpretations.

$$t = t_{1/2} \ln\left(\frac{A_{t0}}{A_{t1}}\right) \Big/ \ln 2\,, \tag{2}$$

$$t = -17.93 \ln\left(\frac{A_{t1}}{A_{t0}}\right), \tag{3}$$

where t is MRT in years, $t_{1/2}$ is half-life. A_{t0} is the input tritium and A_{t1} is tritium in groundwater all in units of "T.U".

The time it takes for dam water to recharge and flow through the groundwater system to BH14 and 15 was estimated. The flow velocity was obtained as a function of the distance from the dam to the respective boreholes. The results are shown in Table 2.

The average groundwater flow velocity is estimated at 202 m/year. Irrigation with dam water also has a potential to increase tritium levels through a diffuse recharge. If irrigation contribution is factored in, then the estimated

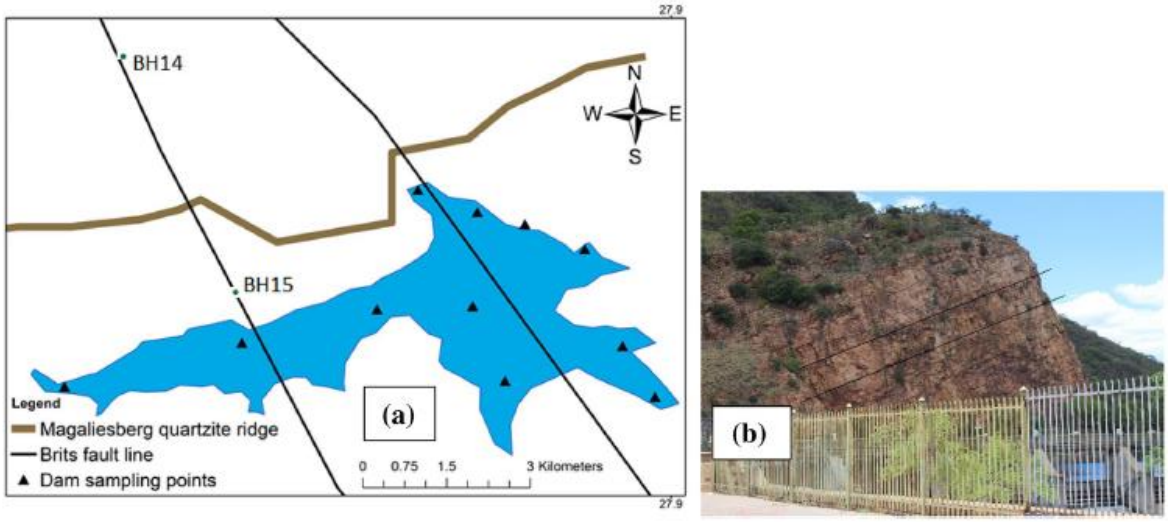

Fig. 7 Schematic of the Hartbeespoort Dam with its main fault lines (**a**) and north-dipping quartzite bedding planes of the Magaliesberg Ridge (Hartbeespoort Dam wall) (**b**)

Table 2 Estimate of groundwater flow period and flow velocity

Site	T.U	Flow period (years)	Distance (m)	Flow velocity (m/year)
Dam	5.9	–	–	–
BH15	4.8	4	750	204
BH14	1.3	27	5400	199
Average				202

flow velocities are assumed to be the minimum-possible flow velocities.

A Reservoir Water Budget on the Hartbeespoort Dam from 15 years (2000–2015) of monthly data indicated that an average net flux of 2,084,131 m^3 surface water is lost to groundwater, possibly by leakage through geological structures. This is the amount of water that could be contributing to focused groundwater recharge which is observed in the environmental isotope interpretations.

Although the study area has agricultural farming of C4 crops like corn andsorghum, much of the catchment remains uncultivated and is covered by grasses and shrubs which are reported by Clark and Fritz (1997) and Kohn (2010) to be vegetation that predominantly undergoes C3 photosynthesis. The evolution of DIC in groundwater is, therefore, assumed to be influenced by CO_2 from C3 vegetation with average $\delta^{13}C$ of − 26‰ as reported by Marfia et al. (2004) and Kohn (2010). The $\delta^{13}C$ values as shown on Table 3 range from − 17.35 to − 5.64‰. The depleted groundwater samples such as those in the carbonate-poor shale, andesite and granitic gneiss indicate open system condition deducing that the source of DIC is soil CO_2. The more enriched values indicate that the groundwater system is closed to soil CO_2. Therefore, it is deduced that the predominant source of DIC in the enriched samples is carbonate dissolution. What is not surprising from the data is that BH23, Nash Farm Spring

Table 3 $\delta^{13}C$ of groundwater in selected boreholes within the UCRB

BH no.	Stratigraphy	Lithology	$\delta^{13}C$ (‰)
BH14	Vlakfontein	Gabbro, norite, anorthosite	− 12.31
BH16	Daspoort/Silverton	Shale and andesite	− 17.35
BH19	West rand Group	Quartzite	− 15.22
BH23	Malmani	Dolomite	− 8.41
BH24	Hekpoort	Shale, andesite	− 15.38
BH25	Halfway house	Granite, gneiss	− 15.3
Nash farm spring-SP1	Malmani	Dolomites	− 6.05
Nouklip spring-SP2	Malmani	Dolomites	− 5.64

and Nouklip Spring which are situated in the dolomites are the most enriched, possibly due to carbonate dissolution. This agrees well with what was reported by Barnard (2000) about the study area, that groundwater containing weak carbonic acid (H_2CO_3) that infiltrates dolomitic terrain flows through planes of weakness such as faults, fractures and joints causing dissolution of dolomite, which leads to soluble bicarbonate in solution as shown by the following chemical reaction:

$$3CaCO_3 \cdot 2MgCO_3 + 5H_2CO_3 \rightarrow 3Ca(HCO_3)_2 + 2Mg(HCO_3)_2 \text{Dolomite} + \text{carbonic acid} \rightarrow \text{calcium} - \text{bicarbonate} + \text{magnesium} - \text{bicarbonate}.$$

BH14 with a $\delta^{13}C$ value of − 12.31‰ shows signs of relative enrichment. This was not expected due to the geochemistry of its host rock (gabbro, norite and anorthosite) which are siliceous and poor in carbonate minerals (Judson et al. 1976). However, as indicated in the analysis of δ^2H, $\delta^{18}O$, and ^3H above, BH14 is recharged by the Hartbeespoort Dam water, which is a receiver of all water from Magalies and Crocodile Rivers. Magalies River constitutes discharge from Nash Farm and Nouklip Springs which are highly enriched in $\delta^{13}C$ as shown on Table 3. This inflow of enriched water into Hartbeespoort Dam could be responsible for enrichment observed in BH14.

Stable isotope interpretations (δ^2H, $\delta^{18}O$) revealed a depleted moisture source for BH16 and the dolomitic springs deducing that they are recharged by rainfall from a similar moisture source, while a difference is observed in $\delta^{13}C$ values. This indicates that, recharge may be occurring from rainfall with a similar moisture source but could be followed by groundwater flow through different aquifer media.

Conclusions

Stable isotope measurements have indicated that groundwater recharge to bedrock aquifers near Johannesburg, South Africa takes place by both diffuse and focused recharge processes. The boreholes in the southern part of the Hartbeespoort dam show depletion especially those on the Transvaal Supergroup formations. This has been attributed to diffuse recharge in the high-elevation undergoing deep circulation through tectonically induced fractures. Focused recharge is observed in the boreholes north of the Hartbeespoort Dam possibly as a result of two semi-parallel north south-facing fault lines that cross the dam and the north-dipping quartzite bedding planes of Magaliesberg quartzite ridge which facilitate lateral flow of groundwater. This is an indication that groundwater is vulnerable to pollution from surface water bodies taking place by infiltration through geological structures. This is also supported by a reservoir water budget method, which indicated a mean annual net flux of 2,084,131 m^3 recharging groundwater from the Hartbeespoort dam water per annum. The average groundwater flow velocity was then determined to be 202 m/year from Hartbeespoort Dam as a recharge source using tritium as a tracer.

Three groundwater clusters are observed from a $\delta^{18}O/d$-excess plot. A high variation in d-excess is said to be a result of recharge episodes from different moisture sources. The evolution of carbon has been observed from both open and closed system considering the $\delta^{13}C$ value in groundwater. Open system was observed in the carbonate-poor shale, andesite and granitic-gneiss aquifers indicating that soil CO_2 is a dominant source of carbon. Closed system was also observed in dolomitic aquifers which had enriched $\delta^{13}C$ and therefore deduced the predominant source of carbon as carbonate dissolution. The observed open and closed $\delta^{13}C$ evolution indicate different groundwater flow-paths through different aquifer media.

Acknowledgements This study was funded in whole or part by the United States Agency for International Development (USAID) and the National Academies of Sciences, Engineering, and Medicine (NAS) through Partnership for Enhanced Engagement in Research (PEER) under cooperative agreement number AID-OAA-A-11-00012 Sub-Grant number: 2000006304 and the Department of Science and Technology, South Africa (UID: 101594). This is where the GRECHLIM project entitled "Understanding recharge in the Limpopo River Basin, South Africa" has been implemented. Any opinions, findings, conclusions, of recommendations expressed in this article are those of the authors alone, and do not necessarily reflect the views of USAID or the NAS, and DST. We would like to thank the Department of Water and Sanitation, Johannesburg Water Authority and South African Weather Services for providing us with different data. Many thanks to the School of Geosciences, University of the Witwatersrand for logistic support, and Ms. Aqeelah Davis for assistance with the Hartbeespoort Dam sampling and logistics. The authors are also very grateful to the anonymous reviewers and the editor-in-chief, Dr. Gunter Dorhofer, whose constructive comments and recommendations helped to improve this work.

References

Abiye TA (2011) Provenance of groundwater in the crystalline aquifer of Johannesburg area, South Africa International. J Phys Sci 6:98–111. https://doi.org/10.5897/IJPS10.119

Abiye TA (2016) Synthesis on groundwater recharge in Southern Africa: a supporting tool for groundwater users. Groundw Sustain Dev 2–3:182–189. https://doi.org/10.1016/j.gsd.2016.10.002

Abiye TA, Mengistu H, Demlie MB (2011) Groundwater resource in the crystalline rocks of the Johannesburg area. S Afr J Water Resour Prot 03:199–212. https://doi.org/10.4236/jwarp.2011.34026

Abiye TA, Mengistu H, Masindi K, Demlie M (2015) Surface water and groundwater interaction in the Upper Crocodile River Basin, Johannesburg, South Africa: environmental isotope approach South African. J Geol 118:109–118. https://doi.org/10.2113/gssajg.118.2.109

Anhaeusser CR (1971) The geology and geochemistry of the archaean granites and gneisses of the Johannesburg—Pretoria dome. Economic Geology Research Unit, University of the Witwatersrand, Johannesburg

Appelo CA, Postma D (2005) Geochemistry, groundwater and pollution, 2nd edn. edn. Balkema, Leiden

Barnard HC (2000) An explanation of the 1:500 000 general hydrogeological map. Pretoria, South Africa

Clark ID, Fritz P (1997) Environmental isotopes in hydrogeology. Lewis Publishers, Boca Raton

Craig H (1961) Isotopic variations in meteoric waters. Science 133:1702–1703. https://doi.org/10.1126/science.133.3465.1702

Department of Water Affairs, Forestry SA (2008) The development of a reconciliation strategy for the Crocodile (west) Water supply system: summary of previous and current studies. Pretoria, South Africa

Eriksson PG, Clendenin CW (1990) A review of the transvaal sequence. S Afr J Afr Earth Sci Middle East 10:101–116. https://doi.org/10.1016/0899-5362(90)90049-k

Froehlich K, Gibson JJ, Aggarwal P (2002) Deuterium excess in precipitation and its climatological significance. In: proceedings of international conference on study of environmental change using isotope techniques: international conference held in Vienna, 23–27 April 2001 proceedings. In: C&S papers series, Vienna Austria, vol 13/P. International Atomic Energy Agency, p 531

Hall AL, du Toit AL (1923) On the section acoss the floor of the Bushveld Complex at the Hartbeesporrt Dam, West of Pretoria (Read 15th October, 1923) vol Plate VII

Harris C, Burger C, Miller J, Rawoot F (2010) O- and H-isotope record of Cape Town rainfall from 1991 to 2008, and its application to recharge studies of Table Mountain groundwater, South Africa South African. J Geol 113:33–56. https://doi.org/10.2113/gssajg.113.1.33

Healy RW (2010) Estimating groundwater recharge. Cambridge University Press, Cambridge

Johnson MR, Anhaeusser CR, Thomas RJ (2006) The geology of South Africa. Council for Geoscience. Geological Society of South Africa and Council for Geoscience, Pretoria, Johannesburg

Judson S, Deffeyes KS, Hargraves RB (1976) Physical geology. Prentice-Hall, Englewood Cliffs

Kohn MJ (2010) Carbon isotope compositions of terrestrial C3 plants as indicators of (paleo)ecology and (paleo)climate. Proc Natl Acad Sci USA 107:19691–19695. https://doi.org/10.1073/pnas.1004933107

Marfia AM, Krishnamurthy RV, Atekwana EA, Panton WF (2004) Isotopic and geochemical evolution of ground and surface waters in a karst dominated geological setting: a case study from Belize, Central America. Appl Geochem 19:937–946. https://doi.org/10.1016/j.apgeochem.2003.10.013

Rivard C, Lefebvre R, Paradis D (2014) Regional recharge estimation using multiple methods: an application in the Annapolis Valley, Nova Scotia (Canada). Environ Earth Sci 71:1389–1408. https://doi.org/10.1007/s12665-013-2545-2

Sami K (1992) Recharge mechanisms and geochemical processes in a semi-arid sedimentary basin, Eastern Cape, South Africa. J Hydrol 139:27–48. https://doi.org/10.1016/0022-1694(92)90193-y

Scanlon BR, Keese KE, Flint AL, Flint LE, Gaye CB, Edmunds WM, Simmers I (2006) Global synthesis of groundwater recharge in semiarid and arid regions. Hydrol Process 20:3335–3370 https://doi.org/10.1002/hyp.6335

Tessema A, Mengistu H, Chirenje E, Abiye TA, Demlie MB (2012) The relationship between lineaments and borehole yield in North West Province, South Africa: results from geophysical studies. Hydrogeol J 20:351–368. https://doi.org/10.1007/s10040-011-0803-5

Tsoelopele-Environmental (2006) Hartbeespoort Strategic Environmental Assessment. Tsoelopele Environmental (pty) Ltd (**unpublished work**)

Witthüser K, Holland M (2008) Hydrogeology of the Cradle of Humankind World Heritage Site, South Africa. In: Paper presented at the 12th international conference of international association for computer methods and advances in geomechanics (IACMAG), Goa, India, 1–6 October, 2008

C.3. Publication 3-Journal of Environmental Earth Sciences

Leketa, K. & Abiye, T. 2019. Modelling the impacts of climatic variables on the hydrology of the Upper Crocodile River Basin, Johannesburg, South Africa. Environmental Earth Sciences, 78, 358. https://doi.org/10.1007/s12665-019-8353-6.

Environmental Earth Sciences (2019) 78:358
https://doi.org/10.1007/s12665-019-8353-6

THEMATIC ISSUE

Modelling the impacts of climatic variables on the hydrology of the Upper Crocodile River Basin, Johannesburg, South Africa

Khahliso Leketa[1] · Tamiru Abiye[1]

Received: 8 October 2018 / Accepted: 31 May 2019
© Springer-Verlag GmbH Germany, part of Springer Nature 2019

Abstract
The impacts of climatic variables on the hydrology of the Upper Crocodile River Basin (UCRB) were modelled using the Precipitation-Runoff Modelling System (PRMS) for the period between 1996 and 2017. The values for the coefficient of determination (R^2) and the Nash–Sutcliffe model efficiency coefficient (E_N) gave a satisfactory correlation between the measured and simulated streamflow values, while a higher root mean square error (*RMSE*) was obtained for the validation period compared to the calibration period. PRMS was confirmed suitable for baseflow simulations because its mean annual recharge estimate of 5.3% was close to that of 7.5%, which was obtained using a separate filter parameter technique, both calculated from baseflow values. The climate scenario simulations revealed that the streamflow components are sensitive to temperature and rainfall. Higher decline in baseflow is observed when temperature increases than when rainfall decreases. Also, a smaller decline is observed in baseflow as compared to total streamflow, indicating the resistance of baseflow to drought. The scenario where temperatures were increased by 1.5 °C and rainfall decreased by 20% resulted in a decrease of 39% in total streamflow and 28% in baseflow. When the natural streamflow decreases by 39%, the wastewater discharge (5 m^3/s) exceeds natural streamflow 80% of the simulation period. As urbanisation increases in the UCRB, wastewater will also increase. It is concluded that, while higher amounts of streamflow currently dilute wastewater, with changing climate variables and increasing urbanisation, less natural streamflow will be available to dilute wastewater, leading to highly polluted surface water. Therefore, better treatment and constraints on wastewater discharge are recommended.

Keywords Precipitation-Runoff Modelling System · Baseflow · Recharge · Changes in climate variables · Wastewater · Johannesburg South Africa

Introduction

The progressively changing climate setting in Southern Africa, characterised by low rainfall and high temperature, leads to reduced terrestrial moisture (Graham et al. 2011; Engelbrecht et al. 2015; ASSAf 2017), which poses a threat to the sustainability of water resources for the current and future generations (Kusangaya et al. 2014). The Intergovernmental Panel on Climate Change (IPCC) has predicted that with increasing carbon dioxide emissions into the atmosphere, by the year 2100, the global temperatures will rise to a range between 1.4 and 5.8 °C (IPCC 2001), while rainfall shall vary with ± 20%. ASSAf (2017) provided the state of climate change in South Africa and predicted that South Africa will continue to warm at a rate higher than 0.15 °C per decade.

The change in temperature and precipitation has a direct impact on the quantity of evapotranspiration and, therefore, streamflow components (Legesse et al. 2010) such as baseflow and runoff. Due to high temperatures, a portion of rainfall that reaches the land surface may rapidly be evaporated back to the atmosphere, which results in reduced surface runoff and infiltration (Markstrom et al. 2015). Direct soil moisture evaporation and transpiration by plants further lead to lower groundwater recharge, which is defined as the downward flow of water reaching the water table, adding to groundwater storage (Healy 2010). The reduced groundwater

This article is part of a Topical Collection in Environmental Earth Sciences on Groundwater resources in a changing environment, guest edited by Okke Batelaan, Fabien Magri, and Martin Sauter.

✉ Khahliso Leketa
lleketa@gmail.com

[1] School of Geosciences, University of the Witwatersrand, Private Bag X3, P.O Box Wits 2050, Johannesburg, South Africa

Published online: 08 June 2019

recharge translates to a declining water table leading to less baseflow to the stream network (Winter 1998). During dry periods, baseflow eventually fails to sustain streamflow, leading to ephemeral streams, which compromise access to water for the aquatic environment, agriculture, human water consumption and socio-economic development (Kusangaya et al. 2014).

Access to water is also compromised by the poor wastewater disposal practices in both peri-urban and urban settings, which lead to polluted groundwater and surface water resources (De and Toor 2017). The effluents from the decentralised onsite septic systems that are predominantly used in the peri-urban settings are potential sources of high nitrogen (N) in groundwater (Humphrey et al. 2013; De and Toor 2017; Toor et al. 2017). On the other hand, wastewater management in the urban centres often consists of centralised wastewater treatment plants, which discharge treated wastewater of lower quality in the stream channels. As a result, the streams that drain large cities are often characterised by poor water quality (Satterthwaite 2008). This condition worsens with increase in urbanisation, an example is the highly urbanised Upper Crocodile River Basin (UCRB) (Fig. 1), which is a catchment that hosts the Johannesburg City and has the highest human impact in South Africa (Department of Water Affairs and Forestry 2008b). The growth in industrialisation in the UCRB presented a high water demand, which necessitated the inter-catchment water transfer of about 550 million m^3/year from the neighbouring Vaal River Basin (Department of Water Affairs and Forestry 2008a). This water transfer, acting as an input into the UCRB, increased the disposal of wastewater from the treatment works into the UCRB surface water resources. As a result, poor surface water quality has been a major concern for several decades, particularly in the Hartbeespoort Dam (Zohary et al. 1988; Department of Water Affairs and Forestry 2008b), which is a receiver of treated wastewater from the Johannesburg area (Department of Water Affairs and Forestry 2008b).

Since rainfall is a source for recharge and temperature is a major driver of evapotranspiration (Healy 2010; Kusangaya et al. 2014; Markstrom et al. 2015), the reduction in rainfall and the increase in temperature are expected to have a negative impact on groundwater recharge (Healy 2010; Kusangaya et al. 2014), leading to reduced discharge

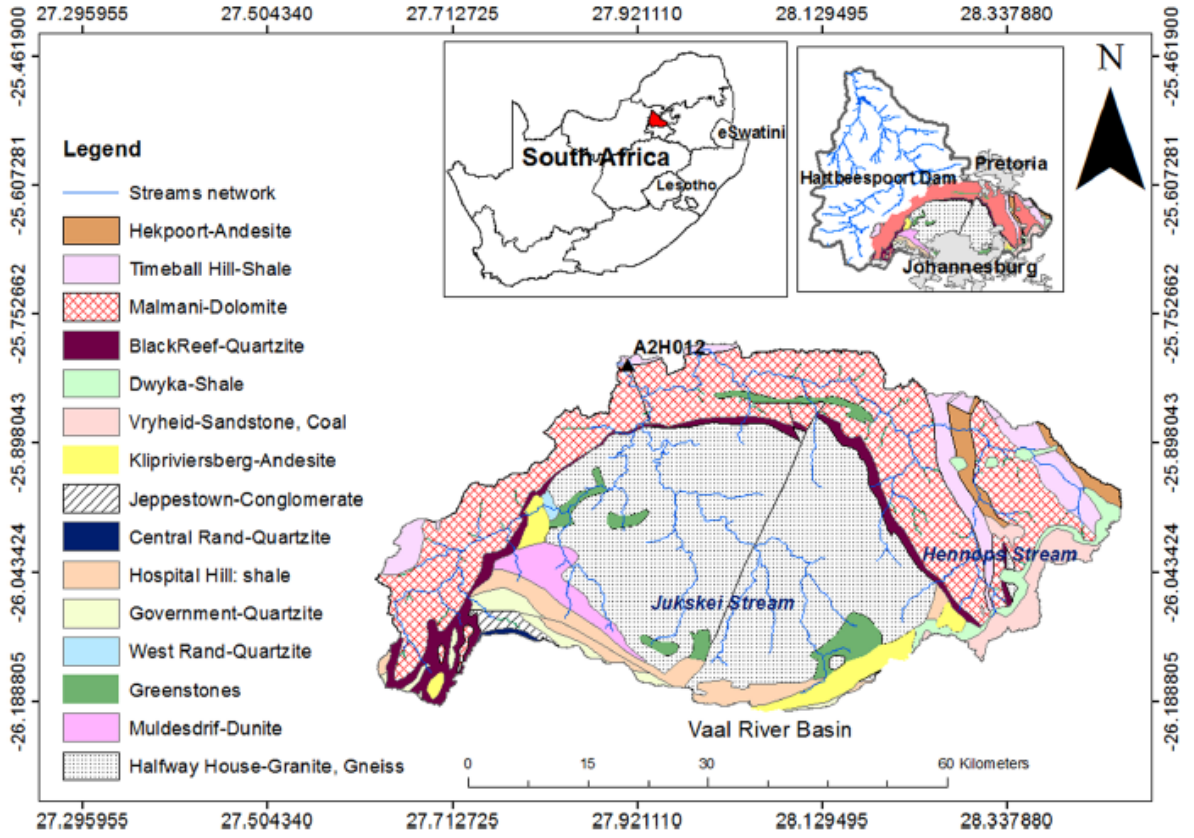

Fig. 1 Combo map of the UCRB and its location in RSA map as insert. Geological data were obtained from the Council for Geoscience

of the streamflow components (Winter 1998; Kusangaya et al. 2014). On the other hand, the growth in industries and urban migration could lead to increased wastewater discharge from water treatment works. This will increase the levels of pollution in the surface water resources, as lesser natural water (baseflow and surface runoff) will be available to dilute the increasing volumes of wastewater. Major et al. (2011) emphasised the need to assess the interaction between changes in climate and wastewater. Therefore, simulations of predictive precipitation-runoff models are necessary to understand how the changes in climate variables will impact the streamflow components and access to clean water for the future generations in the UCRB.

The Precipitation-Runoff Modelling System (PRMS) (Leavesley et al. 1983) has been used in different parts of the world with predominant application in the United States of America (USA) to run the predictive simulations on climate and land use (Markstrom et al. 2015). For example, Markstrom et al. (2012) successfully applied PRMS to assess the climate change response of different watersheds across the USA. Apart from the numerous applications in the USA, PRMS has also been applied in East Africa, Ethiopian Rift Valley with a tropical climate to determine the following, the impacts and sensitivities of streamflow to changes in land use and climate (Legesse et al. 2003; Legesse et al. 2010), and the impacts of changes in climate and land use on the specific hydrological processes, such as groundwater recharge (Abiye et al. 2009).

This study is done in the semi-arid Southern Africa and its objective is to estimate the baseflow and groundwater recharge in the UCRB and to assess the impacts of changes in climate variables on the streamflow components using PRMS. The study further undertakes a comparative assessment of the relative contributions of total streamflow and wastewater under various climate scenarios. Despite many watershed modelling studies that were done in Southern African region (Schulze 2000; Ncube and Taigbenu 2008), there is no record of published work on the applications of PRMS in the region. Various studies that were done in Southern Africa also indicate that changes in climate variables will affect the stream flow (Zhu and Ringler 2010; Graham et al. 2011). Furthermore, it was highlighted by Kusangaya et al. (2014) that the magnitude of climate change impacts will vary in the different catchments. For example, Graham et al. (2011) predicted an 18% streamflow decline in the Thukela catchment in South Africa, Zhu and Ringler (2010) predicted a reduction between 15 and 35% for different parts of the Limpopo River Basin, of which the UCRB is a sub-catchment.

The results of this work shall be beneficial for the water resource managers that deal with sustainable water management strategies. This approach may also be applied in other similar catchments to quantitatively assess the water security challenges that may come with changes in climate variables.

Materials and methods

Overview of PRMS

The Precipitation-Runoff Modelling System (PRMS) is a modular, deterministic, distributed-parameter, physical process-based hydrologic simulation code developed to evaluate effects of various combinations of climate and physical characteristics on hydrologic response and water distribution at the watershed scale (Markstrom et al. 2015; Regan and LaFontaine 2017). The previous versions of PRMS are documented in Markstrom et al. (2015) and Regan and LaFontaine (2017). In PRMS, a watershed is spatially discretised [usually through a geographical information system (GIS) analysis (Markstrom et al. 2015)] into smaller units called hydrologic response units (HRUs) of which each is assumed uniform in the defined properties. HRU properties are defined by the user through a series of PRMS parameters, which specify the physical characteristics of the HRUs and computation coefficients to PRMS. Slope, aspect, land cover, soil type, elevation (z), latitude (y) and longitude (x) of the HRUs, etc., are specified by the user in the Parameter File (parameter.dat) as well as the elevation, latitude and longitude of climate stations and flow and storage computation coefficients such as evapotranspiration, streamflow routing, soil water storage capacities and groundwater flow coefficients. The climate and stream flow data are specified in the Data File (data.dat), while the model execution information, simulation options and output variables are specified in the Control File (control.dat). These files are well described in Markstrom et al. (2015).

PRMS distributes climate data (temperature and precipitation) from the climate stations to each HRU on daily basis. Once climate has been distributed, various amounts of water are apportioned into interception, throughfall, snowpack, evaporation, sublimation, snowmelt, runoff, infiltration, recharge, interflow, baseflow, etc. This apportionment is done based on climate conditions, antecedent storages and the various parameters that define the physical characteristics and computational coefficients of each HRU. A part of evapotranspiration excess will become groundwater recharge, while some becomes surface runoff contribution to streamflow, which encounters further evaporation. A part of groundwater recharge will become baseflow into the stream network. Together with surface runoff (Hortonian and Dunnian) and interflow, baseflow forms the total simulated daily stream discharge at the outlet of the catchment. In PRMS, simulated discharge can be used to calibrate

the model against the measured discharge values (from the stream discharge station).

The PRMS produces several output files including the statistic variable file, which shows the output variable fluxes and storages per day for the entire basin or for the user-selected HRUs. More information on the software requirements and operation of PRMS is given in the user's manual (Markstrom et al. 2015).

Description of the study area

The study area occupies the southern part of the UCRB, which is the most developed part of the basin with the large industries and urban settlements located in northern Johannesburg, Midrand and southern Pretoria (Department of Water Affairs and Forestry 2008a). It drains Jukskei Stream from Johannesburg City in the south of the UCRB and Hennops Stream from Pretoria City in the southeast (Fig. 1). The total basin area that is gauged by the catchment outlet discharge station (A2H012) is 2552 km^2. The study area is characterised by a semi-arid climate with an approximate mean annual precipitation (MAP) of 700 mm/year (Abiye 2011). Due to the semi-arid and industrialised nature of the catchment, there is a high water demand, which cannot be met by the water resources from within the catchment. This, therefore, necessitated augmentation through the inter-basin water transfer from the Vaal Basin in the south of the UCRB (Department of Water Affairs and Forestry 2008a).

The inter-basin water transfer has inflated the discharge in the Jukskei and Hennops streams, through the disposal of urban wastewater from the water treatment works. The disposal of wastewater has adversely affected the quality of surface water resources in the UCRB (Department of Water Affairs and Forestry 2008a). The water quality challenges are mostly observed in the Hartbeespoort Dam, characterised by high levels of eutrophication (Zohary et al. 1988; Department of Water Affairs and Forestry 2008b). Table 1 presents the list of water treatment works and their capacity, which sums up to 400,000 m^3/day (5 m^3/second) (Department of Water Affairs and Forestry 2004). According to the Department of Water Affairs and Forestry (2004), the urban water demand in the UCRB for the year 2000 was approximately 291.4 Mm^3, which is expected to rise to 409 Mm^3 in the year 2025. With the predicted increase in urban water demand, it would be expected that more wastewater shall be generated and disposed in the UCRB streams.

The UCRB is underlain by the Basement Complex, the Witwatersrand Supergroup and the Transvaal Supergroup rocks, which display a northward younging direction (Barnard 2000; Johnson et al. 2006). The Basement Complex is mainly characterised by the Archaean Halfway House granitic and migmatitic bodies that are weathered and fractured, mainly at shallow depth while massive at deeper

Table 1 Average daily wastewater discharge in the UCRB (Department of Water Affairs, South Africa)

Wastewater discharge station	Wastewater volume (m^3/day)
Hartbeesfontein	35,000
Olifantsfontein	38,000
Sunderland Ridge	35,000
Esther Park	400
Johannesburg Northern works	220,000
AECI	7000
Modderfontein	16,000
Midrand South	5000
Percy Stewart	25,000
Driefontein	15,000

levels (Barnard 2000). Overlying the Basement Complex is the Witwatersrand Supergroup, which is represented by the rocks of Government, Hospital Hill and Central Rand (Johnson et al. 2006). The Witwatersrand Supergroup forms the southern boundary of the UCRB (Fig. 1) and mainly consists of quartzite, shale, and outcrops of serpentinite rocks. The Transvaal Supergroup occupies the northern portion of the UCRB and is represented by the Chuniespoort Group and Pretoria Group. The Chuniespoort Group consists of the Black Reef Formation and Malmani Formation, which are represented by the quartzitic and the dolomitic rocks, respectively (Johnson et al. 2006). The Pretoria Group overlies the Chuniespoort Group and appears as small patches on the northern and eastern boundaries of the study area (Fig. 1), represented by Timeball Hill and Hekpoort Formations, which are made of shale and basaltic-andesitic lava rocks.

Barnard (2000) classified the aquifers of the UCRB into the four types, which are, intergranular aquifers, fractured crystalline aquifers, karstic aquifers and intergranular and fractured aquifers. Intergranular aquifers are made of unconsolidated alluvial sands and gravel, fractured crystalline aquifers are made of fractures, fissures and joints within the granitic gneiss and quartzite rocks, while the karstic aquifers are formed in the dolomites. The intergranular and fractured aquifer consists of a combination of intergranular aquifer at the top, and a fractured aquifer at the bottom, which are hydraulically connected (Barnard 2000; Abiye 2011; Abiye et al. 2011). The fractured aquifers are classified as hard rock aquifers generally with low yield, whereas karstic aquifers, because of the dissolution cavities in the dolomites, generally have high yields (Witthüser and Holland 2008; Abiye et al. 2011). High yielding springs associated with karst aquifers are observed in the study area and are able to sustain baseflow during dry seasons. The low yielding

springs are also observed in the study area emerging at the base of Government quartzites and contributing to baseflow in the catchment.

The study area lies within altitudes ranging from 1176 to 1843 m.a.m.s.l. The topography of the study area is mainly influenced by the rock makeup and the historic geological processes. Through geologic history, the progressive upward movement of the Archaean Basement Complex led to the elevation of the older Archaean Basement granites and Witwatersrand Supergroup in the southern part of the catchment (Anhaeusser 1971). This gave way for the younger Transvaal Supergroup to shift towards the low-lying areas of the basin. Erosion also contributed to the topography, such that the more resistant rocks are mostly protruding creating ridges and sub-catchment boundaries, while the less resistant rocks form the valley floors. This is observed most in the Transvaal Sequence among the alternating quartzite, shale and dolostones. The dolostone outcrop has a gentle undulating topography (Abiye 2011), while the quartzites, because of their resistant nature, form elongated ridges.

Construction of the model

Time series data for precipitation and maximum and minimum air temperatures were obtained from the South African Weather Services (SAWS). Stream discharge data for the catchment outlet station (A2H012) were downloaded from the Department of Water Affairs of South Africa (DWS), National data archive. Both climate and river discharge data covered 21 years and 5 months from February 1996 to June 2017.

The description of the geology was obtained from 1:250 000 Barnard (2000) hydrogeological map of Johannesburg. The vegetation description was obtained from South African National Biodiversity Institute (SANBI) vegetation shape files (SANBI 2012). The surface topography was generated from the digital elevation model (DEM) obtained from the United States Geological Survey (USGS) Earth Explorer (https://earthexplorer.usgs.gov/).

ArcGIS Terrain Processing was applied on the DEM to generate a map of 313 HRUs, which are in the form of watersheds as shown in Fig. 2. The slope and aspect maps were generated from the DEM using ArcGIS hydro-tools

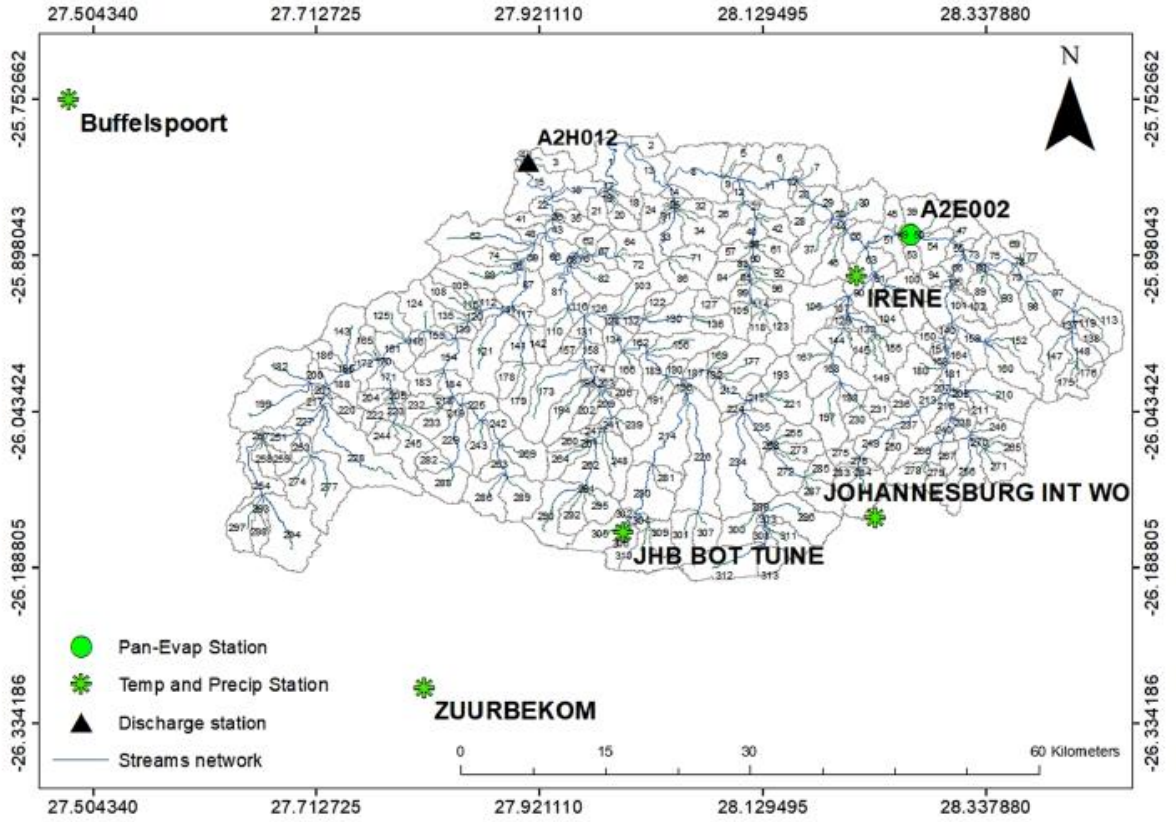

Fig. 2 The constructed hydrological response units (HRUs) in the UCRB with stream network, climate stations and a stream discharge station

and the average slope and aspect values for each HRU were obtained using the zonal statistics tools under ArcGIS hydro-tools. The other properties of the HRUs were obtained by layering the generated HRU map over the individual maps such as geology, land use, vegetation and soil map to obtain the properties of each HRU. In cases where an HRU was underlain by different properties, the dominant property within an HRU was assumed to represent the entire HRU. For example, an HRU which had more surface area coverage of granite than dolomite was assumed to be entirely underlain by granite, therefore, the PRMS properties that are representative of granite were used.

The daily maximum and minimum air temperature, precipitation and stream discharge data were specified in the PRMS Data File. The wastewater discharge of 5 m^3/s that was deduced from the daily total wastewater discharge in the catchment was deducted from the measured daily stream discharge. This is because, Abiye (2016) undertook groundwater recharge assessment in the UCRB using the hydrograph separation method and emphasised that, since this wastewater is a result of inter-basin water transfer from the Vaal Basin into the UCRB, it should be deducted from the measured stream baseflow as it erroneously inflates the baseflow estimate. The description of the HRUs was specified in the PRMS Parameter File. The model execution information including model start date and end, locations of Data File and Parameter File, selection of PRMS modules and selection of variables to be written in the output files were specified in the Control File. The Data File, Parameter File and Control File were constructed according to Markstrom et al. (2015). Missing river discharge, air temperature and precipitation were specified with the value − 19 in the Data File. Table 2 shows the modules used in this study and specified in the control file.

Groundwater recharge estimations

Baseflow was assessed in the UCRB through the application of the Web-based Hydrograph Analysis Tool (WHAT) (https://engineering.purdue.edu/mapserve/WHAT/; accessed July 22nd, 2018), which has been defined by Lim et al. (2005). This exercise was particularly done to address the first objective of this study, which is to estimate recharge through assessing the baseflow component of streamflow. According to Healy (2010), baseflow estimate can be used to calculate recharge assuming that: (1) all groundwater that recharges in the catchment ultimately discharges to a stream; (2) streamflow at dry low flows constitutes groundwater discharge (baseflow); and (3) the area of the aquifer that contributes to groundwater recharge is identical to the surface drainage area.

These assumptions are not all satisfied in the UCRB. The assumption that all recharge eventually discharges into a stream may only be valid in the part of the catchment that is underlain by massive granites with shallow weathered aquifers. Conceptually, when water recharges into such an aquifer system, it will most likely flow laterally towards the stream network, while deep percolation may only occur when it encounters vertical fractures. The dolomitic terrain on the other hand, due to the existence of deep dissolution cavities and fractures (Barnard 2000), is likely to be dominated by deeper percolation, which may not mainly flow to the stream network. However, the calculated baseflow can be referred to as minimum recharge as proposed by Pitman and Vegter (2003) to indicate that the estimated baseflow values only represents part of recharge amount. Vegter (1995) compared recharge estimates from baseflow technique and other methods in various catchments in South Africa, and observed a 50% variance, which was highest in smaller baseflow streams, decreasing with increase in baseflow estimates. The assumption that the aquifer area is

Table 2 Names of modules used to build a PRMS model in this study

Type of module	Purpose	Specified module
Precipitation module (*precip_module*)	Distributes precipitation to each HRU per day	ide_dist
Temperature distribution module (*temp_module*)	Distributes temperature to each HRU per day	ide_dist
Solar radiation module (*solrad_module*)	Computes daily shortwave radiation for each HRU	ddsolrad
Transpiration period module (*transp_module*)	Determines the period of active transpiration	transp_tindex
Potential evapotranspiration (PET) module (*et_module*)	Computes PET for each HRU	potet_jh
Interception module	Computes interception by plants and net precipitation	intcp
Surface runoff module (*srunoff_module*)	Computes surface runoff as an excess of infiltration and soil saturation	srunoff_smidx
Soil zone module (soil zone)	Simulates the hydrologic processes in the soil zone	soil_zone
Groundwater flow module (gwflow)	Simulates storage and inflow to and outflows from the groundwater reservoir	gwflow
Streamflow module (*streamflow_module*)	Computes stream flow leaving the model domain	muskingum

equal to catchment recharge area may not apply in the dolomitic terrain for the same reasons of deeper circulation that enhances inter-catchment groundwater flow. The assumption that all low flows consist of baseflow is assumed valid in this study because the wastewater discharge has been deducted from the measured stream discharge prior to the baseflow estimation.

The single filter parameter approach by Nathan and McMahon (1990) was applied using WHAT to calculate daily baseflow. The approach uses a filter parameter to separate high-frequency flows associated with surface runoff from the low-frequency flows associated with baseflow. The filter parameter value used is 0.995 as confirmed suitable for South African baseflow by Smakhtin and Watkins (1997).

The annual recharge for the 21 years was computed by dividing annual baseflow (m^3/year) by the area of the catchment (m^2) to give recharge in depth units per time (m/year, usually mm/year). The annual rainfall (mm/year) for the corresponding years was used to compute recharge as a percentage of rainfall.

Model sensitivity, calibration and validation

Model sensitivity analysis was conducted to identify the input parameters that have a significant effect on the simulated baseflow output variables (*basin_gwflow_cfs*) and simulated stream discharge output variable (*basin_cfs*). Numerous input parameters invoked sensitivity on the baseflow and streamflow. The parameters that showed significant sensitivity on baseflow were **gwstor_init**, which is groundwater storage at the beginning of a simulation and **gwflow_coef**, which is a coefficient that computes groundwater discharge to streams.

Since baseflow contributes to stream discharge, the simulated *basin_cfs* also showed significant sensitivity to parameters **gwflow_coef**. Over and above those two, **soil_moist_max** and the fast and slow shallow subsurface linear coefficients (**fastcoef_lin**, and **slowcoef_lin**) also invoked sensitivity on the *basin_cfs*. The **soil_moist_max** represents the soil water holding capacity for infiltrated water that is available for evapotranspiration and not for gravity flow as recharge or interflow. The fast and slow linear coefficients (**fastcoef_lin** and **slowcoef_lin**) affect the falling rate of simulated hydrograph limbs after the high flows. The parameter **jh_coef** seemed to affect the entire terrestrial moisture, which includes streamflow, baseflow and direct groundwater recharge. The **jh_coef** is the monthly (January to December) air temperature coefficient used in Jensen–Haise potential evapotranspiration computations. These parameters and variables are well defined in Markstrom et al. (2015).

Calibration of the PRMS model for the UCRB was done using both manual and automatic procedures. Manual calibration was mainly done to identify the acceptable ranges of model sensitive parameters, which were identified during sensitivity analysis. During manual calibration, the model sensitive parameters were adjusted for each consecutive simulation, until a good visual match was observed between the hydrograph of the simulated and measured streamflow and simulated and measured baseflow. The visual similarity of the hydrographs was assessed based on the following characteristics: rising limb slopes, the falling limb slopes, the timing of the peaks and the height of the hydrographs. The calibration data for streamflow were obtained from station A2H012 (Fig. 2), while the daily baseflow data were calculated from A2H012 streamflow data using a single parameter filter method (WHAT). Calibration with the estimated baseflow from WHAT was particularly done to constrain the model to ensure that PRMS is simulating realistic baseflow as compared to a simple single parameter filter method. This places more certainty on the ability of the model to undertake scenario analysis for the baseflow response to changes in climate. Baseflow was calibrated manually by adjusting **gwflow_coef** and **gwstor_init**, while the streamflow component was further calibrated using the automatic procedure as highlighted below.

The automatic calibration of streamflow was done to reduce possible uncertainties, which may have been brought by the user's subjectivity during manual calibration and to ensure that the model closely simulates the hydrological processes of the catchment. This was done through a graphical user interphase (GUI) called Luca (Let us calibrate). Luca is a stepwise, multiple objective calibration program, which was developed for calibration of the models compiled using the United States Geological Survey's Modular Modelling System such as PRMS (Hay and Umemoto 2007). The calibration was done on 7 years and 7 months data (1st February 1996 to 30th September 2003). The first year of calibration (1st February 1996 to 31st January 1997) was used for model initialization. The calibration period was selected, because it had no data gaps in measured streamflows at station A2H012 (see Fig. 2).

The validation period was selected between the 7th February 2007 and the 30th June 2017, mainly because it had a long record of no missing data. Model validation was done to see the accuracy and predictive capability of the model and to demonstrate that a given site-specific calibrated model can make accurate simulations in a different modelling situation or different input data. The model is found to be verified or valid, if its accuracy and predictive capability have been proven to lie within acceptable limits of error by tests independent of the calibration data (Konikow 1978), hence, a verification period that was selected was different from the calibration period. The statistical tools, in addition to the visual graphical analysis, were used to test the correlation between the observed and simulated discharge values in both calibration and

validation periods to give a quantitative measure of correlation. The used statistical tools are coefficient of determination R^2, Nash–Sutcliffe model efficiency coefficient E_N (Nash and Sutcliffe 1970) and the root mean square error (*RMSE*) (Willmott, 1982). R^2 and RMSE were calculated using excel plots, while E_N was obtained from Web-based hydrograph analysis Tool (https://engineering.purdue.edu/mapserve/WHAT/; accessed July 24th, 2018).

Krause et al. (2005) recommended the use of slope and intercept of the regression line in addition to the value of R^2. This is because, a model, which systematically always over or underpredicts, can still have an acceptable R^2 value close to one, even if all predictions are wrong. Therefore, for an acceptable correlation, an intercept would be close to zero, while the gradient should be close to one (Krause et al. 2005). The E_N value should be between 1.0, and $-\infty$ (Krause et al. 2005). For a perfect model fit, the E_N and R^2 value should be 1.0, however, values above 0.5 are also accepted (Santhi et al. 2001; Krause et al. 2005). The *RMSE* was used to assess the closeness of the plotted points to the line $Y=X$ (Pontius et al. 2008). The smaller the *RMSE* value, the more accurate the predictions are and vice versa, such that the values should approach zero for a perfect model (Willmott 1982). Therefore, the *RMSE* was calculated to quantify the magnitude of deviation of the points from the regression line and used to compare the sizes of error between the calibration and the validation periods.

Simulation of climate-based scenarios

The prevailing annual trends of precipitation, air temperature and pan evaporation for the review period were assessed from stations in the UCRB. These were done to assess the prevailing changes in the climate variables for the model period as a way to justify the climate change scenarios. The criteria for selection of stations were based on least data gaps. The station JHB WO was selected for precipitation, maximum and minimum air temperatures. The daily average air temperature was calculated from the daily minimum and maximum air temperatures, from which the annual values were calculated. Since station JHB WO does not measure pan evaporation, the station A2E002 was used to compute annual pan evaporation from an S-class pan. The locations of the two stations are shown in Fig. 2. Precipitation and pan evaporation were given as annual totals, while temperature values were computed as annual averages.

Figure 3a–c show the annual trends of precipitation, temperature and pan evaporation, respectively, for the period 1997–2016. Though these annual values have been

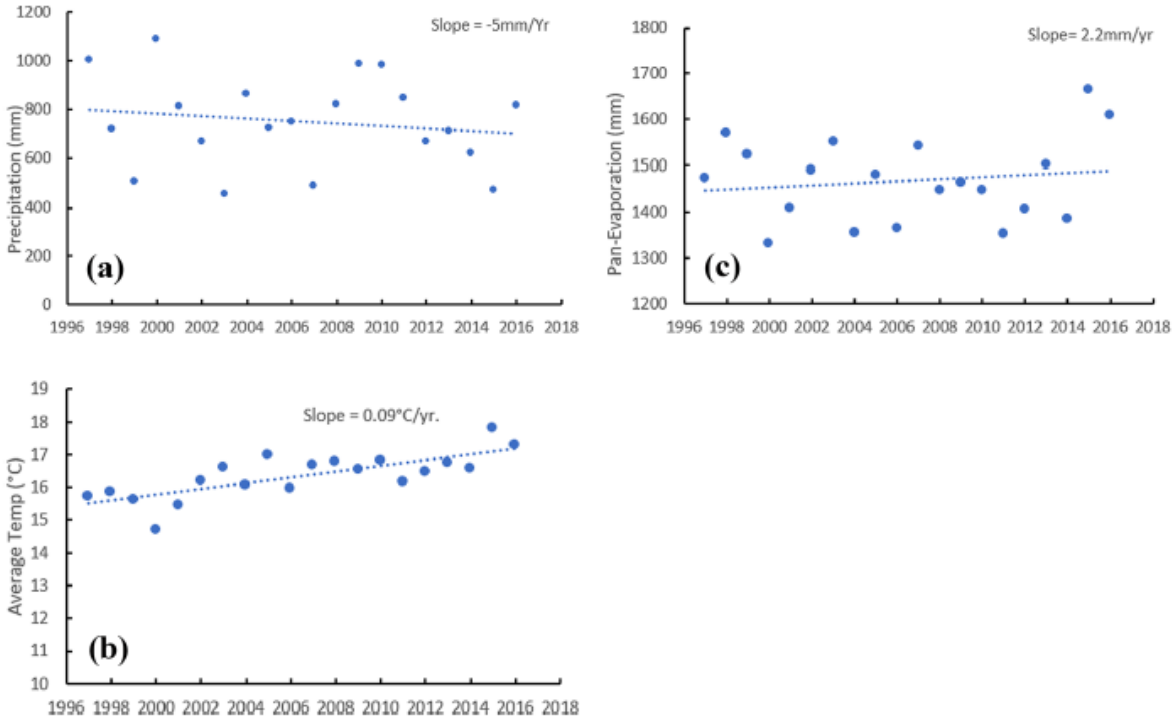

Fig. 3 Annual precipitation (a), temperature (b) and pan evaporation (c) for the period between 1997 and 2016

fluctuating over the review period, the slopes of the trend lines reveal that precipitation has generally been decreasing by 5 mm/year, average temperatures have been increasing by 0.09 °C/year, while pan evaporation has been increasing by 2.2 mm/year. In an assessment of the impacts of changes in climate variables, Kusangaya et al. (2014) reviewed various literature on the projected climate for Southern Africa (such as Graham et al. (2011) and Zhu and Ringler (2010)) and indicated that the various climate models present a consensus that in the future, Southern Africa's climate will become hotter and drier. The observed trends in the UCRB agree with this consensus. Collectively, these trends reveal that terrestrial moisture has been decreasing over the years, which justifies the need to assess the anticipated climate change effects on streamflow in the UCRB.

In this study, the simulations were run for the period 1996–2017 with an increase and decrease of 20% in rainfall and 1.5 °C in temperature. Finally, a combined worst-case scenario was run with a temperature increase of 1.5 °C and rainfall decrease of 20%. The impact of changing climate variables was quantified as a percentage change in streamflow and baseflow during each scenario. The Baseflow Index (BFI) was also assessed to study the relative contributions of groundwater to streamflow in each scenario. The BFI was calculated as the ratio of the mean annual baseflow to the mean annual streamflow for the review period as stipulated in Healy (2010).

Results and discussion

Model calibration and validation

Calibration of the PRMS model in the UCRB gave a value of 0.89 for both R^2 and E_N and 6.6 for the *RMSE* between the simulated and measured streamflow at A2H012. Figure 4a presents a statistical representation, which shows the correlation between measured and simulated discharge values for the calibration period. The correlation values present a characteristic feature of a model that is able to replicate measured data. Santhi et al. (2001) and Krause et al. (2005) stated that, for a good model, the values of R^2 and E_N should be close to one. The gradient of the regression line is 1.0, while the intercept is 0.71. The gradient is equal to the expected value of one and the intercept is close to the expected value of zero for a perfect model, as stipulated by Krause et al. (2005). Figure 5a presents a graphical correlation showing a good visual match between measured and simulated flows for the calibration period. Both the graphical and statistical analyses show that the model is capable of simulating measured flows.

Model validation, which was done for the period between 7th February 2007 and 30th June 2017, yielded a R^2 value of 0.76, E_N value of 0.56 and *RMSE* value of 9.2. Figure 4b presents a statistical representation, which shows the correlation between measured and simulated discharge values for the validation period. However, as can be seen in Fig. 5b, the graphical analysis deduced that the model could not satisfactorily replicate the validation period, particularly the high flows. Despite the lower correlation statistical values compared to calibration period, the validation statistical values still fulfil the requirements for a successful model as stipulated by Santhi et al. (2001) that the correlation statistics should be above 0.5. The gradient of the regression line is close to one, while a bigger deviation is observed in the intercept. The higher value of the intercept means that, where the simulated flow was 0 m^3/s, the measured flow was 3.6 m^3/s deducing that the model is underestimating the low flows. This parameter lowers the level of certainty for the validation period. While the intercept shows a bad correlation, the R^2, E_N and slope satisfy a good correlation and, therefore, means that the model may be applied for scenario analysis. According to the *RMSE* values, the calibration period has a smaller error compared to the validation period.

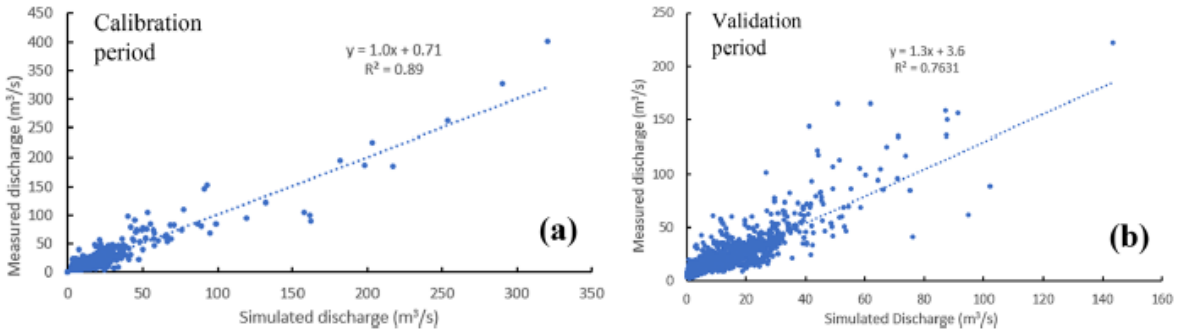

Fig. 4 Statistical correlation between simulated and measured annual flows for the calibration (a) and validation (b) periods

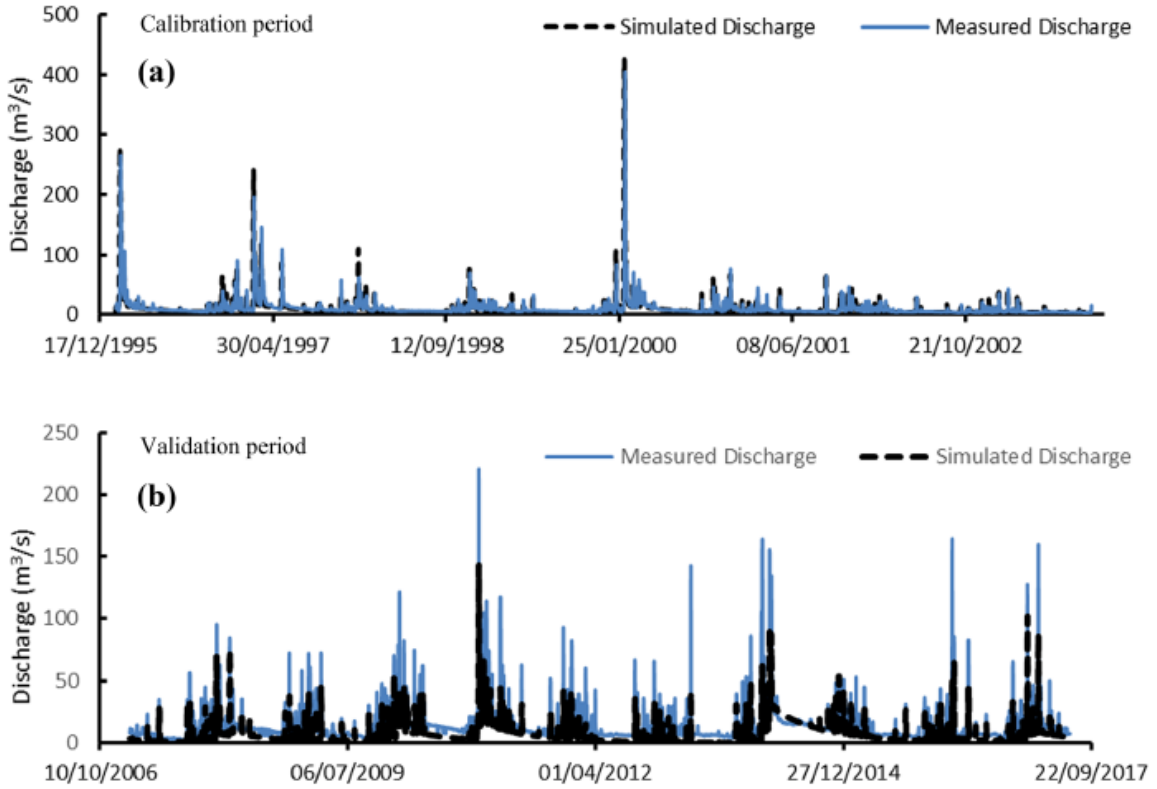

Fig. 5 Daily measured and simulated time series discharge data of the A2H012 for model calibration (a) and validation (b) periods

Recharge assessment

Table 3 shows the annual baseflow for the period 1997–2016 calculated using WHAT and PRMS. The recharge estimates that were calculated from baseflow volume per year and catchment surface area are also presented in Table 3 as percentages of annual precipitation. WHAT gave a recharge estimate range of 5.2–12.5%, with an average of 7.5%, while PRMS on the other hand gave a range of 4.0–6.5% with an average of 5.3%, all as a percentage of total precipitation for the relevant year. These average values are in agreement, and they agree well with the 6.7% estimate that was obtained by Leketa et al. (2018) through application of filter parameter separation method in the UCRB sub-catchments. This indicates that PRMS is simulating sensible baseflow, and therefore, the model is assumed valid for scenario analysis on baseflow in the UCRB.

Simulation of climate scenarios

Table 4 presents the results of climate simulations with increase and decrease in both precipitation and temperature. Both baseflow and streamflow were found to be more sensitive to an increase in rainfall than a decrease. Increasing rainfall by 20% caused an increase of 49% and 52% in baseflow and streamflow volumes, respectively. On the other hand, a reduction in rainfall with the same magnitude caused a reduction of 14% and 23% in baseflow and streamflow, respectively. Slightly more effect was observed in baseflow and streamflow as a result of an increase in temperature than a decrease. Increasing the temperature by 1.5 °C reduced baseflow by 26% and streamflow by 27%, while reduction of temperature in the same magnitude increased baseflow by 23% and streamflow by 18%. Figure 6 shows a monthly time series of simulated baseflow and total streamflow under the changing rainfall scenarios, while Fig. 7 shows the results of changing temperature scenario.

Table 3 Annual baseflow and recharge for the period of study from PRMS and WHAT

Year	WHAT baseflow (m^3)	Recharge (%)	PRMS baseflow (m^3)	Recharge (%)
1997	255 408 701	7.0	237 342 097	6.5
1998	167 359 712	5.9	141 819 568	5.0
1999	149 916 846	8.1	115 091 358	6.2
2000	220 235 876	6.0	221 246 641	6.0
2001	142 983 118	5.2	117 869 811	4.3
2002	114 977 308	5.7	105 817 121	5.3
2003	–	–	–	–
2004	–	–	–	–
2005	–	–	–	–
2006	214 179 140	7.6	135 223 952	4.8
2007	–	–	–	–
2008	229 068 814	7.8	150 423 354	5.1
2009	174 887 205	5.9	123 637 152	4.2
2010	284 385 979	7.8	200 616 347	5.5
2011	291 499 335	8.9	191 274 331	5.8
2012	189 083 892	8.3	108 318 097	4.7
2013	177 831 436	7.2	106 186 603	4.3
2014	388 587 340	12.5	198 365 689	6.4
2015	196 155 577	10.4	119 420 901	6.3
2016	167 059 551	5.9	113 671 422	4.0

Dashed cells represent years where there was missing data

Table 4 Climate simulation results with impacts on baseflow and stream flow

	Current	+20% Rainfall	−20% Rainfall	+1.5 °C Temp	−1.5 °C Temp	−20% Rainfall and +1.5 °C Temp
Baseflow	–	49% more	14% less	26% less	23% more	28% less
Streamflow	–	52% more	23% less	27% less	18% more	39% less
BFI	0.55	0.54	0.61	0.571	0.569	0.65

Having observed that the simulations where temperature was increased and rainfall decreased cause a reduction in both streamflow and baseflow, a further combined worst-case simulation with reduced rainfall and increased temperature was run. The result of the combined simulation was a 28% reduced baseflow and 39% reduced total streamflow. The predicted 39% decrease in streamflow agrees well with the 25.5% decrease that was obtained by Zhu and Ringler (2010) in the Limpopo River Basin (LRB), South Africa. In this prediction by Zhu and Ringler (2010), the rainfall was reduced by a lower value of 15% compared to the 20% in this study (the UCRB is a sub-catchment of the LRB), while potential evapotranspiration was increased by 7.5%. The lower rainfall reduction value of 15% could be the reason why only 25.5% was obtained in the LRB study by Zhu and Ringler (2010), otherwise indicating that if rainfall was reduced at a higher value of 20% in the LRB, streamflow would still decline with a much higher amount similar to the 39% that was obtained in this study.

Figure 8 shows the results of a combined worst-case simulation of increased temperature and reduced rainfall. It shows that there is less drought effect on baseflow compared to streamflow. The baseflow index analysis presented in Table 4 shows that the scenarios that invoke a reduction in terrestrial moisture such as reduced rainfall and increased temperature lead to a higher BFI. This could be attributed to a delayed groundwater drought compared to surface water drought.

A comparative analysis was also done to determine the number of occurrences (days) on which wastewater is more

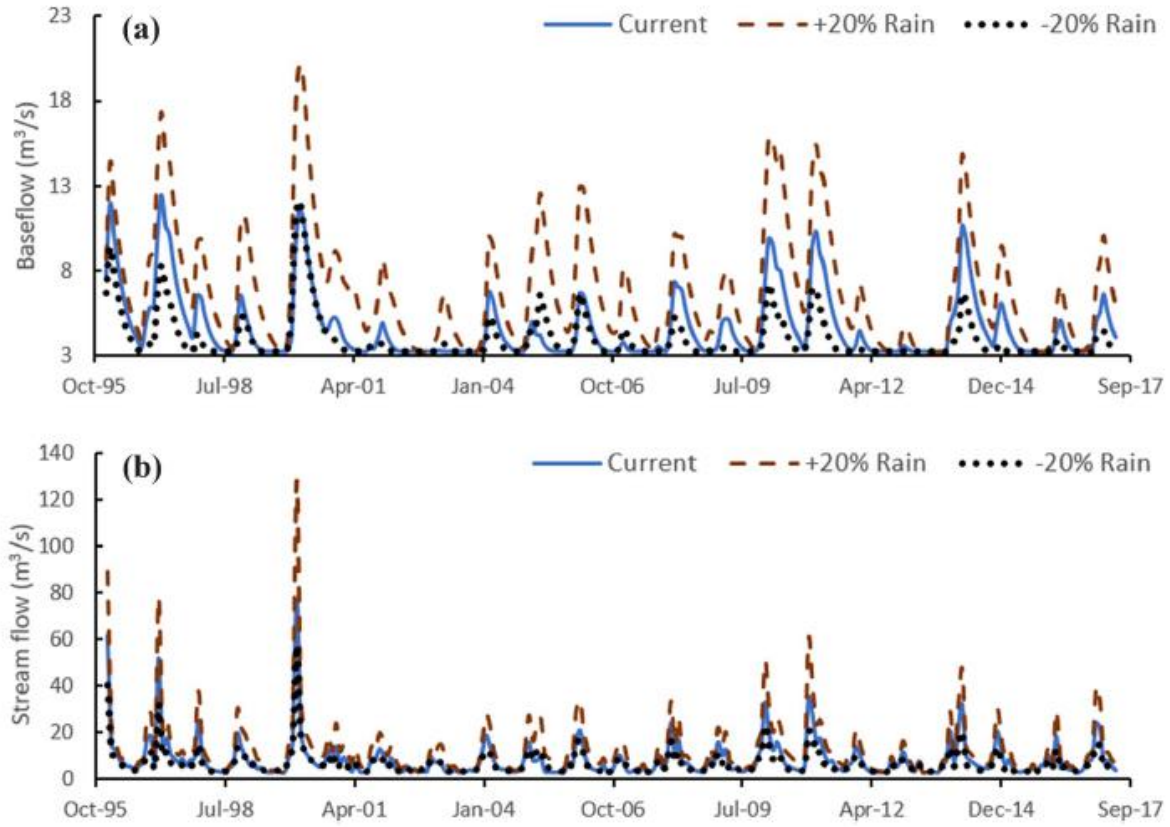

Fig. 6 Scenario simulated for monthly average baseflow (**a**) and stream flow (**b**) with varying rainfall

than natural streamflow (runoff and baseflow) and to determine how the occurrences change with changes in climate variables. Table 5 presents the total number of days out of 7821 of model review days, on which wastewater discharge (5 m^3/s) is greater than daily streamflow (wastewater exceedance days). Currently (1996–2017), 54% of the model review period has wastewater exceeding natural streamflow. When rainfall is reduced by 20% and temperature increased by 1.5 °C, wastewater exceeds streamflow 67% of the time and 75% of the time, respectively. An increase in temperature seems to cause more reduction in streamflow than a decrease in rainfall as was also observed in Table 4. Similarly, the number of occurrences on which wastewater exceeds natural streamflow is higher when temperature is increased than when rainfall is decreased. In the worst-case scenario, where rainfall is reduced and temperature increases, the highest value of 80% is obtained, indicating that wastewater exceeds streamflow 80% of the time. This analysis deduces that as climate variables change, wastewater contribution in the stream is likely to dominate over natural streamflow leading to more polluted water resources. It should however, be noted that this analysis assumes a constant wastewater discharge, meaning that as urbanisation increases, wastewater will increase and the condition will worsen.

Conclusion

The PRMS model was successfully calibrated against the measured streamflow with a R^2 value of 0.89 and 0.76 for the calibration and validation periods, respectively. The E_N values of 0.89 and 0.56 were also obtained for the calibration and validation periods, respectively, while the *RMSE* values were 6.6 for the calibration and 9.2 for the validation period. Since the R^2 and E_N values are close to one, they indicate that the model is capable of replicating measured data. The *RMSE* value also shows a smaller error during calibration compared to the validation period.

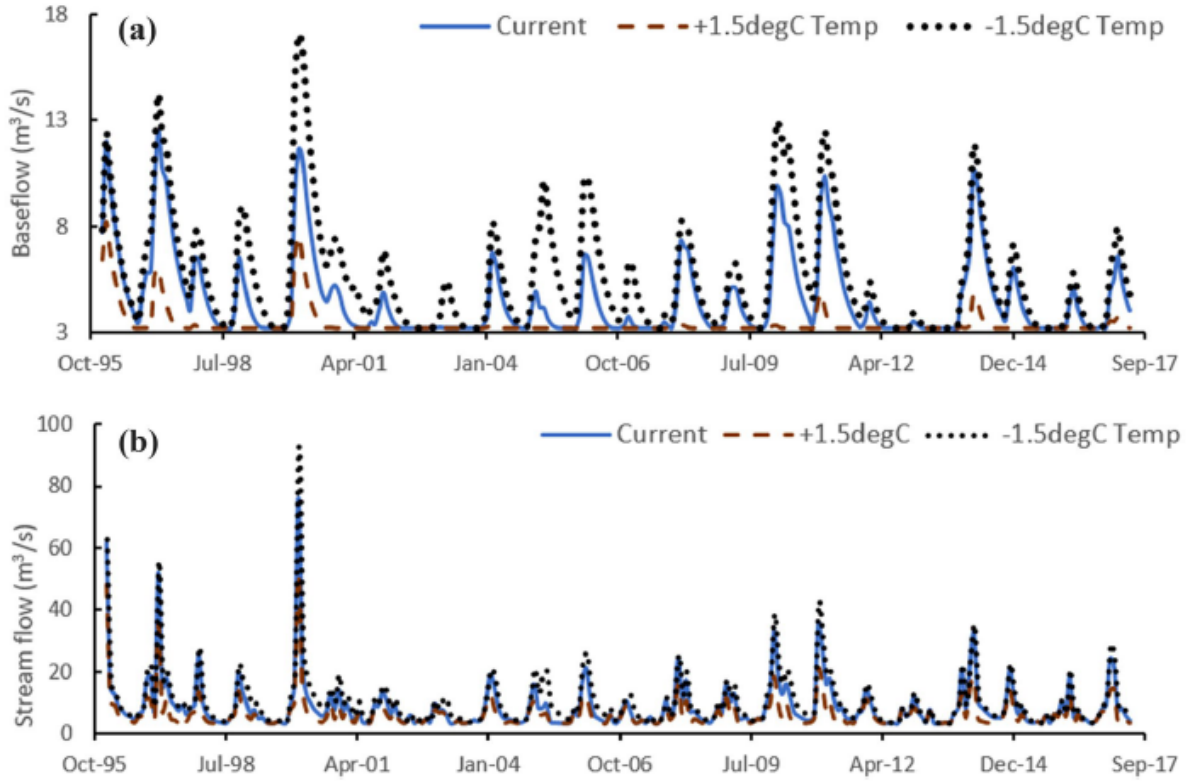

Fig. 7 Scenario simulated for monthly average baseflow (**a**) and stream flow (**b**) with varying temperature

The mean annual recharge estimates were obtained as 7.5% and 5.3% using PRMS and a single filter parameter technique, respectively. Since these mean annual recharge values were calculated using baseflow and catchment area in both techniques, their closeness indicated that PRMS is suitable for baseflow simulations in the UCRB. The simulations indicated a dependence of streamflow components on changes in climate variables. The baseflow shows resistance to drought conditions, with more reduction in baseflow observed when temperature is increased than when rainfall is decreased. The baseflow's resistance to drought is also confirmed by the BFI value; during scenarios where rainfall is decreases and temperature increased, the BFI value tends to increase and the magnitude of decline in baseflow seems to be smaller compared to a bigger decline in total streamflow. The streamflow decreases by 39% and baseflow by 28% during a combined simulation where temperature is increased by 1.5 °C and rainfall decreased by 20%. This behaviour reveals the significance of baseflow in sustaining streams during drought periods.

It is observed that with changing climate variables and increasing urbanisation, the disposal of urban wastewater will constitute a more significant component of stream flow yielding more polluted surface water resources within the UCRB. This condition predicts a potential water quality threat that is brought by a dominance of wastewater discharge in the stream channel as less natural water (baseflow and runoff) will be available to dilute the increasing wastewater discharge. The simulation indicates that under the 20% less rainfall and 1.5 °C increased temperature, the wastewater discharge (5 m^3/s) exceeds streamflow (combined runoff and baseflow) 80% of the time. Over and above that, considering the increasing urbanisation in Johannesburg, the wastewater discharge is likely to increase. Therefore, better

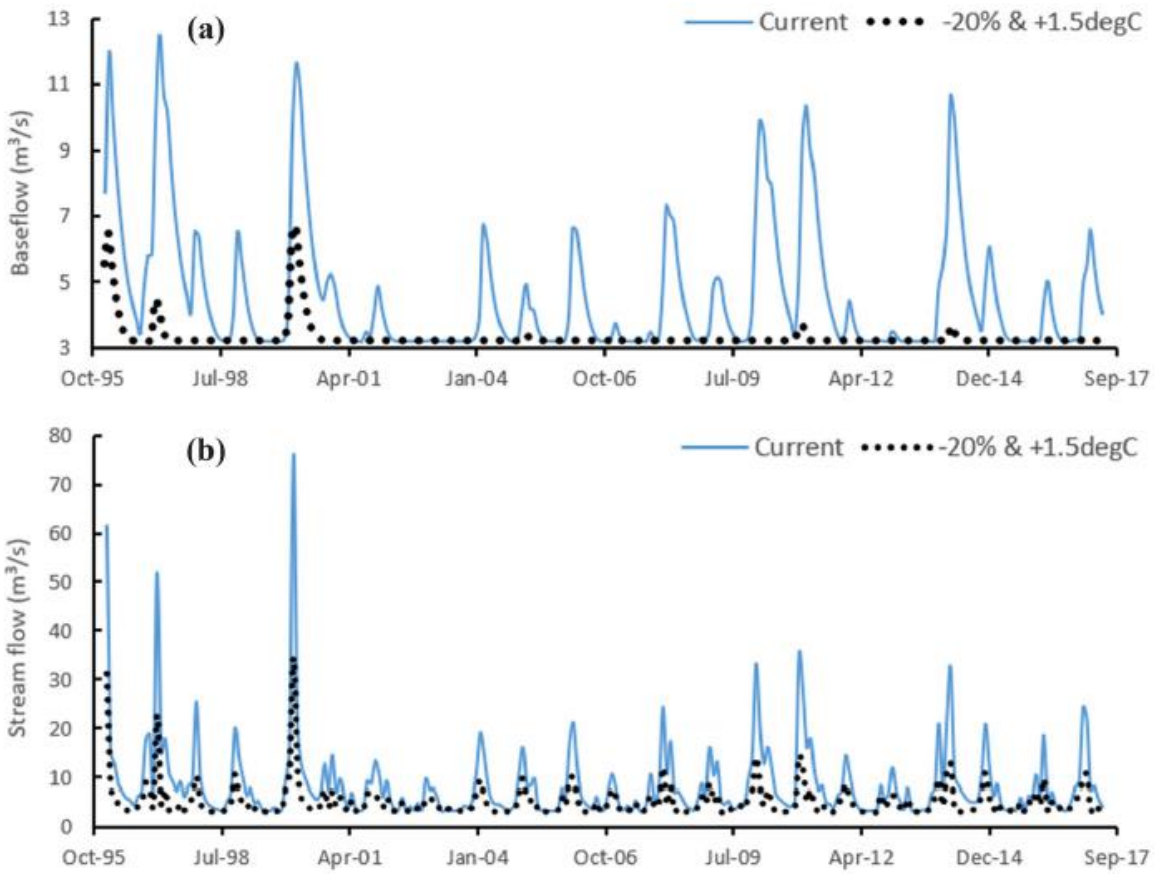

Fig. 8 A Combined scenario simulated for monthly average baseflow (a) and stream flow (b) with increased temperature and reduced rainfall

Table 5 The number of days in which streamflow is less than 5 m^3/s out of 7821 days of modelling period is shown

	Current	+20% Rainfall	− 20% Rainfall	+1.5 °C Temp	− 1.5 °C Temp	− 20% Rainfall & +1.5 °C Temp
No. of days	4204	2149	5222	5883	3106	6292
% days < 5 m^3/s	54%	27%	67%	75%	40%	80%

treatment and constraints on polluting might be required in the future to improve access to clean water for the future generations. With the predicted deteriorating quality of surface water resources, it would also be of interest to assess the water quality impact on groundwater resources, particularly in the riparian zones.

Acknowledgements This study was funded in whole or part by the United States Agency for International Development (USAID) and the National Academies of Sciences, Engineering, and Medicine (NAS) through Partnership for Enhanced Engagement in Research (PEER) under cooperative agreement number AID-OAA-A-11-00,012 Sub-Grant Number: 2000006304 and the Department of Science and Technology, South Africa (UID: 101594). Any opinions, findings, conclusions, of recommendations expressed in such articles are those of the authors alone, and do not necessarily reflect the views of USAID or the NAS, and DST. The authors would like to thank the Department of Water and Sanitation, South African Weather Services Johannesburg City Parks and Council for Geosciences for providing us with different data. Many thanks to the School of Geosciences, University of the Witwatersrand for office provision and administrative support. The authors would also like to thank Robert Steve Regan, Lauren Hay and Richard Healy of the U.S Geological survey for their technical

assistance with PRMS and recharge assessment. The authors would also like to acknowledge the anonymous reviewers and the Editor in Chief Olaf Kolditz, whose comments improved this work.

References

Abiye TA (2011) Provenance of groundwater in the crystalline aquifer of Johannesburg area. S Afr Int J Phys Sci 6:98–111. https://doi.org/10.5897/IJPS10.119

Abiye TA (2016) Synthesis on groundwater recharge in Southern Africa: a supporting tool for groundwater users Groundwater for. Sustain Dev 2–3:182–189. https://doi.org/10.1016/j.gsd.2016.10.002

Abiye TA, Legesse D, Abate H (2009) The impact of climate change on groundwater recharge: a case study from the Ethiopian Rift. In: Groundwater and climate in Africa (Proceedings of the Kampala Conference, June 2008), Kampala, Uganda, 2008. IAHS-AISH Publication, Kampala, pp 174–180. https://eurekamag.com/research/037/181/037181012.php

Abiye TA, Mengistu H, Demlie MB (2011) Groundwater resource in the crystalline rocks of the Johannesburg Area. S Afr J Water Resource Protection 03:199–212. https://doi.org/10.4236/jwarp.2011.34026

Anhaeusser CR (1971) The Geology and geochemistry of the archaean granites and gneisses of the Johannesburg-Pretoria dome. Economic Geology Research Unit University of the Witwatersrand Johannesburg, South Africa. https://books.google.co.za/books?id=aMQKAQAAMAAJ

ASSAf (2017) First biennial report to cabinet on the state of climate change science technology in South Africa. South Africa (ASSAf). https://doi.org/10.17159/assaf.2016/0015

Barnard HC (2000) An explanation of the 1:500 000 general hydrogeological map. Pretoria, South Africa. ISBN 0621299146

De M, Toor GS (2017) Nitrogen transformations in the mounded drainfields of drip dispersal and gravel trench septic systems. Ecol Eng 102:352–360. https://doi.org/10.1016/j.ecoleng.2017.02.039

Department of Water Affairs and Forestry (2004) Crocodile River (West) and Marico water management area: Internal strategic perspective of the Crocodile River (West) catchment. Department of Water Affairs and Forestry, Pretoria, South Africa. http://www.dwaf.gov.za/Documents/Other/WMA/3/Crocodile_ISP.pdf

Department of Water Affairs and Forestry (2008a) The development of a reconciliation strategy for the Crocodile (West) water supply system: Summary of previous and current studies. Department of Water Affairs, Pretoria, South Africa. http://www.dwa.gov.za/Projects/crocodilemaintenance/Documents/CWRS%20Reports/CWRS%20Summary%20of%20Previous%20and%20Current%20Studies.pdf

Department of Water Affairs and Forestry (2008b) The development of a reconciliation strategy for the Crocodile west water supply system version 1: water resource reconciliation strategy version, 1st edn. Pretoria, South Africa. http://www.dwa.gov.za/Projects/crocodilemaintenance/Documents/CWRS%20Reports/CWRS%20Crocodile%20West%20Reconciliation%20Strategy%20Version%201.pdf

Engelbrecht F et al (2015) Projections of rapidly rising surface temperatures over Africa under low mitigation. Environ Res Lett 10:1–17

Graham LP et al (2011) Using multiple climate projections for assessing hydrological response to climate change in the Thukela River Basin. S Afr Phys Chem Earth Parts A/B/C 36:727–735. https://doi.org/10.1016/j.pce.2011.07.084

Hay LE, Umemoto M (2007) Multiple-objective stepwise calibration using Luca, Version 1.0 edn. United States Geological Survey, USA. https://doi.org/10.3133/ofr20061323. http://pubs.er.usgs.gov/publication/ofr20061323

Healy RW (2010) Estimating groundwater recharge. Cambridge University Press, Cambridge

Humphrey CP Jr, O'Driscoll MA, Deal NE, Lindbo DL, Thieme SC, Zarate-Bermudez MA (2013) Onsite wastewater system nitrogen contributions to groundwater in coastal North Carolina. J Environ Health 76:16–22

IPCC (2001) Climate change 2001: The scientific basis. Contribution of working group I to the third assessment report of the intergovernmental panel on climate change. In: Houghton JT, Ding Y, Griggs DJ, Noguer M, van der Linden PJ, Dai X, Maskel K, Johnson CA (eds) Quarterly Journal of the Royal Meteorological Society, vol 128. Cambridge University Press, Cambridge, pp 1038–1039. https://doi.org/10.1002/qj.200212858119

Johnson MR, Anhaeusser CR, Thomas RJ (eds) (2006) The geology of South Africa. First edn. Geological Society of South Africa, Johannesburg/Council for Geoscience, Pretoria, Johannesburg; Pretoria. ISBN 1919908773

Konikow LF (1978) Calibration of groundwater models. In: Verification of mathematical and physical models in hydraulic engineering. University of Maryland & American Society of Civil Engineers, Hydraulics Division, New York, pp 87–93

Krause P, Boyle DP, Bäse F (2005) Comparison of different efficiency criteria for hydrological model assessment. Adv Geosci 5:89–97. https://doi.org/10.5194/adgeo-5-89-2005

Kusangaya S, Warburton ML, Archer van Garderen E, Jewitt GPW (2014) Impacts of climate change on water resources in southern Africa: a review. Phys Chem Earth Parts A/B/C 67–69:47–54. https://doi.org/10.1016/j.pce.2013.09.014

Leavesley GH, Lichty RW, Troutman BM, Saindon LG (1983) Precipitation-runoff modeling system; user's manual. United States Geological Survey, Denver, Colorado. https://doi.org/10.3133/wri834238

Legesse D, Vallet-Coulomb C, Gasse F (2003) Hydrological response of a catchment to climate and land use changes in tropical Africa: case study South Central Ethiopia. J Hydrol 275:67–85. https://doi.org/10.1016/s0022-1694(03)00019-2

Legesse D, Abiye TA, Vallet-Coulomb C (2010) Modeling impacts of climate and land use changes on catchment hydrology: Meki river. Ethiopia Hydrol Earth Syst Sci Discuss 7:4535–4565. https://doi.org/10.5194/hessd-7-4535-2010

Leketa K, Abiye T, Zondi S, Butler M (2018) Assessing groundwater recharge in crystalline and karstic aquifers of the Upper Crocodile River Basin, Johannesburg, South Africa. Groundwater Sustain Dev. https://doi.org/10.1016/j.gsd.2018.08.002

Lim KJ, Engel BA, Tang Z, Joongdae C, Ki-Sung K, Suresh M, Dibyajyoti T (2005) Automated web GIS based hydrograph analysis tool, What I Jawra. J Am Water Resources Assoc 41:1407–1416. https://doi.org/10.1111/j.1752-1688.2005.tb03808.x

Major DC, Omojola A, Dettinger M, Hanson RT, Sanchez-Rodriguez R (2011) Climate change, water, and wastewater in cities. In: Rosenzweig C, Solecki WD, Hammer SA, Mehrotra S (eds) Climate change and cities first assessment report of the urban

modelling system, version 4: US geological survey techniques and methods, book 6, chap. B7. United States Geological Survey, Colorado, USA. http://dx.doi.org/10.3133/tm6B7. https://pubs.usgs.gov/tm/6b7/

Nash JE, Sutcliffe JV (1970) River flow forecasting through conceptual models part I—a discussion of principles. J Hydrol 10:282–290. https://doi.org/10.1016/0022-1694(70)90255-6

Nathan RJ, McMahon TA (1990) Evaluation of automated techniques for base flow and recession analyses. Water Resour Res 26:1465–1473. https://doi.org/10.1029/WR026i007p01465

Ncube M, Taigbenu A (2008) Application of the SWAT model to assess the impact of land cover and land use on the hydrologic response in the Olifants Catchment. In: Paper presented at the 8th WaterNet/WARFSA/GWP-SA annual symposium (31 October–2 November 2007), Lusaka, Zambia

Pitman W, Vegter J (2003) Recharge and stream Flow. In: Xu Y, Beekman HE (eds) Groundwater recharge estimation in South Africa. UNESCO International Hydrologic Programme (IHP), Paris, pp 109–122

Pontius RG, Thontteh O, Chen H (2008) Components of information for multiple resolution comparison between maps that share a real variable. Environ Ecol Stat 15:111–142. https://doi.org/10.1007/s10651-007-0043-y

Regan RS, LaFontaine JH (2017) Documentation of the dynamic parameter, water-use, stream and lake flow routing, and two summary output modules and updates to surface-depression storage simulation and initial conditions specification options with the Precipitation-Runoff Modeling System (PRMS). United States Geological Survey, Reston, VA. https://doi.org/10.3133/tm6B8

SANBI (2012) National vegetation map project (VEGMAP). http://bgis.sanbi.org/vegmap/map.asp. Accessed 22 Sept 2017

Santhi C, Arnold JG, Williams JR, Dugas WA, Srinivasan R, Hauck LM (2001) Validation of the swat model on a large Rwer basin with point and nonpoint sources1. J Am Water Resources Assoc 37:1169–1188. https://doi.org/10.1111/j.1752-1688.2001.tb03630.x

Satterthwaite D (2008) Cities' contribution to global warming: notes on the allocation of greenhouse gas emissions. Environ Urbanization 20:539–549. https://doi.org/10.1177/0956247808096127

Schulze RE (2000) Modelling hydrological responses to land use and climate change: a southern african perspective AMBIO. J Hum Environ 29:12–22. https://doi.org/10.1579/0044-7447-29.1.12

Smakhtin V, Watkins D (1997) Low flow estimation in South Africa. Institute for water research. Rhodes University, Water Research Commission, Pretoria

Toor GS, Yang Y-Y, Mechtensimer S, De M, Obreza TA (2017) A review of the fate and transport of nitrogen, phosphorus, pathogens, and trace organic chemicals in septic systems AU—Lusk. Mary G Critical Reviews in Environ Sci Technol 47:455–541. https://doi.org/10.1080/10643389.2017.1327787

Vegter J (1995) An explanation of a set of National Groundwater Maps. Water Research Commission, Pretoria

Willmott CJ (1982) Some comments on the evaluation of model performance. Bull Am Meteor Soc 63:1309–1313. https://doi.org/10.1175/1520-0477(1982)063%3c1309:scoteo%3e2.0.co;2

Winter TC (1998) Ground water and surface water: a single resource. US Geological Survey circular. US Geological Survey, Denver

Witthüser K, Holland M (2008) Hydrogeology of the cradle of humankind world heritage site, South Africa. In: Paper presented at the 12th international conference of international association for computer methods and advances in geomechanics (IACMAG), Goa, India, 1-6 October, 2008

Zhu T, Ringler C (2010) Climate Change Implications for water resources in the Limpopo River Basin. Internation Food Policy Research Institute (IFPRI), Washington, DC

Zohary T, Jarvis AC, Chutter FM, Ashton PJ, Robarts R (1988) The Hartbeespoort dam ecosystem programme—1980–1988. Council for Scientific and Industrial Research, Pretoria, RSA. http://www.dwa.gov.za/iwqs/eutrophication/Zohary_1988_The_Hartbeespoort_Dam_ecosystem_programme.pdf

Publisher's Note Springer Nature remains neutral with regard to jurisdictional claims in published maps and institutional affiliations.